Electrically Tuneable Membranes: Revolutionising Separation and Fouling Control for Membrane Reactors

Xu, Lili

Award date:
2017

Awarding institution:
University of Bath

Electrically Tuneable Membranes: Revolutionising Separation and Fouling Control for Membrane Reactors

Lili Xu

A thesis submitted for the degree of Doctor of Philosophy

University of Bath

Department of Chemical Engineering

September 2016

Acknowledgements

I would like to express my deepest gratitude to my main supervisor, Dr. Darrell Patterson, who encouraged me to pursue this project. Without his guidance and persistent support this thesis would not have been possible. Thanks to my second supervisor, Dr. Emma Emanuelsson, who gave me lots of invaluable counselling and advice. For her unwavering help, I am truly grateful. I am grateful to Dr. Salman Shahid for many discussions and invaluable advice on the research topic. Thanks to Dr. Junjie Shen for his support and all the discussions. A big special thanks to my friends Nicholas Low, Kim Wu, Yen Chua, Sameer Khare and Parimala Shivaprasad for helping me with the proofreading work. Their support and suggestions are truly invaluable.

I am delighted to take this opportunity to express my vote of thanks to all laboratory technicians – including Fernando Acosta, Alexander Ciupa, Robert Brain, John Bishop, Suzanne Barkley, Daniel Lou-Hing for all their help and support. A big special thanks to the University of Bath for the Overseas University Research Scholarship that funded my PhD.

I would like to thank all the colleagues in our group for their help and provide me a lovely atmosphere to work in the lab. Many thanks to my dear friends here including Luz, Salida, Mi Tian, Kemi, Meng, Abouther, Jifang Zhang, Fei Liang, Saravanan, Molly, Yang and Adam for their encouragement and accompany. I also thank my lovely housemates for all the joy and fun.

Most importantly, I would like to express my deepest gratitude to my parents for their unconditional support, encouragement, affection and love. Also, thanks to my sister and brother in-law who teach me how to believe in myself and give me the indebted care and love. I could not finish the PhD without their support. A special thanks to my best friend Yu Wang, giving me the best support, encouragement and inspiration. Truly without him I would not have achieved my doctor degree.

Abstract

The overall aim of this research is to develop unique conducting polyaniline (PANI) membranes that can be electrically tuned to achieve different fluxes and selectivity. The target application is in a tuneable membrane reactor, where these membranes allow the fouling layer to be pushed off/through membranes by application of external potential.

To achieve this, several different types of PANI membranes were examined. The permeation properties of HCl-doped PANI membranes can be modified electrically to produce in-situ tuneable separations. However, acid dopant leaching and membrane brittleness limit the further application of these membranes. Polymer acid doped PANI membranes using poly(2-acrylamido-2-methyl-1-propanesulfonic acid) or PAMPSA were investigated as a solution. These PAMPSA doped PANI membranes displayed improved mechanical strength and filtration stability. However, the membranes showed decreased electrical conductivity, leading to a limited tuneable permeance and selectivity under applied potential. To overcome this new challenge, expanded graphite and a large acid (dodecylbenzene sulfonic acid or DBSA) were incorporated into the PAMPSA doped PANI membranes to increase the conductivity. Despite increasing both conductivity and electrical tuneability, the resulting membranes were more porous with looser molecular weight cut-off (outside of the desired NF/low UF MWCO range) than without modification. Efforts to tighten PAMPSA doped membranes to the same MWCO as HCl doped membranes using volatile co-solvents (THF and acetone) were unsuccessful: porosity was due to the large acid dopants.

Membranes were examined for their potential for in-situ fouling removal of model foulant bovine serum albumin under applied voltage. This was successful and defouling extent was found to be closely related to membranes with higher conductivity and greater acid stability.

Overall, it has been demonstrated that the conducting polyaniline composite membranes can be made to be stable to acid leaching and be more mechanically robust, whilst also being externally electrically tuned to different molecular selectivities with the potential for in-situ fouling control.

Table of Contents

List of Figures

List of Tables

Abbreviations

4-MP	4-Methylpiperidine
AC	Activated carbon
APS	Ammonium persulphate
B	Benzenoid rings
BSA	Bovine serum albumin
CNTs	Carbon nanotubes
CSLM	Confocal scanning laser microscopy
DBSA	Dodecylbenzenesulfonic acid
DCA	Dichloroacetic acid
DMAc	Dimethylacetamide
DMF	Dimethylformamide
DI	Deionised
DMA	Dynamic mechanical analysis
EB	Emeraldine base
EG	Exfoliated graphite
ELSD	Evaporative light scattering detector
ES	Emeraldine salt
FITC	Fluorescein isothiocyanate
FESEM	Field-emission scanning electron microscopy
FTIR	Fourier transform infrared spectroscopy
GO	Graphene oxide
GS	Gas separation
HCl	Hydrochloric acid
HPLC	High performance liquid chromatography
H_2O_2	Hydrogen peroxide

H_2SO_4	Sulfuric acid
LB	Leucoemeraldine base
LCST	Lower critical solution temperature
MF	Microfiltration
MMMs	Mixed matrix membranes
MW	Molecular weight
MWCO	Molecular weight cut-off
NF	Nanofiltration
NIPS	Non-solvent induced phase separation
NMP	N-methylpyrrolidone
PA	Polymer acid
PAAc	Poly(acrylic acid)
PADPA	p-aminoo-diphenylamine
PAMPSA	Poly(2-acrylamido-2-methyl-1-propanesulfonic acid)
PANI	Polyaniline
PANI-EB	Undoped polyaniline
PANI-ES	Doped polyaniline
PANI-PA	Polymer acid doped polyaniline
PB	Pernigraniline base
PBS	Phosphate-buffered saline
PEG	Polyethylene glycol
PEL	Polyelectrolyte
PMVEA	Poly(methyl vinyl ether-alt-maleic acid)
PP	Polypropylene
PPV	Polyphenylene vinylene
PPy	Polypyrrole

PSF	Polysulfone
PSSA	Poly(styrenesulfonic acid)
PT	Polythiophene
PTFE	Polytetraflouroethene
PVA	Poly(vinylphosphonic acid)
PVDF	Polyvinyldiflouride
Q	Quinoid rings
RGB	Red, green and blue
RO	Reverse osmosis
SEM	Scanning electron microscope
T_g	Glass transition temperature
T_{poly}	Polymerisation temperature
THF	Tetrahydrofuran
UF	Ultrafiltration
UV-Vis	UV–Visible

1 Introduction

1.1 Background

A membrane is a selective barrier regulating the transport of substances from a process stream containing a mixture of components. These are used in a wide range of processes – from pharmaceutical manufacturing to wastewater treatment – to affect a selective separation, creating two purer process streams from a process stream containing a mixture of components. Conventional membranes, however, have two key limitations: they become fouled and cannot have their transport properties tuned in-situ; transport and selectivity of these polymer barriers are controlled by properties fixed during or after fabrication (i.e. polymer type and resulting free volume, surface charge and microstructure) [1-3]. In this regard, the need for developing a tuneable membrane, which transport properties can be changed in-situ, is certainly warranted.

Polyaniline (PANI), as an intrinsically conducting polymer, has been widely researched due to its conductive properties achieved by the protonation of imine nitrogens (=N-). It is particularly attractive for membrane separation, since its porosity can be controlled at a molecular level through simple acid/base doping/dedoping [4, 5]. The transport properties of conducting PANI membranes, such as permeance and selectivity, could be tuned in-situ by applying an electrical potential across acid doped PANI membranes [6]. The applied potential can change the interaction between PANI and acid dopants, thus modifying the membrane properties and allowing permeance and selectivity to be tuned. In the Patterson research group, based on previous work, it has been realised that an electrically conductive PANI membrane could possibly be dynamically responsive by applying an external electrical potential across the membrane, thus inducing several changes in membrane properties that could produce more general membrane tuneability beyond the ion separations that PANI membranes have, in the main, been applied to thus far [6]. These electrically induced changes could include: changing surface charge controlling Donnan exclusion (which is explained in Chapter 2), change in pore size/free volume (via incorporation or expulsion of ions from the acid dopant sites) controlling pore flow transport, and chemical property changes, controlling solution diffusion and volume swelling.

Combined, these make polyaniline an excellent candidate for a more universally electrically tuneable membrane investigation.

Currently, there are two main challenges relating to the successful utilisation of PANI membranes: (i) the small acids used for doping PANI leach out from the membrane during filtration, leading to decreased conductivity; (ii) small acid doped membranes are brittle and thus difficult to handle and use [7-9]. To overcome these two challenges, various polymer acids (PAs) have been used as dopants to improve the filtration stability and mechanical strength of acid doped PANI membranes [8-16]. However, the major limitation of PAs doped PANI membrane is the low electrical conductivity, leading to poor membrane tuneability (permeance and selectivity change) under applied potential. With this concern, incorporating conducting particles into PAs doped PANI membrane and secondary doping have the potential to be the breakthrough solution to overcome the challenge of low membrane conductivity.

Despite extensive efforts in designing PANI membranes, there remains an insufficient understanding of the electrically induced transformations in these membranes, especially their impact on membrane performance (e.g. selectivity and permeance) for separation of neutral species – indeed the tuneable mechanisms outlined above have not been proven. A range of synthesis, doping and external stimulus parameters and factors needs to be studied to fully understand, optimise and control the in-situ tuneable separation performance of these membranes, and give a promising solution to in-situ membrane fouling removal by tuning the membrane separation performance using external stimuli.

1.2 Overall Project Area and Aim

Therefore, this project will be looking to improve the current PANI membranes in order to achieve better in-filtration stability, superior electrical tuneability and reduce membrane fouling. Therefore, the overall aim of this research is to develop unique conducting PANI membranes that can be electrically tuneable to different fluxes and selectivity. The target application is in a membrane reactor, where the primary aim of the new generated tuneable membrane is to allow the fouling layer to be pushed off/through membrane by external potential. The specific objectives of the project will be addressed after the literature review has clarified the specific gaps in the literature to give these further contexts.

1.3 Thesis Structure

This thesis is composed of eleven chapters and appendices, which are highlighted as following:

- Chapter 1 focusses on the introduction and motivation of the research;
- Chapter 2 presents a systematic literature review;
- Chapter 3 details the aims and objectives of the research;
- Chapter 4 describes the methods and materials involved in the membrane preparation and characterisation;
- Chapter 5 details the electrically tuneable PANI membranes, especially the effect of polymerisation temperature (T_{poly}) on in-filtration electrical tuneability of flux and molecular weight cut-off (MWCO);
- Chapter 6 describes a higher resolution one-filtration MWCO method for aqueous based nanofiltration (NF) and ultrafiltration (UF) membranes using polyethylene glycols (PEGs);
- Chapter 7 focuses on fabricating PAs doped PANI membranes to improve the filtration stability and mechanical properties of conducting PANI membranes;
- Chapter 8 focuses on enhancing PAs doped PANI membrane as a stimulating-responsive membrane by exfoliated graphite (EG) incorporation and secondary doping treatment with dodecylbenzenesulfonic acid (DBSA);
- Chapter 9 focuses on the effect of co-solvent (tetrahydrofuran (THF) and acetone) and evaporation time on the performance of PAs doped PANI membrane;
- Chapter 10 focuses on the in-situ fouling removal of stimuli-responsive composite PANI membranes by the application of electrical potential;
- Chapter 11 outlines the overall conclusion and future work.

2 Literature Review

2.1 Membrane Separation Process

A membrane, as a selective barrier between two adjacent phases, separates a feed stream into a retentate (or concentrate) and a permeate fraction [17]. Retentate consists of solutes that cannot pass through the membrane and permeate consists of solutes and solvent that can be transported through the membrane (Fig. 2-1) [18].

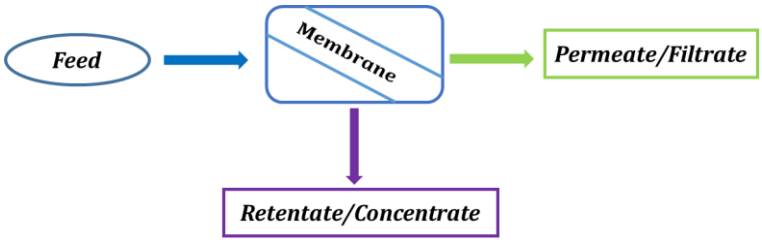

Fig. 2-1 The main stream parameters of membrane separation [18].

2.1.1 Membrane Separation Classifications and Modes

Membrane separation processes are generally categorised into pressure, concentration-gradient and electrical potential driven processes based on the driving forces. This project will focus on pressure-driven membrane processes, so this literature review will focus on these. Pressure-driven membrane processes are classified based on their pore size: microfiltration (MF), ultrafiltration, nanofiltration, reverse osmosis (RO) and gas separation (GS). Fig. 2-2 shows the separation characteristics of four main pressure driven processes such as MF, UF, NF and RO [19].

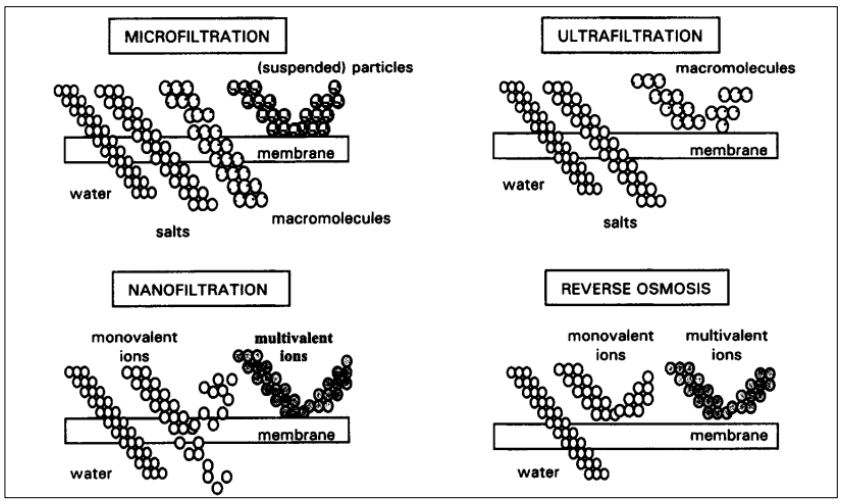

Fig. 2-2 The characteristics of microfiltration, ultrafiltration, nanofiltration, and reverse osmosis [19].

MF membranes have the largest pore size with diameters between 0.1 and 10 μm and are capable of removing particles, colloids and suspensions. MF can be used as prefiltration of UF process in the wastewater treatment or for the retention of proteins from the biochemical solutions [19, 20]. UF membranes have average pore diameters ranging from 10 to 1000 Å. UF processes are suitable for the removal of solids, bacteria, microorganisms and large dissolved molecules, such as natural organic material [19, 21]. NF membranes have pore sizes in the 1 to 10 nm range and a MWCO of 200 to 1000 g mol^{-1}. A typical application for a NF process is to reduce the ionic strength of a solution as well as to remove small organic molecules and colour from surface water or wastewater [22]. RO membranes have dense separation layers without distinct pores. The RO process is effective in removing many types of dissolved matters and monovalent ions, which is most widely known for its application in desalination of seawater and brackish water [23, 24].

Pressure-driven membrane filtration modes can further be divided into dead-end filtration and cross-flow filtration depending on the flow direction on the membrane surface as shown in Fig. 2-3 [25]. In dead-end filtration mode, all the fluid passes through the filter medium. This can result in trapped molecules on the membrane surface starting to form a more concentrated layer that affects the transport through the membrane (so called “concentration polarisation”) and eventually a “fouling layer” which can decrease the flux and significantly change the selectivity of the filtration process (these issues will be covered in more detail in Section 2.1.6 later). In cross-flow filtration mode, the main stream passes across the membrane surface in a parallel direction. Some solute and solvent molecules pass through the membrane and some continue to flow across it. Dead-end filtration is used in industry where a high selectivity needs to be guaranteed. Unlike the dead-end filtration, cross-flow filtration can wash away the “concentration polarisation” and “fouling layer” in the filtration process and is the most frequently used filtration mode in industry [26].

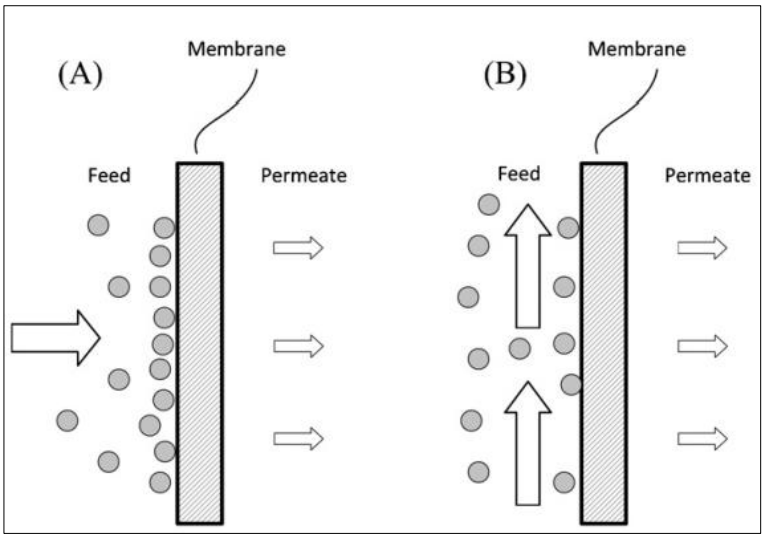

Fig. 2-3 Diagram of dead-end filtration (A) and cross-flow filtration (B) [25].

2.1.2 Membrane Transport Models

The mechanism of mass transport in the permeation processes are mostly covered by three membrane models: the solution diffusion model, pore flow model and Donnan exclusion. All three models can control the transport of solutes and solvents through a membrane – this is especially for membranes in the UF and NF range – as targeted in this project.

(i) **The solution diffusion model** is most widely applied to describe the transport of low molecular weight (MW) components in dense membranes in processes such as GS, pervaporation and RO [27]. In this model, permeants partition into the membrane material and then diffuse to the permeate side of the membrane down a concentration gradient. The feed and permeant phases are separated by the differences of the rate between components dissolving in the membrane and diffusing through the membrane. The model assumes that a membrane is in equilibrium with the adjacent outside phases, and the interactions between membrane materials and solutes determine the transport rate and selectivity [27, 28].

The mass transport in a solution diffusion membrane consists of three relevant steps: (i) sorption of the permeant from the feed liquid into the membrane according to a partition coefficient, (ii) diffusion of the permeant to the permeate side of the membrane according to a chemical potential gradients and (iii) desorption of the permeant from the membrane at the permeate side to the downstream side. Fick's first law can be used to describe solution diffusion:

$$J_i = -D_i \frac{d_{c_i}}{d_x} \qquad \text{Equation 2.1}$$

Where J_i is the flux and d_{c_i}/d_x is the concentration gradient. The term D_i is the diffusion coefficient. This equation is a good description for membrane transport depending on concentration, pressure and so on [28].

(ii) **The pore flow model** is of relevance for the transport of permeants with different sizes or MW through tiny pores in UF and MF processes [29]. In contrast to the solution-diffusion model, it assumes that transport is driven by the pressure gradient. Viscous flow and sieving exclusion achieve the separation and dominate transport rate. In the pore flow model, all molecules larger than the largest membrane pores are completely rejected and all molecules significantly smaller than the smallest pores pass through the membrane. All molecules that are larger in size than the smallest pores but smaller than the largest pores are prevented based on the pore size distribution of the membrane [28]. Mass transport on basis of the pore flow mechanism membrane can be described using Darcy's law illustrated in Equation 2.2:

$$Q = \frac{KAP}{\mu L} \qquad \text{Equation 2.2}$$

Where: Q: the flowrate of the fluid, K: the permeability of the system, A: the cross-section area, P: pressure, *L*: the thickness of the membrane, μ: the viscosity of the fluid.

(iii) **Donnan exclusion** describes the behaviour of charged ions passing through the membrane. The charged membranes selectively adsorb counter ions and exclude identically charged ions (namely co-ions). In order to keep the ion equilibrium between membrane and solution, the transport of counter ions could be affected [30]. The Donnan exclusion model shows that the equilibrium distribution of ions can take place across a membrane and it can be written as (assuming permanent ions are K^+ and Cl^-):

$$\frac{C_{K^+_{in}}}{C_{K^+_{out}}} = \frac{C_{Cl^-_{out}}}{C_{Cl^-_{in}}} \qquad \text{Equation 2.3}$$

2.1.3 Parameters Definition

The selective transport properties of a membrane are determined by two parameters: the flux and selectivity (rejection). Membrane flux is defined as the flowrate of feed stream passing through per unit area of membrane at a given operating pressure. It can be affected by the nature of membranes (materials and structures) and external factors (pressure, temperature and concentration) [21].

$$J = \frac{1}{A}\frac{dV}{dt} \qquad \text{Equation 2.4}$$

Where J is flux, A is effective surface area of membrane, dV is the volume through membrane and dt is the time.

Membrane permeance normalises for pressure applied to the membrane and thus allows for comparisons of filtrations at different applied pressures.

$$Permeance = \frac{J}{TMP} = \frac{1}{TMP \bullet A}\frac{dV}{dt} \qquad \text{Equation 2.5}$$

Where TMP is the transport membrane pressure.

The selectivity of a membrane is generally expressed by the rejection. The value of the rejection varies between 0% (unselective membranes) and 100% (complete retention of the solute). Membrane rejection is generally calculated according to the Equation 2-6:

$$R_{\mathrm{j}}(\%) = \left(1 - \frac{C_{\mathrm{p}}}{C_{\mathrm{f}}}\right) \times 100\% \qquad \text{Equation 2.6}$$

Where R_{j} is the rejection of membrane, C_{f} is the solute concentration in the feed and C_{p} is the solute concentration in the permeate.

The MWCO is a term also used to describe the retention performance of a membrane. It is determined by the lowest MW of a solute at which a rejection of 90% is achieved by the membrane. A solute with a higher MW than the MWCO will get a higher rejection. MWCO curves can be obtained by plotting the rejection of solutes, typically PEGs, dextrans, polystyrenes, or proteins against their molecular weights [31]. The shape of the MWCO curve is more important however – an ideal MWCO curve should have a sharp cut-off, a shallower slope means the membrane will not separate molecules distinctively and is not as useful [18].

A mass balance around the membrane is applied to determine the loss of solutes during the filtration. An overall mass balance, which indicates the extent to which the permeate and retentate have been recovered in the permeate and retentate, compared to the feed, can be calculated by a rearrangement of the overall mass balance around the membrane:

$$\text{Mass balance (\%)} = \frac{Q_p\, C_p + Q_r\, C_r}{Q_f\, C_f} \times 100\% \qquad \text{Equation 2.7}$$

Where Q_f, Q_p and Q_r is the flowrate of feed, permeate and retentate, respectively. C_f, C_p and C_r is the concentration of solutes in feed, permeate and retentate, respectively. For a dead-end filtration, the flowrates can be replaced with volumes, V_f, V_p and V_r.

2.1.4 Membrane Structures

The common symmetric and asymmetric membrane types are shown in Fig. 2-4 [32]. In a symmetric membrane, the structure is identical throughout the entire cross-section of the membrane. The separation characteristics are determined by the entire structure of membrane and the flux is inversely proportional to its thickness. On the other hand, the structure of an asymmetric membrane has a gradient over the cross-section. A typical asymmetric membrane consists of a very thin, dense skin layer on a porous support structure. The skin layer is responsible for the selective behaviour of the asymmetric membrane, whereas the porous substructure only serves as mechanical support and possesses negligible resistance to mass transfer. Good mechanical strength and high fluxes can be achieved in asymmetric membranes due to these properties [29, 33]. Taking the mechanical strength and permeance into account, asymmetric membranes will be the focus in this project.

Phase inversion, a single process which creates an integral structure with the skin and the support structure made from the same material, is commonly employed to prepare asymmetric membranes [29, 34]. As reported in recent years, it has become one of the most economical, versatile and reproducible techniques for the synthesis of an integrally skinned asymmetric membrane, which consist of an ultrathin skin layer on a microporous support substructure [21, 35]. The detailed preparation method will be introduced in the Section 2.4.1.

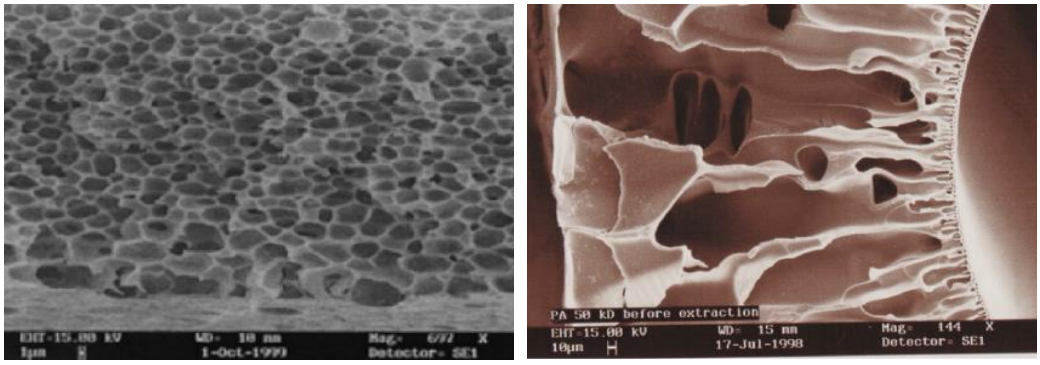

(a) symmetric membrane (b) asymmetric membrane

Fig. 2-4 The structure of cross-sections: (a) symmetric membrane (b) asymmetric membrane [32].

Fig. 2-5 illustrates the morphology of porous and dense membranes [33]. Porous membranes, possessing pore diameters between 1 nm and 10 μm, are commonly employed in MF, UF and dialysis processes [29]. Pore flow and Donnan exclusion related transport controls the separation of solvent and solutes through these porous membranes. Non-porous or dense membranes provide high selectivity but low permeability, which can be applied in the separation of small molecules [36]. Transport rate and selectivity are mainly influenced by chemical affinity between solutes and membrane materials, which can be described by a solution-diffusion mechanism [37]. Membrane structures in dense membranes are generally asymmetric, providing relatively high fluxes as a result of the transport rate-determining very thin selective layer on the porous support layer. Dense membranes are widely used in numerous processes such as RO, GS and pervaporation [29, 38].

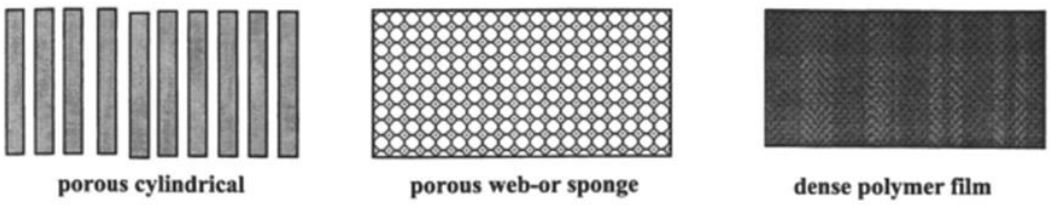

Fig. 2-5 The structure of relevant porous and dense membranes [33].

2.1.5 Membrane Materials

Generally, synthetic membranes can be made from polymers, inorganic materials or a mixture of organic polymer and inorganic materials. By far the majority of membranes are made from polymeric materials such as polysulfone (PSF),

polytetrafluoroethylene (PTFE), polyvinylidenefluoride (PVDF), polypropylene (PP) and polyaniline. Inorganic materials, like metals, ceramics and glasses, are employed for special applications (e.g. the production and purification of high-quality hydrogen and the separation of isotopes at high temperatures) [29, 39]. Polymeric membranes have the advantage of lower cost whereas inorganic membranes are advantageous in applications requiring elevated temperatures and harsh chemical conditions [39]. The combination of these two main types of membranes are known as hybrid membranes, where the main type is mixed matrix membranes (MMMs), incorporating an inorganic dispersed phase within a polymer matrix. MMMs combine the advantages of each phase and have the potential to achieve higher permeability and selectivity for gas mixtures compared to polymeric membranes [40, 41]. However, the MMMs face significant challenges of membrane aging, sensitivity to chemical cleaning and fouling [42]. In terms of this, an asymmetric membrane made by polymer materials in the UF and NF range will be produced in this project. The membrane is expected to be suitable for enzyme rejection in a free enzyme membrane reactor with regard to the target future application of this work.

2.1.6 Concentration Polarisation and Membrane Fouling

Concentration polarisation and membrane fouling are inevitable in pressure-driven membrane processes, which result in the decline of permeate flux over time and affect the membrane performance. Generally, an initial flux decline is primarily caused by concentration polarisation, a rapid solute build-up near the membrane surface. Long-term flux decline is primarily affected by membrane fouling (e.g. cake formation, solute desorption, bacterial growth, *etc*.) [43, 44].

Concentration polarisation is attributed to membrane permselectivity: the retained species accumulate at the upstream membrane/solution interface where their concentration gradually increases, leading to the generation of a concentration gradient at a membrane surface. Fig. 2-6 displays concentration polarisation on a membrane surface in a cross-flow filtration [44]. Concentration polarisation can initiate membrane fouling and considerably decrease membrane separation efficiency. Traditionally, techniques such as increasing the fluid flowrate, promoting turbulent mixing, reducing membrane thickness have been employed to alleviate it [45].

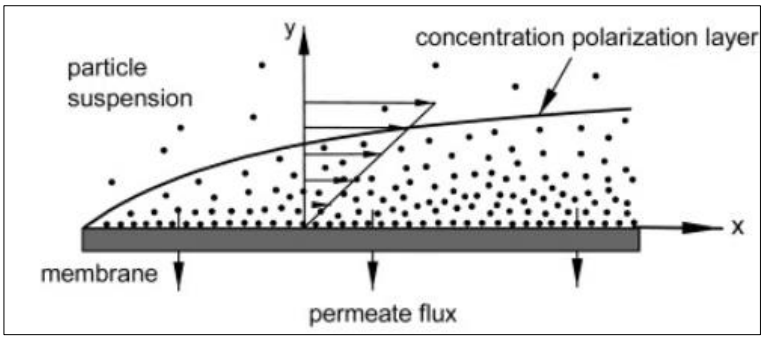

Fig. 2-6 Concentration polarisation on a membrane surface in a cross-flow filtration [44].

Membrane fouling is caused by the accumulation of foulants on the membrane surface, or within the pores, leading to a long-time flux decline and sometimes also to a change in separation characteristics. The main fouling mechanisms include adsorption of certain components, pore clogging, cake layer formation, chemical interaction between foulants and membrane materials and bacterial growth [2, 29, 43]. In general, membrane fouling can be divided into reversible fouling and irreversible fouling. Reversible fouling can be removed by physical means such as hydraulic cleaning or mechanical cleaning, whereas irreversible fouling can only be removed by chemical cleaning.

Numerous improvements have been developed to prevent or minimise membrane fouling, including pre-treatment of feed solution, modifications of membrane surface, optimisation of operation conditions as well as membrane cleaning [20, 29, 43]. Pre-treatment of the feed solution includes chemical precipitation, pre-filtration, pH adjustment, adsorption onto activated carbon, chlorination or addition of complex agents [46]. Incorporating hydrophilic moieties or charged groups into the membrane surface is an effective approach to develop anti-fouling membranes. The optimisation of operation conditions, such as enhancing feed flow velocities or shear rate on the membrane surface, are capable of reducing fouling. Membrane cleaning such as hydraulic cleaning, mechanical cleaning, chemical cleaning and electrical cleaning is a vital step and always employed in practical operation [1]. The choice of prevention methods mainly depends on the membrane type, module configuration, chemical and physical resistance of the membrane and type of foulants treated [45].

Among these techniques, pretreatment generally comes at a great cost and with limited effect [47]. Chemical cleaning can contribute to fouling removal but

interrupts the filtration process [48]. Surface modification has an efficient effect on the initial stage of filtration. However, it cannot play a long-lasting role to fouling suppression once the surface is fouled by deposited contaminants [49]. Regardless of the approaches used, the membrane would eventually be contaminated during filtration. Therefore, it is still a hot issue and remains unsolved for membranes, especially in a free enzyme membrane reactor. Conventional membranes in membrane reactors are difficult to change their morphology and porosity to alleviate fouling once synthesised [50]. In this regard, it could be of great interest to develop tuneable membranes with switchable separation properties by applying external stimuli to mitigate membrane fouling [51]. Hence, this study will focus on developing a stimuli-responsive membrane to remove membrane fouling in-situ by tuning the membrane separation performance using external stimuli.

2.2 Stimuli-Responsive Membranes: Smart Tools for More Controllable Separation Processes

2.2.1 Recent Advances in Stimuli-responsive Membranes

As mentioned before, the existing commercial membranes cannot have their transport properties adjusted in response to external stimuli once fabricated. The stimuli-responsive polymers give a promising solution to reversibly switch their physicochemical properties upon the application of external stimuli. Therefore, responsive polymers are attracting increasing attention and considered to be important materials for developing stimuli-responsive membranes [52].

Table 2-1 summarises the recent stimuli-responsive membranes prepared by stimuli-responsive polymers or modification of membrane surface by incorporating stimuli-responsive polymers [52-57]. The membranes have been designed to respond to some common triggers, including changes in temperature, pH, ionic strength, light, electric and magnetic field. The membrane responsive properties can be explained by conformation changes in the polymers that lead to reversible microphase segregation. The stimuli-responsive membranes have myriad potential applications such as sensors, drug delivery, self-cleaning surfaces, solute separation, selective filtration amongst other applications.

Table 2-1 Some stimuli-responsive membranes [52-57].

Stimulus	Example responsive group	Stimuli-responsive change
Electrical voltage	Polyaniline, polypyrrole (PPy)	The permeation of PANI membrane or PPy coated membrane can be modified electrochemically to produce controllable transportation properties.
Temperature	Poly(N-isopropylacrylamide)	Incorporating responsive groups in the membrane bulk makes a bulk responsive membrane, and this membrane displays decreased barrier properties above the lower critical solution temperature (LCST). Incorporating responsive groups on the membrane surface makes a membrane with surface modifier layers, and this membrane exhibits pore opening above the LCST.
pH and ionic strength	Poly(acrylic acid) (PAAc), polyelectrolyte (PEL)	The membrane with PELs grafted from pore surface exhibits decreased pore size by adjusting pH to ionise the polymer. For PELs based hydrogels, the membrane displays higher solute permeation by adjusting pH to ionise the polymer.
Light	Photo-chromic molecules (Azobenzene, spiropyran, diarylethene, viologen)	Membranes with photo chromic units show reversible changes in molecular properties such as polarity, charge, colour and size and macroscopic properties. Membrane barrier properties can be changed with application of external light energy.
Electric fields	PEL, anisotropic nanoparticles	Membranes using surface coating or anisotropic nanoparticles undergo changeable solute permeation in response to electric field. The solute permeation can be turned on and off by switching electric field on and off.
Magnetic fields	PEL, magnetic nanoparticles,	Magnetic membranes display displacement and can be used to control chemical release under the application of magnetic field.

2.2.2 Key Factors for Stimuli-responsive Membranes

Four essential factors are closely related to the stimuli-responsive membranes. The first key factor is responsivity including response speed and response degree, which is still a challenge in the responsive membrane. Generally, a fast response speed and large response degree is desired whenever the stimulus appears. Compared to temperature and pH, electricity and magnetic field normally give faster response speed as expected. The second key factor is the stable performance during the operation process. The responsive membrane should be robust and maintain their conformations under the fixed stimulus. The reversibility is the third essential factor, which stands for self-regulative adjustment of membranes. The membrane should retain the initial properties or conformations after undergoing repeated exposure to external stimulus. Another key factor is reproducibility, which is important for the large scale or widespread practical application [54].

2.2.3 Stimuli-responsive Membranes for Fouling Control

Recent studies have investigated the application of responsive membranes for the suppression of fouling and most of them have focused on the development of temperature, pH, ionic strength and electrical field responsive membranes [58]. In contrast to the traditional methods, the membrane properties can be tuned by changing the conformation of responsive groups upon the application of external stimuli. For example, oscillating between a more hydrophobic and hydrophilic membrane surface can result in desorption of adsorbed fouling under the stimulus [59]. This indicates that the adsorbed contaminants may be released by switching the confirmations of the responsive polymers in response to applied stimulus.

At present, the fabrication of electrically conductive membranes with tuneable transport properties under applied potential has attracted considerable attention [60]. Many studies focus on the anti-fouling behaviour of membranes by use of external electric field on the membrane surface [61-63]. For example, a conductive MF membrane by incorporating a stainless steel mesh exhibited enhanced anti-fouling performance and could effectively control the fouling by applied potential [61]. Biofouling in polypyrrole (PPy) coated membranes could be reduced by electrochemical polarisation of PPy. The membrane can be applied as an electrochemically switchable membrane [64]. Application of an external electric field is found to be a promising method to enhance the fouling control in electrified

commercialised PVDF ultrafiltration membranes [65]. Electrically conductive membranes demonstrate the ability to remove foulants from membrane surfaces and the membrane can be easily cleaned in-situ via electrical stimulus.

It is found that polyaniline as a conducting polymer with a conjugated backbone has the ability to change its structure at the molecular level by controlling the incorporation or exclusion of ions from the dopant site [3-5]. This provides a promising way to tune the separation properties of PANI membrane by applying external stimuli, thus mitigating the membrane fouling, or allowing defouling in-situ. Taking these into account, this research will focus on utilising PANI as a conducting membrane material and investigating the possibility to remove and/or reduce membrane fouling under external stimuli.

2.3 Polyaniline-A Promising Intrinsically Conducting Polymer

2.3.1 Properties of PANI

Polyaniline, a π-conjugated structure with alternating single and double bonds, has been found to be the most extensively studied intrinsically conducting polymer during the past decade [66]. Compared with other conducting polymers such as polypyrrole, polythiophene (PT), polyphenylene vinylene (PPV), PANI is most widely researched and applied because of good environmental stability, distinct electrochemical properties, simple reversible acid/base doping chemistry as well as cheaper synthesis costs [4, 66-69]. Electrical properties of PANI can be varied and controlled by both oxidative and non-redox protonic acid doping reactions in the conjugated carbon backbones. Also, the characteristic colour of PANI changes in different oxidation states, so each state can be distinguished by its colour. The electrochromatic changes of the polymer have led to its application in redox and pH indicators as well as other display devices [70, 71].

Fig. 2-7 shows the transformation of three basic structures of PANI by redox and doping processes [71]. The three basic structures of PANI range from the completely reduced form called leucoemeraldine base (LB) to the intermediate oxidised state called emeraldine base (EB) to the fully oxidised form called pernigraniline base (PB). Transition from emeraldine to leucoemeraldine and emeraldine to pernigraniline can be observed using cyclic voltammetry [66]. The only electrically conductive form of PANI is the emeradine salt (ES) which can be

formed by the addition of acids that protonates the EB without a change in its oxidation state.

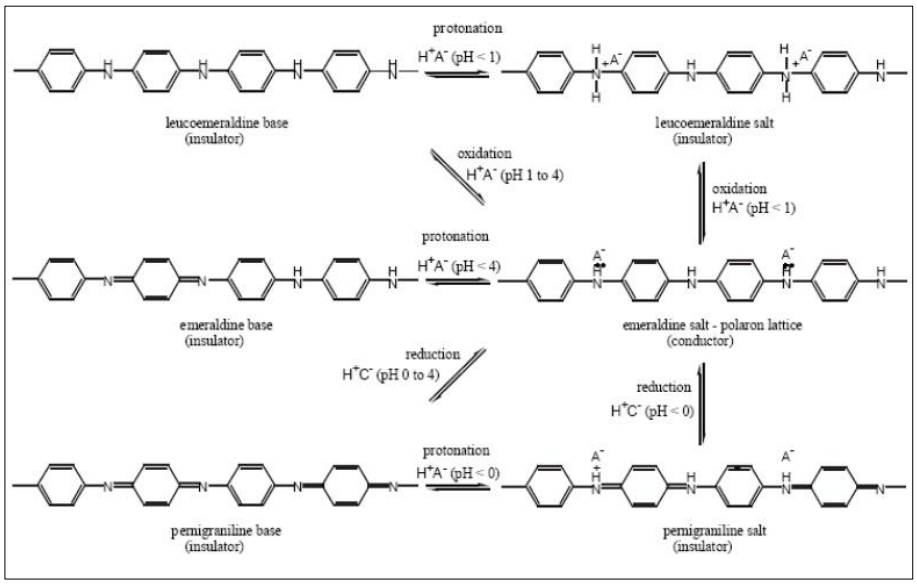

Fig. 2-7 Transformation of PANI into various states by redox and doping/undoping processes [71].

Oxidative and chemical proton doping processes to form the conductive ES state of PANI are shown in Fig. 2-8 [70]. The proton doping process is different from redox doping since it does not include the incorporation or withdrawal of electrons from the PANI backbone. The imine sites (=N-) in the EB can be protonated by acid dopants to form the bipolaron and then the bipolaron dissociates two stable polarons. The polaron structure is responsible for the transport of the electric charge and associated with the conducting regions in the bulk polymer. Then this undergoes a rearrangement along the entire polymer backbone to form a delocalised polysemiquinone radical cation. Consequently, electrical conduction occurs along the chain through electron delocalisation or inter-chain hopping of charge carriers [66, 71, 72].

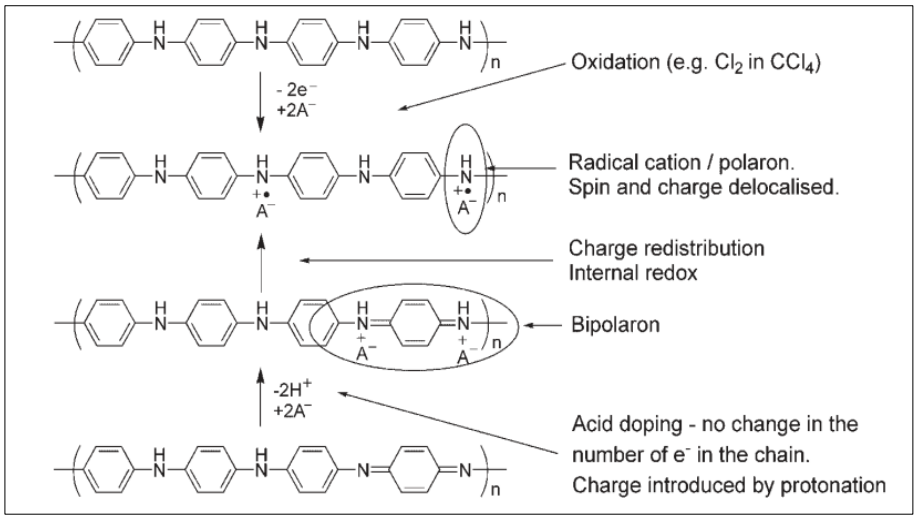

Fig. 2-8 Oxidative and chemical doping mechanisms to form the conductive emeraldine salt [70].

Fig. 2-9 shows the conduction pathway in the polaron structure. The nitrogen cation radical acts as a hole. Electron from the adjacent neutral nitrogen atom jumps to the hole to make it become neutral, the hole then starts to move, creating a second hole. The electron consequently moves along the chain and the hole is formed in the opposite direction of the whole electron motion, leading to conduction in the polaron structure. In the LB and PB structures, the electron movement is less likely since all the nitrogen along the chain are similar, creating less chance for the protonated nitrogen and neutral nitrogen side by side, resulting in the insulating nature of LB and PB [66].

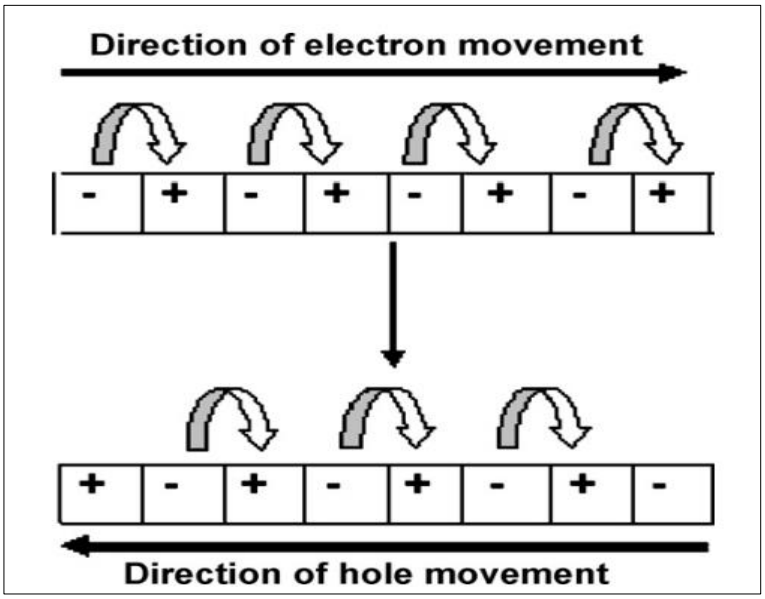

Fig. 2-9 The conduction pathway in the polaron structure (the "+" represents nitrogen cation radical acting as a hole and the "- "represents neutral nitrogen) [66].

2.3.2 Chemical Polymerisation of PANI

Different methods for the synthesis of PANI have been developed, including chemical polymerisation, electrochemical polymerisation, photo-induced polymerisation, enzyme-catalysed polymerisation, plasma polymerisation and a number of other special methods. Among the employed methods, chemical and electrochemical polymerisation techniques are the most commonly used methods for PANI preparation as a result of better reproducibility and control [71]. The electrochemical synthesis technique can obtain a relatively purer PANI form (as no additional chemicals such as oxidant and surfactant are employed) compared to chemical polymerisation [66]. However, electrochemically prepared PANI films are highly porous and thus have poor mechanical properties which limit their usefulness [71]. Also, the incorporation of expensive metals in electrochemical polymerisation increases the fabrication cost. In contrast, chemical oxidative polymerisation has the advantage of producing PANI on a large scale at a cheaper price which can compete with electrochemical polymerisation [4, 71, 73]. It is considered as the most feasible route for commercial production of PANI and will also be used in this project.

For chemical oxidative polymerisation, PANI is synthesised through the oxidation of the respective aniline monomers in acidic solution (pH≤3). Widely used chemical oxidizing agents include aqueous ammonium persulfate ($(NH_4)_2S_2O_8$, APS), $FeCl_3$, H_2O_2-$FeSO_4$, H_2O_2-Fe, $K_2Cr_2O_7$, $KMnO_4$, $KClO_3$, $KBrO_3$ and KIO_3, *etc*. The protonated ES is obtained as the reaction product, which is conductive with a dark green colour [4].

Fig. 2-10 displays the chemical polymerisation mechanism of aniline under acidic conditions. The preparation of PANI is represented by a consecutive reaction of chain growth. In the initial stage, the aniline is protonated and produces corresponding radical cations. In the second step, coupling of N- and para-radical cations occurs and then undergoes rearomatisation of the dication of p-aminoo-diphenylamine (PADPA). Subsequently PADPA is oxidised to form the diradical dication forms [71]. The initial PANI product has been confirmed to be the fully oxidised pernigraniline salt intermediate and the synthesis then proceeds by the subsequent chain propagation. When all oxidant is consumed, the remaining aniline in solution reduces the protonated pernigraniline intermediate to form the

final product, the green ES. Although more than 95% of constitutional aniline units are coupled with "head-to-tail" (i.e., N-para) position, a small fraction of molecules linked in the ortho-coupling way also occur, leading to defects in the polymer conjugation structure [71, 74].

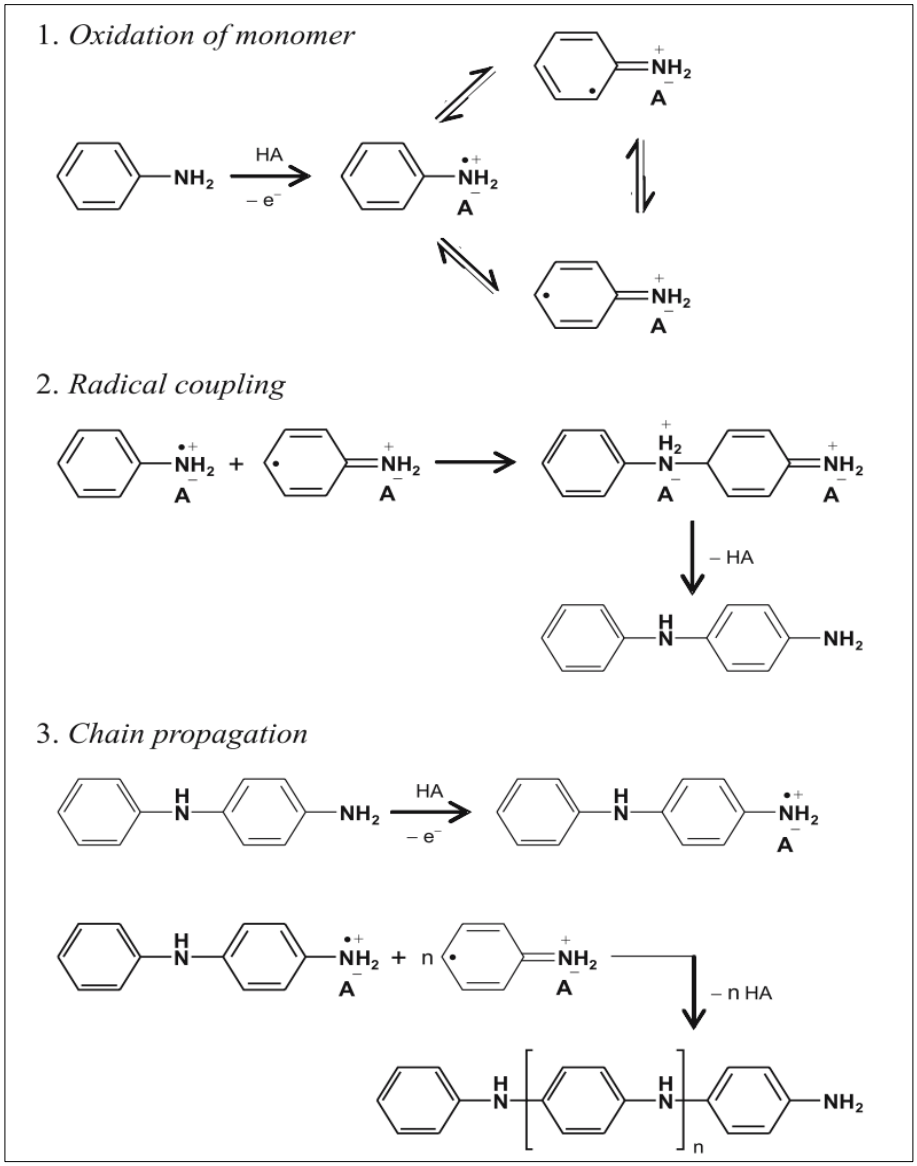

Fig. 2-10 Chemical polymerisation mechanism of aniline [75].

2.3.3 Parameters in Chemical Polymerisation

In the case of chemical polymerisation of PANI, the product properties depend on the polymerisation parameters such as the nature of the acid, chemical oxidants, reaction temperature, the molar proportions of aniline and oxidant [73, 74, 76, 77]. One crucial task of this project is to explore the influence of reaction parameters on the

PANI properties and further link the effect of parameters to the final PANI membrane properties.

Polymerisation temperature is an essential factor which affects the mechanical, chemical and electrical properties of PANI. A lower synthesis temperature favours producing PANI with higher MW and more regular molecular structure than a higher temperature [78-80]. This has led to the synthesis of PANI that has higher mechanical strength with fewer defects and membranes with more interlinked structures [81-83]. Previous studies in the Patterson research group has found that the average MW of PANI synthesised at 15°C and 24°C was 292,347 and 237,301 g mol^{-1} measured by gel permeation chromatography (GPC) - size exclusion chromatography (SEC) method, respectively [6]. In combination with literature, these all suggested that a lower temperature is favourable for the formation of PANI with a higher MW and chain regularity.

The relation between polymerisation temperatures and conductivity, however, is still ambiguous. Ohtani *et al*. and Lee *et al*. claimed that decreasing polymerisation temperature was accompanied by an increased conductivity, while Boara *et al*. found that PANI product with high conductivity could be obtained even at 60°C by optimising the reaction conditions [84-86]. Some studies observed that the conductivity was independent of the polymerisation temperatures [77, 79, 85, 87].

Optimising the PANI polymerisation temperature is key to form optimal PANI polymer, thereby enabling the fabrication of high performance (in terms of tuneability, mechanical robustness and membrane separations) electrically tuneable PANI membranes. Consequently, it is necessary to conduct a critical evaluation on the effect of polymerisation temperatures on the PANI polymer and PANI membrane properties and this research will focus on this and explore the optimisation of the polymerisation temperature to make electrically tuneable PANI membranes a reality.

The acid dopants employed in the aniline polymerisation have been reported to significantly affect the physicochemical properties of PANI products. A wide variety of acids, ranging from mineral acids, organic acids to polymer acids, have been used as dopants for PANI. Small molecular dopants like HCl have the disadvantage of leaching out from PANI, leading to the dedoping of PANI and

decreased conductivity [11]. Polymer acids have the potential to overcome these problems thus improving the long-term chemical stability [4, 10, 11, 73, 76, 88]. This project will incorporate polymer acids into the PANI structure and make more stable acid doped membranes, and the following literature review in Section 2.4.4 will focus on different kinds of polymer acids.

A large range of chemical oxidants have been successfully used in the aniline polymerisation. Previous studies showed there was no obvious correlation between the redox potential of the oxidizing agent and the properties of PANI [73, 76]. $FeCl_3$ enables aniline polymerisation to be carried out in a polar organic solvent [71]. H_2O_2 oxidation of aniline results in low polymerisation yield, but the addition of Fe^{2+} gives a high conversion of polymer products [89]. KIO_3 and $K_2Cr_2O_7$ are found be convenient oxidising agents for the chemical polymerisation of PANI [76]. Among them, $(NH_4)_2S_2O_8$ is reported to be the most widely employed oxidant to initiate the nucleation and growth of PANI [13]. Therefore, APS will be chosen as the chemical oxidant for the PANI synthesis in this project.

2.4 Polyaniline Based Membranes

2.4.1 Preparation of PANI Membranes

Various membrane formation techniques have been used for the preparation of PANI based membranes, such as phase inversion, diffusion cell polymerisation, coating composite polymerisation, electrochemical polymerisation and radiochemical graft polymerisation [66, 81, 90-101]. Among them, some techniques still remain a challenge for the successful and industrially scalable PANI membrane production. In terms of electrochemical polymerisation, the incorporation of expensive metals to allow the deposition of polymer onto the backing support will considerably increase the production cost [102]. In the case of radiochemical graft polymerisation, high energy irradiation grafting would likely deteriorate the bulk properties of the materials [103]. Considering the large scale of application and operational feasibility, phase inversion is the most economical way to produce PANI membranes and will be employed in this project.

Phase inversion, which was originally developed by Loeb and Sourirajan in the 1960s, involves changing of a cast polymeric solution into two separated phases: a solid polymer-rich phase forming a membrane dense skin layer and a liquid

polymer-lean phase forming a membrane porous sublayer [104]. It is a result of the interplay of mass transfer and phase separation. Phase inversion via immersion precipitation, namely non-solvent induced phase separation (NIPS), is the most popular employed method due to its potential to form many membrane morphologies. Typically, a flat phase inversion membrane is prepared by casting a polymer solution to a supporting layer and then immersed in a non-solvent coagulation bath. The polymer is transformed to a solid film due to the exchange of solvent and non-solvent [105]. This research will focus on the synthesis of an integrally skinned asymmetric membrane by the NIPS method.

During the fabrication of phase inversion membranes, there are some parameters controlling the properties of the membrane produced, such as casting solution concentration, choice of solvent, choice of additives, membrane support materials, evaporation conditions, casting speed, membrane thickness, crosslinking treatment, *etc.* [7, 88, 92, 93, 106-112]. Rohani *et al*. in the Patterson research group gave a systematic investigation on the effect of aforementioned parameters on the PANI membrane properties [6]. The optimum preparation parameters have been found to obtain a proof of concept tuneable small acid doped PANI membrane. Addition of co-solvent was found to produce a potentially good membrane with a thinner and denser skin layer [6]. This research work will continue the previous work and co-solvent will be used to adjust membranes in the UF and NF range. In terms of this work to make electrically tuneable PANI membranes, conducting particles will also be considered to make the membranes more conductive. Therefore the following lierature review will focus on these parts.

2.4.2 Co-solvent Addition

It is known that the use of a volatile co-solvent in the polymer solution can cause a change in the fabricated membrane morphology and performance [105, 113]. Addition of co-solvents can alter the instantaneous demixing behaviour, trigger the formation of a skin layer and change the membrane morphology from finger-like voids to sponge-like microstructures [114, 115]. Some highly volatile solvents, such as THF, acetone, dioxane, can be used as co-solvents [116, 117]. The highly volatile solvent can evaporate rapidly from the outermost membrane surface prior to immersion into the non-solvent bath, improving the local polymer concentration in the casting solution [114]. This results in the formation of denser skin layers with

few pores or defects, leading to lower membrane permeance and higher solute rejection.

The evaporation time plays a crucial role in influencing the loss of volatile co-solvents, thereby affecting the local polymer concentration in the casting solution. Generally, a longer evaporation time results in a thicker skin layer with decreased surface porosity while a shorter evaporation time leads to a thinner skin layer with increased surface porosity [118]. During the evaporation step, the skin layer formed at longer evaporation time exhibits more resistance between the coagulation bath and bulk of membranes. As a result, it is more difficult for the in-diffusion of non-solvent and out-diffusion of solvent, thereby delaying the demixing process and affecting the final membrane morphology and performance. Taking these into account, co-solvents will be employed in this research and the influence of evaporation time will also be studied to determine whether the membrane structure can be tightened.

2.4.3 Conducting Particles Incorporation

Various carbon materials, such as activated carbon (AC), carbon nanotubes (CNTs), graphite and graphene, have been investigated to incorporate into the PANI matrix via different processing techniques, in particular chemical polymerisation and solution mixing [119, 120]. In-situ polymerisation of aniline in the presence of carbon materials is the most frequent way. It has been found that aniline can functionalise and solubilise carbon materials via the formation of donor-acceptor complexes. The carbon materials serve as conductive bridges connecting PANI conducting domains and increase the charge transfer mobility, resulting in an enhanced conductivity [121, 122]. Solution mixing, where polymer chains adhere to carbon material through the Van der Waals forces, can also improve the conductivity by intercalating PANI into the interlayer spaces of conducting particles [122]. Table 2-2 presents the conductivity of PANI composites with the most common used conducting particles including AC, CNTs, graphite and graphene.

Activated carbon is an amorphous carbon-based material with outstanding porous structure, high surface area and good electrical conductivity. It has been reported that incorporation of AC into PANI could enhance the electrical conductivity as

well as thermal stability of the composite. This can be considered as the most economical way to synthesise a PANI/carbon complex [123-125]. On the other hand, the carbon networks in AC are less extensive as those in graphite and CNTs, leading to the disordered crystallinity with reduced conductivity than other advanced carbon materials [126].

Graphite is a layered carbon material with higher electrical conductivity (>100 S/cm) than activated carbon and a lower price than carbon nanotubes [127, 128]. It has been found that the graphite/PANI composites exhibited greater conductivities than those of graphite or PANI alone [129]. However, it is difficult to prepare conductive PANI/graphite complexes by direct intercalation due to the small interspacing of the graphite layers. Therefore, chemical modification by H_2O_2-H_2SO_4 method is generally employed to form expandable graphite, which can intercalate aniline monomer or PANI polymers into the pores of the graphite sheet [129, 130].

CNTs, including multi-wall carbon nanotubes (MWNT) and single-wall carbon nanotubes (SWNT), are hexagonal networks of carbon atoms with each end capped with half of a fullerene molecule [119, 131]. CNTs have a narrow distribution size, excellent electrical and thermal conductivity, and show high stability and mechanical strength [132]. The CNTs used should be pre-treated by a mixture of nitric and sulfuric acids, which can convert a hydrophobic CNT to a hydrophilic one by the incorporation of acid functionalities [133]. It has been reported that the incorporation of CNTs into a PANI matrix could enhance the electrical conductivity as well as the mechanical properties of the PANI/CNTs complex [109, 134]. Currently, the high cost is the major obstacle to restrict the large scale application of CNTs [119].

Graphene, a two-dimensional material with carbon atoms arranged in a regular hexagonal pattern, has excellent electron mobility, large specific surface area, extraordinary mechanical strength and potentially low manufacturing cost. This is comparable with, or even better than, CNTs [111, 135, 136]. In most of the previous studies, graphene nanosheets or graphene oxide (GO) are used as starting materials during the in-situ polymerisation of the aniline monomer [135, 137, 138]. It has been proven that PANI and graphene can form synergistic interfacial interactions to enhance the charge transfer of the complex, resulting in improvement of the

electrical conductivity. Unfortunately, graphene nanosheets tend to agglomerate and affect the dispersal extent within the polymer matrix, limiting their usefulness for the synthesis of a conductive complex [111, 135]. GO, with hydroxyl and carboxyl groups, can disperse well to form stable dispersion, but further treatments are needed to convert the insulated GO to conducting graphene [136, 139].

In terms of this project to make conductive PANI membranes, EG will be chosen as conducting particles and carbon nanotube and graphene will be left for future work. Two approaches, in-situ chemical polymerisation and solution mixing will be applied to incorporate EG into the PANI structures.

Table 2-2 Conductivity of PANI composites with different conducting particles by chemical polymerisation.

Conducting Particles	Chemical Polymerisation Methods	Conductivity (S cm^{-1})	Ref.
Activated carbon	In-situ polymerisation in the presence of AC powder with HCl as medium	0.21	[140]
	In-situ polymerisation in the presence of granular AC with HCl as medium	1.53	[125]
	In-situ polymerisation in the presence of AC (RP-20) with DBSA as medium	——	[141]
	In-situ polymerisation in the presence of AC (20 nm) with p-toluenesulfonic acid as medium	1.328	[124]
	Solution mixing polyaniline with AC	——	[123]
Graphite	In-situ polymerisation of aniline in the presence of exfoliated graphite obtained from 80 mesh graphite flake with HCl as medium	33.3 (1.5% graphite / 98.5% PANI)	[128, 130, 142]
	In-situ polymerisation of aniline in the presence of water dispersible colloidal graphite with different acids as medium	350 (90% graphite / 10% PANI)	[143]
	In-situ polymerisation of aniline in the presence of exfoliated graphite obtained from graphite flake with HCl as medium	880 (91% graphite / 9% PANI)	[129]
	In-situ polymerisation of aniline in the presence of graphite powder (4 um particle diameter) with methanesulfonic acid as medium	800 (96% graphite / 4% PANI)	[126]
	In-situ polymerisation of aniline in the presence of exfoliated graphite with DBSA as medium	298.51 (80% graphite / 20% aniline)	[127]
Multi-wall carbon nanotubes	In-situ polymerisation of aniline in the presence of MWNT with HCl as medium	33.3	[144]

Single-walled carbon nanotubes	In-situ polymerisation of aniline in the presence of MWNT with HCl as medium	33.37 (10% MWNT/ 90% PANI)	[132]
	In-situ polymerisation of aniline in the presence of MWNT (10-20 nm) with HCl as medium	——	[145]
	In-situ polymerisation of aniline in the presence of SWNT with HCl as medium	1.26 (8 % SWNT/ 20% aniline)	[122, 134]
	In-situ polymerisation of aniline in the presence of SWNT (Length, 5-15 um; diameter＜2 nm) with HCl as medium	——	[146]
Graphene	In-situ polymerisation of aniline in the presence of graphene sheet with HCl as medium	——	[137]
	In-situ polymerisation of aniline in the presence of graphene oxide with HCl as medium and then reduction and reoxidation- redoping	——	[135]
	In-situ polymerisation of aniline in the presence of graphene oxide with HCl as medium and then reduction-dedoping and redoping	——	[138]
	Solution mixing of chemically converted graphene (CCG) and PANI	5.5 (44% CCG/ 56% PANI)	[136]
	Disperse GO in sulphated polyaniline and then reduction	0.3	[147]

2.4.4 Doping of PANI Membranes

A wide variety of acids, ranging from mineral acids to organic acids, have been used as dopants of PANI. PANI is typically doped with strong mineral acids such as HCl, HBr, HNO_3, H_2SO_4 and H_3PO_4 [148, 149]. The major issue with these small molecular acids is their poor solubility in common solvents so the final materials cannot be feasibly processed. Moreover, these small acid dopants are prone to volatilise, leading to the dedoping of PANI drastically and severely limiting the utility in real membrane systems [11, 70]. Compared to the conventional small acids dopants, the polymer acids as large dopants offer many advantages: (1) the polymer acids are not volatile and eliminate the problem of volatility and diffusivity [88]; (2) polymer acids can form a double strand structure (Fig. 2-11) with PANI by the strong interaction between acid groups and imine nitrogen [14]. The molecular association avoids the dopants leaching and significantly improves the chemical stability of the conducting PANI [8, 11]; (3) the use of such polymer acids dopants results in rubbery behaviour of the composites and greatly enhances the mechanical properties of conducting polyaniline (i.e. makes them less brittle) [9, 14]. In addition, the presence of such macromolecules within the conducting polymers forms different structures and morphologies from small acid doped PANI, which can bring improved properties (such as a wide range of solubility, improved processibility) as well as additional functionalities to the resulting materials [14, 150, 151].

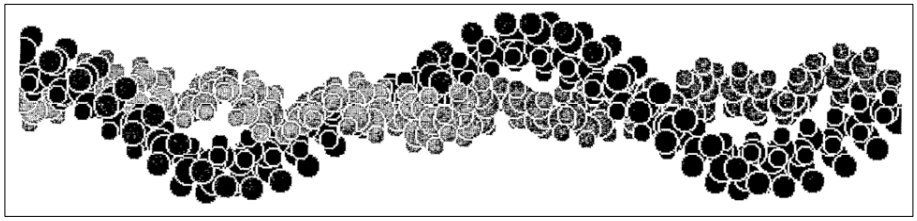

Fig. 2-11 A double strand model for binding between PANI and polymer acids [14].

The polymer acids that have been used as dopants for PANI include poly(2-acrylamido-2-methyl-1-propanesulfonic acid) (PAMPSA) [152, 153], poly(acrylic acid) [8, 13, 108], poly(methyl vinyl ether-alt-maleic acid) (PMVEA) [10], poly(styrenesulfonic acid) (PSSA) [9, 16], poly(amic acid) [15, 154, 155], poly(vinylphosphonic acid) (PVA) [156, 157], polyamidosulfonic acids [152, 158]. Table 2-3 displays the acid dopants used for the PANI and other polymers.

Table 2-3 Summary of acid dopants.

Dopants	Acids-PANI	Solubility (water)	Conductivity ($S\ cm^{-1}$)	Ref
Mineral acid	HR (R means halogen)- PANI	+	1-5	[148]
	H_3PO_4- PANI	+	58	[84]
	Selenious acid- PANI	+	0.02--0.0003	[159]
	Camphorsulfonic acid- PANI	+	200-400 (m-cresol)	[160]
	dodecylbenzene sulfonic acid- PANI	+	100-250	[161]
Organic acid	4-(4-Hydroxy-2-methyl-phenylazo) benzenesulfonic acid- PANI	-	0.05-0.06	[162]
	4-(4-Hydroxy-biphenyl-3-ylazo)-benzenesulfonic acid- PANI	-	0.02-0.05	[162]
	4-[4-hydroxy-2-((Z)-pentadec-8-enyl) phenylazo] benzenesulfonic acid- PANI	+	10^{-2}-10^{-3}	[163]
	Pyrenesulfonic acid- PPy	+	————	[164]
	Esters of 5-sulfo-i-phthalic acid- PANI	+	85 (DCA as solvent)	[165]
	Sulfonic acid of 3-penradecyphenol- PANI	+	0.45-0.60	[166]
	Sulfonic acid of 3-pebtadecylanisole- PANI	+	1.84-2.50	[166]
	Sulfonic acid of 3-pentadecylphenoxy acetic acid- PANI	+	3.30-6.62	[166]

Polymer acid	Poly(acrylic acid)- PANI	+	10^{-3}-10^{-4}	[8, 150]
	Poly(amic acid)- PANI	+	10^{-5}	[154]
	Poly(styrenesulfonic acid)- PANI	+	2-3	[16]
	Poly(2-acrylamido-2-methyl-1-propanesulfonic acid)- PANI	+	0.4-1.1	[153]
	Poly(vinylphosphonic acid)- PANI	+	10^{-2}-10^{-1}	[156, 167]
	Poly(alkylene phosphate)- PANI	+	------	[168, 169]
	Poly(methyl vinyl ether-alt-maleic acid)- PANI	+	3.5×10^{-3}-2.1×10^{-2}	[170]
	Phosphoric acid- PBI (Polybenzinidazole)	+	0.01 (25℃)-0.26 (200℃)	[171]
	Polyglutamic acid- PPy	+	------	[172]
	Poly[2-(3'-thienyl) ethanesulfonic acid]- PVA	+	8×10^{-5} (0.05 molar ratio PVA)	[173]

It is notable that the chemical structure of the polymer acids affect the morphology of the PANI product and the doping efficiency of acid groups on the polymer chains. M. Angelopoulos *et al*. reported that the doping of PANI membrane with poly(amic acid) could be limited due to the geometric constraints of the large rigid acid backbone, leading to decreased conductivity [154]. Zhang *et al*. also reported that compared with the benzene sulfonic group of PSSA and the multiple carboxylic acid groups of PMVEA, PAAc with the smaller size of the acrylic acid group can be easily incorporated as a dopant into PANI and exhibited a relatively higher doping level [10]. Alexander *et al*. found that the rigidity of the poly(amidosulfonic acids) matrix backbone played an important role in the electronic structure of the interpolymer complexes. The flexible-chain polymer acid could adjust its conformation to the rigid chain of PANI while the rigid chain of PANI, in turn, had to adapt its confirmation to match the structure of polymer acid, forming a double-strand structure or brush-type structure [152, 158].

Due to the conformational hindrance created by the polymer chain, it is expected that not all the polymer acids are capable of doping PANI. To date, the polymer acids with carboxylic acid groups and sulfonic acid groups are the most popular used dopants for PANI. This study will choose polymer acids with these acid groups but different molecular structures to determine their ability to incorporate into PANI structures and then effects on the produced PANI systems.

The aforementioned polymer acids can be incorporated into PANI structure by different ways such as chemical oxidation, electrochemical polymerisation and enzymatic synthesis [152, 153, 156, 158]. Among them, chemical oxidation is one of the most common ways due to its simplicity and low cost [174, 175]. This approach involved binding of aniline monomer into polymer acids templates by interactions such as columbic attraction and hydrogen bonding, and then polymerising anilinium cations on the acids templates to obtain polymer acids doped PANI complex. This way ensured the large size of polymer acid dopants entrapped with polyaniline [10, 153, 176].

Based on this, one promising approach to prepare polymer acid doped membranes is to directly use the above mentioned polymer acids doped PANI (PANI-PA) complex as membrane materials. Previous studies also demonstrated some others ways to prepare acids doped membranes, such as blending undoped PANI powder

(PANI-EB) with acids before membrane fabrication, adding acids in the casting solution during membrane preparation, secondary doping with acids after membrane preparation, *etc.* [8, 85, 92-94, 108, 150]. In comparison to blending undoped PANI powder with acids and secondary doping, the new approach could eliminate the subsequent processing steps to dedope acid doped PANI (PANI-ES) by ammonia and then redope PANI-EB by the desired acids. Adding acids in the casting solution generally resulted in a random polymer packing due to the confirmation freedom of both large polymer chains [176]. This new method however, is expected to grow polyaniline along the acid templates and form confined structures in an ordered packing. Therefore, the new method will be used in this study to make polymer acid doped membranes.

Furthermore, the proton doping level is an important factor which influences the conductivity of PANI. The highest achievable conductivity occurs when the EB form (50% oxidised with alternative benzenoid and quinoid rings) is 50% doped by acids, leading to the protonation of the whole quinoid rings as well as the formation of a perfect polaron. At a doping degree beyond 50%, some amine sites are protonated and bipolarons may also form, thereby reducing the polymer conductivity. The doping level lower than 50% will result in inadequate protonation of some imine sites [71]. Therefore, it is necessary to control the proton doping level to achieve high membrane conductivities. It also needs to be mentioned that the conductivity of polymer acid doped PANI is lower than the small acid doped PANI, indicating that some work like secondary doping still needs to be done to further improve the conductivity.

2.4.5 Applications of PANI Membranes

The wide utilisation of conducting polymers in membrane separation processes is mainly due to their high electrical conductivity, electrochemical activity and switchability between various oxidation and doping states [157]. PANI, as one of the most attractive conducting polymers, has distinct advantages in membrane separation because of the pH dependent protonation/deprotonation in addition to the common electrochemical oxidation-reduction switchability.

Initially, interest in PANI as a membrane material stemmed from the research work by Anderson *et al*., where the authors reported that an excellent permselectivity

towards gases was achieved by PANI membranes [148, 149]. The effective free volume of these PANI membranes enabled to be tuned by the doping and dedoping process. Therefore, a high selectivity towards gas mixtures could be obtained by a controlled doping, dedoping and redoping process [148, 149, 177].

After this, PANI has been used to prepare a range of different membranes including pervaporation membranes, proton-exchange membranes and organic solvent nanofiltration membranes [7, 92, 94, 107, 178-180]. In terms of PANI membranes in pervaporation, PANI displayed superior stability in aprotic solvents and can be used in the dehydration of aggressive solvents [81, 108]. For PANI membranes in electrodialysis, the presence of an electroactive PANI layer at the surface of commercial proton-exchange membranes led to an improved selectivity for specific ion transport [107, 180, 181]. In the case of PANI membranes employed in organic solvent nanofiltration, acid dopants acted as soft templates, introducing nanoporosity into the membane structure. After extracting the acid counterion by alkaline, small solvent molecules can pass through the expanded free volume [7, 92, 94].

Furthermore, PANI is employed to modify polysulfone UF membranes by forming a PANI nanofiber layer on the PS membrane surface. It was found that the PANI modified nanocomposite membrane exhibited a much better antifouling performance than the substrate membrane due to the hydrophilicity and steric hindrance effect of the PANI nanofiber layer [98].

2.4.6 Evidence of Stimuli-responsive PANI Membranes

The tuneability of PANI makes it a promising candidate membrane material in numerous applications like sensors, actuators, electrochromic displays and membrane separations. Table 2-4 summarises the tuneable properties and possible applications of PANI membranes. It can be seen that PANI with various tuneability is a promising material for use in responsive membranes. Considering one of the research aims is to develop stimuli-responsive composite membranes for fouling control, it could be great interest to choose PANI as a tuneable membrane material. Based on the conductive properties of PANI and fast response speed requirements of external stimuli, electrical potential will be considered to work as external

stimulus. The effect of electric stimulus on the fouling removal of conductive PANI membrane will also be explored.

Table 2-4 Tuneable properties of PANI-initial proof of stimuli-responsive PANI membrane.

Tuneable properties	Findings	Possible applications
Electrical conductivity	Adjusting the solution pH (≤3) results in protonated PANI which displays electrical conductivity [182]. Dopant type and doping degree influence the electrical conductivity of PANI. At a perfect EB form, the electrical conductivity increases with the increased doping degree, 50% doping displays the highest conductivity. With the degree of doping beyond 50%, the conductivity decreases due to the formation of bipolarons [66]. Changing the oxidation state chemically or electrochemically affects the electrical conductivity. The 50% oxidised with 50% doping is expected to show high conductivity [184]. The electrical conductivity can be significantly improved by integrating PANI with electro-active materials such as metals, metalloid, carbon nanomaterial (EG, CNT, graphene), due to the enhanced carrier mobility and charge transfer in the chain structure [109, 120].	sensors, batteries , actuators, Electrostatic discharge materials, supercapacitors [183]
Morphology and surface charge change	Protonation–deprotonation and oxidation-reduction processes affect the membrane morphology at a molecular level, leading to the selective transport of gas [148] and neutral solution species [56, 108]. Membrane surface charge can also be changed by doping and redox processes, resulting in a selective transport of ions [107].	Smart membrane separation, (gas, ion and neutral solute) and ion-exchange materials [66]
Electrochromisim	PANI exhibits colour change (white-yellow-green-blue-violet) depending on both pH via protonation-deprotonation and the oxidation state via oxidation-reduction process [185].	Electrochromic displays, pH indicators, polymer light emitting diodes [183]

2.5 Implications of the Literature

The above literature review illustrates the tuneable properties of conducting polymer PANI membranes adjusted by doping/dedoping in the conjugated carbon backbone to change the free volume within the membrane. Going beyond this current understanding, this work hypotheses that if a PANI membrane is used under electrical stimulation, there are several possible ways (including this) that flux and selectivity can be changed which will be able to effect a change in separation (selectivity and permeance) for electrically neutral molecules as well as the more commonly studied charged species:

- Membrane charge can change $\longrightarrow$ Donnan exclusion changes
- PANI is piezoelectric (as above) $\longrightarrow$ Pore size and/or free volume changes
- Electrical filed developed $\longrightarrow$ Molecular interaction changes
- Polymer properties change $\longrightarrow$ Solution diffusion through membrane changes

Conventional membranes cannot change their selectivity and pore size in a simple in-situ method to overcome membrane fouling. In reactors incorporating membrane separation, membrane fouling is a serious problem which limits production rate and effluent quality. There is a gap in the literature to incorporate a conducting PANI membrane into a reactor system, ultimately achieving in-situ control for membrane fouling (as well as any species in the permeate/reactor product stream). To achieve this, it is necessary to produce a tuneable PANI membrane reactor which can be tuned to different pore size and molecular selectivity via an external potential.

In a tuneable membrane reactor, foulants will be pushed through and off the membrane by changing the pore size and surface charge. If the foulant is an enzyme, this will allow it to be recovered, saving money and resources. In particular, if pore size can be changed, then irreversible fouling could be overcome, removing a fundamental barrier to continuous membrane reactor adoption. Furthermore, if the conventional membrane becomes fouled with an enzyme or other foulant molecules and/or feed, the flux will decrease and the selectivity will change. A tuneable membrane can be regulated to keep the same flux and selectivity overtime, resolving this problem. Changing MWCO and charge in the PANI membranes could also be used to periodically remove fouling altogether. Conversely, if the fouling layer is key to a high reaction rate, the catalyst film layer

thickness can be controlled using a tuneable membrane. To do this, a robust and functional tuneable membrane must be produced. The PANI membrane appears to be a very promising option for this.

Currently, three main challenges exist for PANI membranes:

- Membranes doped by small acids such as HCl are brittle and severely limit the utility in real membrane systems.
- Small acid dopants are prone to leach during filtration, leading to the dedoping of PANI drastically.
- Doped membranes are often poorly conductive.

Many studies have discussed the limitations of the state-of-the-art in PANI tuneable membranes and some proposed to use polymer acid in the casting solution to fabricate polymer acid doped membrane, but few studies solve these problems by incorporating the long chain acid into the PANI from the very beginning, potentially strongly binding the acid to the PANI structure during the polymerisation for PANI synthesis. Moreover, applying an electrical potential to a doped PANI membrane produces electron flow to change the membrane free volume due to the incorporation or expulsion of ions from the dopant site. Membranes with tuneable selectivity and permeability could be produced and the transport properties can be predictably controlled in-situ using external potential. Therefore, a systematic research study is required to determine the best conditions and species to use to polymerise different polymer acids into the PANI structure and prepare polymer acid doped membrane and then control the membrane selectivity and permeability in-situ by externally applied potential.

3 Aims and Objectives

As stated in Chapter 1, the overall aim of this research is to develop unique conducting PANI membranes that can be electrically tuneable to different fluxes and selectivity. The target application is in a membrane reactor, where the primary aim of the new generated tuneable membrane is to allow the fouling layer to be pushed off/through membrane by external potential.

Based on past literature precedents and the gaps in the literature, the specific objectives of this project are:

- Investigate the influence of T_{poly} on in-filtration electrical tuneability of small acid doped PANI membranes;
- Improve the filtration stability and mechanical properties of acid doped PANI membranes by incorporating the PAs (mainly PAMPSA) into the PANI structure;
- Enhance the electrical conductivity of PAMPSA doped PANI membrane (Memb-PAMPSA) by incorporating EG and secondary doping treatment with DBSA;
- Examine suitable methods for decreasing the MWCO of Memb-PAMPSA;
- Evaluate the membrane in-situ fouling removal ability using external stimuli;
- Develop a higher resolution one-filtration MWCO method for NF/low UF range membranes using electrically neutral molecules for use in determining MWCO changes of electrically connected PANI membranes.

In order to fulfil these objectives, a technical route has been formulated in Fig. 3-1.

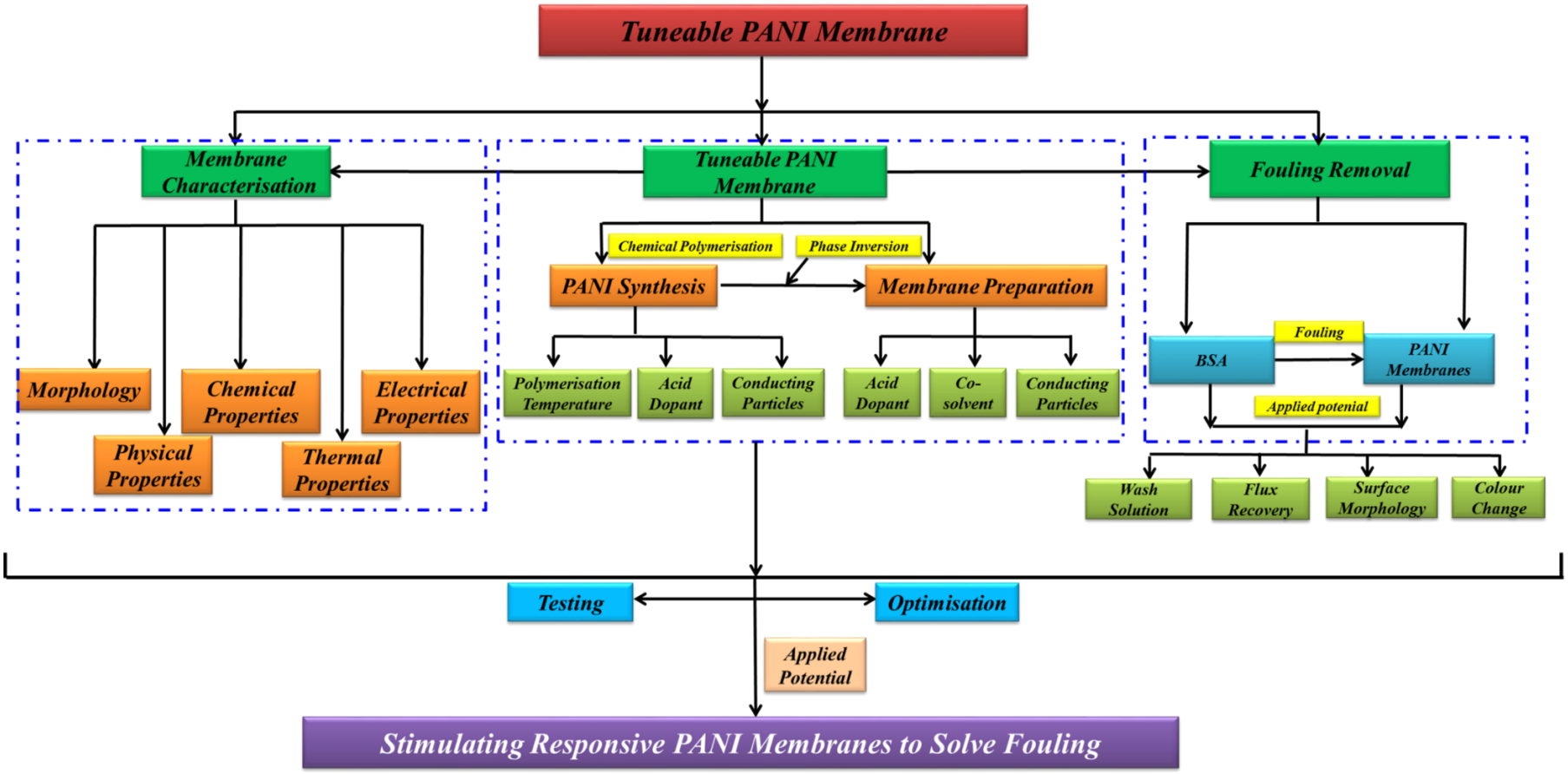

Fig. 3-1 Technical route.

4 Materials and Methods

4.1 Materials

Aniline, ammonium persulfate, hydrochloric acid, acetonitrile (HPLC grade), tetrahydrofuran, N-methyl-2-pyrrolidone, 4-methyl piperidine, poly(acrylic acid) (MW=450,000 g mol^{-1}, powder), poly(styrenesulfonic acid) (MW=75,000 g mol^{-1}, 18 wt% in water), poly(methyl vinyl ether-alt-maleic acid) (MW=80,000 g mol^{-1}, powder), rose Bengal (dye content 95%), DBSA and fluorescein isothiocyanate (FTIC) were purchased from Sigma-Aldrich (UK). Ammonia solution, methanol, poly(2-acrylamido-2-methyl-1-propanesulfonic acid) (MW=800,000 g mol^{-1}, 10 wt% in water), hydrogen peroxide (H_2O_2, 30 wt% solution in water), sulfuric acid (H_2SO_4, 96% solution in water) and isopropanol were obtained from Fisher (UK). Graphite powder (2-15 μm) was purchased from Alfa Aesar (UK). Polyethylene/polypropylene mixture backing layer − Novatexx 2431 (140 μm) was supplied by Freudenberg Filter (Germany). All solutions were prepared with DI water produced from an ELGA deioniser (PURELAB Option).

Table 4-1 displays the commercial PEG and purer PEG standard obtained from different companies. Commercial grade PEGs (PEG 1000, 1500, 2000, 4000 and 6000) were purchased from Alfa Aesar (UK). A purer grade PEG 1000 standard was purchased from Fluka (Switzerland). Commercial grade PEG 3000 was obtained from EMD Millipore (UK). The properties of commercial membranes are provided in Table 4-2. GE Osmonics™ (GE, GK, GH) and TriSep UA60 were purchased from Sterlitech (US). The Millipore disk membranes (Ultracel PLAC04310, Ultracel PLBC04310) were purchased from Sigma-Aldrich (UK). GE Osmonics™ GE and Millipore Ultracel PLAC04310 are NF membranes while GE Osmonics™ GH, GE Osmonics™ GK, TriSep UA60 and Millipore Ultracel PLBC04310 are UF membranes.

Table 4-1 Supplier and MW of the commercial grade PEGs and purer grade PEG standard used.

Chemical	Supplier	MW (g mol^{-1})
PEG 1000 (Commercial grade)	Alfa Aesar	950-1050
PEG 1000 (Purer grade)	Fluka	950-1050
PEG 1500 (Commercial grade)	Alfa Aesar	1450-1500
PEG 2000 (Commercial grade)	Alfa Aesar	1800-2200
PEG 3000 (Commercial grade)	EMD Millipore	3000
PEG 4000 (Commercial grade)	Alfa Aesar	3600-4400
PEG 6000 (Commercial grade)	Alfa Aesar	5400-6600

Table 4-2 Characteristics of the commercial membranes used to benchmark the new PEG MWCO technique.

Membranes	Nominal MWCO range (g·mol^{-1})	Membrane materials	Type
GE Osmonics™ GE	1000 [186, 187]	Composite Polyamide	NF
GE Osmonics™ GH	1000-2500 [186, 188-190]	Thin Film	UF
GE Osmonics™ GK	2000-3500 [186, 188, 189, 191]	Thin Film	UF
TriSep UA60	1000-3500 [192]	Polypiperazine-amide	UF
Millipore Ultracel PLAC04310	1000 [193]	PLAC cellulosic (regenerated cellulose)	NF
Millipore Ultracel PLBC04310	1000-3000* [194, 195]	PLBC cellulosic (regenerated cellulose)	UF

4.2 Chemical Oxidation Polymerisation of PANI-EB

Fig. 4-1 shows the setup used for the synthesis (chemical polymerisation) of PANI. 18.23 mL of aniline was dissolved in 200.0 mL of HCl solution (1.0 M). In a separate reagent bottle, 45.63 g of oxidant agent APS was dissolved in 128.0 mL of HCl solution (1.0 M), then the APS was slowly added into aniline solution by peristaltic pump (20 mL h^{-1}) for about 8 h to have a proper control of the polymerisation reaction and the total reaction time was 24 h [6]. T_{poly} were set at 5°C, 15°C and 25°C, respectively.

PANI is non-conductive unless doped with acids − the anions of dopants incorporated into PANI can be electrostatically attracted to the doped nitrogen on the PANI backbone to produce the conductive form of PANI [196]. The prepared emeraldine salt PANI-ES (note that this nomenclature indicates that PANI is in the

acid doped state) was filtered and intensively washed with six successive 250 mL DI water (6× 250 mL) to remove unreacted chemicals. Subsequently, the obtained powder was stirred in a 250 mL of aqueous ammonia solution (33.3%, w/v) for about 12 h to deprotonate PANI-ES.

The PANI-EB (note that this nomenclature indicates that PANI is in the undoped state) containing ammonia solution was then re-washed with DI water (3× 500 mL) to remove the excess ammonia, and then with methanol (3× 250 mL) to remove the PANI oligomers. The polymer was dried in a vacuum oven at 60°C for 24 h. Finally, non-conductive powder was ground in a mortar and pestle to generate a fine purple-bronze PANI-EB product. The PANI powder synthesised at 5°C, 15°C and 25°C will be denoted as PANI-EB-5, PANI-EB-15 and PANI-EB-25 in the paper, where the number indicates T_{poly}, respectively.

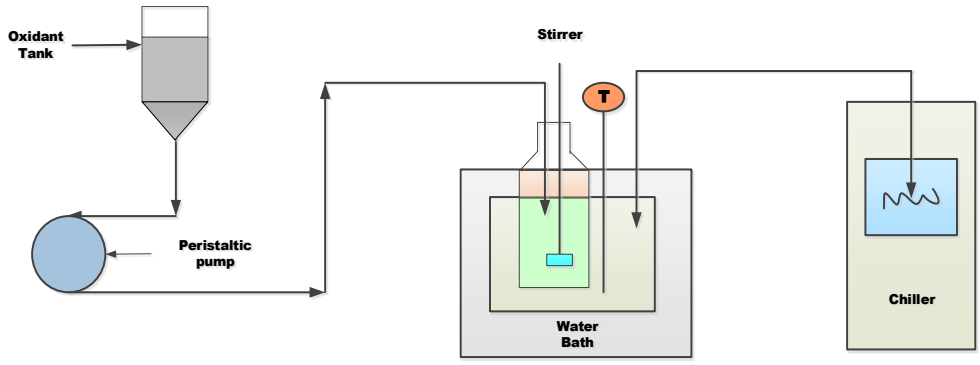

Fig. 4-1 Setup for chemical polymerisation of aniline.

4.3 Chemical Oxidation Polymerisation of PANI-PA

The setup in Fig. 4-1 was also used for PANI-PA preparation. Aniline, at 4:1 monomer to acid repeat unit molar ratio, was dissolved in the polymer acid solution namely PAMPSA, PSSA, PAAc and PMVEA (0.1 M). In a separate reagent bottle, oxidant agent APS (at 1:1 molar ratio to aniline monomer) was dissolved in water. The difference between PANI-EB and PANI-PA synthesis was that HCl used to dissolve aniline and APS was replaced by polymer acid solution and water, respectively. The polymerisation temperature was controlled at 15°C and the reaction time was 24 h. The reactant product was washed with 6× 250 mL of DI water and 3× 250 mL of acetone, and then dried in a vacuum oven at 60°C for 24 h. The obtained powder was ground in a mortar to give a fine black green PANI-PA product.

4.4 Preparation of Exfoliated Graphite

The exfoliated graphite was prepared using $H_2O_2 - H_2SO_4$ methods, following the process reported in the literature [129, 142]. The graphite powder was added to the concentrated sulfonic acid and stirred until well dispersed, and then H_2O_2 was added into the mixture followed by stirring for 2 h. The as-treated graphite was then washed with DI water until the pH of the filtrate reached 6 and subsequently dried at 100℃ for 24 h. After that, the dried power was heated in a furnace at 700℃ for 2 min. The graphite worm was then dispersed in a 50 wt% isopropyl alcohol solution and sonicated for 2 h, subsequently washed with DI water and dried under vacuum at 60℃ for 24 h.

4.5 Small Acid Doped PANI Membrane Fabrication

The membranes were prepared via NIPS at room temperature. DI water was used as the non-solvent in the coagulation bath. NMP has been recommended as the best solvent to dissolve PANI-EB for PANI membrane preparation. 4-MP showed good gel inhibiting ability for PANI membrane synthesised in NMP [6, 7, 50, 106]. Therefore, NMP and 4-MP was used in this study to prepare PANI membrane by phase inversion. PANI-EB (11.55 g, 20 wt%) was slowly added to a mixture of NMP (42.43 g) and 4-MP (3.77 g) using a funnel in small portions over 5 min. The mixture was stirred at a high mixing speed (300 rpm) for 4 h to obtain a homogeneous solution and then left overnight (12 h) to remove air bubbles.

It has been reported that some forms of aggregation or clumping could occur in PANI/NMP solution due to a strong inter-/intra-chain interaction between the PANI molecules [197-200]. Also, the degree of PANI aggregation increases with an increasing PANI concentration [198]. There is no visible aggregation or clumping in the solution in our case, so the solution was used to cast PANI-EB membranes without any other treatment.

The membrane backing layer was secured using scotch tape on a flat glass plate and the solution was added into the reservoir of the doctor blade (Elcometer 3700), then the membranes were cast to the backing layer at 250 μm casting thickness using an adjustable film applicator (Elcometer 4340 automatic film applicator, Elcometer, UK). Evaporation time of 15 s was used before immersing the casted membrane solution into a DI water coagulation bath. The membrane was kept immersed in DI water at room temperature for at least 24 h and then rinsed with

fresh water and stored in DI water for later use. The membranes prepared by PANI-EB-5, PANI-EB-15 and PANI-EB-25 were denoted as Memb-EB-5, Memb-EB-15 and Memb-EB-25, respectively. Fig. 4-2 displays the membrane preparation by NIPS method.

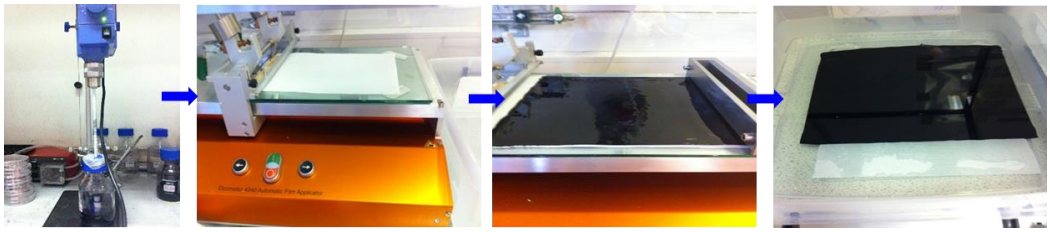

Fig. 4-2 PANI membrane preparation by non-solvent induced phase separation.

Doping of membrane was carried out in 1.0 M HCl solution since the conductivity of PANI in 1 M aqueous HCl reached an equilibrium value [182]. Doping of PANI changed the membranes colour from bronze purple to a dark green. In terms of HCl doped membrane used in Chapter 5, the membranes were initially doped for 24 h and membranes characterised at this doping time up until initial tuneability assessment using dynamic droplet penetration analysis (Section 5.3.5). However, these membranes were found to be too brittle to be used in cross-flow testing and therefore the effect of doping time was then studied and was discussed in more detail in Section 5.4.1. The Memb-EB-5, Memb-EB-15 and Memb-EB-25 doped with HCl were denoted as Memb-ES-5, Memb-ES-15 and Memb-ES-25, respectively.

4.6 Polymer Acid Doped PANI Membrane Fabrication

The above mentioned NIPS procedure (Section 4.5) was used in the preparation of polymer acid doped PANI membrane. In contrast to HCl doped membranes, polymer acid doped PANI membranes were prepared by using PANI-PA complexes as membrane materials. Unlike the PANI-EB solution in Section 4.5, some clumping occurred during the solution preparation, so the solution was heated at 80°C for 30 min to reduce the clumping of the PANI-PA complexes in NMP solutions prior to casting.

In order to tighten the PAMPSA doped PANI membrane (Memb-PAMPSA), different solvents (dimethylformamide (DMF), dimethylacetamide (DMAc)), co-solvents (THF, acetone) and evaporation times (0-120 s) were studied as detailed in **Error! Reference source not found.**.

Table 4-3 Membrane preparation conditions: casting solution composition and evaporation time.

Membrane notation	Solvent/co-solvent (mass ratio)	Gel inhibitor	Evaporation time (s)
M1	NMP	No 4-MP	---
M2	DMF	No 4-MP	---
M3	DMAc	No 4-MP	---
M4	NMP	4-MP (4-MP/PANI tetrameric repeat unit molar ratio=1.2:1)	0 s
M5	NMP/Acetone (70/30)	4-MP (4-MP/PANI tetrameric repeat unit molar ratio=1.2:1)	---
M6	NMP/THF (70/30)	4-MP (4-MP/PANI tetrameric repeat unit molar ratio=0.5:1)	---
M7	NMP/THF (70/30)	4-MP (4-MP/PANI tetrameric repeat unit molar ratio=1.2:1)	0 s
M8	NMP/THF (70/30)	4-MP (4-MP/PANI tetrameric repeat unit molar ratio=1.2:1)	10 s
M9	NMP/THF (70/30)	4-MP (4-MP/PANI tetrameric repeat unit molar ratio=1.2:1)	20 s
M10	NMP/THF (70/30)	4-MP (4-MP/PANI tetrameric repeat unit molar ratio=1.2:1)	30 s
M11	NMP/THF (70/30)	4-MP (4-MP/PANI tetrameric repeat unit molar ratio=1.2:1)	45 s
M12	NMP/THF (70/30)	4-MP (4-MP/PANI tetrameric repeat unit molar ratio=1.2:1)	60 s
M13	NMP/THF (70/30)	4-MP (4-MP/PANI tetrameric repeat unit molar ratio=1.2:1)	120 s

***** Temperature: 22-23℃; Humidity: 40-50%.

Visual defect analysis (Section 4.8.2) was used to detect defects, such as pinholes and cracks on the membrane surface. This can make sure membranes with good quality was used throughout the experiment.

4.7 Incorporating EG and DBSA into Memb-PAMPSA

Three different approaches as illustrated in Fig. 4-3 were applied to incorporate EG into Memb-PAMPSA.

Method 1 (in-situ polymerisation): involved incorporating EG in the in-situ polymerisation of aniline with PAMPSA as acid medium. Three different weight percentages of EG (25 wt%, 50 wt% and 75 wt%), with respect to aniline were used during the in-situ polymerisation of aniline, and the synthesised PANI-PAMPSA-EG complex with the highest conductivity was selected to make membranes.

Method 2 (mechanical mixing): involved mechanically mixing EG and PAMPSA doped PANI (PANI-PAMPSA) complex, and two different weight

percentages of EG (25 wt% and 50 wt%) with respect to PANI-PAMPSA were used. The mixture with higher conductivity was chosen to make membranes.

Method 3A (solution mixing): involved two steps: the first step was to disperse EG in solvent with 2 h ultrasonication at a low temperature (5°C); the second step was to add PANI-PAMPSA into the solution portion by portion with magnetic stirring overnight. The obtained casting solution was then used to make membranes.

Method 3B (solution mixing): involved dispersing EG and PANI-PAMPSA separately in the solvent, and then the EG solution was added drop by drop into PANI-PAMPSA solution with ultrasonication for 2 h at a low temperature (5°C) and magnetic stirring overnight. The obtained homogeneous mixture was used to make membranes.

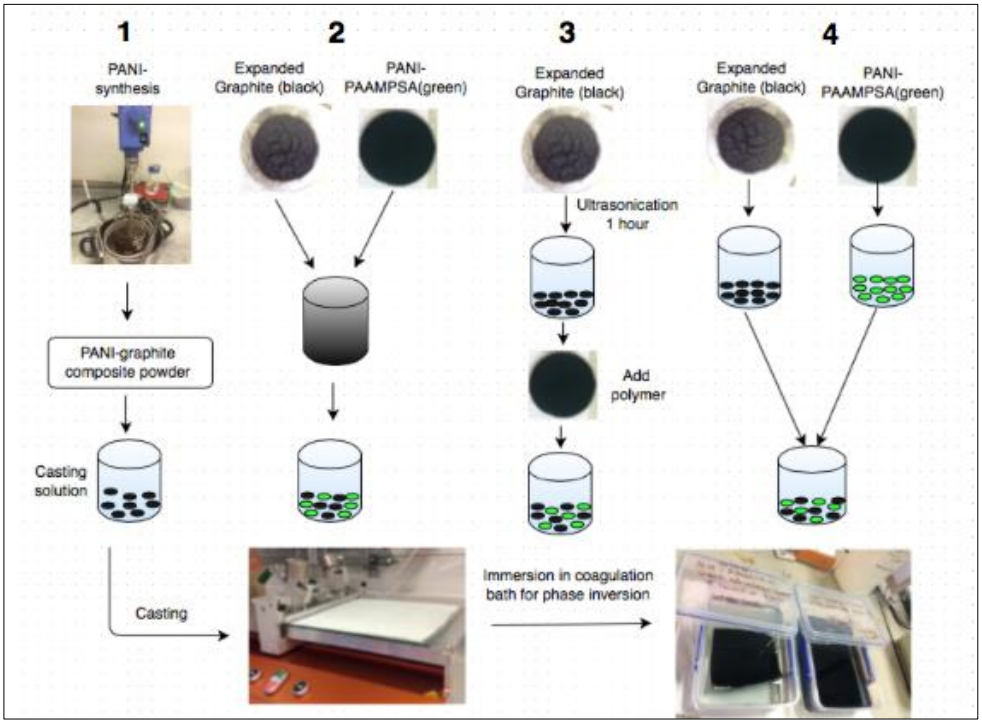

Fig. 4-3 Different approaches to incorporate EG into membranes: (1) In-situ polymerisation in presence of EG, (2) mechanically mixing EG and PANI-PAMPSA, (3) dispersing EG in solvent and then adding PANI-PAMPSA, (4) dispersing EG and PANI-PAMPSA in solvent separately and then mixing together.

The membrane was prepared using NIPS method as per Section 4.5. The formed membranes then doped in 1.0 M DBSA for 24 h at room temperature to obtain secondary doped membranes (Memb-PAMPSA-EG/DBSA).

4.8 Characterisation Techniques

4.8.1 Fourier Transform Infrared Spectroscopy (FTIR) and UV–Visible Spectroscopy (UV-Vis): Chemical Analysis

The FTIR spectra of dry PANI samples (both powder and membranes) were obtained by using a Spectrum 100™ - FTIR Spectrometer (PerkinElmer, USA) fitted with an attenuated total reflectance (ATR) detector. A background scan was run prior to sample testing and spectra were recorded from 4000 to 650 cm^{-1} in transmission mode with a spectral resolution of 4 cm^{-1} and 32 scans. Thin slices of PANI membranes were measured directly. The PP/PE backing layer was also tested for comparison with the fabricated membrane.

The UV-Vis analysis of PANI-EB powder was carried out using UV-Vis equipment (UV-1601, Shimadzu, Japan). 10 mg of PANI were dissolved in 10 mL of NMP to prepare 1.0 g L^{-1} solution; the obtained solution was then diluted into 0.01 g L^{-1} by NMP. Spectra were recorded at wavelengths from 250 to 850 nm at room temperature.

4.8.2 Visual Defect Analysis

A backlit LED light box was used to detect any visible defects.

4.8.3 Field-emission Scanning Electron Microscopy (FESEM): Membrane Morphology

The morphological properties of the membranes were imaged by using FESEM (JSM-6301F, JEOL, Germany). The samples were prepared by breaking them in liquid nitrogen to obtain a smooth cross-section and then mounted on the SEM stubs by conductive double-sided tape and dried overnight. The samples were coated with chromium using a sputter coater (Q150T S, Quorum) under argon flow to reduce sample charging under the electron beam. The samples were imaged using an acceleration voltage of 5 kV.

4.8.4 Mechanical Strength Analysis: Membrane Robustness

The tensile strength and elongation at break of membranes were determined using a standard mechanical testing instrument (Instron 3369). The samples prepared in this manner were cut by a razor blade into rectangular strips of approximately 5 mm × 75 mm for testing. The samples were gripped using clamps and all tests

were conducted with a pull speed of 2 mm min^{-1} at room temperature. Membrane thickness was measured using standard Vernier callipers. An average of three membrane samples was recorded.

4.8.5 Dynamic Mechanical Analysis (DMA): Glass Transition Temperature (T_g)

The T_g of membranes were obtained by using a dynamic mechanical analyser (Mettler-Toledo, DMA1, STARe System) up to a temperature of 300°C with a heating rate of 5°C min^{-1} and at a frequency of 1 Hz. The membranes were cut into strips of 25 mm (L) × 5 mm (W).

4.8.6 RGB Colour Analysis: Membrane Doping State via Colour Changes

Colour analysis RGB (Red, Green and Blue) was used to quantitatively evaluate the colour of PANI membranes. A RGB value of (0, 0, 0) represents a black colour whereas a value of (255, 255, 255) represents white. Consequently, a higher RGB value indicates a lighter colour. A scanner (CanoScan 9000F, Canon, Japan) was used to scan the membrane samples to obtain membrane images, and Image J software was employed to analyse the images and give the mean value of RGB. The reported values are the mean values of different points from at least two different membrane samples. The colour variation (ΔRGB) after doping (R_d, G_d, B_d) can be calculated by subtracting the data before doping (R_0, G_0, B_0), in accordance with Equations 4.1-4.3:

$$\Delta R = R_d - R_0 \qquad \text{Equation 4.1}$$

$$\Delta G = G_d - G_0 \qquad \text{Equation 4.2}$$

$$\Delta B = B_d - B_0 \qquad \text{Equation 4.3}$$

4.8.7 Four-point Probe Conductivity Meter: Membrane Conductivity

The membrane surface conductivity was investigated at room temperature by using a four-point probe conductivity meter (RM3000, JANDEL, UK). The measured bulk resistivity (ρ) was calculated by the following relationship in Equation 4.4:

$$\rho = 4.532 \times V \times t/I \qquad \text{Equation 4.4}$$

Where ρ is resistivity, V is the measured potential, I is the provided current, and t is the membrane thickness. The conductivity was calculated from the conversion of the resistivity. Each sample was measured a minimum of 10 times with average and standard deviation reported.

4.8.8 Dynamic Droplet Penetration Analysis: Initial Tuneability Assessment

The dynamic droplet penetration over time with, or without, applied potential through the membranes was measured by use of a contact angle goniometer (Contact Angle System OCA 15Pro, Dataphysics, Germany). The membrane sample was placed on an analytical platform which electrodes were connected to provide voltage across the membrane, as illustrated in Fig. 4-4. A small drop of water (2.0 µL) was placed onto the membrane surface at a dosing rate of 1.0 µL s^{-1} using a Hamilton syringe. A video camera was used to record images of the water drop with and without applied potential. The programme software was used to calculate the effective contact angle and droplet height change on the membrane surface.

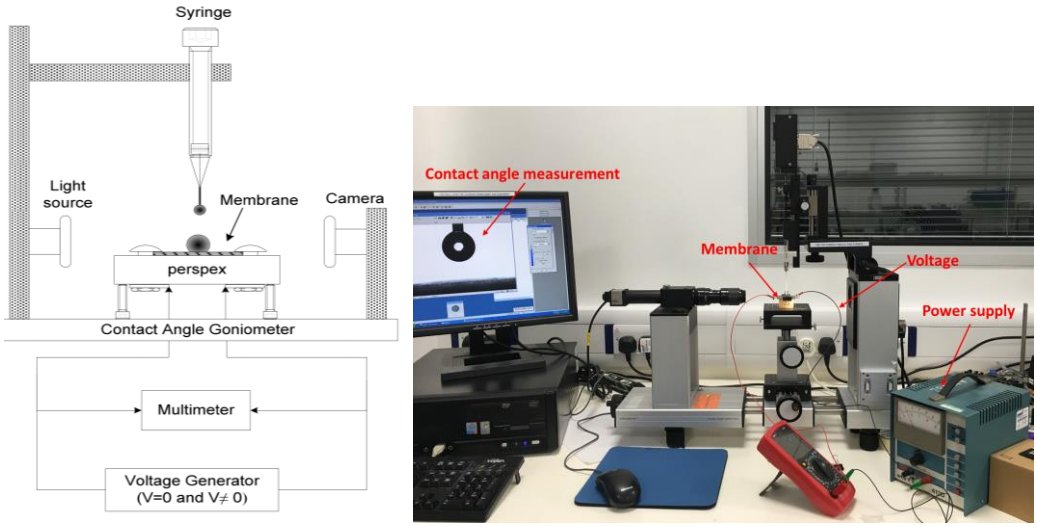

Fig. 4-4 The membrane assembly in the contact angle goniometer [6].

4.8.9 Dead-end Filtration: Membrane Transport Property

Membrane filtration was performed in a stirred high pressure stainless steel dead-end filtration cell (HP 4750, Sterlitech, USA). The membrane with an effective area of 14.6 cm^2 was placed on a sintered metal plate. During filtration, the filtration cell was immersed in a water bath at a temperature of 25°C and a magnetic stirrer at 300 rpm was used to minimize the effect of concentration

polarisation in the membrane surface. The driving force for filtration was provided by nitrogen gas. All membranes were pre-conditioned with DI water until a steady state flux was achieved. After reaching steady state, DI water or PEG mixture solution were added into the filtration cell and the permeate was collected in a measuring cylinder. Permeate mass versus time was recorded by using a computer operated digital mass balance (Sartorius LC3201D-00M, Germany) to determine the permeate mass flux. Solute rejection was calculated using Equation 4.5:

$$R_{\mathrm{j}}(\%) = \left(1 - \frac{C_{\mathrm{p}}}{C_{\mathrm{f}}}\right) \times 100\% \qquad \text{Equation 4.5}$$

Where R_{j} is the rejection of membrane, C_{f} is the PEGs concentration in the feed and C_{p} is the PEGs concentration in the permeate. MWCO curves are obtained by plotting the rejection of the individual oligomers in the PEG mixtures against their molecular weight, determining the molecular weight at which a rejection of 90% was achieved.

4.8.10 MWCO analysis method

(1) PEG mixture concentration determination

The PEG mixtures used for MWCO analysis included commercial PEG 1000, 1500, 2000, 3000, 4000 and 6000. PEG, were selected as MWCO molecular probes since they are available in a wide range of MW from a number of different manufacturers, are low price compared to other MWCO probes (e.g. polystyrenes), are electrically neutral, are soluble in water over a wide range of concentrations and have minimum chemical interactions with membranes compared to more polar and charged molecules [201, 202]. They were dissolved in DI water to obtain PEG oligomer mixture solution. In terms of each commercial PEG with the same weight concentration, PEG 1000 exhibited much higher peak heights and areas than the other higher MW PEGs (e.g. PEG 1500, 2000, 3000, 4000 and 6000). In order to make sure the comparable peak response for all the commercial PEGs and get a relatively similar peak signal across the entire HPLC chromatogram, the weight concentration of larger MW PEGs (PEG 1500-6000) needed to be three times higher than PEG 1000 in the PEG mixtures.

In terms of the construction of calibration curve, the lowest concentration used was 75 mg L^{-1} for PEG 1000 and 300 mg L^{-1} for PEG 1500 to 6000 considering the sensitivity of the detector. Below the lowest concentration, the detector baseline

appeared to drift and showed excessive noise. The feed concentration used for the MWCO determination of commercial membranes was 600 mg L^{-1} for PEG 1000 and 2400 mg L^{-1} for PEG 1500 to 6000. Feed concentration was expected to be as low as possible to prevent the possible concentration polarisation which could affect the MWCO value and so the feed concentration applied in the study was comparable to the previous publications [201, 203]. Since the retentate should still be measurable, the highest concentration used for the calibration curves was 1200 mg L^{-1} for PEG 1000 and 4800 mg L^{-1} for PEG 1500 to 6000. Therefore, the calibration curve covered a wide range of concentrations to give a comprehensive coverage of the expected feed, permeate and retentate concentrations. The calibration curves were established by diluting a stock solution of PEG mixture (1200 mg L^{-1} for PEG 1000, and 4800 mg L^{-1} for PEG 1500 to 6000). The peak areas versus concentrations of PEG oligomers were quantified by ELSD detector to construct the calibration curve.

Purer PEG 1000, as an external standard, was employed to accurately identify the MW of the individual oligomers in its MW range using the stated average MW range as the highest peaks eluted, thereby accurately determining the identity of several peaks in the series.

(2) Analysis method

A high performance liquid chromatograph (HPLC) coupled with an evaporative light scattering detector (ELSD) were used for the identification of individual PEG oligomers. An ELSD detector was used since previous work in this research group and elsewhere has demonstrated that it is the most robust, reliable and sensitive detector for close MW PEG oligomers signal detection if coupled with an appropriate gradient elution [201, 202, 204]. The HPLC apparatus (Agilent 1260 infinity series, Agilent Corporation, USA) consisted of an autosampler (G1329B), a Colcom column oven (G1316A), a Quat pump (G1311B), a degasser and an Agilent data interface. The detection was performed utilising an Agilent ELSD (Agilent 1260 infinity G4260B, Agilent Corporation, USA) with drift temperature set up at 60℃. An Agilent Poroshell 120 EC-C18 column (4.6 mm length × 5.0 mm I.D., 2.7 μm particle size) was used to achieve the separation of peaks with temperature set at 50℃. A flowrate of 1.0 mL min^{-1} was used with mobile phase A: acetonitrile and B: water. The gradient used to separate the individual peaks of

the PEG mixtures is presented in Table 4-4. A sample volume of 50 μL was injected throughout the whole work. The analysis was based on the peak areas and each peak corresponded to a PEG oligomer with a certain molecular weight.

Table 4-4 HPLC gradient for the separation of PEG oligomer.

Elution time/min	Gradient A (acetonitrile)/vol. %	Gradient B (water)/vol. %
0	15	85
2	25	75
20	25	75
92	50	50
95	20	80

4.8.11 Cross-flow Filtration and Electrical Tuneability under Applied Potential

Fig. 4-5 shows the electrically connected cross-flow filtration setup. The setup is comprised of two custom made PTFE cross-flow electro-filtration cells (effective area of 14.6 cm^2, Auckland Engineering workshop) based on metal cross-flow cells (METXF-2.5-041-01, stainless steel, Membrane Extraction Technology, UK) [6]. Two stainless steel membrane electrodes were employed in this study. A good electrical contact between the membrane surface and electrodes was ensured before each experiment. The operating pressure was supplied by a precision metering pump (Hydra-Cell seal-less diaphragm pump model G10XKSGHFEMH, Michael Smith Engineering, UK) and potential was provided by a variable power supply (413D, Weir, UK). Current was measured using a digital multi-meter (UT58C, Maplin, UK). The temperature was kept at 25°C by a water bath (SBB Aqua 12 Plus, Grant instrument, UK).

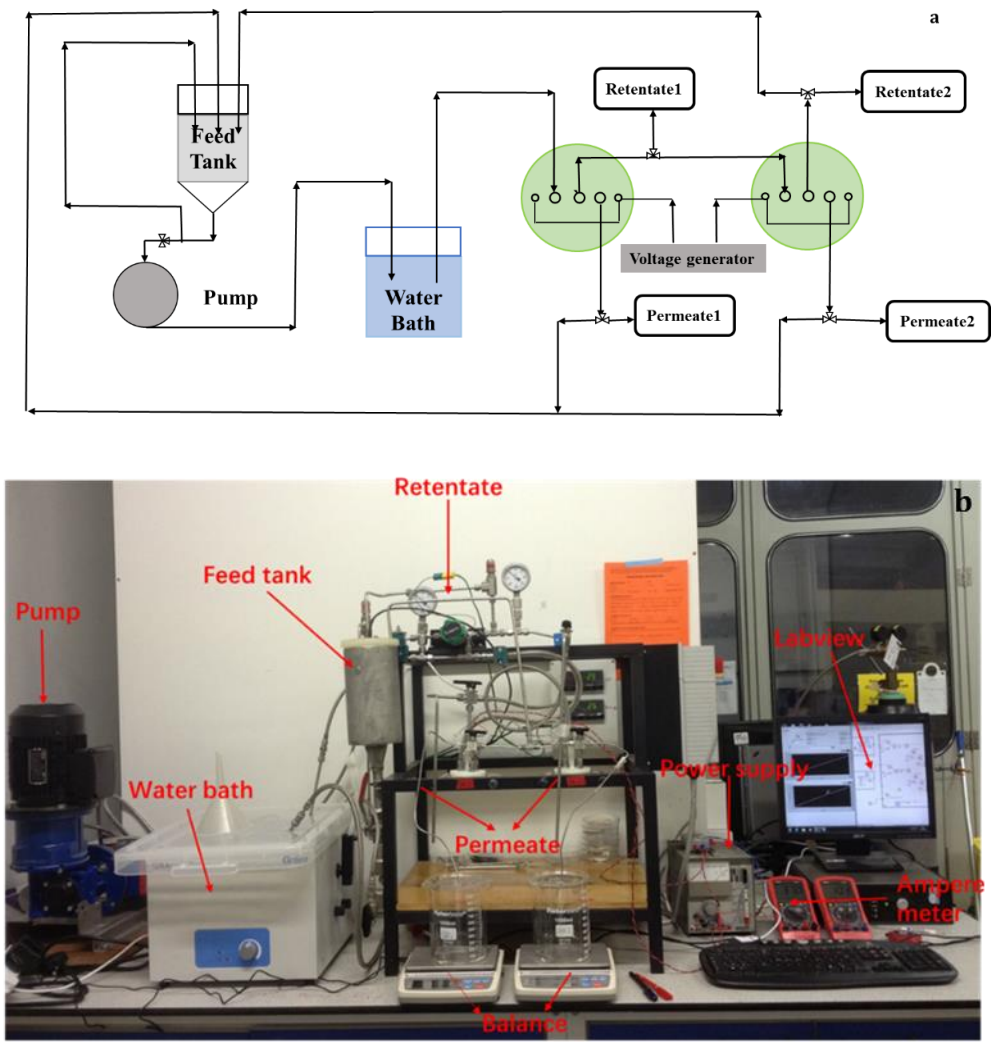

Fig. 4-5 (a) Schematic of the electrically connected cross-flow filtration rig, (b) labelled photo of the electrically connected cross-flow rig.

In a typical experiment, PANI membrane was placed in the cross-flow membrane cell, and then 1.5 L of DI water or PEG solution (PEG 1000, 1500, 2000, 3000, 4000 and 6000) was transferred to the reservoir tank. The flowrate was set at about 1.2 L min^{-1} as too high flowrate might cause unstable operating pressure whereas too low flowrate might lead to membrane fouling. Permeate was collected at a constant pressure.

To test the electrical tuneability, membrane filtration experiments were performed with different electrical potentials, with 0, 9 and 30 V for small acid doped membrane in Chapter 5 and 30 V for PAMPSA doped membranes in Chapter 7 and 8. For the 0 V potential experiment, the first permeate sample (denoted t = 0 min) was taken after constant pressure was continued. Further permeate samples

were taken at 30, 60 and 120 min intervals after this. The same procedure was also used to study the effect of electrical potential (9 and 30 V) on membrane filtration.

The permeate samples were kept in HPLC vials for the HPLC-ELSD analysis and MWCO was determined for each permeate collected as detailed in Section 4.8.10. Membrane mass flux was calculated from the permeate mass versus time data recorded by using a computer operated digital mass balance (A&D Instruments, GR-300, UK). In order to avoid the effect of small acid leaching from the membrane (Chapter 5) during cross-flow filtration, the same membrane was redoped prior to the filtration for each electrical potential. In this study, at least two different membrane samples were used to characterise each type of membrane.

4.9 Fouling test and Post-Fouling Characterisation

4.9.1 Dead-end Filtration: Permeance Determination

Four kinds of membranes were chosen for the subsequent fouling evaluation tests. Dead-end filtration was used to determine the permeance of virgin, BSA fouled and cleaned membranes. The membrane was firstly preconditioned with DI water, and then 200 mL of DI water was used to determine the flux of virgin membranes, after that 200 mL of 1.0 g L^{-1} BSA solution was added to the cell to foul the membrane, and then 200 mL of DI water was run again to measure the flux of fouled membranes. After cleaning with applied potential, the flux of cleaned membranes was measured with 200 mL of DI water. All the filtration was run at 25°C with a stirring rate of 300 rpm. Permeate mass versus time was recorded by using a computer operated digital mass balance (Sartorius LC3201D-00M, Germany) to determine the permeate mass flux.

4.9.2 Fouling Removal with Applied Potential

Fig. 4-6 displays the setup used for the fouling removal of membranes under an applied potential at room temperature. Firstly, the membrane was immersed in 800 mL water in a beaker, and then applied potential of 30 V was applied on the membrane and lasted for 2 h. The wash solution sample was taken at 0, 30, 60, 90 and 120 min. In addition, the two control experiments were run on BSA fouled membranes in the absence of applied potential and unfouled membrane in the presence of applied potential.

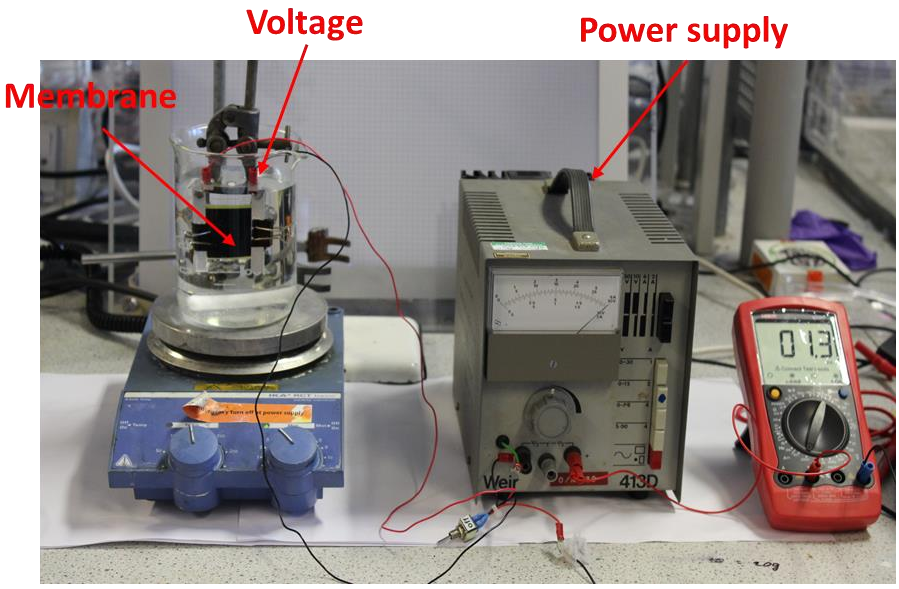

Fig. 4-6 Setup for evaluating membrane fouling removal.

4.9.3 UV-Vis of the Wash Solution: Component Identification Analysis

UV-Vis was used to analyse the components of the wash solution (obtained from Section 4.9.2) to evaluate membrane defouling behaviour by the application of external potential. A calibration curve was built in order to measure the BSA concentration in the wash solution. Spectra were recorded in the range from 200 to 900 nm.

4.9.4 Confocal Scanning Laser Microscopy (CSLM): Visual Examination of Membranes

CSLM (Carl Zeiss LSM, Germany) were utilised to visualise the BSA-fluorescein on the membrane surface and distinguish the membrane defouling action upon electrical stimulus.

The membrane samples (virgin, fouled and cleaned by external potential) were stained using FITC dye for 1 h and then washed with phosphate-buffered saline (PBS) to remove extra dye, after that the sample was viewed at two different magnifications.

5 Electrically Tuneable PANI Membranes: Influence of T_{poly} on in-filtration Electrical Tuneability of Flux and MWCO

5.1 Introduction

The high selectivity and flux needed for current membranes to outcompete other separation technologies is often limited by fouling and the inability to precisely fine tune flux and selectivity of these membranes. The development of smart membranes, where the selectivity and flux can be tuned by external stimuli during operation, has the potential to be the breakthrough solution to overcome these major challenges [6]. Polyaniline (PANI), a π-conjugated structure with alternating single and double bonds, is the most extensively studied intrinsically conducting polymer during the past decade [4, 5]. Its electrical properties can be varied and controlled by both oxidative and non-redox protonic acid doping reactions in the conjugated carbon backbone [69-71]. It has attracted considerable attention because of good environmental stability, distinct electrochemical properties, simple reversible acid/base doping chemistry as well as lower synthesis costs [66, 69].

PANI has been widely studied in membrane based separations, such as gas separation, pervaporation, selective ion separation and organic solvent nanofiltration during the past two decades [7, 81, 88, 94, 107, 148]. It has been shown that PANI membrane structure can be altered at a molecular level by controlling the incorporation or exclusion of ions from the dopant site - even after synthesis- which is very difficult to accomplish with conventional polymer membranes [3-5]. The controlled movement of ion solutes in aqueous systems through PANI and other conductive polymer membranes in permeation cells has been well studied [205, 206]. Despite extensive efforts in designing ion selective PANI membranes, there remains an insufficient understanding of electrically tuneable membranes for pressure filtration systems [15, 207], especially their impact on membrane performance for separations of non-ionic species in particular (with only two examples available in literature) [56].

We have realised that an electrically conductive PANI membrane could possibly be dynamically responsive by applying an external electrical potential across the membrane, thus inducing several changes in membrane properties that could produce more general membrane tuneability beyond the ion separations that PANI

membranes have, in the main, been applied to thus far. These electrically induced changes include: changing surface charge controlling Donnan exclusion, change in pore size/free volume (via incorporation or expulsion of ions from the acid dopant site) controlling pore flow transport, and chemical property changes controlling solution diffusion and volume swelling. All these properties make polyaniline an excellent candidate for a more universally electrically tuneable membrane investigation.

Previous studies in Patterson research group has found that the transport properties of conducting PANI membrane, such as permeance and selectivity, could be tuned in-situ during cross-flow pressure filtration by applying an electrical potential across acid doped PANI membranes [6, 208]. The electrical potential changes the interaction between PANI and acid dopants and thus modifying the membrane properties and allowing membrane permeance and MWCO to be tuned. These tuneable membranes can thus offer a promising solution to optimise and control the in-situ tuneable separation performance in relevant industrial operations.

PANI can be synthesised by several methods, including chemical polymerisation, electrochemical polymerisation, photo-induced polymerisation, enzyme-catalysed polymerisation, plasma polymerisation and other special methods [4, 71, 73]. Among the employed synthesis methods, chemical oxidative polymerisation has the advantage of producing PANI on large scale more economically with good reproducibility and control, which allows for commercial application [4].

Many studies have focused on the optimum reaction conditions for the aniline polymerisation as well as the influence of the synthesis conditions on the PANI properties [73, 77, 79, 82, 84, 87, 209, 210]. Among these conditions, T_{poly} plays a crucial role in the oxidative chemical polymerisation of PANI and it is known to influence the mechanical, chemical and electrical properties of PANI [79, 85, 86, 184]. A lower T_{poly} favoured producing PANI with a higher molecular weight than room temperature, which was desirable to form a membrane with more interlinked structures and higher mechanical strength [81-83]. The relationship between T_{poly} and electrically conductivity, however, is still ambiguous. Ohtani *et al*. and Lee *et al*. claimed that decreasing T_{poly} was accompanied by an increase in conductivity, while Boara *et al*. found that high conductivity of PANI could be obtained even at 60°C by optimising the reaction conditions [84-86]. Other studies reported that the

conductivity was independent of T_{poly} [77, 79, 85, 87]. Stejska *et al*. studied the effects of T_{poly} on properties of PANI and found that PANI prepared below 0°C showed an increase in molecular weight and crystallinity while little dependence of conductivity of PANI on the T_{poly} [79]. While it is known that T_{poly} affects the properties of PANI, there is no study that reports the effect of T_{poly} on the transport properties and electrical tuneability (i.e. electrically tuneable permeance and selectivity)) of PANI in pressure driven filtration processes. As T_{poly} affects the properties of PANI, it could subsequently influence the transport properties of PANI membranes and their electrical tuneability. Therefore, it is necessary to conduct a systematic evaluation of the effect of T_{poly} on above mentioned membrane properties and their electrical tuneability.

Consequently, this study is the first rigorous study on the effect of T_{poly} on the properties of PANI membranes and its impact on the electrical tuneability of flux and MWCO during cross-flow filtration of neutral species. PANI was synthesised via chemical oxidative polymerisation at different T_{poly}. Based on literature reports [211, 212], three T_{poly} (5°C, 15°C and 25°C) were chosen. Subsequently, flat sheet PANI membranes were prepared via NIPS method. The membrane properties (chemical, electrical, physical and mechanical) were investigated by a multitude of physicochemical techniques, e.g. FTIR, UV-Vis, DMA, FESEM, four-point probe conductivity, dynamic contact angle goniometry, membrane permeance and MWCO. Cross-flow filtration under applied potential was used to determine the change in membrane performance caused by external voltage changes. The membrane properties at different T_{poly} were compared and an understanding of the relationships among T_{poly}, membrane performance properties and electrically tuneability of membranes, were developed for the first time.

5.2 The Effect of T_{poly} on the PANI Powder Properties

5.2.1 Yields of PANI Powder

PANI-EB powder was synthesised from aniline monomer at 5°C, 15°C and 25°C. Table 5-1 describes the weights and yield of PANI powder versus T_{poly}. It can be seen that each T_{poly} produced similar weights and gave around 71% yield based on the aniline monomer. The result illustrates that T_{poly} had no significant effect on the yields of PANI powder ($P>0.05$) as also observed in literature [78]. This

indicates that the synthesis undertaken can be benchmarked against other PANI synthesis work in the literature.

Table 5-1 Weight and yield of PANI-EB powder obtained at different T_{poly}.

PANI-EB-T_{Poly}(°C)	Weight (g)	Yield (%)
PANI-EB-5	13.34±0.41	71.56±2.22
PANI-EB-15	13.14±0.31	70.50±1.67
PANI-EB-25	13.25±0.47	71.13±2.51

5.2.2 UV-Vis and FTIR Analysis

UV-Vis absorbance spectra of the PANI-EB samples with different T_{poly} dissolved in NMP are shown in Fig. 5-1 (a). The spectra presented two significant absorption peaks at 330 and 639 nm respectively. The 330 nm band (B-band) corresponds to the π- π^* transition associated with π electrons of benzenoid rings (B) [213]. The absorption in the visible range, at 639 nm (Q-band), is ascribed to excitation of an electron from the highest occupied orbital of benzenoid rings to the lowest unoccupied orbital of the quinoid rings (Q) [214]. The absorption of the Q-band reflects both intra- and inter-chain interaction; therefore, its absorption intensity and wavelength change with the EB chain configuration, which is affected by the solubility, additive, concentration, oxidisation level and molecular weight. On the other hand, the B-band is mainly a function of intra-chain interaction; therefore, the solution properties have a less impact on its intensity and wavelength [215, 216]. Therefore, the absorbance ratio of the Q-band and B-band, Q/B ratio, may be used to determine the oxidation level of PANI chains. The value of Q/B = 0.86 indicates an ideal PANI-EB while a Q/B below 0.69 typically indicates higher or lower levels of oxidation.

For the powder synthesised, UV-Vis spectra of the three different PANI-EB forms (PANI-EB-5, 15 and 25) showed a slight decrease of Q/B absorbance ratio with increasing T_{poly}, i.e., 0.88 for PANI-EB-5, 0.86 for PANI-EB-15 and 0.81 for PANI-EB-25 while the wavelength of Q-band and B-band remained almost constant. The differences in Q/B ratios are most likely related to the structural differences (i.e. oxidation state and molecular weight) of PANI-EB resulting from the different T_{poly} [78]. Specifically, Yang *et al*. reported that when the MW of PANI was less than 30,000 g mol^{-1} the Q/B ratio decreased to 0.48 and increased as the

molecular weight increased becoming constant at 0.89 when the MW was greater than 30,000 g mol^{-1} [217]. Therefore, in the present case, a slight increase in the Q/B ratio at low T_{poly} suggests that a lower T_{poly} produces a higher molecular weight PANI-EB and/or PANI-EB with increased content of non-protonated Q units. This confirms other results in the literature [79, 87].

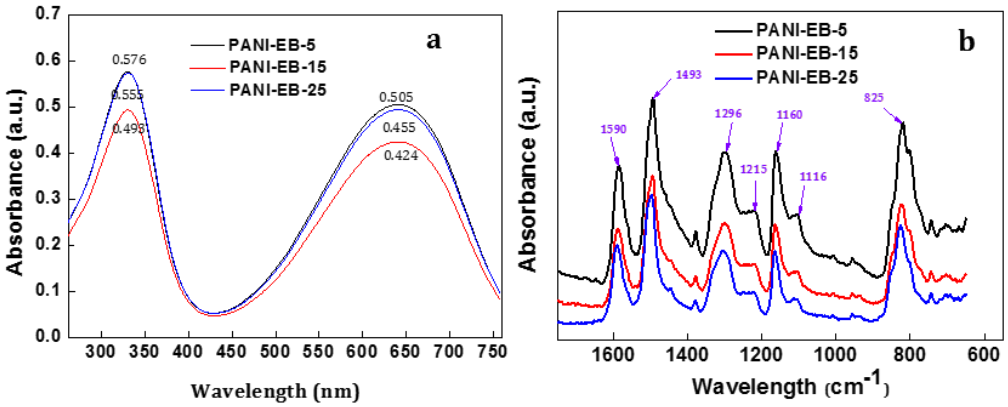

Fig. 5-1 (a) UV-Vis absorbance spectra of PANI-EB at different T_{poly}. (b) FTIR spectra of PANI-EB powder synthesised at different T_{poly}.

Table 5-2 FTIR bands representing PANI at different wavelengths [184, 218].

PANI band Characteristics	**Wavelength (cm^{-1})**
C=C stretching vibrations of benzenoid rings	1485-1498
C=C stretching vibrations of quninoid rings	1560-1598
C-N-C stretching of secondary aromatic amine	1296-1286
C-N+· stretching in polaron form of PANI (ES)	1231-1245
-NH^{+}= structure upon doping (Electronic like bands)	1145-1150
C-H out of plane blending of 1,4-ring	815-830
C-Cl stretching vibration	620-630

Fig. 5-1 (b) shows FTIR spectra of the PANI-EB at different T_{poly}, with characteristic peaks of PANI identified in Table 5-2. The spectra show the characteristic bands of PANI at 1590 cm^{-1} (stretching of N=Q=N), 1493 cm^{-1} (stretching of N-B-N), 1296 cm^{-1} (C-N-C stretching of the secondary aromatic amine), 1160 cm^{-1} (C-H in plane blending of 1,4-ring) and 825 cm^{-1} (C-H out of plane blending of 1,4-ring) [184, 218]. The characteristic absorption peaks of PANI appeared in the UV-Vis and FTIR spectra, indicating that PANI-EB was indeed produced in the experiment [219].

The spectra of all PANI-EB samples were very similar but they slightly differed in the intensity of the shoulders occurring at 1116 and 1215 cm^{-1}. The band at 1116 cm^{-1} is assigned to the vibration mode of protonated units Q = NH^{+}-B or B-$NH^{+\cdot}$-B present in PANI-EB [220]. As can be seen in Fig. 5-1 (b), the intensity of shoulder at 1135 cm^{-1} increased from PANI-EB-5 to PANI-EB-25, which indicates that the content of residual protonated units in a PANI-EB form is an increasing function of T_{poly}. The band at 1215 cm^{-1} showed the opposite behaviour and decreased as T_{poly} increased. In the literature, this band had been assigned to $V_{CN} + \delta_{CH}$ modes in Q units and authors observed a decrease in this band intensity with increasing content of self-doped units in PANIs prepared with the $FeCl_3/H_2O_2$ catalyst system [220]. The intensity decrease of the band at 1215 cm^{-1} implies a decrease in the content of non-protonated Q units with increasing T_{poly} from 5°C to 25°C. These results are consistent with the UV-Vis results.

5.3 The Effect of T_{poly} on PANI Membrane Properties

Membranes were prepared from PANI-EB powder synthesised at different T_{poly} as detailed in Section 4.5. These membranes were then characterised using a range of techniques. Subsequently, a comparison was made to conclude the T_{poly} which produce most optimal electrically tuneable membranes (aiming for robust, conductive membranes with widely tuneable flux and MWCO).

5.3.1 PANI Membrane Morphology: Defect Analysis and FESEM Imaging

A backlit LED light box was used to detect any visible defects, such as pinholes and cracks, on the membrane surface. Fig. 5-2 shows the images of Memb-EB and Memb-ES. Memb-EB-5 and Memb-ES-5 had smooth and shiny membrane surfaces without any visible cracks. Memb-EB-25 and Memb-ES-25 were brittle with defects and cracks formed on the surface, indicating that the membrane was likely to perform poorly in filtration experiments. As a stability test, membranes were kept at room temperature for a period of two months. Memb-EB-15 surface developed some cracks similar to Memb-EB-25; there were no visible changes to Memb-EB-5 during this time.

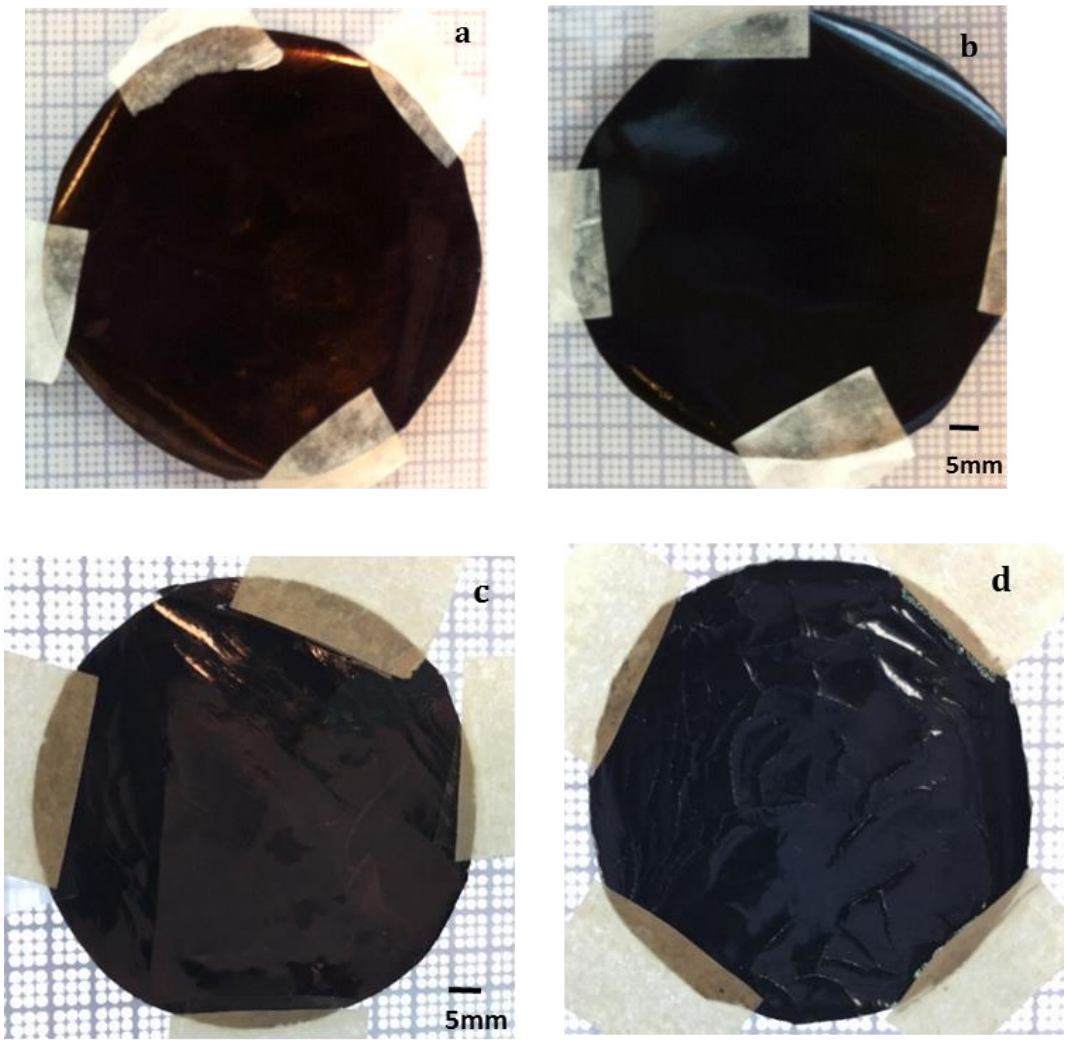

Fig. 5-2 Defects examination of membrane surfaces by light box: (a) Memb-EB-5 (purple bronze), (b) Memb-ES-5 (dark green), (c) Memb-EB-25 (purple bronze) and (d) Memb-ES-25 (dark green)

Fig. 5-3 presents the effect of T_{poly} on the membrane morphology. All the membranes displayed characteristic cross-sections of NF membranes, showing three layers [221]: a denser top skin layer, a transition region and a relatively porous layer of PANI on a support layer. Macrovoids are present in all membranes. In general, membrane structures depend on both the thermodynamic interactions between components in the casting solution, as well as on the phase inversion kinetics [222]. Structures with macrovoids are expected in the studied system due to the high mutual affinity between NMP and water, which generally leads to instantaneous demixing. NMP with higher density than water leads to the diffusion of water into the membrane, forming the finger-like voids. The presence of macrovoids is both desirable and undesirable: they are desirable as they can lead to high membrane fluxes by reducing the membrane diffusional resistance below

the dense active layer, whilst they are undesirable since they increase the compaction of the membrane at the elevated pressures during filtration [223].

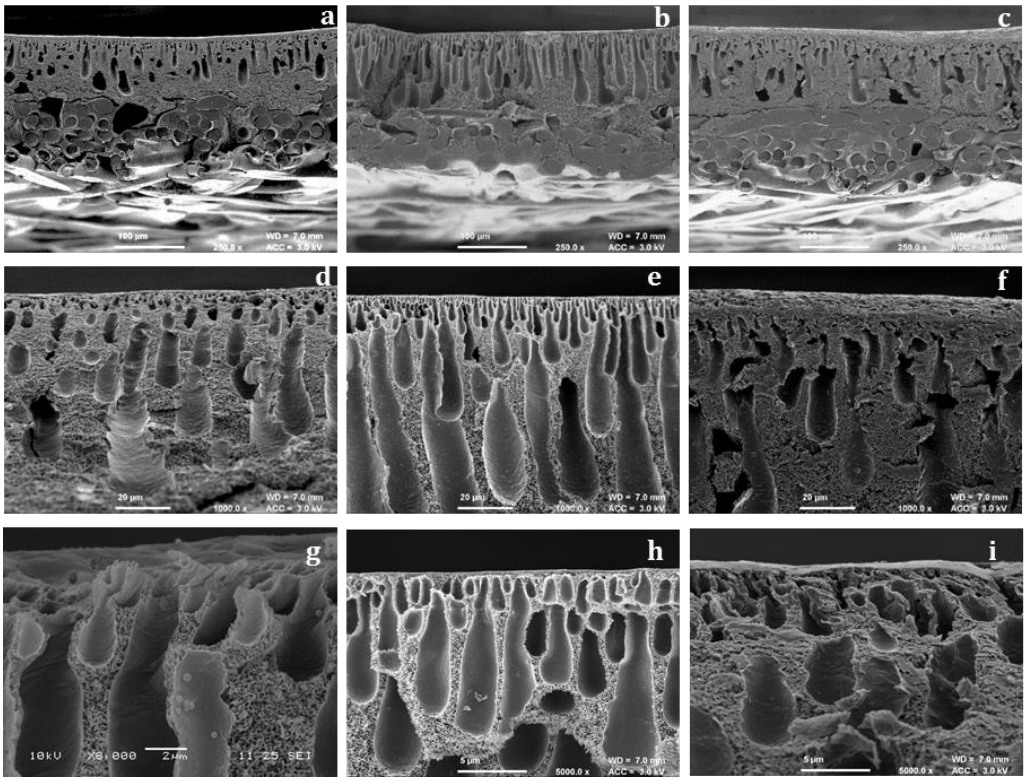

Fig. 5-3 FESEM images of (a, d, g) Memb-EB-5, (b, e, h) Memb-EB-15 and (c, f, i) Memb-EB-25 at three different magnifications (magnifications refer to the original image when captured by the FESEM) showing the overall membrane structure (a-c), membrane layer (d-f) and detail of the top layer (g-h).

The Memb-EB-15 had larger macrovoids, while Memb-EB-5 and Memb-EB-25 had denser, more spongy structures, respectively. It is known that PANI synthesised at a lower T_{poly} typically has a higher molecular weight [79, 87] . Increased molecular weight of PANI results in higher viscosities of casting solutions thus causes more entanglement of polymer chains in the casting solutions. This would slow down demixing during NIPS and would result in denser membranes with fewer macrovoids. Indeed, somewhat fewer macrovoids are present in Memb-EB-5 prepared from PANI polymerised at lower T_{poly}. With more delayed demixing, the membrane morphology transitions from macrovoids to more spongy structures. However, Memb-EB-15 also had the longer macrovoids than Memb-EB-25. One possible reason could be that the smaller MW PANI polymers in Memb-EB-25 could also be more mobile during the phase inversion process and fill in some of the macropores formed.

Overall, the visual defect analysis and SEM results therefore indicate a new result for PANI membranes - that T_{poly} directly affects PANI membrane morphology.

5.3.2 FTIR and Colour Analysis of PANI Membranes

Fig. 5-4 shows the FTIR spectra of Memb-EB and Memb-ES – again refer to Table 5-2 for the characteristic peaks shown in the undoped and doped membranes. The bands at 1595 and 1498 cm^{-1} were assigned to C=C stretching vibration of both quinoid and benzenoid rings, respectively. The band at 1295 cm^{-1} corresponds to C-N stretching vibrations of secondary amine of PANI backbone. Doping of the PANI is confirmed to occur in all samples, since addition of the acid transforms the imine group (=N−) into amine groups (−N˙−). The absorption peaks of the quinoid and benzenoid rings were shifted from 1595 cm^{-1} and 1498 cm^{-1} to a lower wavelength on acid doping. Additionally, the protonation caused by acid doping can be identified by the presence of a strong peak for C-H aromatic amine appeared at approximately 1140 cm^{-1} in the Memb-ES, which is representative of an "electronic-like band". This particular peak is also associated with a high degree of electron delocalisation and a high electrical conductivity [224, 225]. Meanwhile, the band at 620 cm^{-1} relates to C-Cl stretching vibration.

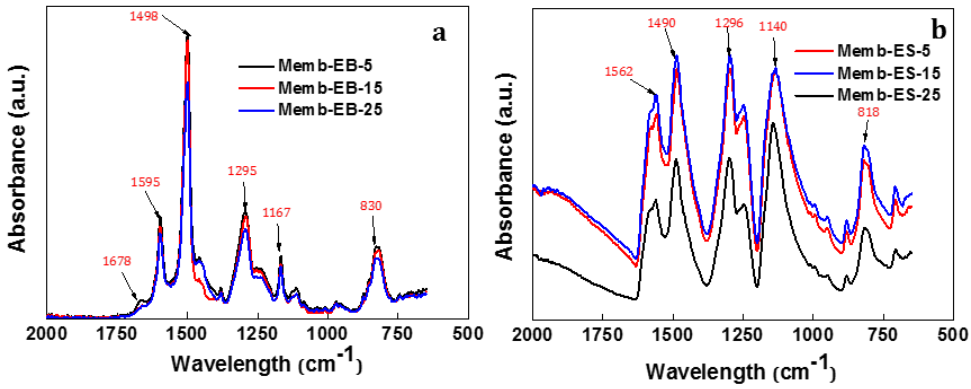

Fig. 5-4 FTIR spectra of (a) Memb-EB and (b) Memb-ES as a function of T_{poly}.

The bands in the region 1400-1600 cm^{-1} were normalised so that the intensity ratios (Q/B) of quinoid and benzenoid peaks can be compared. The Q/B ratio can be used as a measure of the extent of oxidation of the PANI. Fig. 5-5 shows the degree of oxidation based on the Q/B in the PANI-EB and Memb-EB taken from the FTIR data. The Q/B value was calculated by the ratio of the peak height of 1595 cm^{-1} (associated with Q) versus 1498 cm^{-1} (associated with B) from the FTIR spectra. PANI-EB samples showed a similar Q/B ratio (from FTIR data) as compared to

Q/B ratio calculated from UV-Vis results. Based on Q/B ratio, it can be concluded that all undoped PANI-EB samples have an oxidation degree lower than 0.8, indicating that the individual chains contain more benzenoid rings than quinoid rings.

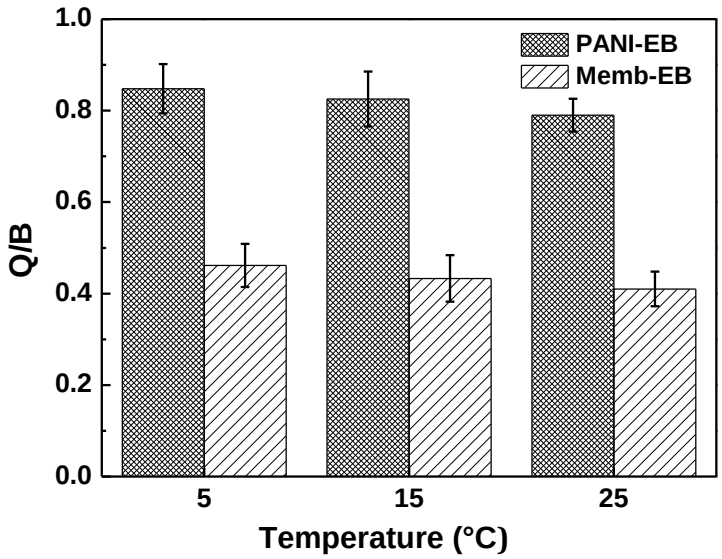

Fig. 5-5 (a) Q/B (oxidation degree) of the PANI-EB and Memb-EB samples.

For the case of Memb-EB samples a peak appeared at 1678 cm^{-1} that corresponds to the C=O vibration coming from NMP, indicating that the carboxylic groups in NMP are involved in the interaction. For Memb-EB system, a significant decrease was also found in the Q/B ratio when dissolving PANI-EB in NMP solvent to prepare Memb-EB. The decrease in the Q/B ratio of Memb-EB can be related with the suppression of Q units by the NMP that would lead to increase in the B units [226, 227]. This can also be confirmed by the huge intensity increase of peak at 1498 cm^{-1} (B units) in Memb-EB compared to the PANI-EB.

Table 5-3 Image J derived colour data of Memb-EB and Memb-ES.

Colour	Red	Green	Blue
Memb-EB-5	12.6	18.8	18.4
Memb-ES-5	11.4	20.0	20.9
Memb-EB-15	13.0	19.2	19.1
Memb-ES-15	11.5	19.4	18.7
Memb-EB-25	12.3	18.3	19.4
Memb-ES-25	11.1	20.0	19.1

The colour of PANI films is characteristic of the PANI oxidation state. With doping, the PANI membranes produced change colour from a purple bronze when undoped (EB) to dark green when doped (ES). Colour quantification of these states is in Table 5-3. The increase in green and decrease in red for all membranes irrespective of T_{poly} indicates that the membranes have been doped by acid, confirming the FTIR results. The doped membranes are therefore expected to be conductive.

5.3.3 Electrical Conductivity

Fig. 5-6 shows the electrical conductivity of doped PANI membranes as function of T_{poly}. It can be found that the membrane conductivity increased with increasing T_{poly}. Bhadra *et al*. reported that the electrical properties of PANI membrane could be influenced by four important factors including: oxidation state, doping degree and dopant type, crystallinity and molecular weight or chain length [66, 184]. The above mentioned UV-Vis and FTIR results indicate different extent of oxidation and molecular chain length of PANI-EB-5, PANI-EB-15 and PANI-EB-25. Theoretically electrical conductivity is very weakly dependent on the chain length of PANI [228]. In cases, when the charges hopping between different polymer chains are much faster in comparison with the life time of the charge on one chain, i.e. when the interchain transport happens more frequently than the intrachain one. In such cases, PANI would resemble an intermolecular conductor rather than an intramolecular one-dimensional conductor i.e. conjugated polymers (charge mobility along the chain). Thus, higher conductivity of PANI for higher T_{poly} is not because of the larger chain lengths but because the polymer backbone has a higher structural regularity, i.e. the counter-ions are distributed along the backbone in a more regular way, increasing the charge carrier mobility. Thus, from the conductivity results, higher T_{poly} was beneficial for the higher structural regularity of PANI-EB, leading to the increased electrical conductivity when formed in membranes.

The PANI-EB-5 with relative longer chain lengths and more interlinked structures formed at a lower T_{poly} is prone to forming a “compact coiled” conformation in the polymer solution with high concentration, which would restrict the electron delocalisation or hopping [229, 230].

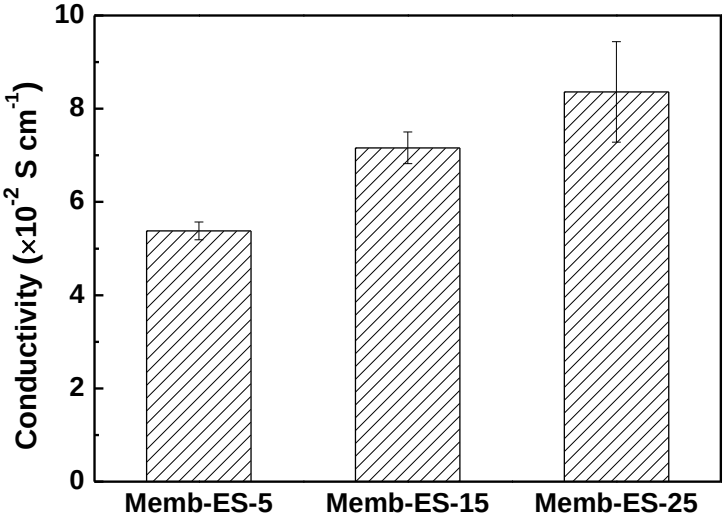

Fig. 5-6 Surface conductivity of Memb-ES.

5.3.4 PANI Membrane Robustness: Mechanical Strength and T_g

Table 5-4 shows both tensile strength and elongation at break of Memb-EB decreased with increasing T_{poly}. The decrease in tensile strength and % elongation can be attributed to the increased brittleness of the membranes. Mechanical properties are also closely related with the molecular weight of the polymer. Long chain polymers show improved mechanical properties compared to short chain polymers. Higher tensile strength and larger % elongation of Memb-EB is indicative of a higher molecular weight of PANI-EB prepared at low T_{poly}, which would have a higher degree of entanglement between the polymer chains, a higher weak bonding interaction (Van der Waal interactions etc.), a higher molecular compaction and consequently are more resistant to tensile stress[231].

When the PANI membranes are doped (Memb-ES), similar trends with increase in tensile strength and % elongation with T_{poly} are still apparent. However, the tensile strength and % elongation decreased even further after the membranes were doped with acid. This can be related to the changes in intermolecular reconfiguration of PANI backbone by acid dopant. In doped PANI membranes the polymer chain experiences significant steric hindrance to chain movement thus making the polymer structure more rigid. In addition, PANI membranes were prepared using NMP as solvent and it would not be surprising that these membranes still contain residual amounts of NMP. This residual NMP has a plasticising effect on the Memb-EB structure. On the other hand, doping of Memb-EB increases the free volume of the membranes thus removing the residual NMP

trapped in the empty pockets between polymer chains, making the membrane less flexible (plasticised) or more rigid.

Table 5-4 Mechanical properties of membranes.

Membrane	Overall membrane appearance	Tensile strength (MPa)	Elongation at break (%)
Memb-EB-5	Smooth surface	3.84±0.08	1.56±0.11
Memb-EB-15	Smooth surface	3.71±0.05	1.22±0.02
Memb-EB-25	Rough surface	3.43±0.02	1.04±0.06
Memb-ES-5	Smooth surface	2.59±0.01	1.20±0.10
Memb-ES-15	Smooth surface	2.98±0.03	1.09±0.24
Memb-ES-25	Rough surface	2.46±0.03	0.89±0.27

Table 5-5 gives the measured glass transition temperatures of membranes. The T_g of Memb-EB increased with the increasing T_{poly}, indicating that higher T_{poly} tend to increase the rigidity of the polymer chains, making membranes more brittle. This is consistent with the mechanical properties results.

Table 5-5 Glass transition temperatures of membranes.

Membrane	**Memb-EB-5**	**Memb-EB- 15**	**Memb-EB- 25**
T_g/°C	160	175	190

(Note: The Memb-ES got damaged before getting the T_g point.)

The combined results of Fig. 5-2, Table 5-4 and Table 5-5 illustrate that decreasing T_{poly} produces more robust PANI membranes with fewer defects and better mechanical (tensile strength) properties that are desirable in a membrane application. It has been shown previously in the Patterson group [6] and by other authors [77, 81, 87] that lower T_{poly} led to higher molecular weight of PANI. This produced PANI with longer polymer chains and more interlinked structures, with concomitant superior mechanical properties.

The reason for the poor mechanical properties of Memb-EB-25, could be the lower degree of entanglement between the polymer chains and insufficient adhesion to the backing layer. At lower T_{poly}, the improvement in mechanical properties is therefore likely due to the higher molecular weight PANI chains present, which entangle to a greater extent and has a higher weak bonding interaction (Van der

Waal interactions, *etc*.), a higher molecular compaction and consequently are more resistant to tensile stress [231].

Considering all of the above membrane characterisation results, it can be concluded that higher T_{poly} showed higher membrane conductivity, which would result in a more electrically tuneable membrane structure but with poorer mechanical properties. Furthermore, the membranes prepared from PANI polymerised at 25°C had significantly lower mechanical stability and were found to be too brittle to be used for useful filtration to be obtained (in the main due to cracking). Therefore, henceforth membranes synthesised from PANI polymerised at 5°C and 15°C only are now further characterised.

5.3.5 Initial Tuneability Assessment: Dynamic Droplet Penetration Analysis of Membranes

Dynamic droplet penetration analysis using a contact angle goniometer was used to characterise the solute permeation rate through the conducting PANI membrane. The tuneability was determined by the change in effective contact angle and droplet height over time without and with applied potential of 9 V. Fig. 5-7 shows the changes in effective contact angle and droplet height of Memb-ES-5 and Memb-ES-15 over time at 0 and 9 V of applied potential. As the pH of the doping solution can influence the contact angle measurements [196], all membranes were doped under same conditions.

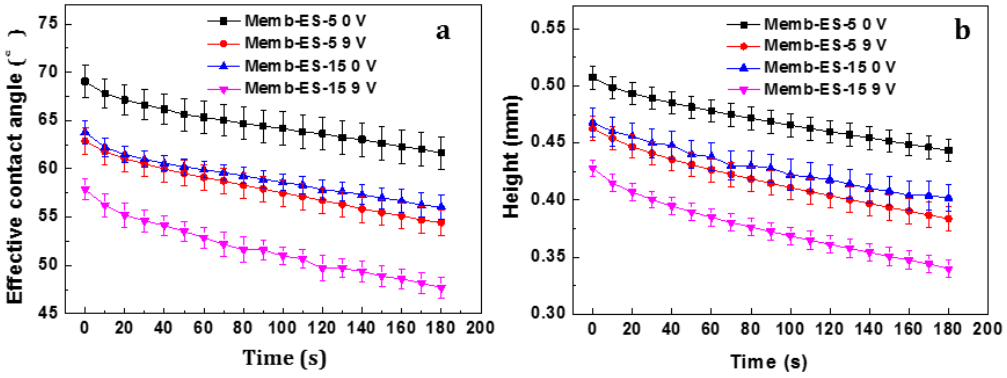

Fig. 5-7 (a) The effective contact angle and (b) droplet height change of Memb-ES over time with and without potential.

Memb-ES-5 shows a higher effective contact angle at a fixed time compared to the Memb-ES-15 (Fig. 5-7 (a)). The lower effective contact angle of water for Memb-ES-15 suggests that the wetting of the water on Memb-ES-15 surface is better

compared to Memb-ES-5. This may be indicative of relatively stronger intermolecular attractions between water and the Memb-ES-15 hydrophilic surface. These results are qualitatively consistent with the relatively higher conductivity of Memb-ES-15 (Fig. 5-6). The decreased effective contact angle and droplet height for membrane surfaces under applied potential can be related with the increased surface energy or polarity of the surface [232]. The applied potential altered the dynamic wetting behaviour of water on the conducting surface by increasing the charge transfer by hopping between the conducting domains [56, 233, 234].

The difference in overall rate of change of effective contact angle and droplet height with time between 0 and 9 V measurements gives a further quantitative indication of the electrical tuneability of the membranes. This shows that the applied potential has a significant effect on the surface energies of the membranes, with the rate of effective contact angle change from 4.1×10^{-2} θ s^{-1} to 4.7×10^{-2} θ s^{-1} for Memb-ES-5 and from 4.3×10^{-2} θ s^{-1} to 5.6×10^{-2} θ s^{-1} for Memb-ES-15 (Fig. 5-7 (a)). Moreover, the rate of change of droplet height increased from 3.6×10^{-4} mm s^{-1} to 4.4×10^{-4} mm s^{-1} for Memb-ES-5 and from 3.7×10^{-4} mm s^{-1} to 4.9×10^{-4} mm s^{-1} for Memb-ES-15 ((Fig. 5-7 (b)). This strongly indicates that the flux of a conducting PANI membrane can be tuned by applied electrical stimulus, with Memb-ES-15 being the most tuneable. The higher tuneability of Memb-ES-15 can be attributed to its higher electrical conductivity and optimal membrane morphology [6, 56, 235] and their relationship of the hypothesised tuneability of these membranes. Memb-ES-15 has a higher conductivity, which allows greater electron movement and creates a more hydrophilic membrane surface due to the greater mobility of charged ions in the membrane. In addition, the external potential could oxidise the conjugated structure and cause the movement of acid dopants, changing the dopants attachment or steric position in the polymer structure leading to a free volume change in membrane [236, 237]. Therefore, all three mechanisms of tuneability are potentially increased to a greater extent: surface charge controlling Donnan exclusion, change in pore size/free volume controlling pore flow transport, and chemical property changes controlling solution diffusion and volume swelling.

5.4 Electrical Tuneability of Flux and MWCO in Cross-flow Filtration

5.4.1 Increasing the Mechanical Robustness of PANI Membranes: Effect of Doping Time

The PANI-ES membranes characterised so far were sufficiently robust to handling and characterisation. However, it was found that the PANI-ES doped for 24 h were too brittle to survive the cross-flow testing. Therefore, the mechanical robustness of the membranes was examined to overcome this issue.

Doping time of the membrane is an important parameter to ensure the transformation of EB to ES form that could influence the performance properties of the PANI-ES membranes and so was explored to determine if this could be used to produce less brittle membranes. Currently, there is no clear information on this topic in the literature. In order to find an optimum doping time and to study the effect of doping time on PANI membranes, PANI-EB membranes (purple bronze colour) were doped with 1.0 M HCl for 2, 6 and 24 h to convert them into PANI-ES form (dark green colour). For this purpose, only Memb-ES-15 was studied at different doping times.

Mechanical testing was performed on Memb-ES-15 from the different doping times (Table A1, Appendix A). Memb-ES-15 with doping time of 2 h showed the highest tensile strength and Young's modulus. At higher doping times of 6 and 24 h, Memb-ES-15 showed similar tensile strength while lower Young's modulus for 24 h Memb-ES-15. In addition, the % elongation decreases as the doping time increases. All above mechanical properties showed that at longer doping times the membranes become more brittle compared to a shorter doping time of 2 h. To determine why this the chemical groups present (by FTIR) and conductivity were examined at different doping times.

Fig. A1 (Appendix A) shows the FTIR spectra of Memb-ES-15 as a function of different doping times. The FTIR spectra show no significant changes in the chemical structure of the PANI with doping time. Fig. A2 (Appendix A) shows the effect of doping time on the conductivity of Memb-ES-15. The membranes showed a similar conductivity for all doping times. This indicates that doping time does not affect the tuneability of the membranes (which is related to conductivity), but does effect mechanical properties. This may indicate that longer doping times

disrupt the inter-polymer interactions (perhaps decreasing entanglement) rather than changing the PANI itself.

The protonation of polyaniline doped by HCl is believed to give rise to a polaronic conduction band leading to a metallic state that enhances the conductivity of the PANI. The imine sites are believed to be protonated in preference, which gives the bipolaron form. However, this undergoes dissociation and proportionate to form a delocalised polaron lattice or polysemiquinone form. It has been reported that the protonation consists of both chemical and diffusion processes [238]. The chemical reaction occurs between the proton in the aqueous acidic solution and the nitrogen atom on the imine unit of the PANI chains to form a polysemiquinone. On the other hand, diffusion processes correspond to diffusion of proton and counter-ions from an aqueous acidic solution into the membrane. Wan *et al*. reported that the doping processes at the initial stage were controlled by a chemical reaction, whereas the doping processes at the later stage were dominated by a diffusion processes [238]. In addition, it was found that the protonation processes became independent of the doping time when doping time is over a critical doping time – this would be when the chemical reaction is complete and sufficient diffusion has taken place to the doping sites. In our particular case, we have thin film membranes which would allow swift diffusion – allowing the acid to affect the inter-polymer interactions (making the polymer more brittle) once doping has completed. Thus, it can be concluded that the doping time of 2 h is already over the critical doping time of PANI membranes by 1.0 M HCl solution.

Considering the mechanical property, electrical conductivity and FTIR results, it can be concluded that the doping time of 2 h is the best choice (not affecting key properties but making the membranes more mechanically robust) and therefore was selected as the minimum doping time for the membranes for used for cross-flow testing.

5.4.2 Membrane Electrical Tuneability under Cross-flow Filtration

The conductive Memb-ES-5 and Memb-ES-15, doped for only 2 h, were tested to determine the effect of T_{poly} on the membrane tuneability under pressure and flow conditions in electrically connected cross-flow cells.

Permeance changes with applied potential: An electrically neutral PEG mixture mixed with deionised water was used as feed and the change in flux and MWCO under applied potential was examined. Table 5-6 and Fig. 5-8 shows that the permeance with the PEGs slightly decreased and the current increased with the increased potential. The current and the permeance of Memb-ES-15 were always higher than that of Memb-ES-5. These results from PEG mixtures filtration also indicated that the membranes became tighter under applied potential. At the end of 30 V run, the permeance reduced by 24.8% for Memb-ES-5 and 30.8% for Memb-ES-15 (Table 5-6), slightly higher reduction compared to the water permeance. This may be related to slight membrane fouling.

Table 5-6 PEG mixtures permeance of membranes under applied potential.

Membrane	0 V	9 V	30 V
	Permeance (L m^{-2} h^{-1} bar^{-1})		
Memb-ES-5	4.0±0.4	3.4±0.5	2.8±0.2
Memb-ES-15	4.9±0.5	4.5±0.2	3.7±0.4

(Note: The first highest point was not included in the permeance calculation.)

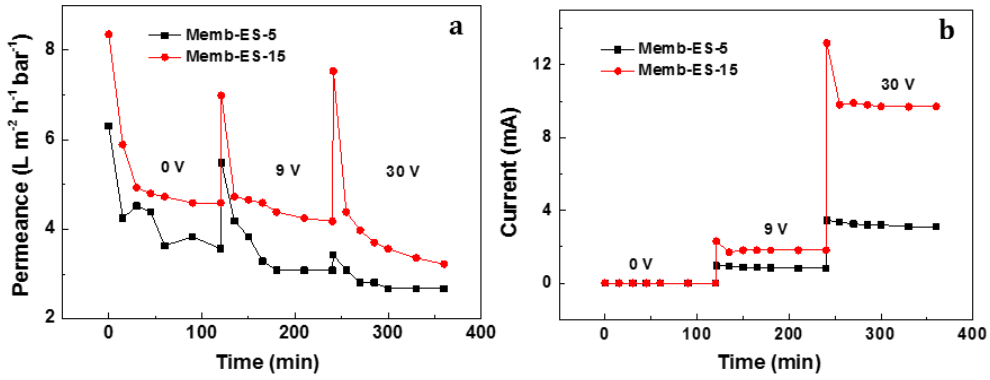

Fig. 5-8 (a) Permeance and (b) current of Memb-ES under applied potential from 0 to 30 V (20 bar, 25°C, PEG mixtures).

MWCO changes with applied potential: Table 5-7 summarises the overall MWCO results after 120 min filtration – the trend in MWCO at different voltages and filtration sample times can be seen in Fig. 5-9 and Fig. 5-10. It can be observed that a higher potential led to a lower MWCO of membranes. This indicates a tightening of the membrane leading to a reduced transport of high MW PEG oligomers through the membrane structure, concomitant with the decrease in permeance. Furthermore, Memb-ES-15 showed lower MWCO compared to

Memb-ES-5 under the same applied potential. This could again be related with the electrical conductivity of the membrane as the higher current passed though Memb-ES-15 than Memb-ES-5, leading to more significant MWCO change of Mem-ES-15. The potential mechanisms for this will be discussed below.

Table 5-7 MWCO change of membranes after filtration time of 120 min under applied potential.

Membrane	0 V	9 V	30 V
	MWCO (g mol^{-1})		
Memb-ES-5	>6,000	5,400±200	3,750±150
Memb-ES-15	>6,000	4,800±800	2,800±200

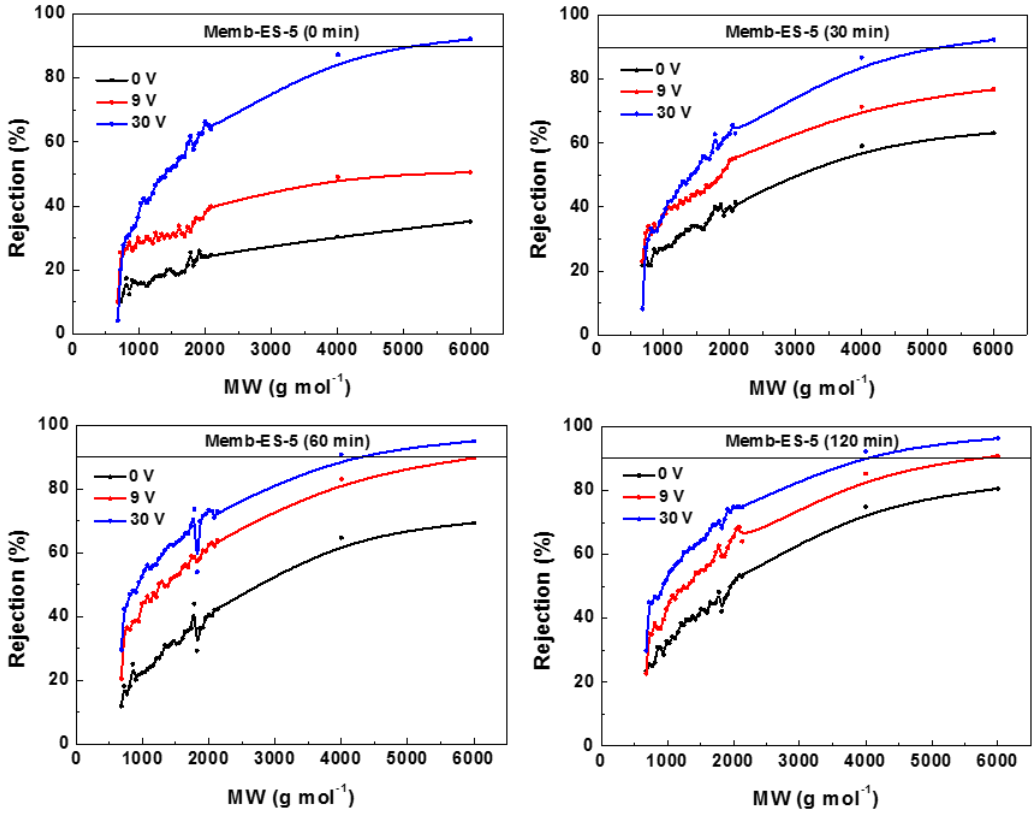

Fig. 5-9 The rejection of Memb-ES-5 in different filtration time (0, 30, 60 and 120 min) under applied potential of 0, 9 and 30 V (20 bar, 25℃, PEG mixtures).

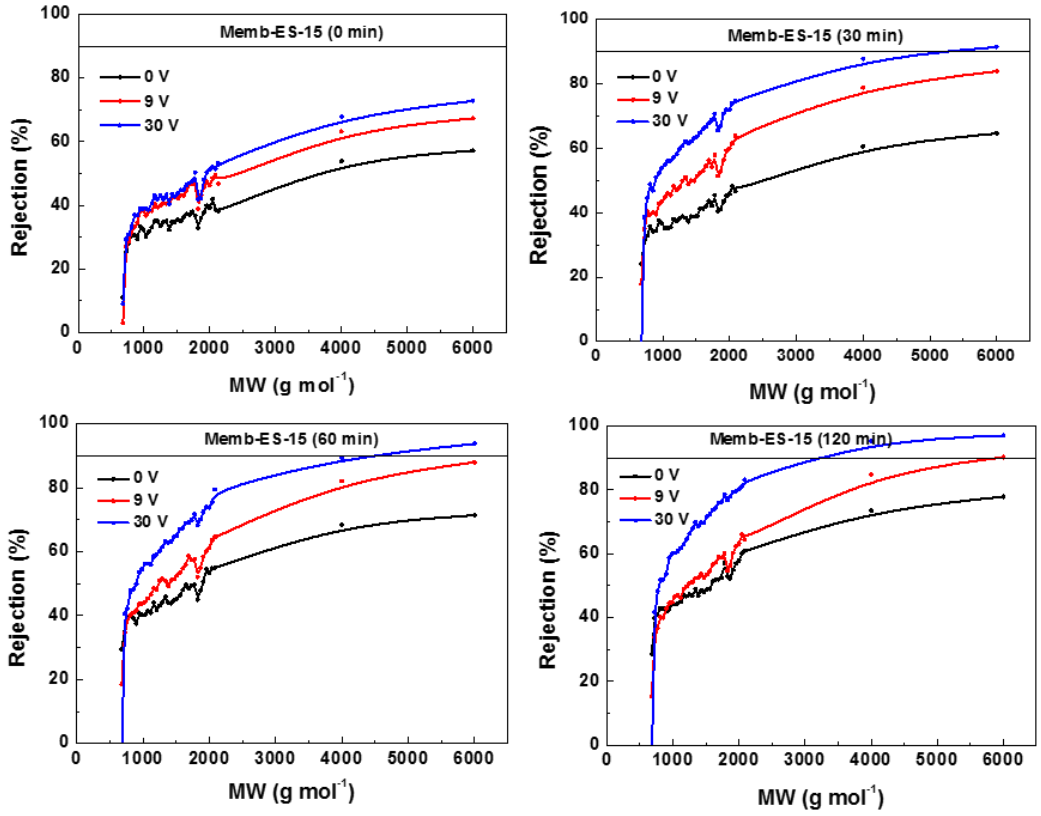

Fig. 5-10 The rejection of Memb-ES-15 in different filtration time (0, 30, 60 and 120 min) under applied potential of 0, 9 and 30 V (20 bar, 25℃, PEG mixtures).

Electrical tuneability membranes with pure water flux: Control experiments were undertaken using DI water as feed, and the permeance and current passing though the membranes under applied potential (from 0 and 30 V) were shown in Table 5-8 and Fig. 5-11. At the end of 30 V run, water permeance decreased by 17% for Memb-ES-5 and 22% for Memb-ES-15, compared to 0 V run. This shows that the water permeance also slightly decreases with the applied potential, again indicating that the membrane structure became tighter with higher applied electrical potential.

Table 5-8 Water permeance of membranes under applied potential.

Membrane	0 V	9 V	30 V
	Permeance (L m^{-2} h^{-1} bar^{-1})		
Memb-ES-5	5.57±0.30	5.05±0.44	4.61±0.60
Memb-ES-15	5.86±0.42	5.84±0.78	4.56±0.61

(Note: The first highest point was not included in the permeance calculation.)

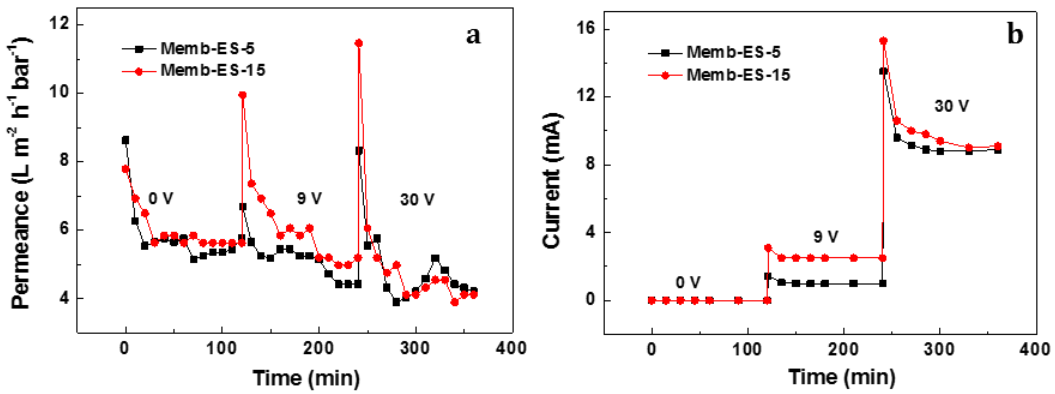

Fig. 5-11 (a) Water permeance (b) current of Memb-ES under applied potential from 0 to 30 V (20 bar, 25°C, DI water).

The current passing through the membrane significantly increased with the increased potential from 9 to 30 V. Memb-ES-15 showed higher current compared to Memb-ES-5 under the same applied potential, which can be explained by the higher electrical conductivity of Memb-ES-15. It was also found that the current of each run decreased significantly during the first 15 minutes attributed to membrane equilibration and leaching of some of the acid dopant. After that, the current became stable as the residue acid dopant kept membrane conductive. The FTIR, colour change results showed that the acid leached out from the membrane during the long time filtration (Fig. A3 and Table A2, Appendix A). Therefore, the membrane was redoped in HCl after each run. This is also the reason for the spikes in the current and permeance values at the start of each fixed electrical potential run. Fig. A4 and A5 (Appendix A) shows that the membrane permeance stays stable in time at a fixed electrical potential eliminating the effect of dopant leaching in time.

The permeance of Memb-ES-15 was always higher than that of Memb-ES-5 for both the PEG and DI water filtrations (which is also consistent with the dead-end filtration results without applied potential in Fig. A6 (Appendix A). This is therefore a membrane structural and native surface charge issue (since it is present without applied potential) and so can be explained by the presence of larger macrovoids and thinner membrane thickness of Memb-ES-15 (Fig. A7, Appendix A), leading to decreased membrane diffusion resistance during filtration. Membrane hydrophilicity also plays an important role on the water transport resistance as more hydrophilic membranes tend to have higher permeance. As

from contact angle results, we know that Memb-ES-15 showed relative higher hydrophilicity than Memb-ES-5, thus leading to lower water transport resistance and higher permeability.

5.4.3 MWCO and Flux Electrical Tuneability Mechanism

It has been shown through electrically stimulated cross-flow filtration that the permeance/flux and MWCO can be tightened with increasing applied voltage in these PANI MWCO membranes, which is best for the 15°C synthesised PANI. This leads to the question what allows this to be the best polymerisation conditions in this case and what mechanisms cause this filtration tuneability?

Zhou *et al*., studied the FTIR of dried PANI membranes and reported that external voltage could produce large average hopping energy, which allowed the charge transfer by hopping between the conducting domains during 0-75 V while the Joule heating effect (dopant displacement) resulted in the deprotonation of PANI at voltages from 75 to 175 V [239]. As the maximum potential applied in this study was much less than 75 V, we can eliminate the presence of joule heating effects (dopant displacement) and propose that membrane swelling is the dominant phenomenon in reducing the PANI membrane permeance. There is no published literature that discusses the effect of higher potential (above 1.2 V) on the chain structure and membrane morphology of PANI.

In this absence, we propose that high potential can cause the movement of acid dopants, changing the dopants attachment or steric position in the polymer structure that would slightly swell the polymer chains. Thus, reducing the free volume/pore size of the membrane and posing an extra resistance to water transport [236, 237]. Therefore, it is likely that change in membrane volume has a significant effect on the transport properties, however all three mechanisms of tuneability are potentially still having an effect here: surface charge controlling Donnan exclusion (which would interact with the dipole of the water), change in pore size/free volume controlling pore flow transport, and chemical property changes controlling solution diffusion and volume swelling. This is inconsistent with dynamic droplet penetration results, but it can be concluded that the decrease in contact angle and droplet height were because of increased wetting or

hydrophilicity of the membrane surface and not because of increased permeation rate through the membrane.

This work demonstrates that an optimal T_{poly} exists (here 15°C), which is related in part to the higher PANI molecular weight that lower T_{poly} should produce, and to a higher electrical conductivity from PANI synthesised at higher T_{poly}. It is clear that optimising the in-filtration electrical tuneability of flux and MWCO of HCl doped conductive polyaniline membranes will not be via increasing or decreasing one parameter to produce the most versatile electrically regulated separation changes. Instead, as in this study, a range of synthesis, doping and external stimulus parameters and factors will need to be simultaneously studied and optimised to fully understand, optimise and control the in-situ tuneable separation performance of these membranes. More work is underway to study and understand the detailed mechanism of PANI membrane transport under high applied potential and its effect on the dedoping behaviour, membrane solute transport and electrical resistance (impedance) during filtration and on the development of non-ideal joule heating effects.

5.5 Conclusions

The effect of T_{poly} of PANI on the membrane properties and their impact on the electrical tuneability of flux and MWCO during cross-flow filtration were investigated in this paper. PANI was synthesised via chemical oxidative polymerisation at three different T_{Poly} (5°C, 15°C and 25°C) and flat sheet membranes were prepared using NIPS technique. T_{poly} was found to influence the molecular structure, morphology, thermal, mechanical and electrical properties of PANI membranes. The results showed that the lower T_{poly} of 5°C and 15°C formed membranes with improved mechanical properties, relatively lower electrical conductivity and fewer macrovoids. While the higher T_{Poly} (25°C) produced membranes with highest electrical conductivity but rough surface, relatively brittle membranes with lower tensile strength, which could not be used in the pressure driven filtration experiments.

The trans-membrane flux and MWCO of PANI membranes were measured for neutrally charged PEG feed solutions as a function of the applied potential from 0 to 30 V. The doped PANI membranes showed the highest MWCO (< 6000 g mol^{-1} at zero applied potential), irrespective of T_{poly}. These membranes showed a

decrease in permeance and MWCO under the applied potential in the PEG cross-flow filtrations, with Memb-ES-15 showing the greatest decrease, in permeance (30.8 %) and MWCO (down to 2800 g mol^{-1}) at 30 V compared to 0 V. This may be attributed to movement of acid dopants or dopants steric position in the polymer structure that would slightly swell the polymer chains. The greater tuneability was found to be related to the membranes with relatively higher electrical conductivity. Considering the mechanical robustness, membrane performance and electrical membrane tuneability, Memb-ES-15 provided the best performance compared to other two membranes, Memb-ES-5 and Memb-ES-25.

This work demonstrates that the polymerisation conditions producing PANI need to be carefully controlled in order to optimise the properties affecting the in-filtration electrical tuneability of flux and MWCO of HCl doped conductive polyaniline membranes produced from them.

6 A Higher Resolution One-filtration MWCO Method for Aqueous Based NF and UF Membranes Using PEGs

6.1 Introduction

Pressure driven membrane separations have been widely applied in many industries as they enable separations to become more energy efficient and environmental friendly [201, 202]. It is of great importance to understand the membrane transport properties and separation ability when using a commercial membrane or developing a new membrane. The MWCO of a membrane is defined as the molecular weight (MW; also known as molecular mass) value where a 90% rejection of the filtered solutes through the membrane is obtained. It is a universally applied parameter to evaluate and benchmark membrane selection properties [240]. A reliable technique for measuring MWCO values is crucial to provide an indication of the potential selectivity for end users to make an appropriate choice of membrane in order to buy, test and apply over the wide range of applications, solvents and solutes that are wanted for a particular membrane [31, 241].

A range of methods and MWCO molecular probes are currently used, including styrene oligomers [7, 31, 94], PEGs [201, 242-244], dextrans [245-250], alkanes [251, 252], sugars [253, 254], dyes[255], acids [243], and others [254, 256-258]. These existing methods, however, have several limitations:

(1) The detection of multiple compounds in a single filtration is difficult to accomplish, thus most of the methods require multiple and repetitive test filtrations of individual solutes to obtain the MWCO curve, which is both time consuming and costly compared to a single filtration method [31, 201, 258, 259].

(2) In terms of the available MWCO molecular probes, pure alkanes and dextrans are only commercially available with MW of below 400 g mol^{-1} and above 1000 g mol^{-1}, respectively. Styrene oligomers are expensive in comparison to all other molecules used and therefore this limits their application at a larger scale. Dyes are mainly charged molecules and therefore will also potentially be rejected by Donnan Exclusion, which does not reflect the MW (size/mass) based separation that MWCO should primarily reflect. Furthermore, it is not easy to source a suitable variety of dyes with similar molecular structures and that have a similar interaction with the membrane. Other solutes, like alkane and polypropylene

glycol, have limited solubility in water, especially at higher MWs, which limits their use [202, 255].

(3) Some of the methods are for organic solvent based separations and limited to the nanofiltration (NF: 200-2000 g mol^{-1}) range and, due to limited water solubility of the probe, cannot be directly employed in aqueous systems [31, 201, 259]. For aqueous systems, many of the methods that have been developed only have a limited range of MWs that can be probed, with many mainly focused on the NF range [202, 260, 261]. This limits the potential membranes that can be screened and characterised, for example low MWCO ultrafiltration membranes have attracted considerable attention as they are widely used in oil/organic solvent separation [262], food industry for sweeteners purification [189], metal ions removal [263] and drinking water treatment [264]. Moreover, when a new membrane is synthesised and the MWCO is unknown, a method that allows a wide range of MWs to be tested with relative precision and resolution would allow a faster characterisation time, which in turn provides faster feedback in order to speed up development time – something needed for high throughput synthesis of membranes, for example [265]. Consequently, it is of importance to develop an approach for the MWCO determination of both NF and low UF membranes over the widest possible MW range with the highest possible resolution between adjacent MWs.

Therefore, this research aims to develop a reliable, cost effective, high resolution, single filtration MWCO evaluation method covering a wider MW range than any other MWCO method for aqueous based NF and low MWCO UF membranes.

6.2 HPLC-ELSD Characterisation of the Single PEG and PEG Mixtures

Each of commercial PEGs from PEG 1000 to 6000 was run using HPLC-ELSD to separate peaks. Higher MW PEG oligomers displayed longer retention times. This can be explained by the separation mechanism based on the competition between the solubility of PEG oligomers in the mobile phase and the selective adsorption on the C18 column [202]. Higher MW PEGs with longer non-polar chains tended to be retained in the C18 column, thus prolonging the elution time. Fig. 6-1 shows that the HPLC method could separate the individual oligomers in each commercial PEG mixture apart from PEG 6000. Therefore, the method gave finely resolved PEG oligomer peaks from PEG 1000 to 3000 with straight and stable baselines. The peaks of PEG 4000 were also well separated although a level baseline could

not be achieved. The unseparated PEG 6000 oligomers were eluted separately and so was regarded as one peak representing an average MW of 6000 g mol^{-1}. This new method presents a significant improvement on baseline stability and the wide range of MW oligomers resolved and identifiable compared to previous methods [201, 202].

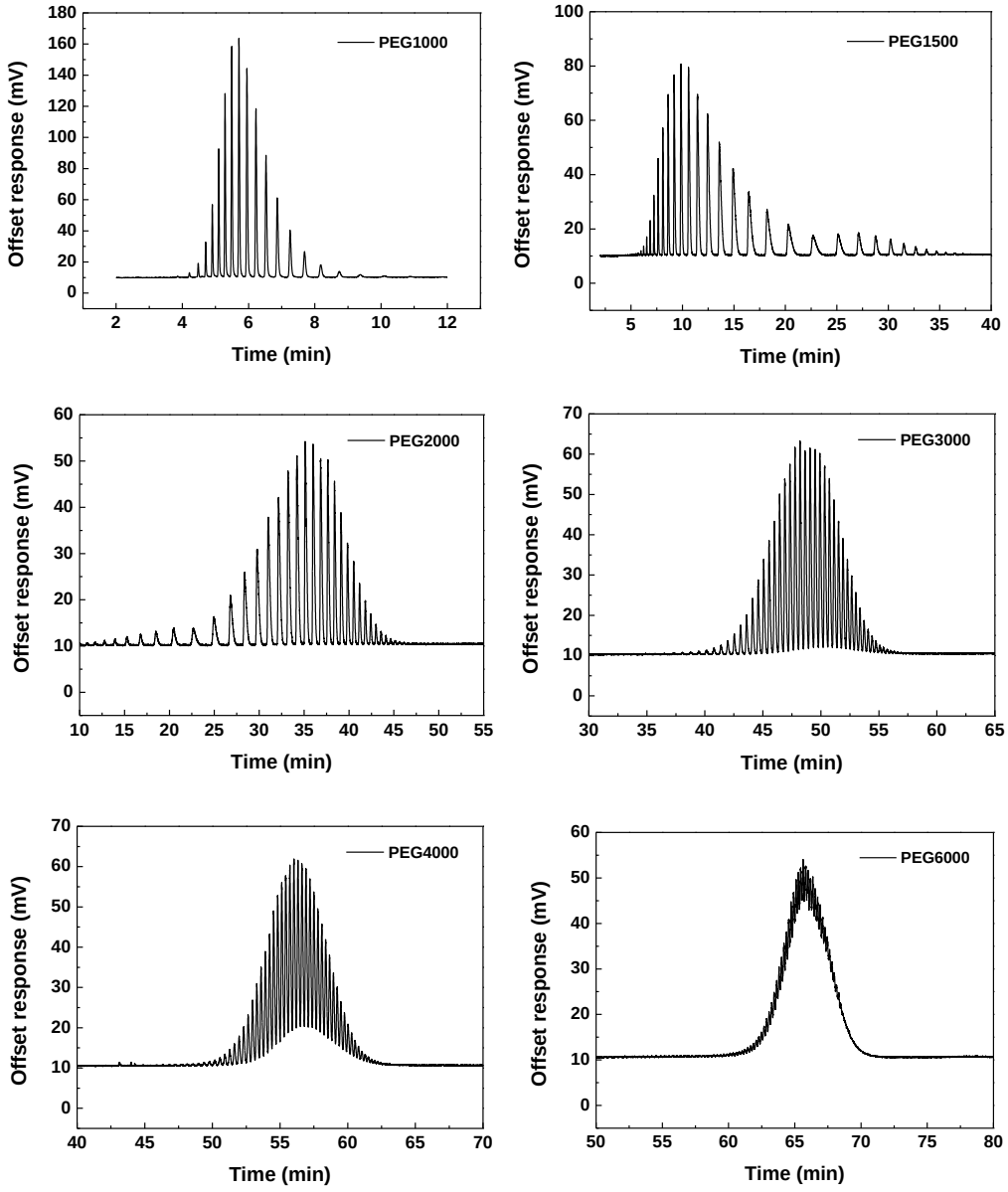

Fig. 6-1 HPLC-ELSD characterisation of the single PEGs from 1000 to 6000 g mol^{-1}.

When all of these commercial PEGs are mixed together and a sample run using HPLC method, the individual peaks could still be resolved with a clear and stable baseline, as shown in Fig. 6-2. Varying the concentration of the PEG mixture (for calibration curves – see Fig. B1 in Appendix B), it was found that the peak area increased with increased mixture concentration without losing the baseline resolution. It can therefore be concluded that the employed ELSD was applicable for practical analysis of PEG mixtures.

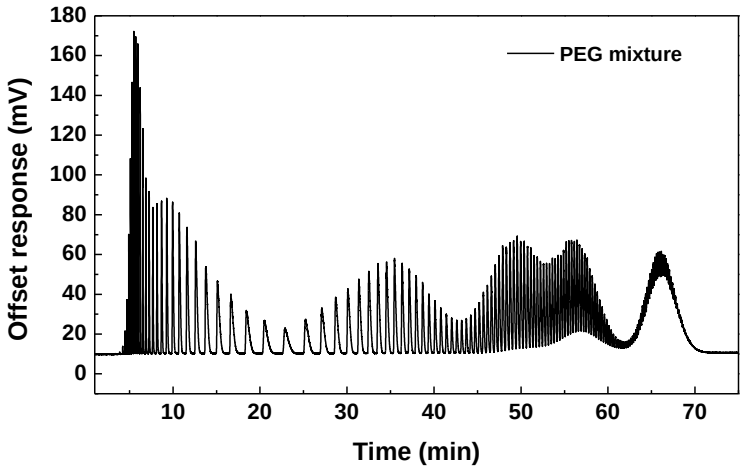

Fig. 6-2 The oligomer peak separation and detection in the PEG mixture (400 mg L^{-1} for PEG 1000 and 1600 mg L^{-1} for PEG 1500-6000) by the developed HPLC-ELSD method.

6.3 Identification of Individual PEG Oligomers

A purer PEG 1000 standard was used to positively identify peaks within the PEG mixture. In the PEG 1000 standard chromatogram, four consecutive peaks with retention time of 5.73, 5.98, 6.25 and 6.57 min displayed the first four highest peaks (Table B1 in Appendix B). The supplier declared M_n range of the purer PEG 1000 standard was 950 to 1050 g·mol^{-1}, which therefore identified these four peaks as corresponding to PEG oligomers with MWs of 942, 986, 1030 and 1074 g·mol^{-1}. In the PEG mixture, the four closest corresponding peaks (with retention times of 5.71, 5.96, 6.23 and 6.53 min) were assigned these MWs (Table B1 and B2 in Appendix B).

In order to further guide the MW identification of each peak, the highest response peaks from each individual commercial grade PEG (PEG 1000-6000) were identified in the HPLC chromatogram of the PEG mixture as shown in Fig. 6-3. This highest peak will approximately correspond to the PEG oligomer MW that is closest to the average MW (M_n) of commercial grade PEGs given by the manufacturer. Although this does not give a direct identification of the oligomers MWs (since there are no pure PEG oligomers with MW of 1000, 1500, 2000, 3000, 4000 and 6000 g mol^{-1}), this method however does help guide the assignment of the peaks to those close to that MW [202].

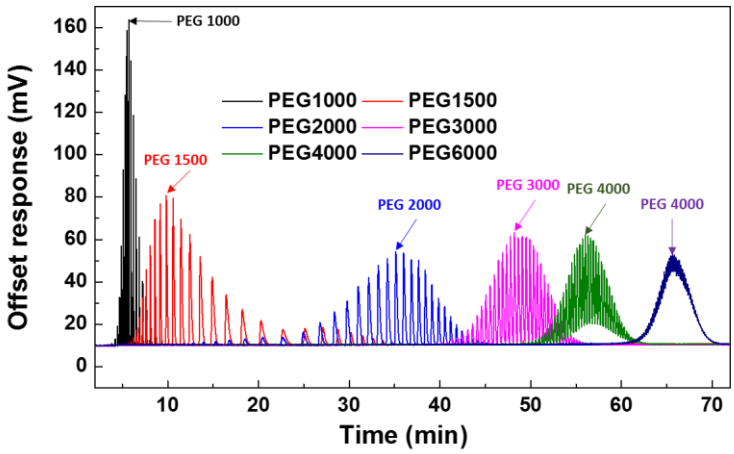

Fig. 6-3 The oligomer peaks of each single commercial grade PEGs (400 mg L^{-1} for PEG 1000 and 1600 mg L^{-1} for PEG 1500-6000).

Using the four identified peaks as a starting point, the remaining MWs were assigned by adding the 44 g mol^{-1} difference above and below to each oligomer peak (which is the MW associated to the repeating structural unit of CH_2-O-CH_2 in the PEG). The average MW of the commercial grade PEGs (as per Fig. 6-3) was then used as a confirmation that this process yielded accurate peak MW assignment – there was good correspondence between the peak MW expected at these highest peaks within the assignment process indicating that the peak MW assignment was accurate (as summarised in Table 6-1). Fig. 6-4 summarises the identified and assigned MWs of each peak in the PEG mixture.

Table 6-1 Summary of the retention time and peaks with the identified molecular weight.

Retention time of the highest peak (min)	**5.96±0.02**	**11.53±0.10**	**35.29±0.25**	**48.25±0.077**	**56.08±0.071**	**65.88±0.35**
Commercial PEGs M_n from suppliers (g mol^{-1})	950-1050	1450-1500	1800-2200	3000	3600-4400	5400-6600
Finalized PEG mixture oligomers' MW (g mol^{-1})	986	1470	2174	3142	4110	6000

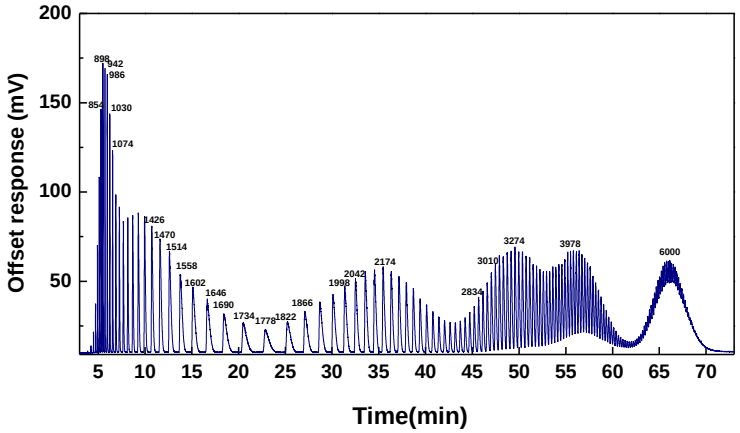

Fig. 6-4 Identification of individual PEG oligomers mixture from 678 to 6000 g mol^{-1}.

6.4 Obtaining Calibration Curves

As discussed in Section 4.8.10, the PEG mixture concentration used for the calibration curve covered a broad range from 75-1200 mg L^{-1} for PEG 1000 and 300-4800 mg L^{-1} for PEG 1500 to 6000. Based on this, different mixture concentrations were analysed to establish a set of external calibrations for each PEG oligomer. One complication identified is shown in Fig. 6-3, where some peaks from oligomers were present in two adjacent commercial PEGs from PEG 1000 to PEG 4000. These peaks are called "crossover" or "combined" peaks, whose peak area is a combination of the concentration of that oligomer in both adjacent commercial PEGs in the mixture. The "crossover" peaks have been mentioned in a previous study in this research group [202]: the equations and methods to deal with them have been directly adopted from this work. Consequently, the equations used in this study are listed in Equation B1 and B2 in the Appendix B. Using all of this information and procedures, a calibration curve for each PEG oligomer was established – detailed information is presented in Fig. B1 in Appendix B.

Generally, a linear response between peak area and concentration is preferable for routine quantitation of concentration [204]. In this study, a linear relationship could be obtained for all the PEG oligomers with the correlation coefficients (R^2) 0.98 and above. However, it is noticeable that the response became slightly non-linear at lower concentrations, especially for higher MW PEG oligomers. MWCO curves are a plot of rejection (Equation 4.5) vs MW. So, despite a high R^2, extensive testing and comparison of predicted MWCO to expected MWCO of commercial membranes (work not presented) has shown that the difference between the correlations at the lower concentrations (i.e. permeate concentration in Equation 4.5 and higher concentrations (i.e. feed concentration in Equation 4.5 in for these PEG oligomers can lead to over or under prediction of the rejections and therefore the MWCO. Therefore, to ensure the rejection of each MW PEG oligomer is calculated from an equivalent part of the calibration curves it is recommended that the feed and permeate concentration used come from the same section of the calibration curve. To ensure this, calibration curves are divided into two ranges: the high concentration range and low concentration range (Fig. 6-5). The range to use in the rejection calculation for a particular membrane is decided by comparing

the overall ELSD response of the permeate with that of the feed. If the membrane rejects much of the PEG mixture, resulting in a permeate ESLD response that is approximately below 1/3 of the feed ELSD response (for ease, this can be qualitatively assessed by comparing the resulting HPLC chromatograms of the ELSD response), it is considered to be part of the low concentration range. In this case, the feed needs to be diluted to be closer to the permeate concentration to avoid calibration error. Otherwise, if the permeate response is within a similar concentration range to the feed (i.e. in the high concentration range in Fig. 6-5, the response from both can be used directly without need for feed dilution.

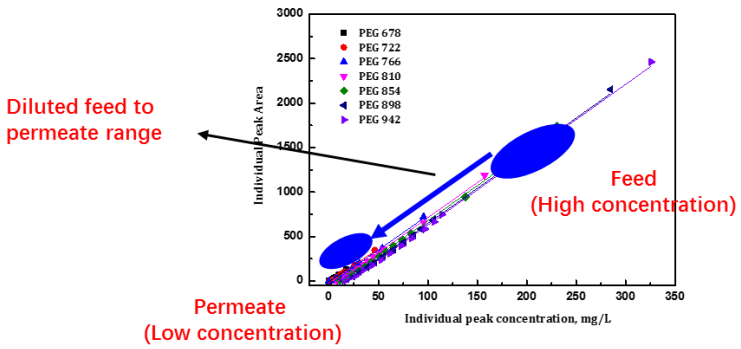

Fig. 6-5 Example of the two ranges of concentration that need to be considered to minimise rejection calculation error: high concentration range and low concentration range. Feed samples must be diluted to within the permeate concentration range if the ELSD response is approximately more than 2/3 higher than the permeate response.

6.5 Determination of MWCO in Commercial Membranes

Commercial membranes were characterised to benchmark the MWCO using the developed PEG method. An example of the HPLC chromatograms of the feed, permeate and retentate samples that are obtained for a membrane (a GE Osmonics™ GH) that is within the MWCO range of the method are given in Fig. 6-6. The resulting HPLC chromatograms from all of the other commercial membranes are given in Fig. B2-B7 in Appendix B. For all, the ELSD response of permeate was always lower than that of the feed and the ELSD response for the retentate was always higher than that of the feed, suggesting the membrane separation was as expected. The permeate ELSD response for the GE Osmonics™ GE and GH, Millipore Ultracel PLAC04310 and PLBC04310 were all lower than 1/3 of the feed ELSD response, therefore for these the feed was diluted into the permeate range for the rejection calculations for the MWCO curves. The permeate

of GE Osmonics™ GK exhibited an ELSD response of more than 1/3 of feed, and so the feed response was directly used for the rejection calculation without dilution.

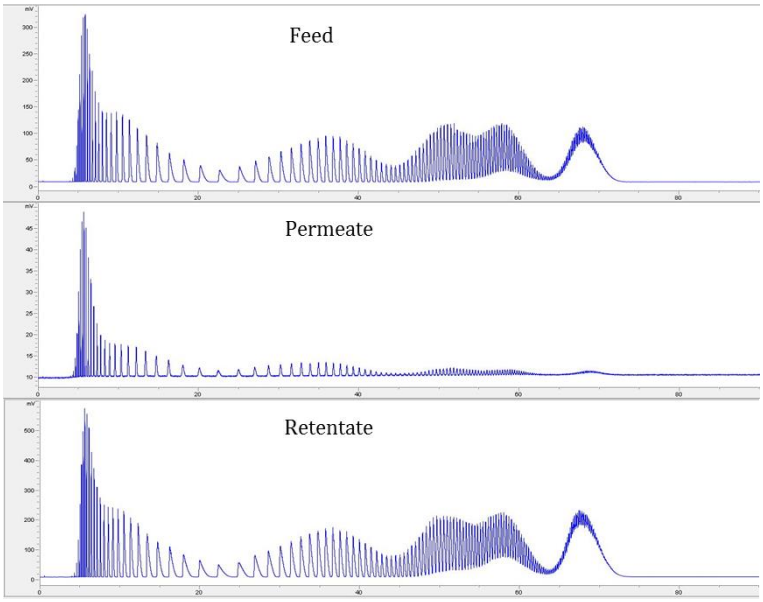

Fig. 6-6 HPLC chromatograms of feed, permeate and retentate from GE Osmonics™ GH.

The permeance of the membranes with pure water and the PEG mixture (Table 6-2) differed slightly, indicating that for the concentrations used there may be some unavoidable concentration polarisation, which is likely inevitable when using a mixture of soluble polymers with NF/low UF membranes.

Rejection of each of the PEG oligomers as a function of the corresponding MW were plotted to give MWCO curves for each of the membranes as shown in Fig. 6-7. The MWCO from these were compared to the information provided by the manufacturer and in literature (Table 6-2). Table 6-2 shows that five of the six membranes tested (GE Osmonics™ GE, GK and GH; Millipore Ultracel PLAC04310 and PLBC04310) gave MWCOs that are in good agreement with the manufacturers values – all of which will have been determined using a different MWCO analysis than this. This indicates that this MWCO method is robust and accurate for most membranes.

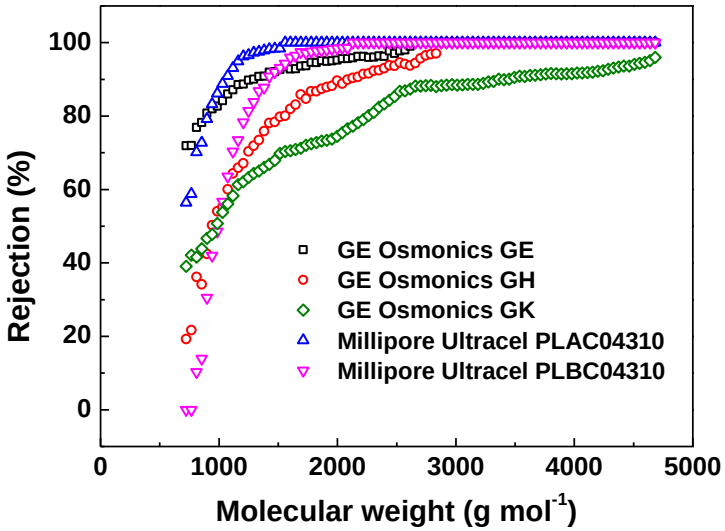

Fig. 6-7 MWCO curves of commercial membranes using the HPLC-ELSD method.

However, what about the one membrane that deviated? The TriSep UA60 membrane gave a zero ELSD response for all permeate samples, with the retentate giving the strongest ELSD response of the six commercial membranes. This indicates a 100% rejection of all MWs in the PEG mixture, with the TriSep UA60 therefore having a MWCO lower than 678 g mol^{-1} (the lowest MW PEG oligomer in the method). This is unexpected, since the MWCO according to the manufacturer is expected to be 1000-3500 g mol^{-1}. Therefore, Rose Bengal was also used to determine the membrane rejection and the permeate was colourless (Fig. B8 in Appendix B). A high rejection indicated that the MWCO of TriSep UV60 is less than 974 g mol^{-1} (the MW of Rose Bengal) confirming this result. Based on these two separate and different MWCO tests, it is assumed that the MWCO of the TriSep UA60 stated by the manufacturer is incorrect for the membranes supplied. It is recommended that the manufacturer retest their membrane MWCO, perhaps using the method in this work.

Therefore, overall these results confirm that the newly developed one-filtration PEG method is accurate and comparable to MWCO determined by other methods used by membrane manufacturers. Moreover, this new method gives the widest MWCO range with the highest resolution for aqueous based membranes in a single filtration so far, and so it is recommended that it could be adopted as the new standard MWCO test for NF and low UF membranes for aqueous based separations.

Table 6-2 Membrane separation properties (Permeance and MWCO) of different commercial membranes obtained using the methods outlined in this paper compared with MWCO from the membrane manufacturers.

Membrane type	**Permeance in water ($L\ m^{-2}\ h^{-1}\ bar^{-1}$)**	**Permeance in PEG ($L\ m^{-2}\ h^{-1}\ bar^{-1}$)**	**Permeance in water supplied by manufacturer ($L\ m^{-2}\ h^{-1}\ bar^{-1}$)**	**MWCO measured ($g{\cdot}mol^{-1}$)**	**Nominal MWCO range ($g{\cdot}mol^{-1}$)**
GE Osmonics™ GE	1.9±0.1	1.1±0.1	1.1	1294±20	1000 [186, 187]
GE Osmonics™ GH	3.2±0.2	1.7±0.1	3.3	1866±373	1000-2500 [186, 188-190]
GE Osmonics™ GK	9.3±1.0	5.6±0.5	5.7	3956±716	2000-3500 [186, 188, 189, 191]
TriSep UA60	9.4±0.7	5.1±0.4	7.9	<678	1000-3500 [192]
Millipore Ultracel PLAC04310	2.5±0.1	2.0±0.02	---	1030±62	1000 [193]
Millipore Ultracel PLBC04310	7.0±0.7	4.6±0.4	---	1404±31	1000-3000* [194, 195]

***** Manufacturer states a MWCO of 3000 but notes that the MWCO could be 2-3 times smaller than the molecular weight of the solute to be retained when using regenerated cellulose.

6.6 Conclusions

A reliable, cost effective, single filtration method for evaluating the MWCO of aqueous based NF and low MWCO UF membranes has been developed. This method covered the MW range from 678 to 4594 g mol^{-1} with a difference of just 44 g mol^{-1} and further extended to 6000 g mol^{-1}. Utilising the HPLC-ELSD technique allows a single filtration of individual PEG oligomers and can be easily run to characterise the MWCO of membranes. MWCO determination of five commercial membranes from GE Osmonics™ and Millipore showed good agreement with manufacturer and literature values, confirming the accuracy of the method. The MWCO for a TriSep UA60 membrane was lower than that stated by the manufacturer (< 678 g mol^{-1}), however a rejection test with Rose Bengal (MW of 974 g mol^{-1}) indicates that it may be that the MWCO of the supplied membranes is in fact incorrect. It is recommended that the manufacturer retests their membrane MWCO, perhaps using the method in this work.

Consequently, this work is a significant extension to the MWCO method arsenal, with the single filtration MWCO range significantly extended from 678 to 4594 g mol^{-1} with a MW difference of just 44 g mol^{-1} and an additional MW at 6000 g mol^{-1}. This new method therefore gives the widest MWCO range with the highest resolution for aqueous based membranes in a single filtration so far.

7 Fabrication and Characterisation of Stimulating Responsive PAs Doped PANI Membranes

7.1 Introduction

In Chapter 5, it was found that applying an electrical potential across HCl doped PANI membranes (Memb-HCl) changed the interaction between HCl and PANI, thereby changed the membrane properties allowing membrane selectivity and permeability to be tuned. However, two main problems exist in the small acid doped PANI membranes: (i) the acids used for doping PANI membranes leach out from the membrane during filtration, leading to decreased conductivity; (ii) small acid doped membranes are brittle and severely limit the successful utilisation in real filtration systems [9, 11, 13, 150].

To overcome these two challenges, various PAs have been used as dopants, including poly(2-acrylamido-2-methyl-1-propanesulfonic acid) (PAMPSA) [152, 153], poly(acrylic acid) (PAAc) [8, 13, 108], poly(methyl vinyl ether-alt-maleic acid) (PMVEA) [10], poly(styrenesulfonic acid) (PSSA) [9, 16], poly(amic acid) [15, 154, 155], poly(vinylphosphonic acid) (PVA) [156, 157] and polyamidosulfonic acid [152, 158]. PAs enable the formation of a double-stranded structure with PANI due to the strong intermolecular interactions between them. In comparison with small acids which only form a single-stranded structure with PANI, the double-stranded structure can reduce acids leaching and display good stability of the conductive state [14]. In addition, PAs can be expected to improve the flexibility and mechanical properties of PANI membranes, making these membranes easy to be handled and used [9, 266]. As mentioned in Section 2.4.4, chemical oxidation of aniline whereby PAs serve as templates is one of the most common ways to incorporate PAs into PANI structure. This approach ensures the binding of PAs into PANI to obtain PAs doped PANI complexes.

Acids doped PANI membranes have been conventionally prepared by different approaches, such as blending undoped PANI powder with acids before membrane fabrication, adding acids in the casting solution during membrane preparation and secondary doping with acids after membrane preparation [8, 85, 92-94, 108, 150]. The methods, such as blending undoped PANI powder with acids and secondary doping need to firstly dedope emeraldine salt (PANI-ES) by ammonia and then redope emeraldine base (PANI-EB) by the desired acids. Such methods are time

consuming and complicated. Adding acids in the casting solution during membrane preparation generally produces a membrane with disordered polymer packing and random distribution of acids [88].

To overcome these issues, in this chapter, a new membrane preparation method to prepare polymer acid doped membranes is proposed. PANI-PA complexes are firstly prepared by chemical oxidation of aniline on the templates of PAs which are directly used as the membrane materials. In contrast to blending undoped PANI powder with acids and secondary doping, the new developed approach could eliminate the subsequent dedoping and redoping processes. Compared with adding acids in the casting solution, the proposed method is expected to grow polyaniline along the acids template and produces more ordered packing of the PANI-PA structure [176].

Therefore, the aims of this chapter are to:

- Design a feasible route to fabricate PAs doped PANI membrane by incorporating different PAs during the PANI synthesis.
- Investigate the properties (chemical, electrical, physical and mechanical) of PAs doped PANI membranes as well as the in-situ tuneable separation performance under applied potential.

Four types of polymer acids were employed in the preparation of PA-doped PANI membranes, namely PAMPSA, PSSA, PAAc and PMVEA. Their properties are given in Table 7-1.

Table 7-1 The properties of polymer acids.

Polymer acids	Chemical structure	MW (g mol^{-1})	Physical form	pH (0.1 M)
PAMPSA	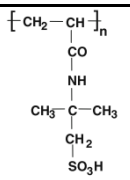	800, 000	10 wt% in water	2.0±0.1
PSSA	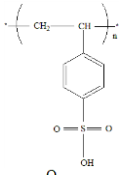	75, 000	18 wt% in water	1.4±0.1
PAAc	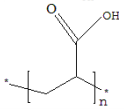	450, 000	powder	2.5±0.1
PMVEA	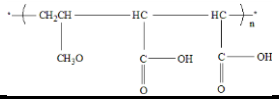	80, 000	powder	2.9±0.1

The properties of the PANI-PA complexes and their membranes were investigated by means of FTIR, SEM, four-point probe conductivity meter, dynamic contact angle goniometry. The membrane filtration performance (permeance and rejection) was characterised by dead-end filtration. A bespoke in house cross-flow filtration rig with external conductive probes in contact with the surface of the membrane was used to investigate the membrane tuneability by external voltage under industrially relevant membrane filtration conditions.

7.2 PANI-PA Complex Powder Properties

7.2.1 Morphology of PANI-PA Complexes Powders

Fig. 7-1 shows the FESEM images of PANI-PA complexes obtained from the chemical oxidation of aniline in the presence of PAs. Incorporation of polymer acids into the PANI structure resulted in different morphologies which were unique to each type of PANI-PA complex. In particular, the PANI-PAMPSA complex (Fig. 7-1 (a)) produced a fibrous network with good adhesion to PANI, which may be due to the formation of hydrogen bonding between the –NH groups of PAMPSA with the unsaturated nitrogen atoms of PANI (–NH···N=) [12]. PANI-PSSA (Fig. 7-1 (b)) showed the largest particle size compared to the other PANI-PA. It was reported that the size of PANI-PA complex could be controlled by the acidity of solutions and a stronger acid generally led to a larger size [267]. PSSA

with sulfonic acid groups was a stronger acid than PAAc and PMVEA with carboxylic acid groups, and thus resulting in a larger particle size [10].

PANI-PAAc (Fig. 7-1 (c)) showed uneven particle sizes with loose structures, likely due to the irregular aggregation of aniline on the PAAc template. During the chemical oxidation of aniline on the template of polymer acids, aniline interacted with polymer acids to form aniline-PA complex by the ionic attractions between positively charged anilinium and negatively charged counter ions. The oxidant ammonium persulfate attacked the aniline to initiate the polymerisation. PAAc with weak negatively charged ions formed weak ionic interactions between acid groups and aniline, thereby leading to the loose anchoring of PANI on the PAAc template [268]. PANI-PMVEA (Fig. 7-1 (d)) showed a uniform globular morphology and a much more intense and compact structure than undoped PANI (PANI-EB) (Fig. 7-1 (e)). The reason is that PMVEA created templates for the polymerisation of aniline and formed new nucleation sites for PANI deposition [12]. It was observed in the experiment that the PANI-PA complexes with sulphonic acids groups were harder to grind and much more rigid than PANI-PA complexes with carboxylic acids groups, which may be due to the stronger interaction between the sulphonic acids and conjugated structure of PANI. The different morphologies formed by the incorporation of different PAs are expected to bring novel properties to the membrane materials.

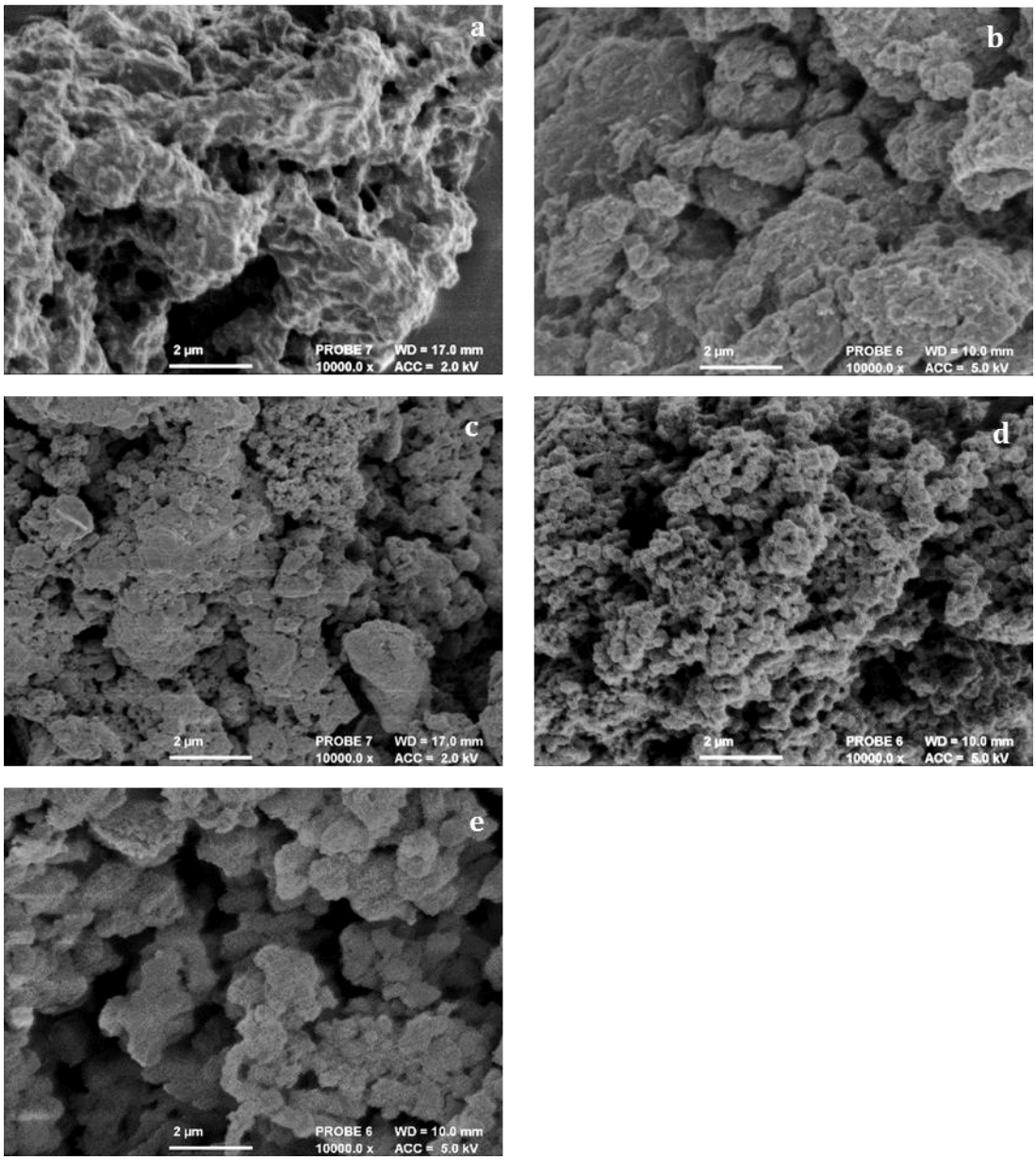

Fig. 7-1 FESEM of PANI-PA complexes (a) PANI-PAMPSA, (b) PANI-PSSA, (c) PANI-PAAc, (d) PANI-PMVEA and (e) undoped PANI (for comparison).

The elemental compositions of the PANI-PA complexes were determined using EDS analysis as shown in Fig. 7-2. All PANI-PA complexes possessed a much higher O content compared with PANI-EB as a result of the incorporation of the sulfonic acid and carboxylic acid groups, confirming the incorporation of polymer acids into the PANI structure. PANI-PAMPSA and PAN-PSSA also showed higher S content due to the incorporation of sulfonic acid groups. PANI-PSSA showed higher C content compared with other PANI-PA complexes due to the benzenoid ring in the PSSA. S content was also found in the PANI-PAAc and PANI-PMVEA. The reason is probably that the reduction of ammonium persulfate

produced counter ions (HSO_4^-/SO_4^{2-}), which were incorporated into PANI structure to maintain a charge balance during the polymerisation [170]. This is undesirable as it may affect the ionic interaction between polymer acids and PANI, giving PANI with a lower doping level of PAs.

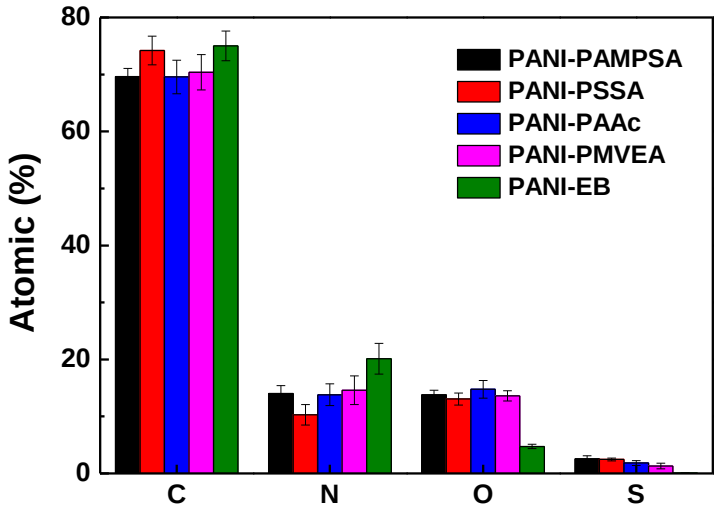

Fig. 7-2 EDS analysis of PANI-PA complexes.

7.2.2 FTIR Analysis of PANI-PA Complexes Powders

Table 7-2 shows the characteristic peaks presented in the PANI-PA complexes. Fig. 7-3 shows the FTIR spectra of the PANI-PA complexes powders. The presence of the peaks from polymer acids confirms their successful incorporation into PANI structures. Two main peaks of PANI-EB at 1491 cm^{-1} and 1588 cm^{-1} corresponded to the benzenoid and quinoid rings of PANI [212]. The peak of PANI-PAMPSA at approximately 1030 cm^{-1} corresponded to the symmetric stretching of -SO_2-, which was representative of sulfonate salts. The peak near 1653 cm^{-1} was assigned to the C=O stretching in PAMPSA [12]. In the PANI-PAAc complex, the characteristic bands at 1245 cm^{-1} and 1702 cm^{-1} were ascribed to the absorption carboxylic acid group [8, 10]. In the PANI-PSSA complex, S=O stretching of sulfonic acid group was present at 1028 cm^{-1}. The benzenoid bands at 1491 cm^{-1} shifted to lower wavelength, probably due to the partial overlapping by the benzene ring in PSSA structures. In the PANI-PMVEA, the C-O and C=O stretch of carboxylic acid group appeared at 1241 cm^{-1} and 1712 cm^{-1}, respectively. The peak at 1412 cm^{-1} can be ascribed to the interaction between C-O stretch and C-O-H in-plane bending of the carboxylic acid group of PMVEA [150].

Table 7-2 Band characteristics of PANI-PA complexes presented in FTIR spectra.

Compound	Band Characteristics	Wavelength (cm^{-1})
PANI-EB [124, 140, 269]	C=C stretching of benzenoid rings	1491-1497
	C=C stretching of quninoid rings	1588-1594
	C-N stretching of benzenoid rings	1284-1286
	C=C stretching of quninoid rings	1102-1104
PANI-PAMPSA [12, 141, 270, 271]	S=O stretching of sulfonic acid group	1028-1032
	symmetric $-SO_2$ stretching of sulfonic acid group	1150-1152
	asymmetric SO_3^- stretching of sulfonic salts	1173-1174
	C=O stretching of amide group	1644-1653
PANI-PSSA	S=O stretching of sulfonic acid group	1028-1032
PANI-PAAc [8]	C=O stretching of carboxylic acid group	1702-1713
	C-O stretching of carboxylic acid group	1225 -1245
PANI-PMVEA [8]	C=O stretching of carboxylic acid group	1702-1713
	C-O stretching of carboxylic acid group	1225 -1245

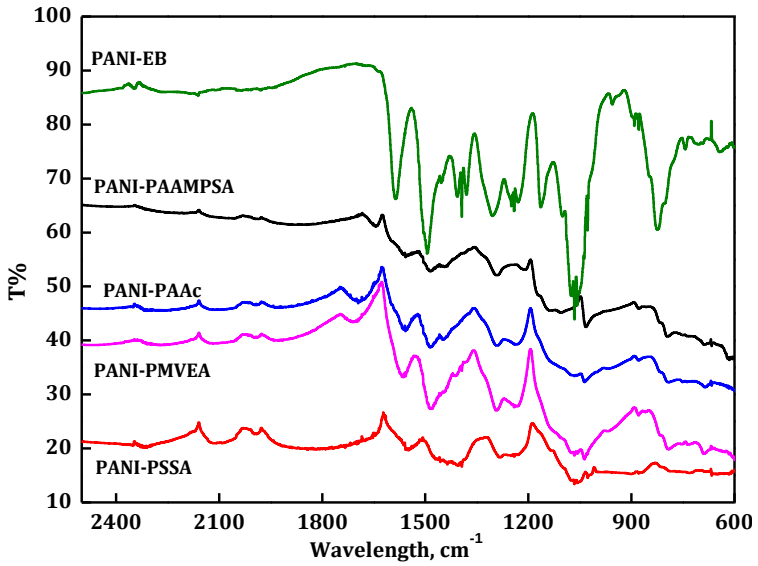

Fig. 7-3 FTIR spectra of the various PANI-PA complexes powders.

It is also interesting to observe that the quinoid ring peak at 1590 cm^{-1} in the PANI-EB showed a noticeable shift to approximately 1564 cm^{-1}, 1561 cm^{-1}, 1563 cm^{-1} and 1569 cm^{-1} in PANI-PAMPSA, PANI-PSSA, PANI-PAAc and PANI-PMVEA, respectively. This indicates that there was an interaction between π-conjugated

quinoid structure of PANI and polymer acids, associated with the degree of charge delocalisation on the polymer backbone [124]. Previous studies reported that the weak shoulder at around 2500 cm^{-1} was assigned to the stretching mode of protonated imine nitrogen ions (NH^+) while the abroad absorption bands close to 2735 cm^{-1} was ascribed to the stretching of protonated amine nitrogen ions (NH_2^+) [8]. In all the PANI-PA complexes, the peaks were around 2500 cm^{-1}, indicating that the protonation took place preferentially on imine nitrogen atoms. This is consistent with previous studies, confirming that the imine nitrogen atoms of PANI were preferentially protonated compared to amine nitrogen atoms of PANI [8].

7.2.3 Electrical Conductivity of PANI-PA Complexes

Fig. 7-4 shows the surface electrical conductivity of the PANI-PA complexes as measured using a four-probe conductivity meter. The protonation of PANI by polymer acids formed conductive PANI-PA complexes. This suggests that delocalised polarons were formed in the PANI-PA complexes and charge transfer occurred along the polymer chains. It was observed that PANI-PA with sulfonic acid groups showed higher conductivity compared to PANI-PA with carbolic acid groups. PANI-PSSA showed higher conductivity than PANI-PAMPSA. PANI-PMVEA, which has the PMVEA moiety working as a binary carboxylic acid, exhibited higher conductivity than PANI-PAAc as the PAAc moiety functions as a monoacid.

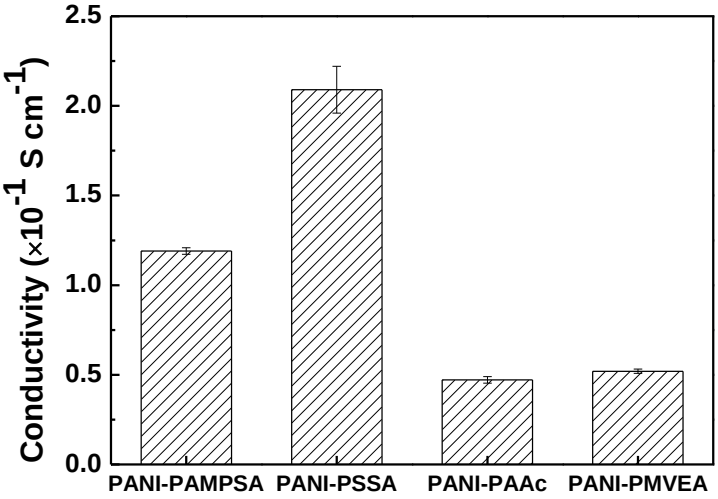

Fig. 7-4 Conductivity of polymer acids doped PANI complex.

Electrical conductivity is dependent on the oxidation state, doping degree and dopant types, crystallinity and molecular weights or chain length [66, 184]. The

structure of the polymer acid templates used in this study plays a crucial role in determining the electrical conductivity of the final complex. Previous studies indicated that the doping became increasingly inefficient with increasing molecular weights because of the mass transfer limitation of high molecular weight polymers [153], which are in line with the current results, where PSSA with the smallest molecular weight and highest acidity produces the most conductive PANI-PA complex.

PAMPSA with the largest molecular weight gave the next highest complex conductivity. PAMPSA possesses a highly flexible backbone of which its conformation can be adjusted to match the rigid conjugated macromolecule of PANI [152, 158]. This allows the PAMPSA chain to form a stronger interaction with PANI during in-situ polymerisation of aniline. In this respect, it would be advantageous to provide a high local concentration of protons and form regular and uniform chain structures.

The conductivity of carboxylic acid doped PANI was lower than sulfonic acid doped PANI. The reason is that the conductivity of doped PANI is dependent on the pKa of the acids [272]. Lower pKa exhibits a higher efficiency to donate H^+ and induces crystalline domains, which promotes electron mobility along the polymer backbone and results in high conductivity [196, 273]. The PAAc formed PANI-PAAc with the lowest conductivity among the four types of PAs, indicating PAAc was not an effective dopant for PANI, confirming previous studies [8, 150]. This previous work suggested that the PAAc chain could not form conformation adaptabilities with PANI backbones to align an ordered structure of PANI-PAAc due to its conformational hindrance and bulkiness [88, 150]. Considering all of the above results, it can be stated that the conductivity of PANI-PA complex is closely related to the properties of the PAs. Higher acidity, flexible backbone and smaller molecular weights of polymer acids are desirable to produce highly conductive PANI-PA complexes.

It is also noticed that it was ineffective to incorporate polymer acids into the PANI structure by immersing PANI-EB in the polymer acid solution at room temperature. The conductivity of obtained powder was two or three orders of magnitude lower than that formed by in-situ polymerisation. As discussed in Chapter 5, the protonation process through immersion uptake consists of both a chemical reaction

and a diffusion process. The reaction occurs at the initial doping stage between acid group and imine nitrogen of PANI chains. Diffusion occurs at the middle and final stage through the diffusion of proton and counter ions from an aqueous acidic solution into the membrane [238]. In the reaction stage, doping generally takes place in a random packing between the large structure of acids and rigid chain of PANI [176]. In the diffusion stage, it is difficult for the polymer acids with large molecular weights to be incorporated into the PANI structure through immersion uptake due to the mass transfer limitation and potential steric hindrance [150, 153]. On the contrary, the chemical oxidation of aniline whereby PAs serve as templates ensures that polyaniline grows along the acid templates and forms confined structures in an ordered packing [176]. This experiment confirms that the chemical oxidation of aniline templated with polymer acids is more effective at incorporating polymer acids into the PANI structure.

7.3 PA doped PANI Membrane Characterisation

7.3.1 Preparation of PA doped PANI Membranes

All four types of PANI-PA complexes powders were used in the preparation of conductive membranes via NIPS method. Table 7-3 summarises the results of membrane preparation using the different PANI-PA complexes.

PANI-PAMPSA formed a viscous solution in the solvent and produced a flat and shiny membrane surface when immersed in the water bath.

PANI-PSSA was not stable during the non-solvent phase separation and broken into smaller fragments in the water bath after a short time and consequently delaminated from the backing layer.

PANI-PAAc was not completely soluble in the solvent and became aggregated, thus cannot form solid film after 24 h immersion in the water bath.

PANI-PMVEA formed brittle membranes with cracks and defects on the membrane surface.

Table 7-3 Lists of membrane fabrication results by different PANI-PA complexes.

Sample	Membrane preparation Results	Images of membranes in water bath	Images of membranes after NIPS
PANI-PAMPSA	Flat membrane with smooth surface		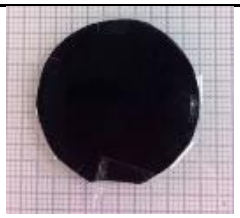
PANI-PSSA	Not stable to water non-solvent immersion		
PANI-PAAc	Insoluble in the solvent		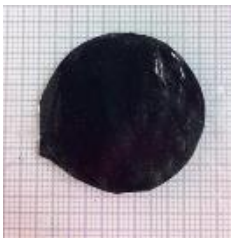
PANI-PMVEA	Brittle membrane with surface cracks		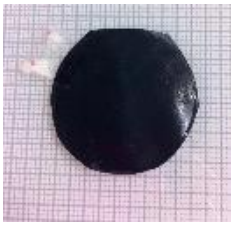

Based on the different membrane preparation results, several possible reasons are found to explain the phenomenon according to the different PANI-PA complexes used.

(1) The polymer acids have different functional groups, leading to different hydrophilicities of the different PANI-PA complexes [153, 274, 275]. The selection of polymer/solvent/non-solvent systems in the NIPS method is key to form membranes with the desired performance [105]. If the polymer has affinity to the non-solvent system, then the nucleation and growth of polymer-rich or polymer-lean phase will be suppressed when immersing polymer solution in the non-solvent bath [276]. In terms of PANI-PSSA (with the highest conductivity), it is expected that the PANI-PSSA complex had a strong affinity to water by cation or anion exchange in aqueous solutions, which is less suitable for NIPS method [176].

(2) Generally, non-conducting PANI can be readily processed in NMP as solvent while the conducting PANI is found to be insoluble in most solvents [66, 274]. Finding an appropriate solvent is of great importance to form films with the desired properties. Although PANI is modified by incorporating dopant acids with different substituents to make them more solution processable, suitable solvents are still limited and the presence of substituents also has reducing effect on the PANI conductivity [270, 275, 277]. Typically, a "good" solvent can change the molecular conformation of doped PANI from "compact coil" structures to more expanded structures [160, 278, 279]. This can reduce π-conjugation defects in the polymer backbone and increase the regularity of chain structure, thus promoting greater charge mobility and higher conductivity [229]. In the case of PANI-PAAc, it could be attributed to the weak interaction between the polymer chain and NMP solvent, leading to the tendency of PANI-PAAc chains to aggregate in the NMP [150, 229]. The insolubility of PANI-PAAc in solvent makes it not suitable to form the soluble polymer solution for the preparation of flexible membranes.

(3) Polymer acids serve as templates for aniline polymerisation and attract aniline by columbic attraction or hydrogen bonding. The ionisation degree of the polymer acids influences the distribution of anilinium on the acid backbones and strong ionisation forms a highly organized assembly [151]. In the case of PANI-PMVEA, the lower ionisation degree may lead to a less regular arrangement of polymer chains – arrangements with a random and amorphous structure. It could be the low degree of entanglement between polymer chain and the ordered packing which hindered the formation of membranes with high mechanical strength.

Among the four types of PANI-PA complexes, PANI-PAMPSA alone, under the casting conditions and solvents considered was able to form a membrane with a flat and rubbery surface. Therefore, all following studies focused on the fabrication and characterisation of PAMPSA doped PANI membranes (Memb-PAMPSA).

7.3.2 Memb-PAMPSA Robustness Analysis

The membrane surface analysis, mechanical strength and glass transition temperature were determined in this study to provide an evaluation of the stability of Memb-PAMPSA. Fig. 7-5 (a) and (b) show the images and RGB colour index of Memb-PAMPSA. The membrane was smooth with a shiny top surface. The

RGB index of Memb-PAMPSA was higher than undoped (Memb-EB) and small acid doped PANI membranes (Memb-HCl), showing that the polymer acid doped membrane was much darker. In the case of Memb-EB, the R:G:B value ratio was 0.25: 0.38: 0.37. After being doped by HCl, the R:G:B value ratio changed to 0.23:0.39:0.38 with a slightly higher green value than blue value. However, the R:G:B value ratio of Memb-PAMPSA was 0.22:0.35:0.43 with a much lower green colour than blue colour. The colour of Memb-EB generally changed from purple bronze to dark green after acid doping. The blue colour in Memb-PAMPSA was much higher than the green colour, indicating the Memb-PAMPSA was not fully doped (i.e. only partially doped).

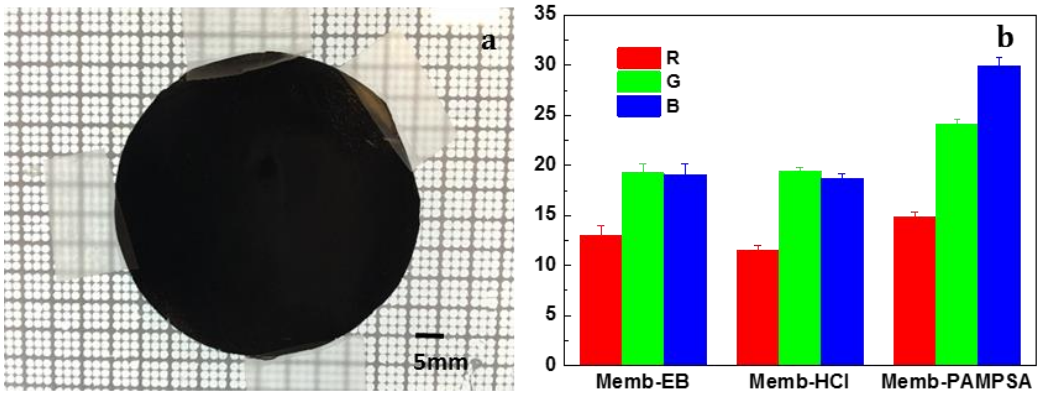

Fig. 7-5 (a) images and (b) RGB colour index of Memb-PAMPSA.

Fig. 7-6 shows the tensile strength and Young's modulus of Memb-HCl and Memb-PAMPSA. Compared to small acid doped membranes, Memb-PAMPSA displayed increased tensile strength and Young's modulus, suggesting an improvement in the mechanical strength. This can be explained by the SEM images in Fig. 7-9, showing that the finger-like voids in the Memb-PAMPSA were reduced compared to small acid doped membranes. As discussed in Chapter 5, finger-like voids were undesirable as they weakened the membrane mechanical strength and resulted in their collapse at high operating pressures [105]. Another possible contributing factor is the plasticising effect of residual NMP on the Memb-PAMPSA. The membranes were prepared using NMP as solvent and it is possible that these membranes still contained residual amounts of NMP. This residual NMP can have a plasticising effect on the membrane structure [227]. On the other hand, doping of the membranes with small acids would remove some if

not all of the residual NMP trapped in the space between the polymer chains, making the membrane more rigid/ less flexible [150].

It was also observed during the experiment that the Memb-PAMPSA was less brittle and much easier to handle in comparison with small acid doped membranes. The improved durability and flexibility were also reported by previous researchers, showing that the polymer acid doped PANI membranes exhibited good elastic behaviour due to the ionic bonds and double-stranded network between polymer acids and PANI chains [9].

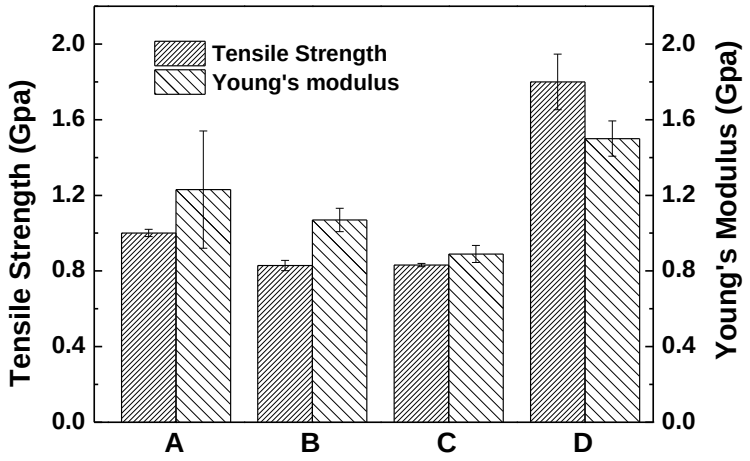

Fig. 7-6 Tensile strength and Young's modulus of Memb-HCl and Memb-PAMPSA. (A=Memb-HCl (2 h doping time); B= Memb-HCl (6 h doping time); C= Memb-HCl (24 h doping time); D= Memb-PAMPSA)

The T_g of Memb-PAMPSA was determined by dynamic mechanical analysis in Fig. 7-7 to understand the membrane physical properties. In Fig. 7-7, the first drop at 132°C was due to the backing layer (PP/PE mixture), and the second drop at 163°C showed the T_g of Memb-PAMPSA, which was slightly lower than small acid doped membranes in Chapter 5. This gives more evidence on the improved membrane properties in terms of flexibility and elasticity [150, 266]. Above all, it can be concluded that the produced Memb-PAMPSA possesses good mechanical strength: it was less brittle and more flexible than small acid doped membranes.

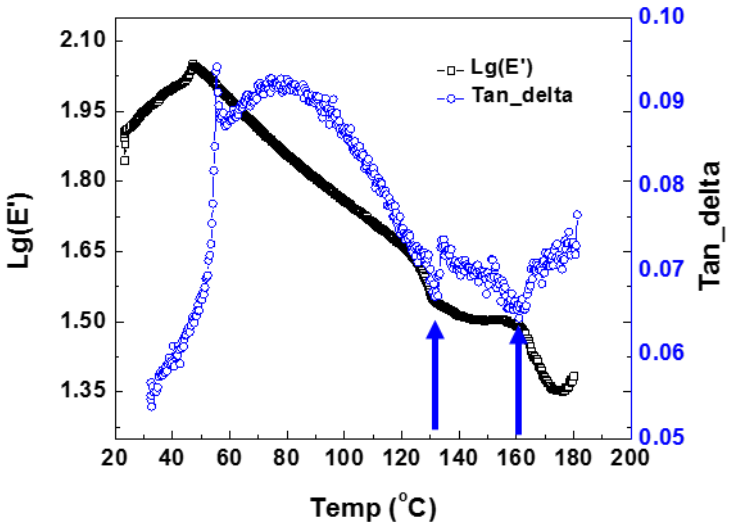

Fig. 7-7 Dynamic mechanical analysis of Memb-PAMPSA.

7.3.3 FTIR of Memb-PAMPSA

To further understand PAMPSA doped membrane properties, FTIR was employed to investigate the chemical structure in the membrane. FTIR spectra in Fig. 7-8 shows the spectra of Memb-PAMPSA and Memb-EB. The main absorption peaks of the quinoid and benzenoid rings appeared at 1495 cm^{-1} and 1598 cm^{-1} in Memb-EB, and at 1495 cm^{-1} and 1590 cm^{-1} in Memb-PAMPSA. The quinoid ring was found to shift by approximately 30 cm^{-1} compared to Memb-EB with fully small acid doped membranes (Memb-HCl) in Chapter 5. In the case of Memb-PAMPSA, the shift of quinoid rings was not as significant as the fully doped membranes, again indicating that the Memb-PAMPSA was not fully doped (i.e. only partially doped). The peaks in Memb-PAMPSA at approximately 1030 cm^{-1} and 1653 cm^{-1} corresponded to the S=O stretching of sulfonic acid group and C=O stretching, respectively. The peak at 1158 cm^{-1} was assigned to asymmetric SO_3^- stretching, which was representative of sulfonate salts. This peak was broader, probably due to the overlapping with the vibrational band of the nitrogen quinone [176]. Overall, the presence of characteristic FTIR peaks of Memb-PAMPSA confirms the incorporation of PAMPSA into PANI membranes through the interactions between the imine nitrogens of PANI and the sulfonic acid groups of PAMPSA.

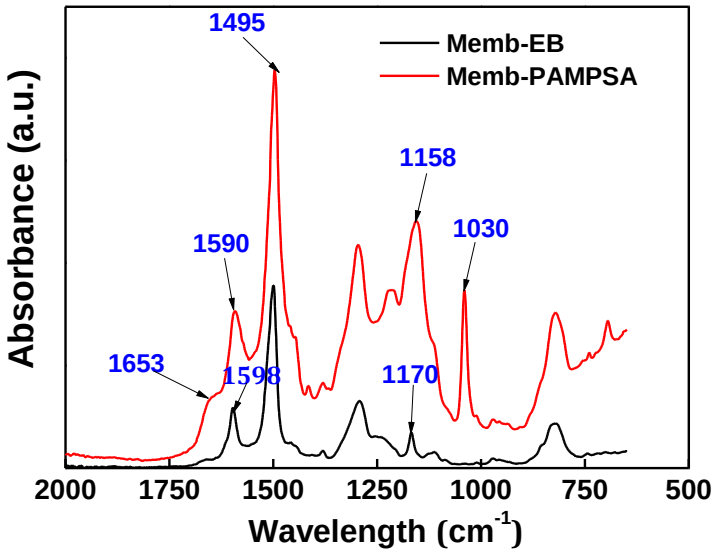

Fig. 7-8 FTIR spectra of Memb-PAMPSA and Memb-EB.

7.3.4 Morphology of Memb-PAMPSA

The surface and cross-section of Memb-PAMPSA are shown in Fig. 7-9. It can be observed that the Memb-PAMPSA surface was rougher compared to that on Memb-EB in Chapter 5. This indicates that NMP was not a "good" membrane film making solvent for the PANI-PAMPSA. Other solvents such as DMF and DMAc were also used in the study, but were not as effective as NMP due to the poorer solubility of PANI-PAMPSA in these solvents. As can be seen from the cross-section, Memb-PAMPSA shows highly porous and loose structures. This suggests that the use of larger dopants produced greater intermolecular spacing between PANI polymer chains and clusters and therefore expanded the membrane pore structures, and facilitated the formation of a loose membrane with higher porosity and larger free volume.

Compared with Memb-EB, the growth of finger-like macrovoids was restricted in the Memb-PAMPSA. Generally, the formation of finger-like macrovoids can be hindered by increasing the polymer concentration in the polymer solution, increasing solvent evaporation time and/or choosing a solvent/non-solvent pair with low miscibility [280]. The same evaporation time and solvent/non-solvent pair were used in the phase inversion procedure in all experiments unless stated otherwise. Although the same concentration of polymer was used, the PANI-PAMPSA formed a more viscous casting solution than PANI-EB, which is in part due to a different dissolution in the solvent. Compared to PANI-PAMPSA, PANI-

EB was more easily dissolved in the solvent and the casting solution flowed more quickly than PANI-PAMPSA. The viscosity of solution plays an important role in the formation of microstructures by influencing the convective flows and demixing process. Greater viscous hindrance forces slow down the precipitation rate, inhibiting the formation of finger-like macrovoids [280]. Another contributing factor is that PANI-PAMPSA was more hydrophilic than the PANI-EB, and needed a longer time to coagulate in the water bath to form films. Slower coagulation rate is desirable to form membranes with "sponge-like" substructures [105]. Generally, finger-like macrovoids are undesirable because they weaken the mechanical strength of membrane. Possible compaction or collapse would take place when the membrane is used in high operating pressure [281, 282]. These results therefore further confirm that incorporating PAMPSA into PANI membranes can improve their mechanical properties.

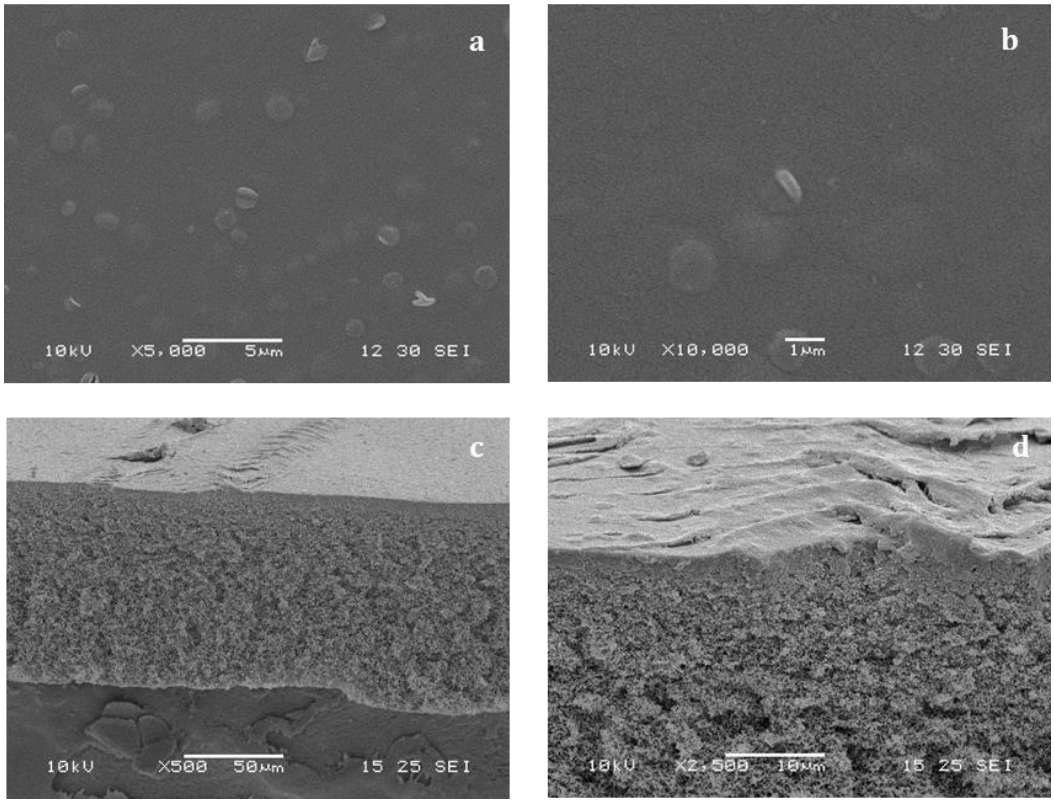

Fig. 7-9 The surface (top) and cross-section (bottom) of Memb-PAMPSA

7.3.5 Permeance and Rejection of Memb-PAMPSA

Permeation of Memb-PAMPSA and Memb-HCl tested by water and the PEG MWCO mixture solution is shown in Fig. 7-10 (a). The permeance of Memb-PAMPSA with water and PEG mixture as feed was 202±12 and 180±16 $L \cdot m^{-2} \cdot h^{-}$

^{1}·bar^{-1}, respectively compared to Memb-HCl with 5.6±0.2 and 4.9±0.5 L·m^{-2}·h^{-1}·bar^{-1}, respectively. Dynamic droplet penetration results in Section 7.3.8 confirm this result that Memb-PAMPSA is more permeable. The higher permeance of Memb-PAMPSA can be explained by two reasons. Firstly, excess pendent sulfonic acid groups of PAMPSA can increase the membrane hydrophilicity [153]. Secondly, Memb-PAMPSA exhibits a loose microstructure with larger free volume and higher porosity as a result of the incorporation of large acids, as shown in Fig. 7-9, which is expected to lead to an increased permeance if pore flow dominates transport. Hence, water molecules can permeate rapidly through the porous membrane structure, leading to an enhanced water permeance [98].

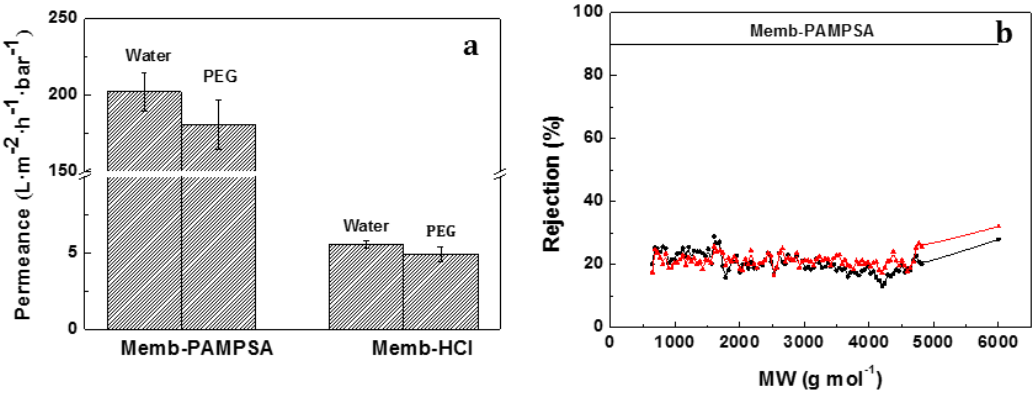

Fig. 7-10 (a) Permeance of Memb-PAMPSA and Memb-HCl and (b) PEG MWCO mixture rejection of Memb-PAMPSA in dead-end filtration.

In addition, Memb-PAMPSA showed a rejection of PEG 1000–6000 with 10%–30%. The low rejection of the PEG mixture may be caused by the larger free volume and higher porosity of Memb-PAMPSA if pore flow is the main transport and rejection mechanism. Complete rejection of BSA (MW of 66, 000 g mol^{-1}) was achieved by the Memb-PAMPSA, indicating that the MWCO of Memb-PAMPSA was much higher than 6000 g mol^{-1} but lower than 66, 000 g mol^{-1} with the BSA as MWCO probe.

7.3.6 Stability of Memb-PAMPSA in Filtration

In order to test the membrane stability during dead-end filtration, pHs of the membrane permeate during different filtration stages were measured to determine the extent of acid dopant leaching. Fig. 7-11 shows the pHs of the permeate (before filtration, after preconditioning and after the actual filtration) in dead-end filtration. The permeate pHs of Memb-HCl decreased during filtration, indicating that HCl

had leached from the membrane. However, the permeate pHs of Memb-PAMPSA were stable, indicating that this new generation PANI membrane overcame the acid leaching problem and was therefore more stable in filtration. This is likely because PAMPSA has a flexible backbone and it can adapt its flexible-chains to the rigid conjugated structure of polyaniline [152]. Accordingly, an interwoven and/or double-stranded structure in a side-by-side chain configuration can be formed between PANI and PAMPSA chains [14, 152]. Compared to the traditional single-stranded configuration in Memb-HCl, the stronger double-stranded and/or interwoven structure between PAMPSA and PANI chains leads to increased chemical stability of Memb-PAMPSA. Additionally, the leaching of PAMPSA can be more difficult on account of the mass-transfer limitations of high molecular weight acids leaving the membrane porous structure [11]. The PAMPSA is expected to be confined locally in the double-stranded structure, making leaching more difficult to happen.

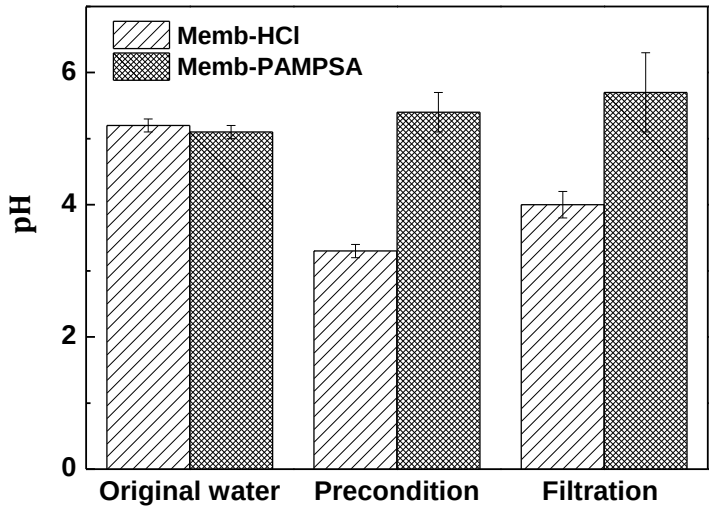

Fig. 7-11 pH change of Memb-HCl and Memb-PAMPSA in dead-end filtration.

7.3.7 Electrical Conductivity of Memb-PAMPSA

In terms of the actual tuneability evaluation of Memb-PAMPSA in Section 7.3.8 and 7.3.9, dry membranes were used in the dynamic droplet penetration analysis while wet membranes were used in the electrically connected cross-flow filtration. Based on this, the surface electrical conductivity was measured in both a dry and wet state to match the membrane conductive properties with the actual tuneability test.

The conductivity of Memb-PAMPSA in a dry and wet state was measured to be (8.56±1.01) $\times 10^{-7}$ and (8.68±0.89) $\times 10^{-4}$ S cm^{-1}, respectively. It is not surprising that the conductivity in a wet state was higher (as a result of the adsorbed moisture) than that in a dry state. The presence of moisture would act as carriers and solvate the counter anions, leading to better mobility of charged ions and greater delocalisation of polarons. Moreover, additional protonation might occur with the exposure to water, promoting more efficient charge transfer along the polymer chains and increasing the electrical conductivity [150, 273].

It was observed that the conductivity of Memb-PAMPSA was significantly lower than Memb-HCl in Chapter 5. This is consistent with the previous research, showing that small acid doped PANI membranes displayed significantly higher conductivities than polymer acid doped PANI membranes [88, 279, 283]. There are several reasons associated with the lower conductivity of polymer acid doped membranes.

(1) NMP is a basic, polar solvent and can form strong hydrogen bonding with acids, so there exists a competition between base-acid reactions of PANI with polymer acids and hydrogen bonding of NMP with acids. This results in an equilibrium and coexistence of doped and undoped PANI in the NMP solvent [226]. In addition, the conductivity of the Memb-PAMPSA was several orders of magnitude lower than the PANI-PAMPSA powder. This indicates that the dedoping happened when dissolving PANI-PAMPSA powder in NMP. FTIR and colour characterisation results in Section 7.3.2 and 7.3.3 also show that the Memb-PAMPSA was not fully doped after being cast from NMP solvent. Although it was reported less dedoping occurred in the more concentrated polymer solution, the PANI with more compact packing could cause a coiled confirmation to be formed, which is unfavorable for charge transfer [226]. These all contribute to the low conductivity when the membrane was cast from NMP.

(2) The polymer acid chain is long (since PAMPSA with a large molecular weight was used) and tends to be more tangled with a more expanded lattice, thus forming a PANI-PAMPSA complex with higher amorphous content and lower crystallinity, affecting the charge delocalisation [284]. It was reported that PANI produced on the template of PAMPSA with a molecular weight of 724, 000 g mol^{-1} had the tendency to form “compact coil” structures [153]. This structure exhibits a narrow

polaron interband transition and decreased conjugation length which limits the charge delocalisation of the protonated imines. In terms of the membranes produced in this work, the molecular weight of PAMPSA used was 800, 000 g mol^{-1} – an even larger structure – so it is deduced that the "compact coil" structures exist in the PANI-PAMPSA complex.

The membrane conductivity can be further improved to different extent by secondary doping with different acids. The conductivity (measured at a dry state) improved by only one order of magnitude after being doped by PAMPSA, while three orders of magnitude improvement was found by secondary doping with DBSA. The reason is assumed to be the mass-transfer limitations of the large structure of PAMPSA in comparison with the long chain DBSA. This also indicates that the efficiency of secondary doping depends on the dopant types (i.e. molecular weight, dopant structure).

7.3.8 Initial Tuneability Assessment: Dynamic Droplet Penetration Analysis

As in Chapter 5, the solute permeation rate through acid doped membranes with or without applied potential was used to characterise the membrane initial tuneability. The change of effective contact angle and droplet with time indicates the solute permeation rate. Considering the low conductivity of Memb-PAMPSA, the highest voltage (30 V) used on the small acid doped membrane was applied on Memb-PAMPSA to determine the effect of applied potential on the membrane transport properties. Fig. 7-12 shows the effective contact angle and droplet height change with time at 0 and 30 V of applied potential. As can be seen, the applied potential did not have a significant effect on the water permeation rate through Memb-PAMPSA, with effective contact angle of 2.2×10^{-1} θ s^{-1} at 0 V and 2.1×10^{-1} s^{-1} at 30 V, and the droplet height of 3.6×10^{-3} mm s^{-1} at 0 V to 4.1×10^{-3} mm s^{-1} at 30 V.

As stated in Chapter 5, the solute permeation rate change with or without applied potential is affected by the membrane conductivity. Small acid doped membranes with higher conductivity can produce more active electron movement under applied potential and thus enhance the charge transfer between the conducting domains. This produces stronger intermolecular attractions and further alters the dynamic wetting behaviour between water and membrane surface.

Applying this here: despite the strong bonding between polymer acids and PANI, the conductivity of Memb-PAMPSA was much lower than small acid doped membranes. It is not surprising that the mobility of delocalised charge and electron movement were weak under applied voltage. Another possible reason is that the solute permeation rate through Memb-PAMPSA was much higher than small acid doped membranes. Considering the accuracy limitation of the equipment, it is not easy to detect the difference of dynamic contact angle when the membrane tuneability was not significant but the solute permeation rate was fast.

It is also found that the solute permeation rate of Memb-PAMPSA was much faster than the small acid doped membrane, with effective contact angle change of 0.2 θ s^{-1} for Memb-PAMPSA compared to 4.3×10^{-2} θ s^{-1} for small acid doped membranes. This is consistent with membrane permeance results in the dead-end filtration, indicating an increased attracting force across the interface between water and Memb-PAMPSA. Acid dopants namely PAMPSA and HCl possess different chemical structures, which may be responsible for the different surface energies and polarities between Memb-PAMPSA and Memb-HCl [196]. PAMPSA with amide group can form additional hydrogen bonding with water, thus enhancing the water permeation rate [153].

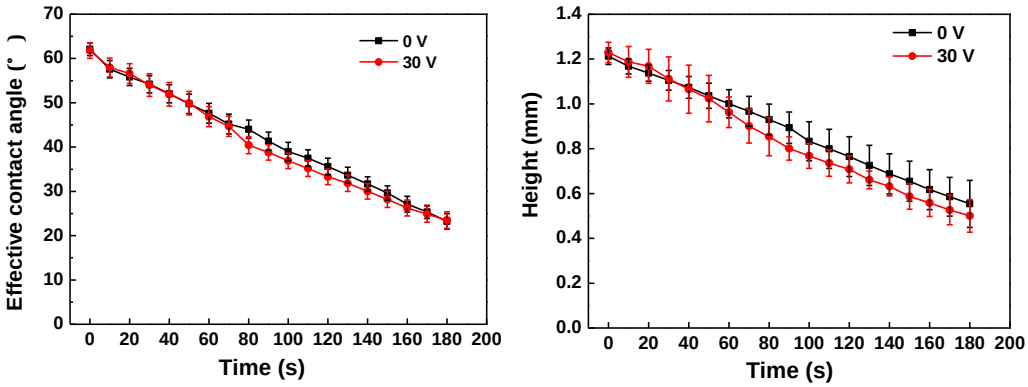

Fig. 7-12 The effective contact angle and droplet height change of Memb-PAMPSA over time with and without potential (30 V). Error bars represent ± SE.

7.3.9 Electrically Connected Cross-flow Filtration

Electrically connected cross-flow filtration is a main way to conduct a critical evaluation on the tuneable properties of Memb-PAMPSA in the absence and presence of applied potential. In order to investigate the influence of applied potential on membrane tuneability of pressure driven filtration of non-ionic species,

aqueous PEG MWCO mixtures were chosen as feed. Considering the loose structure of Memb-PAMPSA, PEG mixtures used for low UF membranes were applied in the electrically connected cross-flow filtration.

Electrical tuneability of PEG mixture: Fig. 7-13 shows the rejection of Memb-PAMPSA in different filtration time (0, 30, 60 and 120 min) under applied potential of 0 and 30 V (2 bar, 25°C, PEG mixtures). It can be found that the rejection of PEG solute mixtures decreased in the presence of external electrical stimulus. Fig. 7-14 shows the water permeance and current of Memb-PAMPSA with PEG UF mixture as feed under applied potential in the absence and presence of applied potential (2 bar, 25°C, PEG mixtures). A slightly faster permeance was found when voltage was applied on the membrane. Moreover, the current passing through Memb-PAMPSA kept stable when applied potential was used.

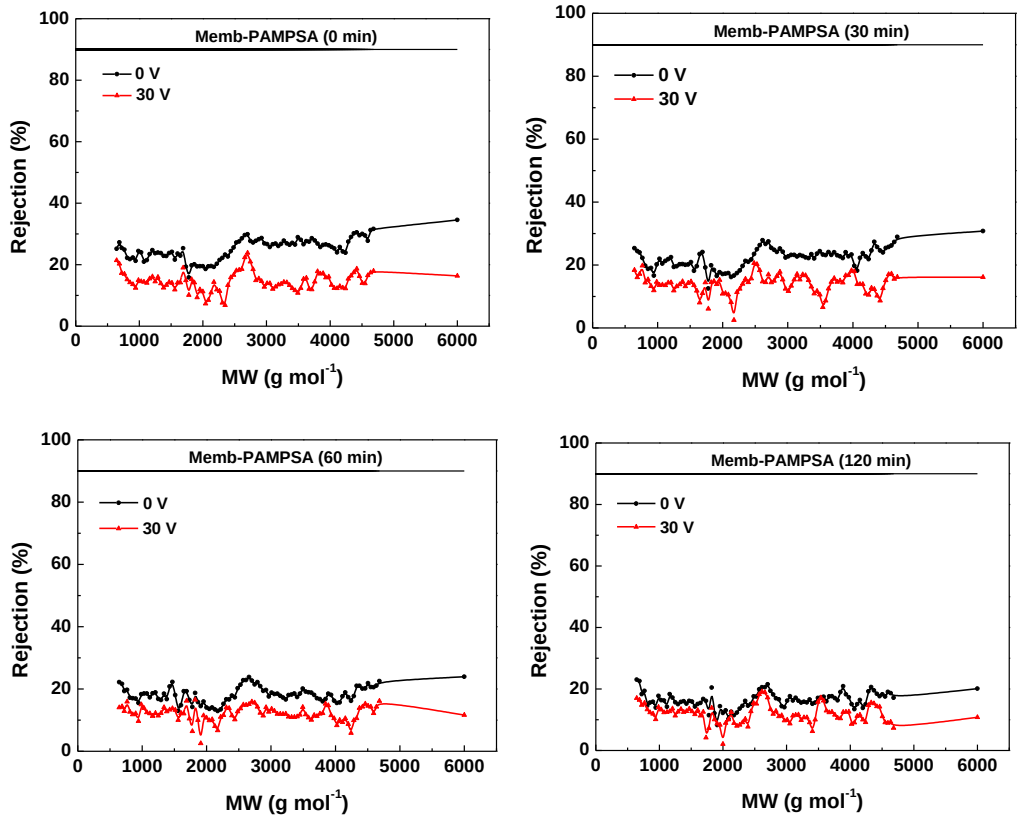

Fig. 7-13 The rejection of Memb-PAMPSA in different filtration time (0, 30, 60 and 120 min) under applied potential of 0 and 30 V (2 bar, 25°C, PEG mixtures).

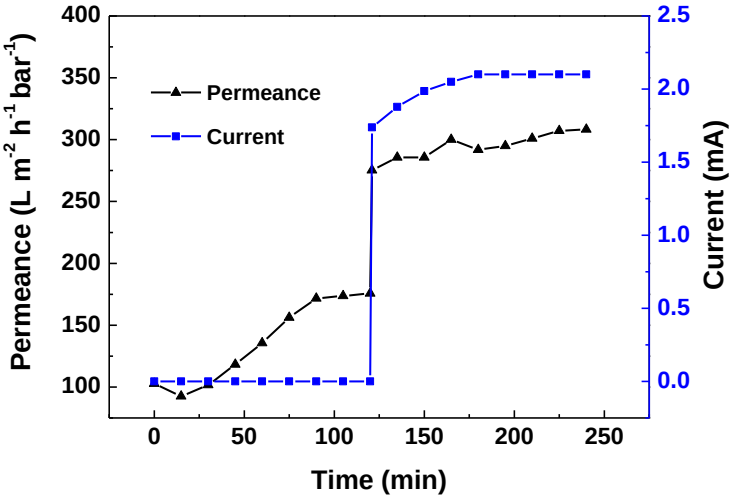

Fig. 7-14 Water permeance and current of Memb-PAMSA under applied potential of 0 and 30 V (2 bar, 25°C, PEG mixtures).

Electrical tuneability of pure water: In order to evaluate the effect of voltage on the membrane permeance, DI water was used as the feed, and the permeance and current passing though the membranes under applied potential were recorded with time (2 bar, 25°C, water). Fig. 7-15 shows that the water permeance increased from 248±3 to 261±7 $L \cdot m^{-2} \cdot h^{-1} \cdot bar^{-1}$ when the external potential was applied. Another cycle was also tried to test the repeatability of membrane tuneability, and the permeance changed from 244±3 $L \cdot m^{-2} \cdot h^{-1} \cdot bar^{-1}$ without applied potential to 255±3 $L \cdot m^{-2} \cdot h^{-1} \cdot bar^{-1}$ with applied potential. This indicates that the membrane structure became looser under applied potential. It is also found that the current passing through the membrane was lower than small acid doped membrane but did not decrease at a fixed 30 V voltage, indicating that the polymer acid doped membrane was less conductive but more stable than small acid doped membranes. These correlates well with the previous membrane conductivity and filtration stability results in this work.

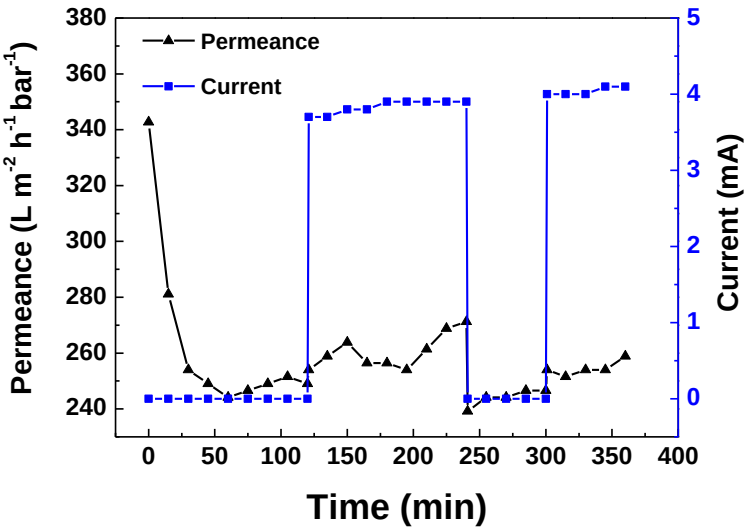

Fig. 7-15 Water permeance and current of Memb-PAMSA under applied potential of 0 and 30 V (2 bar, 25°C, water).

It is hypothesised that several properties changes in Memb-PAMPSA contribute to the tuneable separation under applied potential. Solution-diffusion, pore-flow and Donnan exclusion are the three main models to describe the transport mechanisms of solutes through NF and UF membranes.

Solution-diffusion is widely used to describe the transport of small molecular weights of solutes through dense membranes [27]. The applied potential is expected to facilitate the electron movement along the polymer chain, generating the charge transfer between conducting domains. This would affect the interaction between the solutes and membranes, making the solutes sorption, diffusion and desorption process easier to happen.

Pore flow is believed to occur when the large solutes permeate through tiny pores in the membrane [285, 286]. The applied potential facilitates the mobility of charged ions in the membrane, which in turn changes the free volume in the membrane structure. The changeable structure influences the selectivity and transportation of neutral solutes, producing membranes with tuneable separation [6]. The presence of acids in the membrane makes free volume potentially available, resulting in a tuneable permeability. Compared with small acids, PAMPSA as a flexible polymer acid with large benzene ring sulfonyl groups, allows a larger void formation associated with greater free volume when it arranges its structure under electrical potential. Greater free volume provides more space for the solutes to pass through the membrane, producing the decrease in rejection.

Donnan exclusion describes the behaviour of charged ions passing through membranes [285]. The applied potential facilitates the charge transfer and electron movement through the membranes, potentially increasing the polarity of membrane surface, thus water transport through membrane would be increased due to its dipole.

All of the above results indicate that the Memb-PAMPSA has a limited tuneable permeance and selectivity in non-ionic species under applied potential. The conductivity needs to be increased to improve this and this will therefore be the focus of the next chapter.

7.4 Conclusions

In order to overcome the two challenges (acid leaching and membrane brittleness) of small acid doped PANI membrane, this chapter develops a feasible route to fabricate PAs doped PANI membrane and investigates the properties of the new generated membrane. This is a new way to prepare acid doped PANI membranes by allowing PAs to be primary dopants and polymerising aniline on the template of PAs.

The results show that:

- Among the four types of PANI-PA complexes (PANI-PAMPSA, PANI-PSSA, PANI-PAAc and PANI-PMVEA), PANI-PAMPSA produced the optimal practical membranes with smooth and shiny surface under the casting conditions and solvents considered.
- The in-situ synthesised PANI-PAMPSA complex produced smooth and integral membranes that addressed two of the main problems with conventional mineral acid doped PANI membranes: brittleness and leaching of acid dopant. The Memb-PAMPSA had a Young's modulus and tensile strength twice that of mineral acid doped PANI membranes and permeate pH during filtration remained relatively constant compared to conventional mineral acid doped PANI membranes.
- Memb-PAMPSA exhibited a limited tuneable permeance and selectivity in non-ionic species under applied potential. A higher permeance and lower rejection in non-ionic species was observed under applied potential,

suggesting that the membrane structure can be tuned to be looser by the external stimuli.

- The electrical conductivity of Memb-PAMPSA was much lower than small acid doped membranes, with (8.56±1.01) $\times 10^{-7}$ and (8.68±0.89) $\times 10^{-4}$ S cm^{-1} measured in a dry and wet state, respectively, indicating the next step is to improve the conductivity of polymer acid doped membrane.

8 Enhancing Memb-PAMPSA as a Stimulating-responsive Membrane by EG Incorporation and DBSA Treatment

8.1 Introduction

Compared to small acid doped membrane, PA doped membrane displayed improved mechanical strength and filtration stability. However, the major limitation of PA doped membrane is that the membrane was not fully doped after casting it from NMP and the electrical conductivity was significantly lower than small acid doped membrane. This leads to poor membrane tuneability (permeance and selectivity change) under applied potential. In terms of the overall objective of this research to develop unique conducting PANI membranes that can be electrically tuneable to different fluxes and selectivity and to apply these to control membrane fouling, it is of great importance to improve the electrical conductivity of current PA doped membranes.

Graphite is a layered carbon material with higher electrical conductivity than activated carbon and relatively lower price than carbon nanotubes [127, 128]. It has been found that the intercalation of PANI into graphite at certain ratios exhibited conductivities greater than the individual PANI [129]. However, it is difficult to prepare conductive PANI/graphite complex by direct intercalation as a result of the small interlayer space of graphite layers. Accordingly, a certain chemical or physical modification is needed to prepare expandable graphite or exfoliated graphite with increased interspace compared to neat graphite [127]. The formed EG nanosheets with a loose and porous structure can intercalate aniline monomer or PANI polymer into the interspacing of graphite layers [130]. EG nanosheets can serve as conductive bridges connecting PANI conducting domains and increase the charge transfer mobility, resulting in an enhanced conductivity [120, 128, 129].

Thus far, incorporating conducting polymers like PANI into the interlayer spacing of carbon materials like EG has attracted considerable attention as a result of the high electrical conductivity [120, 126]. Numerous potential applications have focused on supercapacitors [138], sensors [287], rechargeable batteries [288], conductive inks [289] and microbial fuel cells [145], *etc*. To the best of our knowledge, there have been no reports of incorporating EG into PA doped PANI membranes to improve the membrane conductivity, and then realise the aqueous tuneable separation under applied potential. Therefore, studies of combining EG with PA doped PANI

membrane have the potential to be the breakthrough solution to overcome the challenge of low membrane conductivity. This will also potentially open new applications of electrically tuneable membrane separation beyond the traditional applications.

In Chapter 7, PAMPSA as a primary dopant was incorporated into PANI structure during the chemical polymerisation of aniline. When PANI-PAMPSA was cast with NMP as a solvent, the doping level of resulting membranes reduced, suggesting that not all imine nitrogens were protonated by PAMPSA. With this concern, another promising way to improve the membrane conductivity is to perform a secondary doping. Secondary dopants, applied to a primary-doped PANI, can further dope the PANI and induce dramatic conformation change in the molecular network of PANI, resulting in an increased electrical conductivity [229]. It was reported that the conductivity of PAMPSA doped PANI can be improved by more than two orders of magnitude by dichloroacetic acid (DCA) treatment. DCA induced the structural rearrangement of PANI-PAMPSA from "compact coil" to "extended chain". These structural relaxations promoted more efficient charge transport, which was responsible for the improvement in the electrical performance of PANI membrane [290]. However, DCA as a small acid, could also leach out during the filtration process. On the other hand, a long chain acid namely DBSA possesses some attractive advantages like strong acidity, effective doping and plasticisation for PANI, thereby can be considered as a promising secondary dopant for primary polymer acid doped PANI [291, 292].

Considering this, EG was incorporated into PAMPSA doped PANI membrane for the first time in this study, aiming at achieving membranes with a high electrical conductivity and stable performance. Three different methods of incorporating EG into PANI were used including in-situ polymerisation of aniline, mechanical mixing of EG and PANI-PAMPSA powder and solution mixing. Solution mixing was further divided into two different ways of adding EG. In addition, the formed membrane was doped by a secondary dopant DBSA to further improve the electrical conductivity. The properties of obtained polymers and membranes were investigated by different characterisation techniques, e.g. SEM, FTIR and four-point probe conductivity. The dead-end filtration was used to determine the membrane filtration performance (permeability and selectivity). The electrically

connected cross-flow filtration was applied to investigate the membrane tuneability by external voltage under industrially relevant membrane filtration conditions.

8.2 Incorporating EG into Memb-PAMPSA by Three Different Methods

As stated in Section 4.7, three different approaches were used to incorporate EG into Memb-PAMPSA to enhance the electrical conductivity. The resulting membranes were then screened to choose the one with the highest electrical conductivity for the evaluation of membrane performance (i.e. transportation, tuneability, *etc*.).

8.2.1 Method 1: In-situ Polymerisation

(1) Weight and Yield of PANI-PAMPSA-EG composites

Table 8-1 describes the weight and yield of PANI-PAMPSA-EG composites. The yield increased by increasing the EG content, from 77.7% in PANI-PAMPSA-25%EG to 87.5% in PANI-PAMPSA-75%EG. This could be related to the better interaction between π- conjugated structure of the EG and the quinoid ring of PANI-PAMPSA which could reduce the loss of PANI-PAMPSA or EG during the washing process. It is noted that different weight percentages of EG with respect to aniline were used in Method 1. However, different weight percentages of EG with respect to PANI-PAMPSA were utilised in Method 2 (Section 8.2.2) and Method 3 (Section 8.2.3). Therefore, the corresponding EG/PANI-PAMPSA ratio in Method 1 was calculated in order to obtain a parallel comparison among different methods.

Table 8-1 Weight and yield of PANI-PAMPSA-EG composites.

Composites	EG weight (g)	Product weight (g)	Yield (%)	EG/PANI-PAMPSA (%)
PANI-PAMPSA-25%EG	1.40	7.85	77.7	21.7
PANI-PAMPSA-50%EG	2.80	9.50	82.6	41.8
PANI-PAMPSA-75%EG	4.20	11.3	87.5	59.3

(Note: Aniline=5.59 g, PAMPSA=3.11 g, wt% EG with respect to aniline.)

(2) Method 1: Morphology and particle size of EG

Fig. 8-1 describes the morphology of EG prepared by treating graphite using H_2O_2 - H_2SO_4 methods, followed by 2 h ultrasonic treatment in isopropyl alcohol

solution. As can be seen in Fig. 8-1, EG was torn into multilayer graphite nanosheets with interspace between different layers. Such a laminated morphology is desirable as it can provide interlayer spacing for aniline monomer to polymerise and facilitate the formation of conductive networks in the polymer matrix [293]. Previous studies pointed out that there were correlations between the shape of graphite particles and electrical conductivity [294, 295]. Flake-type particles were found to result in higher conductivities than sphere-type particles due to their large specific surface areas and effective surface-to-surface contact [294, 295]. Based on this, the obtained flake-type particles in the study were expected to provide effective conducing networks which could promote the charge transfer along the polymer matrix.

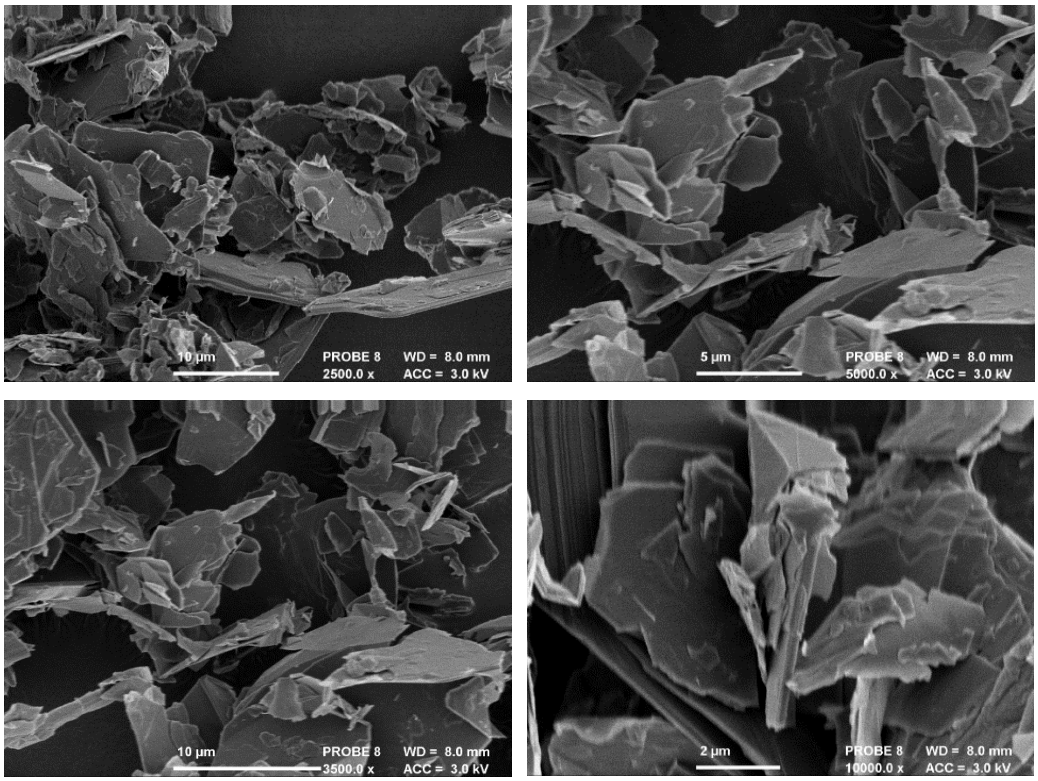

Fig. 8-1 SEM images of EG at different scale bars.

Fig. 8-2 displays the particle size of EG measured by two approaches: mastersizer laser diffraction and SEM image calculation. In terms of laser diffraction, two types of dispersion solvents including water and isopropanol were utilised. The particle size distribution was found to be related to the dispersion solvent, with D (V, 0.1) = 4.7±0.03 µm, D (V, 0.5) =11.1±0.1 µm and D (V, 0.9) = 24.0±0.7 µm in isopropanol dispersion and D (V, 0.1) = 6.1±0.1 µm, D (V, 0.5) =15.3±0.8 µm and D (V, 0.9) = 68.5±8.9 µm in water dispersion. The smaller particle size in

isopropanol was likely due to the stronger isopropanol-EG interfacial interaction, which could prevent the EG agglomeration and allow better dispersion in isopropanol [296]. Image calculation results of SEM (Fig. 8-1) show that the average sheet diameter of EG is 12.0±0.4 μm, similar to the mastersizer laser diffraction results.

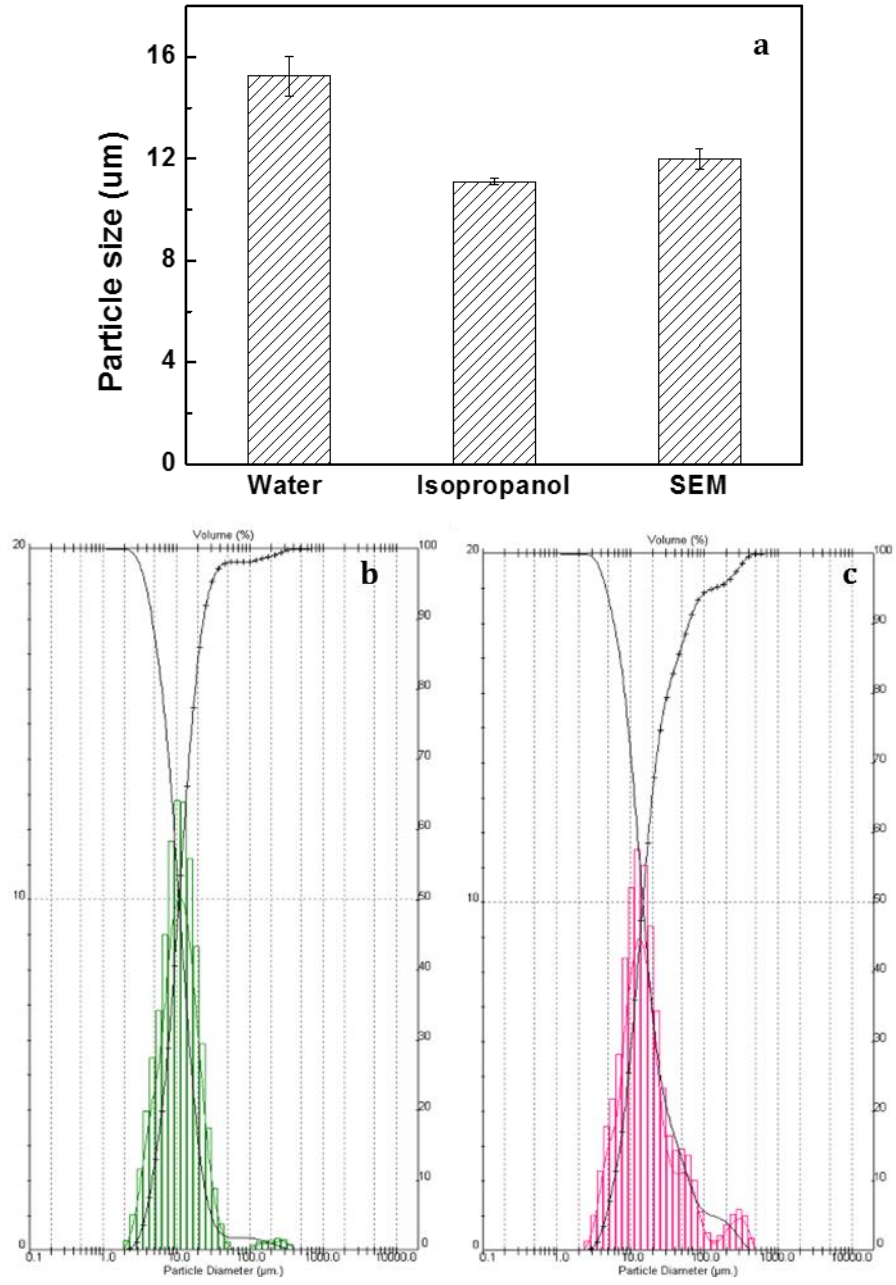

Fig. 8-2 (a) Average article size of EG measured by mastersizer laser diffraction and SEM image calculation, (b) particle size distribution in isopropanol as a dispersion solvent and (c) water as a dispersion solvent.

It has been reported that the particle size of conducting particles plays an important role in the electrical conductivity. Generally, a small particle size is desirable to form enhanced conductive networks by efficiently connecting the conductive pathways, but powders with a small particle size tend to aggregate, thereby increasing voids and porosity in the polymer system [295, 297]. In terms of this, getting good dispersion of EG in the polymer dope solution is a key factor to obtain membranes with desired performance and minimum defects.

(3) Method 1: FTIR of PANI-PAMPSA-EG composites

Fig. 8-3 (a) shows FTIR spectra of the neat graphite and EG. The spectrum of EG did not exhibit new peaks compared to neat graphite. This would indicate that heating EG in a furnace at 700℃ removed all the sulfonic acid groups that were used for the exfoliation of neat graphite. Fig. 8-3 (b) displays the spectra of PANI-PAMPSA-EG powder synthesised at different percentages of EG. The main absorption peaks of quinoid and benzenoid rings appeared at 1562 cm^{-1} and 1485 cm^{-1} in the PANI-PAMPSA-EG composites. The absorption peaks of the quinoid rings shifted by 28 cm^{-1} in comparison with 1590 cm^{-1} in the undoped PANI in Chapter 5, indicating that the imine nitrogen of PANI interacted with PAMPSA and EG. The peaks at approximately 1031 cm^{-1} and 1650 cm^{-1} were assigned to the S=O stretching of sulfonic acid group and C=O stretching, respectively. The broader peak at 1168 cm^{-1} which overlapped with vibrational band of nitrogen quinone was assigned to the asymmetric SO_3^- stretching of sulfonate salts [176]. The presence of a strong peak at approximately 1140 cm^{-1} was representative of an "electronic-like band", indicating that charge-transfer occurred between EG and the quinoid unit of PANI [143].

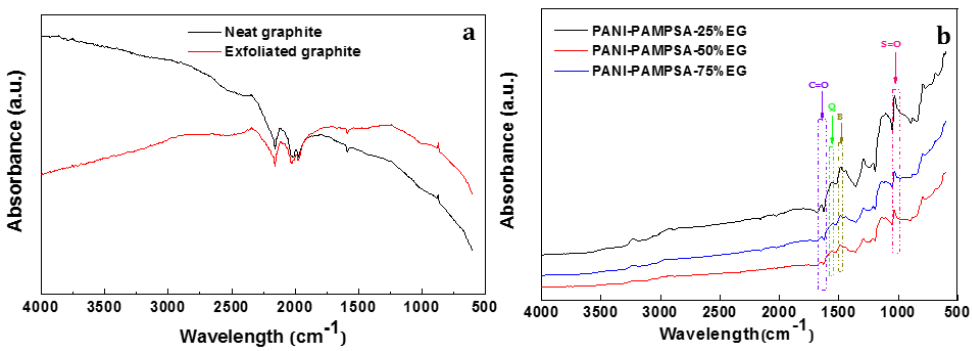

Fig. 8-3 FTIR spectra of (a) neat graphite/EG and (b) PANI-PAMPSA-EG composites (with different EG ratio to aniline).

(4) Method 1: Morphology of PANI-PAMPSA-EG composites

Fig. 8-4 illustrates the morphology of PANI-PAMPSA-EG composites (with different EG ratio to aniline). As stated in Chapter 7, PANI-PAMPSA exhibits a fibrous network. After introduction of EG, the PANI-PAMPSA molecular chain formed on the EG nanosheets and intimately intertwined and linked to the EG. It can also be observed that the aniline monomers were polymerised not only on the surface of EG, but also in the interspace of EG during the in-situ polymerisation, which was similar to the previously reported data [127]. Binding PANI-PAMPSA and EG together was beneficial for the charge transfer along the polymer chain. It can be deduced that PANI chains formed along the acid template by ionic interaction or along EG through π-π interaction. With the increased amounts of EG, more surface area was provided for aniline to be polymerised around EG [146]. The incorporation of EG into PANI was expected to form the electrical conductive network which could accelerate the charge transfer process and improve the electrical performance.

Fig. 8-4 also shows that the particle sizes of PANI-PAMPSA-EG composites increased by increasing EG content, with particle sizes at approximately 16 μm for PANI-PAMPSA-25%EG, 36 μm for PANI-PAMPSA-50%EG and 88 μm for PANI-PAMPSA-75%EG. This indicates that PANI-PAMPSA-EG composites were more prone to aggregate with increased EG content. The aggregation of composites was undesirable as it might decrease the mechanical strength of the polymer systems. Moreover, aggregation could result in poor powder dispersion in the solvent; cracks can easily propagate through the area where there was no good adhesion between PANI-PAMPSA and EG in the polymer matrix [298].

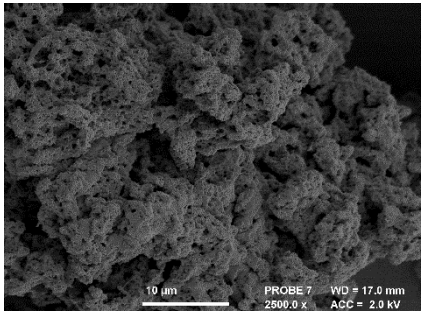

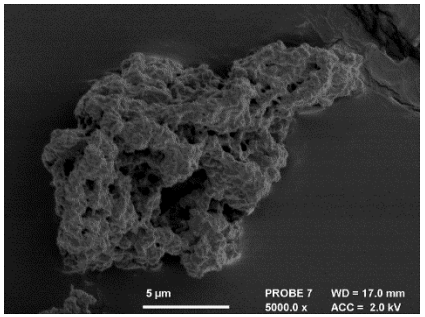

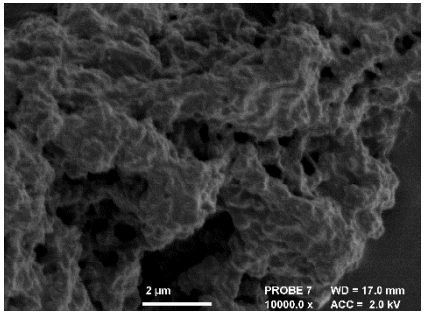

PANI-PAMPSA

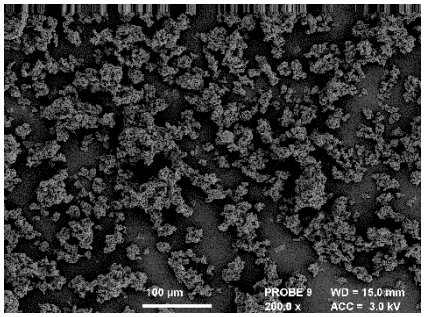

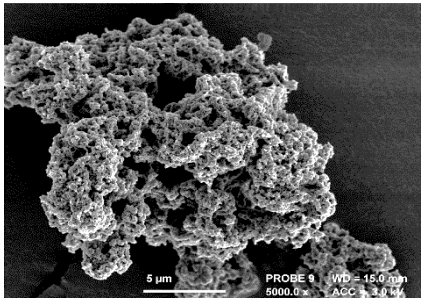

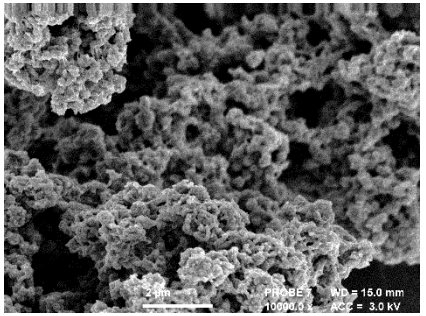

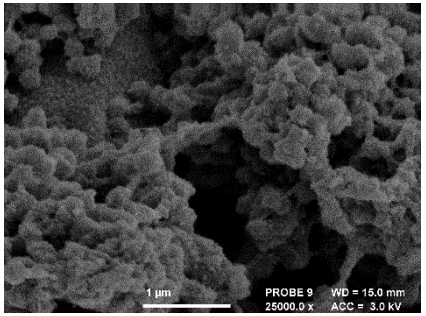

PANI-PAMPSA-25%EG

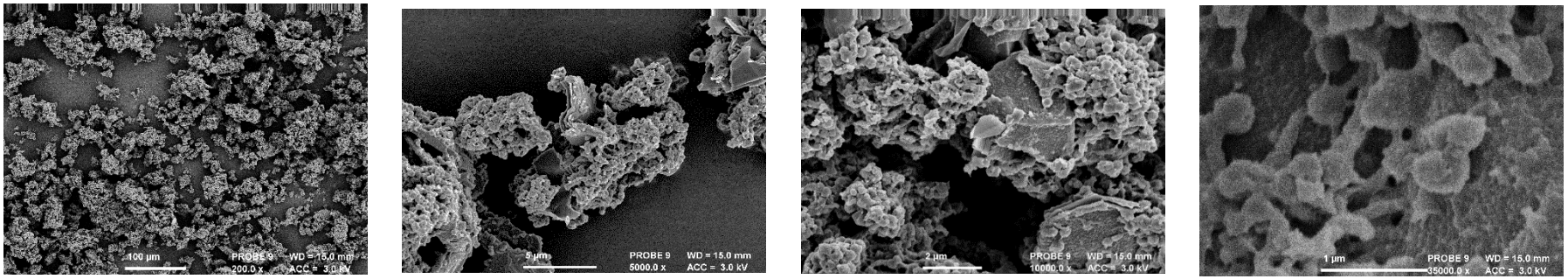

PANI-PAMPSA-50%EG

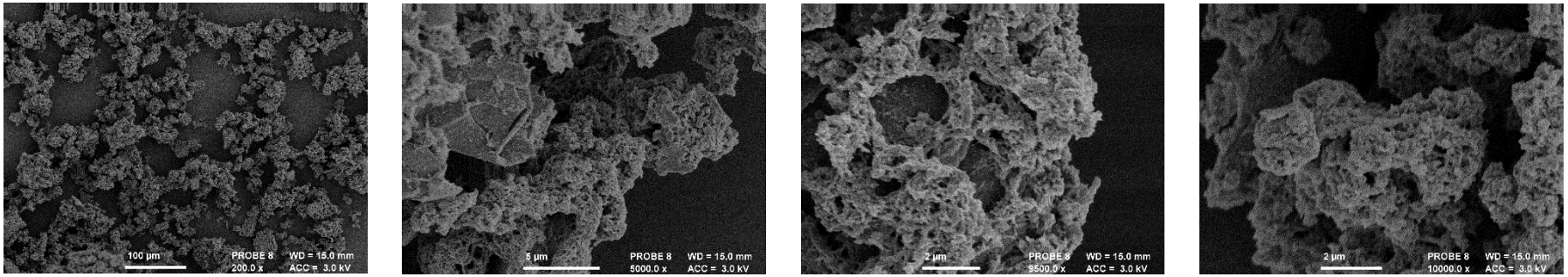

PANI-PAMPSA-75%EG

Fig. 8-4 Morphologies of PANI-PAMPSA-EG prepared by in-situ polymerisation (with different EG ratio to aniline).

(5) Method 1: Electrical conductivity of PANI-PAMPSA-EG composites

Fig. 8-5 shows the electrical conductivity of PANI-PAMPSA-EG as a function of EG ratio. It can be clearly observed that the presence of EG improved the electrical conductivity of the composites, suggesting the successful intercalation of conducting polymers into the interlayer space of EG nanosheets. It was reported that the π-bonded surface of EG could interact with the conjugated structure of PANI through the quinoid ring, and EG served as "conducting bridge" connecting conducting domains of PANI and facilitated charge transfer [132]. In addition, the electrical conductivity of PANI-PAMPSA-EG composites was found to increase by increasing EG ratio. The reason was that enhancing EG ratio could promote more activated electrons, which enabled to enhance the electron transfer and charge mobility through the polymer structure [127].

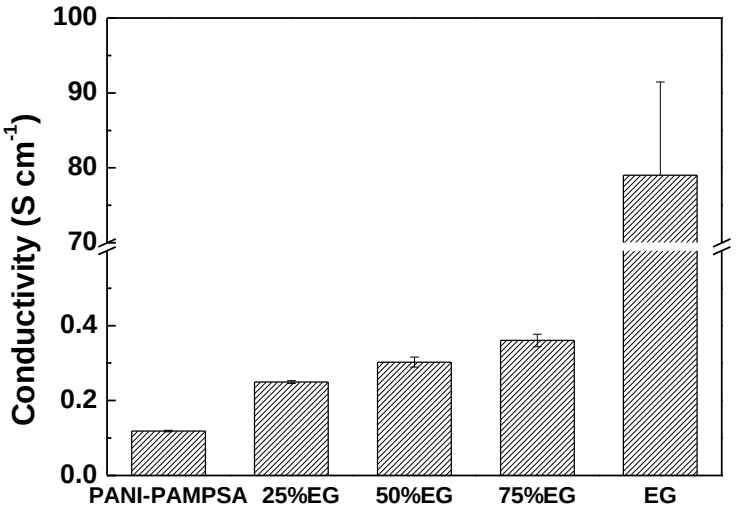

Fig. 8-5 Electrical conductivity of PANI-PAMPSA-EG composites prepared by in-situ polymerisation (with different EG ratio to aniline).

It was found in few previous studies that the intercalation of conducting polymers into the interlayer space of EG at certain ratios exhibited electrical properties greater than the individual pure components [143]. However, this phenomenon was not observed in the present case, and the conductivity showed an improvement, but was still much lower compared to the high conductivity of EG. Several possible reasons could explain the observed conductivity:

(1) It has been reported that the interaction of graphite with aniline during the in-situ polymerisation induced defects on the graphite, resulting in a less ordered

structure for final composites [129]. Based on this, the possible disorder in the EG lattice may lead to a lower conductivity.

(2) Carbon materials were found to serve as dopants for PANI to improve the electrical conductivity through doping effects or charge transfer interaction between basal plane of EG surfaces and quinoid ring of PANI chain [143, 146]. EG may have competition with the sulfonic acid group of PAMPSA during the interaction with conjugated structure of PANI. The competing phenomenon has been found in other studies, for example carbon nanotubes competed with HCl, perturbing the hydrogen bonding between the acid and PANI [132]. This is undesirable as it would to some extent affect the acid doping level of PANI.

(3) In general, the overall electrical conductivity of composite materials depends on the less conductive component. In terms of PANI-PAMPSA-EG composites, PANI-PAMPSA possessed lower conductivity and the weak charge mobility could restrict the electron transfer between the doped PANI and EG [132].

(4) The steric hindrance caused by the large size of PAMPSA and EG particles could also affect their interaction with PANI, thereby reducing the doping level of PANI. These all factors could be associated with the low conductivity of PANI-PAMPSA-EG composites.

8.2.2 Method 2: Mechanical Mixing

(1) Electrical conductivity of PANI-PAMPSA and EG mixture

In contrast to Method 1 incorporating EG into PANI through in-situ polymerisation of aniline, mechanical mixing of PANI-PAMPSA and EG was used in Method 2. Fig. 8-6 displays the conductivity of PANI-PAMPSA and EG mixture by mechanical mixing. The conductivity did not change much with the EG content of 25%, which indicated that a certain amount was needed for the sufficient dispersion of EG throughout the polymer matrix to form conductive networks [298]. It is not surprising to find that the conductivity increased by increasing the EG content from 25% to 50%. Compared with the conductivity of PANI-PAMPSA-EG composites at 41.8 % and 59.3 % of EG content with respect to PANI-PAMPSA in Method 1 (Fig. 8-5), the conductivity of PANI-PAMPSA and EG mixture at 50% of EG content to PANI-PAMPSA was much higher. This indicated that mechanical mixing was more effective in enhancing the composites

conductivity in comparison with in-situ polymerisation. Full analysis of the resulting powders (as per Method 1) is not presented because the EG used was characterised in Method 1 and PANI-PAMPSA was characterised in Chapter 7.

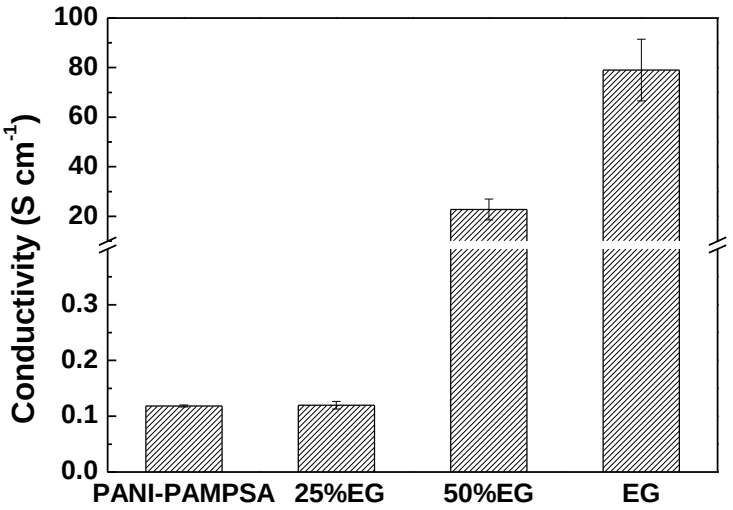

Fig. 8-6 Conductivity of PANI-PAMPSA and EG mixture by mechanical mixing.

8.2.3 Method 3: Solution Mixing by Two Ways

In Method 3, solution mixing by two ways was used to incorporate EG into Memb-PAMPSA. One way (Method 3A) was to disperse EG in NMP with ultrasonication and then add PANI-PAMPSA into the solution portion by portion to make a homogenous solution. The other way (Method 3B) was to separately disperse EG with ultrasonication and PANI-PAMPSA in NMP and then mix them together. Previous studies reported that NMP was the most promising solvent to disperse EG and the applied ultrasonication during dispersion process was favourable to prevent aggregation [293, 299, 300]. These two ways of solution mixing were found to form stable suspension of EG and produced homogenous casting solution, which was expected to form strong networks between polymer matrix and EG filler.

With this method, EG as per Method 1 was used and mixed with the PANI-PAMPSA powder that was fully characterised in Chapter 7. No further analysis of the powder or EG is therefore needed – only the resulting membranes differ from previously presented results.

8.3 Membrane preparation results: Methods 1, 2 and 3

8.3.1 NIPS Observations and Electrical Conductivity

The PANI-PAMPSA-EG composites prepared by Method 1 and PANI-PAMPSA and EG mixture made by Method 2 were dissolved in NMP solvent and then formed into membranes by NIPS method. The casting solution in Method 3 was used to make membranes by the same preparation method. The prepared membranes (Memb-PAMPSA-EG) from the above different approaches were then doped in DBSA for 24 h to obtain secondary doped membranes (Memb-PAMPSA-EG/DBSA).

Table 8-2 Lists of membrane fabrication results and conductive properties of different methods.

Method used	**Results**	**Electrical conductivity (S cm^{-1})**	
		Water bath	**Secondary doping**
Method 1	Not stable to water non-solvent immersion	$<10^{-7}$	$(1.38\pm0.24)\times10^{-4}$
Method 2	Not stable to water non-solvent immersion	$<10^{-7}$	$(2.10\pm0.40)\times10^{-4}$
Method 3A	**Stable to water non-solvent immersion**	**$(2.47\pm0.47)\times10^{-5}$**	**$(5.10\pm0.27)\times10^{-4}$**
Method 3B	Stable to water non-solvent immersion	$(2.24\pm0.40)\times10^{-5}$	$(4.32\pm0.19)\times10^{-4}$

Table 8-2 describes the membrane preparation results as well as the electrically conductive properties from different methods. The phase separation in Method 1 and 2 was not stable as the composites from Method 1 and mixture from Method 2 partially leached into the coagulation bath and the water as non-solvent changed brown in colour. These were clearly more water soluble and so water as non-solvent bath resulted in release of polymer composites into it.

It was observed that the phase separation in Method 3 (A and B) was feasible to make membranes. Method 3B had slight EG loss during the solution transfer process. The highest conductivity was found in the membrane prepared by Method 3A, and the electrical conductivity increased by two orders of magnitude compared with Memb-PAMPSA in Chapter 7. Some possible reasons for the feasible phase separation and high membrane conductivity in Method 3 are:

(1) NMP is a promising solvent to disperse carbon materials and the strong interaction between NMP and EG could further exfoliate EG [301, 302]. The applied sonication also enabled further break-up of the macroscopic aggregates of EG to form a more homogeneously dispersed solution than with the other methods [301]. Such dispersion allowed the subsequent combination of PANI-PAMPSA with EG, possibly promoting the intercalation of conducting polymers into the interlayer space of EG. Therefore, solution mixing in Method 3 allows the better dispersion of EG and PANI-PAMPSA, and gives a more ordered and better distributed polymer dope solution compared to Methods 1 and 2 [292].

(2) It was also observed that the casting solution of Method 3 became more viscous with the addition of EG, which made the casting process more difficult. Previous work in the literature [303, 304] also found that the viscosity of the polymer solution increased with nanoparticles loading. It was suggested that the increased viscosity was due to the strong interaction of nanoparticles and polymer blends. The viscous casting solution in Method 3 implied that a good interaction between EG and PANI-PAMPSA occurred during the solution mixing stage.

(3) The EG in Method 3 (with high specific surface area, surface activity and adsorption properties) facilitated the intercalation of PANI-PAMPSA into its nanosheets in the solution mixing process and so was able to quickly reach an equilibrium state [305, 306]. Some studies have shown that PANI-PAMPSA can function as an acceptor compound via the radical cations generated by PAMPSA and graphite can act as the electron donor [126]. The strong interaction between PANI and the basal plane of EG surfaces led to charge stabilisation and an increased tendency for PANI-PAMPSA to coat on the EG to form a stable composite [134]. This can also make PANI-PAMPSA contact intimately with EG layers, facilitating a larger charge transfer and thus a higher conductivity.

It can be concluded that solution mixing was the most promising method of the three examined to incorporate EG into PAMPSA doped membranes. As discussed in Chapter 7, there exists a competition between base-acid reaction of PANI with acid and hydrogen bonding of NMP with acid, suggesting the dedoping of PANI-PAMPSA in NMP solvent. By introducing a secondary dopant into membranes (prepared by Method 3), it was observed that the electrical conductivity was further improved by approximately twenty times. This implies that a bonding between

sulfonic acid group of DBSA and unsaturated imine nitrogen of PANI was formed, thereby favouring a better electron delocalisation and charge transfer.

Some studies showed that secondary dopants can strongly interact with the PANI backbone and/or primary dopant, and decrease structural defects and polarisation by creating an ordered structure [291]. In addition, secondary doping induced structural relaxations and promoted more efficient charge transfer, contributing to an improvement in membrane conductivity. The secondary dopant DBSA improved the conductivity of PANI composites and electron transfer between secondary doped PANI and EG became less restricted compared to primary PA doped PANI with EG. Therefore, it could lead to an improvement in both the carrier number and charge mobility, contributing to an overall enhancement of electrical conductivity [143]. The increased conductivity due to secondary doping also implies that the conducting PANI part plays an important role in the conductivity of Memb-PAMSPA-EG [143]. The ability to improve the electrical conductivity of the acid doped PANI part could be advantageous to the overall membrane conductivity enhancement. The solution mixing (Method 3A) produced membranes with the highest electrical conductivity, so the following studies focused on the investigation of the obtained Memb-PAMPSA-EG and Memb-PAMPSA-EG/DBSA.

8.3.2 Membrane Robustness Analysis

As in previous chapters a backlit LED light box was used to detect any visible defects, such as pinholes and cracks, on the membrane surface (Fig. 8-7 (a)). It was observed that the EG was dispersed evenly on the membrane and formed a rougher surface than Memb-PAMPSA. After secondary doping, the membrane exhibited a relatively smoother surface and seemed to be more relaxed compared to Memb-PAMPSA-EG.

RGB colour index was again utilised to characterise the membrane colour change (Fig. 8-7 (b)). It was found that the RGB value of Memb-PAMPSA-EG was higher than Memb-PAMPSA, suggesting that the membrane became darker in colour. This confirmed the incorporation of black EG into the membrane. As discussed in Chapter 7, the R:G:B value ratio of Memb-PAMPSA was 0.22:0.35:0.43. The R:G:B value ratio of Memb-PAMPSA-EG and Memb-PAMPSA-EG/DBSA was

0.23:0.34:0.43 and 0.23:0.36:0.41, respectively. The green colour value increased and blue colour value decreased after DBSA doping, suggesting an improved PANI doping level caused by the incorporation of DBSA. These also implied that the Memb-PAMPSA-EG was not fully doped (i.e. only partially doped), therefore secondary doping can be considered as a promising way to further improve the membrane conductivity combined with primary polymer acid doping.

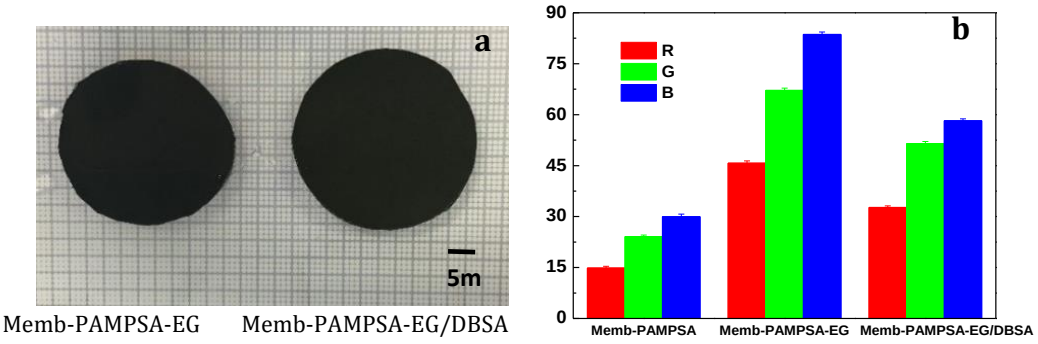

Fig. 8-7 (a) images and (b) RGB colour index of Memb-PAMPSA-EG and Memb-PAMPSA-EG/DBSA.

Fig. 8-8 shows the Young's modulus and elongation at break of Memb-PAMPSA, Memb-PAMPSA-EG and Memb-PAMPSA-EG/DBSA. The Young's modulus did not show any significant changes with the addition of EG but elongation at break showed a decrease, which suggested the membrane flexibility decreased with the addition of EG. This decreased flexibility might be caused by the brittleness and rigidity of EG which was also found in some other studies [298, 307, 308]. Additionally, no significant difference of mechanical strength was found after secondary doping by DBSA, suggesting that DBSA as a secondary dopant was desirable to further improve the membrane conductivity without losing the mechanical strength.

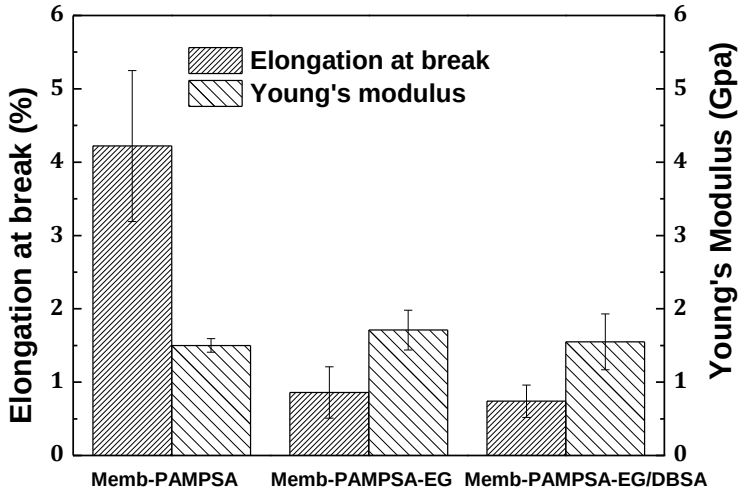

Fig. 8-8 Membrane mechanical properties for Memb-PAMPSA, Memb-PAMPSA-EG and Memb-PAMPSA-EG/DBSA: Young's modulus and elongation at break (%).

8.3.3 FTIR Analysis of Membranes

FTIR spectra in Fig. 8-9 indicates the chemical groups that are present in Memb-PAMPSA, Memb-PAMPSA-EG and Memb-PAMPSA-EG/DBSA. In the three membrane samples, the peaks at 1030-1037 cm^{-1} and 1154-1158 cm^{-1} were assigned to S=O stretching of sulfonic acid group and asymmetric SO_3^- stretching of sulfonate salts, respectively. The peak at 1653-1657 cm^{-1} corresponded to C=O stretching of PAMPSA. The presence of these peaks was indicative of the incorporation of PAMPSA into membranes. Generally, the characteristic bands of benzenoid and quinoid rings appeared at approximately 1495 cm^{-1} and 1598 cm^{-1} in undoped PANI membrane (Chapter 5). Upon the incorporation of PAMPSA, the quinoid stretching mode of PANI red shift from 1598 cm^{-1} to 1590 cm^{-1}, implying the interaction between sulfonic acid and imine nitrogens of PANI. Memb-PAMPSA was only partly doped as mentioned in Chapter 7. Upon the addition of EG, the quinoid stretching mode at 1590 cm^{-1} further red shift, likely indicating that the undoped imine nitrogen interacted with the basal plane of EG surfaces by π-π interaction [309].

As in Chapter 5, the PANI oxidation state is reflected by the ratio of quinoid and benzenoid (Q/B) structure, which can be calculated by the corresponding peak height ratio [310]. The Q/B ratio calculated from FTIR was 0.31 for Memb-PAMPSA, 0.76 for Memb-PAMPSA-EG and 0.83 for Memb-PAMPSA-EG/DBSA. By the incorporation of EG and DBSA, the Q/B ratio of the

corresponding membrane was much nearer to unity, suggesting an increased conductivity [310]. This is consistent with the improved conductivity of Memb-PAMPSA-EG and Memb-PAMPSA-EG/DBSA compared to Memb-PAMPSA in Section 8.3.1.

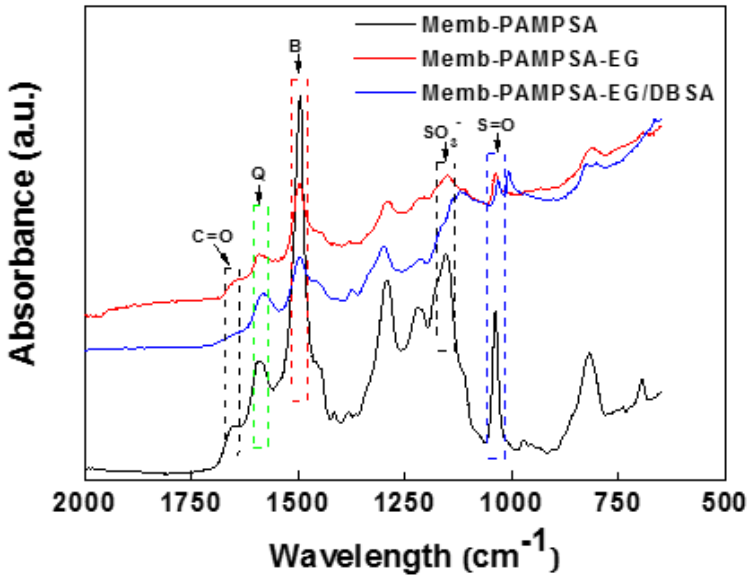

Fig. 8-9 FTIR spectra of Memb-PAMPSA, Memb-PAMPSA-EG and Memb-PAMPSA-EG/DBSA.

8.3.4 Morphology of the Membranes

Fig. 8-10 shows the surface morphology of Memb-PAMPSA-EG and Memb-PAMPSA-EG/DBSA. It can be seen that the EG nanosheets were uniformly dispersed in the matrix and a good interfacial contact was established at the interface, forming a conducting network. Some studies showed that the graphite particles aggregated into larger clusters but this was not observed here. As previously outlined, EG was better dispersed in NMP with the aid of ultrasonication [301]. After doping by DBSA, the membrane surface became smoother, consistent with the membrane appearance in Fig. 8-7 (a). This was likely due to DBSA doping changing the molecular conformation of PANI-PAMPSA from “compact coil” to expanded chain [311]. It has been reported that the packing of particles influenced the macroscopic conductivity [312]. Inter-particle conductivity is dependent on the connectivity by direct contact among the particles while intra-particle conductivity is related to the conductive path length along the crystal domains of particles. Intra-particle conductivity is dominant when conducting particles are fully compacted [295]. In terms of the packing of EG on the

membrane surface, it can be assumed that the intra-particle conductivity plays a significant role in the macroscopic conductivity of membranes.

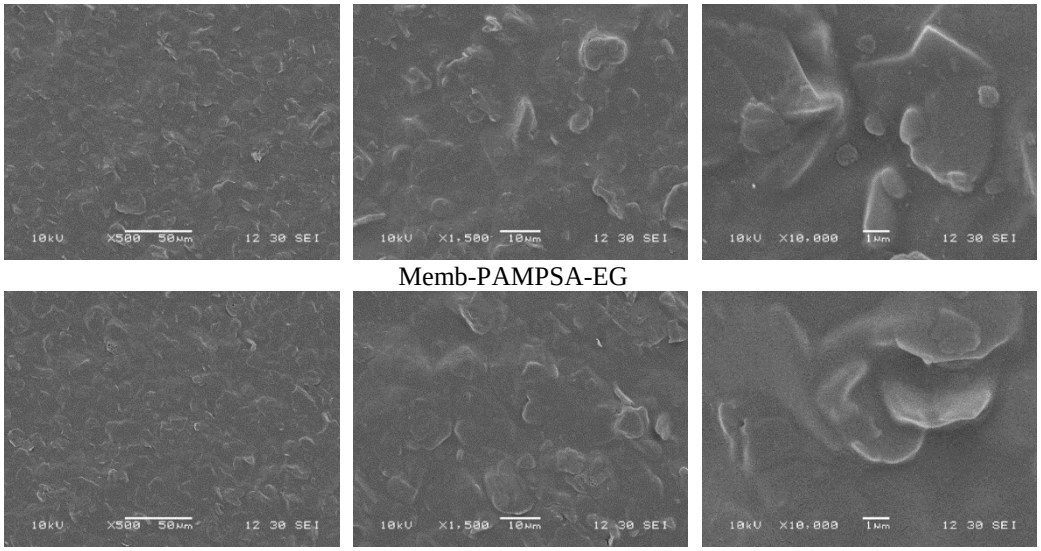

Fig. 8-10 Surface morphology of Memb-PAMPSA-EG (top) and Memb-PAMPSA-EG/DBSA (bottom).

Fig. 8-11 shows the cross-section of Memb-PAMPSA and Memb-PAMPSA-EG. Memb-PAMPSA-EG consisted of a dense top layer, a transition region and a porous layer with large macroscopic-voids. This indicates rapid demixing during the phase inversion process compared to the more uniform structure of Memb-PAMPSA, which is indicative of slow demixing. This also implies that EG had a considerable impact on the phase inversion process. Another important observation was that EG appeared to make the membrane more porous. The increased porosity was likely caused by the dislocation of EG in PANI-PAMPSA-EG composites during the solvent exchange process, leading to more cavities in the membrane structure [51]. Also, rapid demixing generally leads to more porous structures and if there are defects during solidication caused by poor contact between the solids and polymers, this makes the membrane more porous.

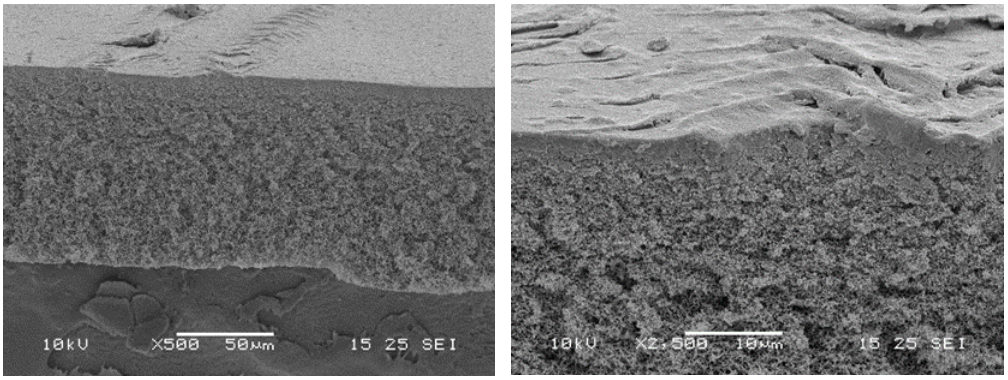

Memb-PAMPSA

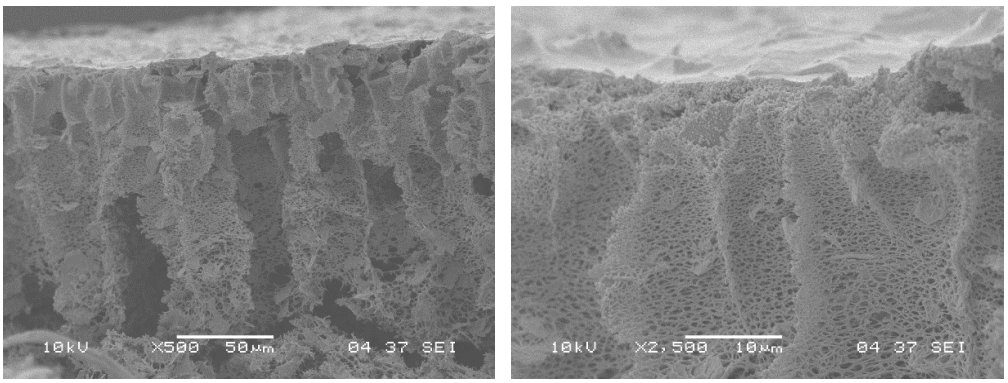

Memb-PAMPSA-EG

Fig. 8-11 Cross-section of Memb-PAMPSA (top) and Memb-PAMPSA-EG (bottom).

8.3.5 Transport Properties of Membranes

Initial permeance and selectivity of Memb-PAMPSA-EG and Memb-PAMASA-EG/DBSA were conducted in dead-end filtration and BSA nanoparticles were utilised to evaluate the membrane rejection. Fig. 8-12 (a) illustrates the permeance of Memb-PAMPSA-EG and Memb-PAMPSA-EG/DBSA. Upon the addition of EG, the membrane permeance increased to 399±19 $L \cdot m^{-2} \cdot h^{-1} \cdot bar^{-1}$, which was twice higher than Memb-PAMPSA. One possible reason was that the presence of EG opened the pores of membranes and resulted in higher porosity, which was evidenced by the membrane morphology in Fig. 8-11. Another possible reason was due to the more hydrophilic membrane surface as a result of EG incorporation [303, 304]. The effective contact angle in Fig. 8-14 was found to change from 62±2° in Memb-PAMPSA to 54±2° in Memb-PAMPSA-EG, illustrating the surface of Memb-PAMPSA-EG was more hydrophilic. The increased membrane permeance results were consistent with the dynamic contact angle results in Fig. 8-14, implying that the introduction of EG resulted in a higher solute permeation rate.

In terms of secondary doping with DBSA, the membrane permeance slightly decreased to 357±24 $L \cdot m^{-2} \cdot h^{-1} \cdot bar^{-1}$. The possible reason was that the free volume between polymer chains was filled with long chain acids (DBSA), which made the diffusion of water solute more difficult [313]. Fig. 8-12 (b) illustrates the BSA rejection of Memb-PAMPSA-EG and Memb-PAMPSA-EG/DBSA. Both the Memb-PAMPSA-EG and Memb-PAMPSA-EG/DBSA exhibit above 90% rejection of BSA (MW= 66, 000 g mol^{-1}), which suggested that the MWCO of membranes was less than 66, 000 g mol^{-1} with BSA as the MWCO probe.

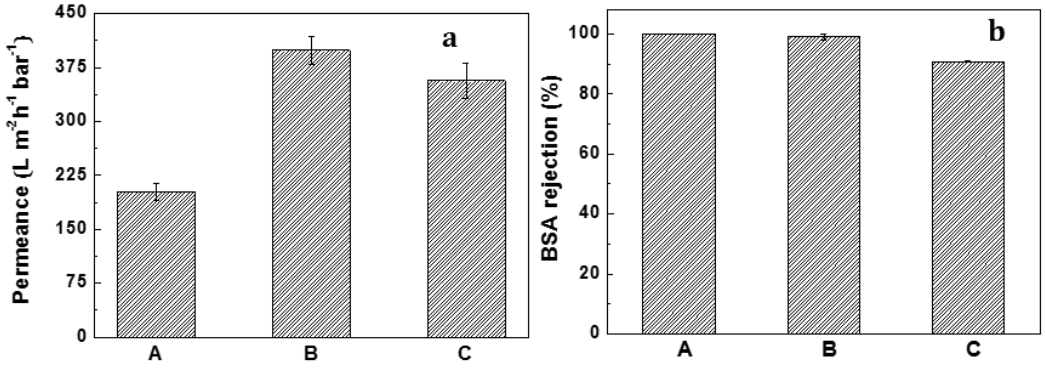

Fig. 8-12 (a) Permeance and (b) BSA rejection of Memb-PAMPSA-EG and Memb-PAMPSA-EG/DBSA (A= Memb-PAMPSA; B=Memb-PAMPSA-EG; C= Memb-PAMPSA-EG/DBSA).

As in Chapter 7, in order to test the membrane stability during filtration, the pHs of the membrane permeate during different filtration stages were measured. Fig. 8-13 presents the pHs of water permeate (before filtration, after preconditioning and after the actual filtration) in the dead-end filtration. The permeate pH in the preconditioning stage slightly varied with higher pH in Memb-PAMPSA-EG and lower pH in Memb-PAMPSA-EG/DBSA. The higher pH in Memb-PAMPSA-EG could be due to the residual NMP entrapped in the membrane. As discussed in Chapter 5 and 7, PANI membranes were prepared using NMP as a solvent and therefore it would not be surprising if these membranes still contained residual amounts of NMP. Doping of Memb-PAMPSA-EG with DBSA could remove the residual NMP trapped in the space between polymer chains. The slightly lower pH in Memb-PAMPSA-EG/DBSA was likely due to the redundant DBSA which stayed on the membrane surface going into the permeate during filtration, but this can be regarded as negligible compared to the leaching of small acids as stated in Chapter 5.

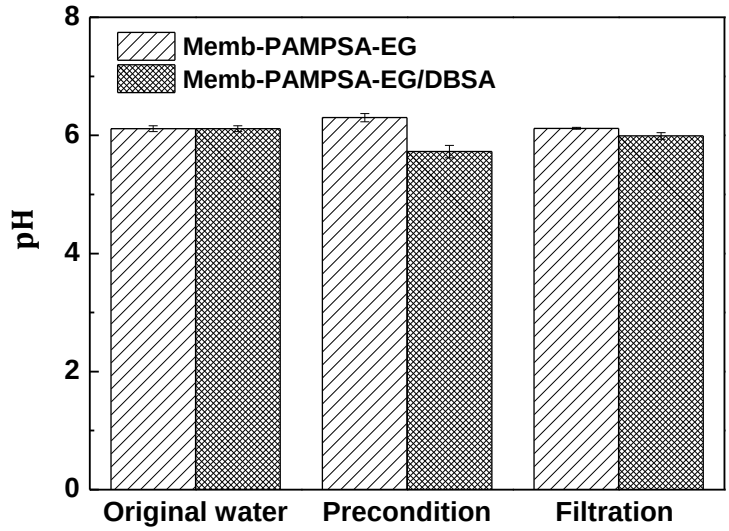

Fig. 8-13 pH change of Memb-PAMPSA-EG and Memb-PAMPSA-EG/DBSA in dead-end filtration.

It is expected that the DBSA leaching would not be a problem in this study for two reasons:

- DBSA, with long alkyl side chains, had weak molecular mobility compared to small acids, making leaching more difficult to happen.
- The interaction of DBSA with PAMPSA and PANI could immobilise and entangle DBSA in the chain structure [314].

In the actual filtration stage, the pHs of Memb-PAMPSA-EG and Memb-PAMPSA-EG/DBSA permeate kept stable, which indicated that both membranes were more stable in filtration compared with Memb-HCl in Chapter 5.

8.3.6 Initial Tuneability Assessment of Membranes

As in previous chapters, in order to determine the membrane initial tuneability, dynamic droplet penetration through the membranes with or without applied potential was examined. The variation of effective contact angle and droplet height with time indicated the solute permeation rate. Fig. 8-14 shows the effective contact angle and droplet height change with time at applied potential of 0 and 30 V. As can be seen, the applied potential had a significant impact on the water permeation rate through both membranes. The effective contact angle varied from 1.1 to 1.8 θ s^{-1} for Memb-PAMPSA-EG and from 1.3 to 2.0 θ s^{-1} for Memb-PAMPSA-EG/DBSA. The droplet height changed from 1.6×10^{-2} to 2.3×10^{-2} mm s^{-1} for Memb-PAMPSA-EG and from 1.7×10^{-2} to 2.4×10^{-2} mm s^{-1} for Memb-

PAMPSA-EG/DBSA. Compared to Memb-PAMPSA whose effective contact angle did not change between 0 and 30 V measurements, the significant dynamic contact angle change of Memb-PAMPSA-EG and Memb-PAMPSA-EG/DBSA gives a further quantitative indication of the electrical tuneability of these membranes.

It was also found that the solute permeation rate was much faster by the addition of EG, with effective contact angle change of 1.1 θ s^{-1} for Memb-PAMPSA-EG compared to 2.1×10^{-1} θ s^{-1} for Memb-PAMPSA. This was consistent with membrane permeance results in dead-end filtration (Fig. 8-12), indicating that the presence of EG formed a more hydrophilic membrane surface and promoted an increased attracting force across the interface between membranes and water. Furthermore, the membrane became more porous due to the addition of EG, as outlined in Section 8.3.4, resulting in a faster permeation rate.

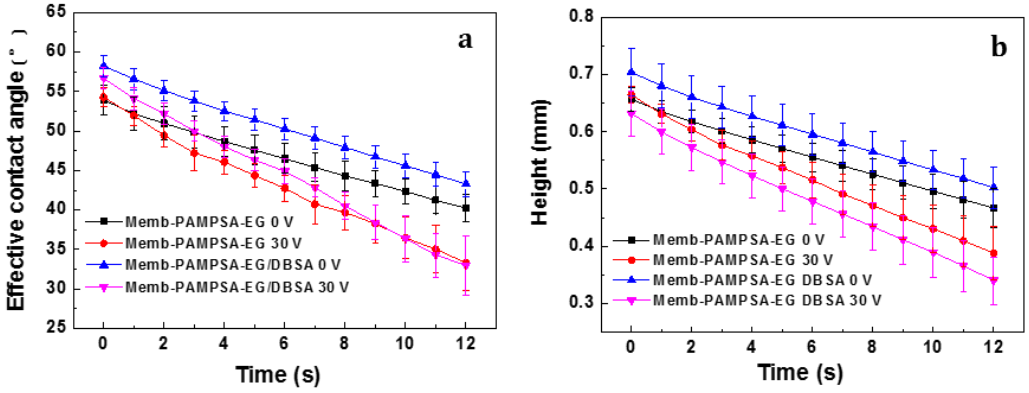

Fig. 8-14 (a) The effective contact angle and (b) droplet height change of Memb-PAMPSA-EG and Memb-PAMPSA-EG/DBSA over time with and without potential (30 V).

As discussed in Chapter 7, an applied potential can bring about several changes that could produce a more general membrane tuneability beyond ion separations. These include: changing surface charge controlling Donnan exclusion, change in pore size/free volume (via incorporation or expulsion of ions from the acid dopant site) controlling pore flow transport, and chemical property changes controlling solution diffusion. Applying an electrical potential to the membrane resulted in a transition to a higher water permeation rate, indicating the bulk volume swelling and water dipole interaction are likely to be the main reason for the increased permeation rate. Some previous studies [307] reported that the applied potential could oxidise the membrane, leading to the expansion of membranes. As graphite

had little or no volume change under applied potential, the film expansion was mainly due to the conformational changes of the doped PANI chain.

EG possesses highly mobile electrons that results in a high electrical conductivity. Compared to Memb-PAMPSA, the incorporation of EG into membranes facilitated the rapid charge transport and electron delocalisation between the PANI backbone and the aromatic structure of EG as discussed previously. Applying an external potential, more polarons were formed to move along the polymer backbone, causing a greater motion of anions or cations on the polymer chains. This created more voids or free volume, allowing more water to pass through the membrane [60]. It can be concluded that membrane with higher conductivity displayed more significant dynamic contact angle change under applied potential. This is consistent with the results in Chapter 5, implying that the initial significant tuneability in the dynamic droplet penetration was closely related to the high membrane conductivity.

8.3.7 Electrically Connected Cross-flow Filtration of Membranes

Electrically connected cross-flow filtration was used to quantify under realistic filtration conditions the tuneability of membrane flux and selectivity at a fixed applied potential compared to zero applied potential. As mentioned in Chapter 7, neutral PEG UF mixture was utilised as feed to evaluate the effect of voltage on the membrane selectivity. However, the membrane structures are very porous and loose due to the incorporation of EG. No significant difference was observed on the PEG rejection of Memb-PAMPSA-EG and Memb-PAMPSA-EG/DBSA with and without applied potential (Fig. C1 and C2, Appendix C). The MWCO technique used is for NF/low UF membranes and therefore does not have the ability to resolve this change in MWCO pattern, which is significantly outside of the intended range. A different technique was not used to quantify this either, since the membranes wanted for this project should be in the NF/low UF MWCO range.

In terms of the permeance of Memb-PAMPSA-EG and Memb-PAMPSA-EG/DBSA under applied potential of 0 and 30 V with PEG UF mixture as feed, the membranes are too permeable for any of the tuneability mechanisms to have a significant effect on the bulk flow of solvent through the membrane (Fig. C3, Appendix C). Again, there is no real discernible effect on the permeance with DI

water as feed with voltage (Fig. C4, Appendix C), which again can be attributed to the very porous nature of the membranes studied compared to those in previous chapters.

It was observed that the Memb-PAMPSA-EG/DBSA displayed higher current in comparison with Memb-PAMPSA-EG (Fig. C3, Appendix C), which was in good agreement with the electrical conductivity results. The current passing through the membrane was found to remain stable, indicating good membrane stability during filtration.

In summary, the addition of EG has made the PAMPSA doped membrane too porous (increasing their MWCO) for the electrical tuneability effects to be observed in the MWCO range wanted for these membranes (i.e. in the NF/low UF MWCO range). This indicates that although the addition of EG increased the conductivity and consequently should increase the electrical tuneability of the membranes according to the findings of Chapter 6 and 7, it also unfortunately made the membranes looser in terms of MWCO) – the opposite effect to what was wanted based on the conclusions of Chapter 7. Therefore, work needs to be done to find a solution to tightening the MWCO of the PANI-PAMPSA membranes – this will be covered in Chapter 9.

The current membranes however will have sufficiently low MWCO to be used for large molecule filtrations – such as with a model foulant such as BSA. Therefore, these membranes will be used to determine their potential as anti-fouling membranes. This is covered in Chapter 10.

8.4 Conclusions

In order to enhance the electrical conductivity of Memb-PAMPSA, EG and secondary dopant DBSA were utilised to incorporate into the membrane in this chapter. The results showed that:

- Different methods, including incorporating EG in the in-situ polymerisation of aniline, mechanical mixing of EG and PANI-PAMPSA powder and solution mixing were chosen to incorporate EG into Memb-PAMPSA. Among these methods, solution mixing was found to be an efficient way to incorporate EG into the membrane.

- The conductivity of PAMPSA doped membrane could be improved by two orders of magnitude by the incorporation of EG, and further enhanced by twenty times using a long chain acid DBSA as a secondary dopant without losing the mechanical strength.
- Compared with Memb-PAMPSA (contact angle of 62±2^{o}), the surface of Memb-PAMPSA-EG became more hydrophilic (contact angle of 54±2^{o}) and the membrane permeance doubled as a result of the incorporation of EG.
- Dynamic droplet penetration showed that Mem-PAMPSA-EG and Mem-PAMPSA-EG/DBSA exhibited enhanced membrane permeation rate under applied potential. Compared to Memb-PAMPSA whose effective contact angle did not change between 0 and 30 V measurements, the significant dynamic contact angle change of Memb-PAMPSA-EG and Memb-PAMPSA-EG/DBSA gives a further quantitative indication of the electrical tuneability of these membranes.
- The addition of EG has made the membrane too porous (lower PEG rejection) for the electrical tuneability effects to be observed in the MWCO range wanted for these membranes (i.e. in the NF/low UF MWCO range). Further work is needed to tighten the MWCO of these membranes. Also, the overall objective is to test the tuneability of the conducting PANI membranes. Therefore, large molecule filtrations – such as BSA will be used to further determine the responsiveness of the current membranes (even though the membrane produced showed high flux and low selectivity).

9 The Effect of Co-Solvent and Evaporation Time on the Performance of Memb-PAMPSA

9.1 Introduction

Compared to undoped PANI membranes, the incorporation of PAMPSA into a PANI network formed a more open pore structure with higher porosity and larger free volume. These membranes were found to be within the loose UF range based on the PEG mixture and BSA rejection determined in Chapter 7. These membranes however were not conductive enough to produce a significant change in selectivity and permeance with applied potential and were not at a tight enough MWCO range as desired (NF range membranes are wanted). To increase conductivity, EG was added which increased conductivity but also decreased the rejection. Therefore, the major challenge for Memb-PAMPSA is to tighten the MWCO.

In order to investigate whether the membranes can be tightened to the same MWCO range as the small acid doped membranes in Chapter 5, attempts have been made by changing the membrane preparation parameters. Therefore, the aims of this chapter are to:

- Investigate the effect of membrane preparation parameters on the tightening of Memb-PAMPSA.
- Study the effect of co-solvent and evaporation time on the properties of Memb-PAMPSA.

This work however is not complete due to time limitations at the end of the 3year funded PhD period and therefore will only give an initial indication of the feasibility of this method.

It is known that the use of a volatile co-solvent in the polymer solution can cause a change in the membrane morphology and performance [105, 113]. Addition of co-solvents can alter the instantaneous demixing behaviour, trigger the formation of a tighter skin layer and change the membrane morphology from finger-like voids to sponge-like microstructures [114, 115]. THF and acetone are commonly applied highly volatile co-solvents used in membrane fabrication through the NIPS method [114, 117, 315]. The evaporation of co-solvents prior to immersion into the coagulation bath and different demixing rate during NIPS produce a region with locally increased polymer concentration, desirable for the formation of a tighter defect-

free skin layer [114, 316, 317]. On the other hand, the evaporation time plays a crucial role on the thickness and porosity of the formed skin layers of membranes [117, 318]. In general, a longer evaporation time results in a thicker skin layer with decreased surface porosity, while a shorter evaporation time leads to a thinner skin layer with increased surface porosity [118].

In order to investigate the effect of membrane preparation parameters on the tightening of Memb-PAMPSA, different co-solvents (THF and acetone) and evaporation times were selected in this study. The effect of adding volatile co-solvents on the final membrane properties was determined by different characterisation techniques. SEM was employed to analyse the fabricated membrane morphologies. Dead-end filtration was utilised to determine the membrane separation performance. FTIR, four-point probe conductivity meter and the electrically connected cross-flow filtration were applied to further investigate the membrane tuneability in terms of the overall objectives of the thesis.

9.2 Membrane Preparation

Table 9-1 displays the notation and preparation conditions of membranes used in this study. As it is well known, 4-MP, as a secondary amine additive, plays a crucial role in the enhancement of PANI dissolution [50, 106]. It can form hydrogen bonding between the hydrogen of the amine and the imine nitrogen of polyaniline. The sufficient steric bulk can inhibit the gelation in concentrated PANI solutions [200, 319]. However, 4-MP is found to be correlated with polymer degradation, which could result in the low conductivity and poor mechanical strength [200, 320]. Therefore, decreasing the content of 4-MP in the casting solution was crucial to avoid the drawback of using secondary amines. The 4-MP used in the previous chapters was in the molar ratio of 1.2:1 to PANI tetrameric repeat unit. It was observed (Table 9-1) that decreasing the amount of 4-MP led to gelation of membrane preparation solution. Just like PANI, the PANI-PAMPSA solution was also observed to become a gel at a high polymer concentration in the absence of an anti-gelling agent (e.g. 4-MP). The casting solution (mass ratio of NMP/Acetone at 70/30) became a gel at a molar ratio of 4-MP/PANI tetrameric repeat unit of 0.5/1. Therefore, the molar ratio of 4-MP to PANI tetrameric repeat unit was kept at 1.2/1 for the following membrane preparation.

In terms of THF and acetone as co-solvents, it was found that acetone led to gel formation, while THF formed a viscous solution that could be cast into membranes. Based on the experimental phenomenon, it was observed that THF was a relatively weak solvent for PANI-PAMPSA compared to NMP while acetone was a strong non-solvent for PANI-PAMPSA. Hence, adding acetone into the solvent led to the agglomeration of PANI-PAMPSA particles (gelation); this can be attributed to hydrogen bonding between the PANI chains. This gelation made the attempts to prepare PANI-PAMPSA membranes with acetone as a co-solvent unsuccessful. On the other hand, the addition of THF produced a viscous polymer solution: therefore, membranes were cast at different evaporation times and investigated further.

Table 9-1 Preparation parameters (composition of casting solution, evaporation time) and resulted membrane solution.

Membrane notation	Solvent/co-solvent (mass ratio)	Gel inhibitor	Evaporation time (s)	Result
M1	NMP	No 4-MP	---	60%-70% dissolved
M2	DMF	No 4-MP	---	40%-50% dissolved
M3	DMAc	No 4-MP	---	60%-70% dissolved
M4	NMP	4-MP (4-MP/PANI tetrameric repeat unit molar ratio=1.2:1)	0 s	Viscous solution, able to cast
M5	NMP/Acetone (70/30)	4-MP (4-MP/PANI tetrameric repeat unit molar ratio=1.2:1)	---	Gels
M6	NMP/THF (70/30)	4-MP (4-MP/PANI tetrameric repeat unit molar ratio=0.5:1)	---	Gels
M7	NMP/THF (70/30)	4-MP (4-MP/PANI tetrameric repeat unit molar ratio=1.2:1)	0 s	Viscous solution, able to cast
M8	NMP/THF (70/30)	4-MP (4-MP/PANI tetrameric repeat unit molar ratio=1.2:1)	10 s	Viscous solution, able to cast
M9	NMP/THF (70/30)	4-MP (4-MP/PANI tetrameric repeat unit molar ratio=1.2:1)	20 s	Viscous solution, able to cast
M10	NMP/THF (70/30)	4-MP (4-MP/PANI tetrameric repeat unit molar ratio=1.2:1)	30 s	Viscous solution, able to cast
M11	NMP/THF (70/30)	4-MP (4-MP/PANI tetrameric repeat unit molar ratio=1.2:1)	45 s	Viscous solution, able to cast
M12	NMP/THF (70/30)	4-MP (4-MP/PANI tetrameric repeat unit molar ratio=1.2:1)	60 s	Viscous solution, able to cast
M13	NMP/THF (70/30)	4-MP (4-MP/PANI tetrameric repeat unit molar ratio=1.2:1)	120 s	Viscous solution, able to cast

***** Temperature: 22-23℃. Humidity: 40-50%

9.3 Cross-section Morphologies of Memb-PAMPSA/THF

To explore the influence of THF on the membrane morphology, membrane cross-sections were investigated using SEM as shown in Fig. 9-1. It was observed that the distinguishable skin layer was formed by adding THF into the casting solution, indicating a delayed demixing process. THF can be driven off under forced convection conditions, resulting in a loss of the co-solvent from the outermost membrane surface. This behaviour led to the coalescence and rapid vitrification of polymer-rich regions and thus formed an oriented skin layer [276]. The skin layer acting as a barrier slowed down the counter-diffusion between the solvent and non-solvent, leading to a slower demixing process in the coagulation bath. Furthermore, the membranes prepared under a longer evaporation time (namely 45, 60 and 120 s) exhibited a thicker skin layer, followed by a transition region with a porous structure. This reduced the tendency of forming defects and pinholes on the membrane surface. However, membranes prepared using a shorter evaporation time (namely 0 s) displayed a thinner skin layer followed by a finger-like void morphology, which could cause the formation of pinholes on the membrane surface [315]. In terms of the overall aims of this project, membranes prepared at the evaporation time of 60 s, being the best performing membranes, were employed to investigate the impact of co-solvent on the membrane properties including transport properties, electrical conductivity and tuneability.

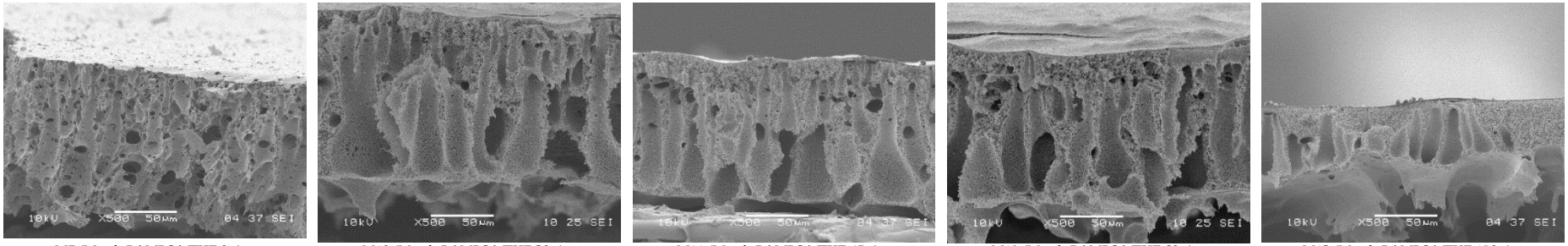

Fig. 9-1 Cross-section morphologies of Memb-PAMPSA/THF at different evaporation times.

9.4 Memb-PAMPSA/THF Robustness Properties

Fig. 9-2 (a) and (b) show the membrane image and RGB colour index of Memb-PAMPSA/THF (evaporation time of 60 s), respectively. The membrane surface was smooth and shiny, very similar to the Memb-PAMPSA in Chapter 7. The RGB index of Memb-PAMPSA/THF was found to be higher than Memb-PAMPSA, showing that the addition of THF produced denser and darker membranes. It was observed that PANI-PAMPSA exhibited lower dissolution in THF compared to NMP, and the formed casing solution was more viscous. The higher viscosity of PANI-PAMPSA solution would result in a denser membrane compared to Memb-PAMPSA without THF as a co-solvent.

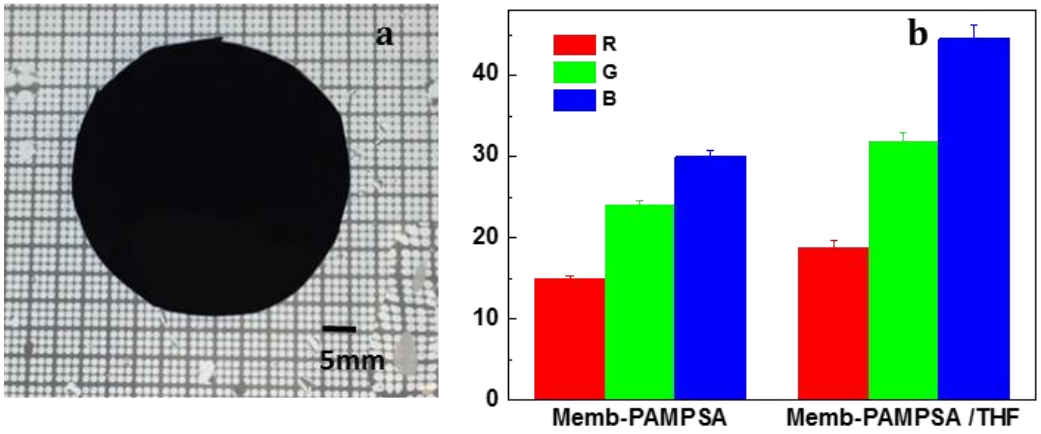

Fig. 9-2 (a) images and (b) RGB colour index of Memb-PAMPSA/THF.

The tensile strength and Young's modulus of Memb-PAMPSA and Memb-PAMPSA/THF are depicted in Fig. 9-3. Memb-PAMPSA/THF displayed a slight improvement in the tensile strength and Young's modulus, implying an enhancement in the mechanical strength compared to Memb-PAMPSA. This can be explained by the formation of a denser skin layer by utilising THF as a co-solvent (Fig. 9-1). In addition, the entanglement of polymer chains in a more viscous solution was favourable to form membranes with minimum defects [118]. These all contributed to the relatively high mechanical strength of Memb-PAMPSA/THF.

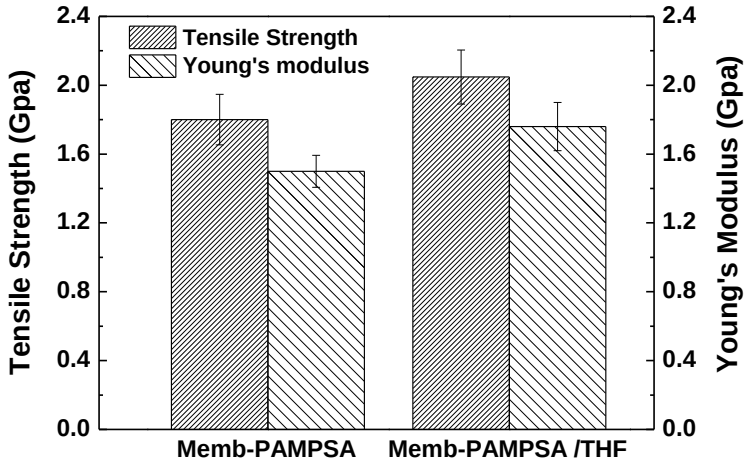

Fig. 9-3 Tensile strength and Young's modulus of Memb-PAMPSA and Memb-PAMPSA/THF.

9.5 Surface Morphology of Memb-PAMPSA/THF

The surface morphology of Memb-PAMPSA/THF is shown in Fig. 9-4. Similar to the Memb-PAMPSA in Chapter 7, the surface was observed to be rough with aggregates. NMP was relative a "good" solvent for the PANI-PAMPSA in comparison to DMF and DMAc as mentioned in Chapter 7. The roughness was probably due to the undissolved clusters of PANI-PAMPSA. This indicated that a better dissolution method or a longer dissolution time is needed to better dissolve the PANI-PAMPSA complex powder.

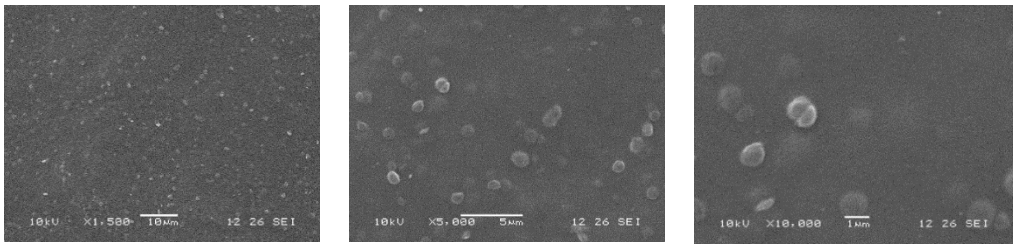

Fig. 9-4 Surface morphology of Memb-PAMPSA/THF.

9.6 Permeance and Rejection of Memb-PAMPSA/THF

Fig. 9-5 shows the permeance and rejection of Memb-PAMPSA/THF tested by water and PEG mixture solution. Compared to Memb-PAMPSA, the permeance of Memb-PAMPSA/THF with water and PEG mixture as feed was decreased by 59.6% and 61.8%, respectively. The rejection of PEG 1000-6000 was 30%-40% for Memb-PAMPSA/THF, in comparison with 10%-30% for Memb-PAMPSA. This suggested that the membrane was slightly tightened after adding THF as co-solvent. This is most likely due to the formation of denser skin layer contributed to the decreased permeance and increased rejection. However, Memb-

PAMPSA/THF cannot be tightened into the MWCO range of small acid doped membranes, indicating that the increased porosity in Memb-PAMPSA was mainly due to the large MW of PAMPSA, which creates a greater free volume in the membrane structure.

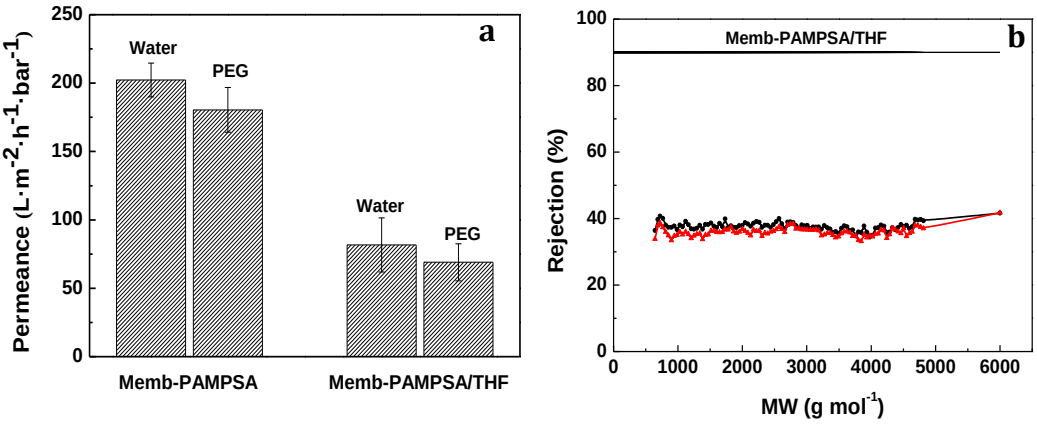

Fig. 9-5 (a) Permeance and (b) PEG rejection of Memb-PAMPSA/THF.

9.7 Electrical Conductivity of Memb-PAMPSA/THF

Fig. 9-6 illustrates the electrical conductivity of Memb-PAMPSA and Memb-PAMPSA/THF. Addition of co-solvent THF decreased the electrical conductivity of membranes. A possible explanation for this is a conformation change of the PANI polymer chain in the presence of THF. Results may support this – for example a more viscous solution was observed to form by the addition of THF into the polymer solution. It is likely that the aggregation of PANI-PAMPSA was enhanced as a result of polymer chain entanglement in the viscous solution, forming "compact coil" structures [113, 321]. The PANI-PAMPSA with a "compact coiled" conformation is closely associated with the low electrical conductivities [322].

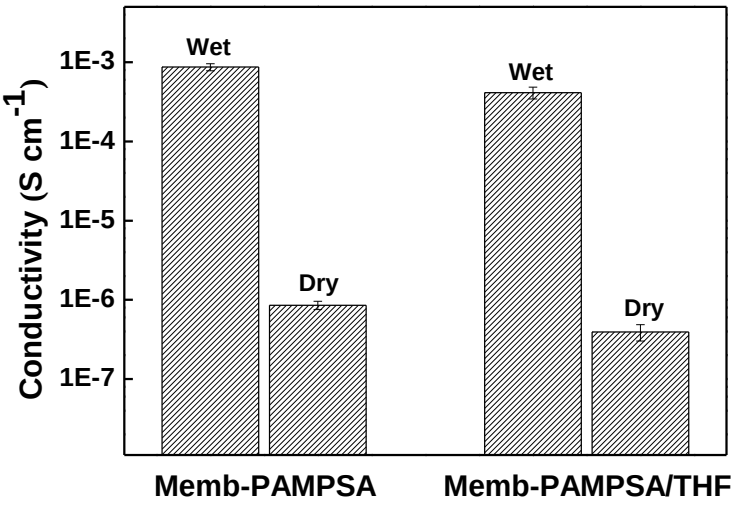

Fig. 9-6 Electrical conductivity of Memb-PAMPSA and Memb-PAMPSA/THF.

9.8 Electrically Connected Cross-flow Filtration

Electrically connected cross-flow filtration is employed to conduct a critical evaluation on the tuneable properties of produced membranes. It is expected that these membranes will have poor tuneability due to the low electrical conductivity, however for completeness experiments were run to confirm this.

Fig. 9-7 shows the rejection of Memb-PAMPSA/THF at different filtration times (0, 30, 60 and 120 min) under an applied potential of 0 and 30 V (2 bar, 25°C, PEG mixtures). There was no difference in the rejection of PEG solute mixtures with and without electrical potential. Fig. 9-8 shows the water permeance and current of Memb-PAMPSA/THF with and without applied potential. Similarly, no significant permeance change was observed in the presence and absence of applied potential. The current passing through Memb-PAMPSA/THF was also lower than Memb-PAMPSA in Chapter 7, consistent with the lower conductivity of Memb-PAMPSA/THF. This all demonstrates again that high conductivity is key to high membrane tuneability. It is possible that the entanglement of the polymer chains in the Memb-PAMPSA/THF caused inefficient charge delocalisation and electron transport [322]. The weak mobility of delocalised charge and electron movement might be responsible for the loss of membrane tuneability.

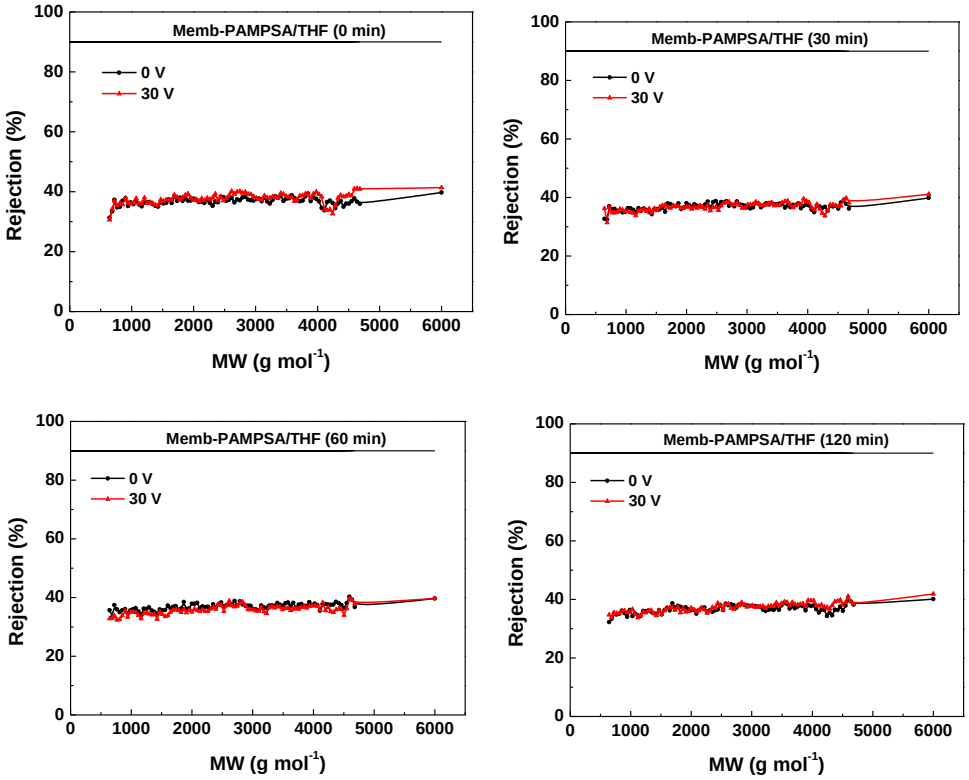

Fig. 9-7 The rejection of Memb-PAMPSA/THF at different filtration times (0, 30, 60 and 120 min) under applied potential of 0 and 30 V (2 bar, 25°C, PEG mixtures).

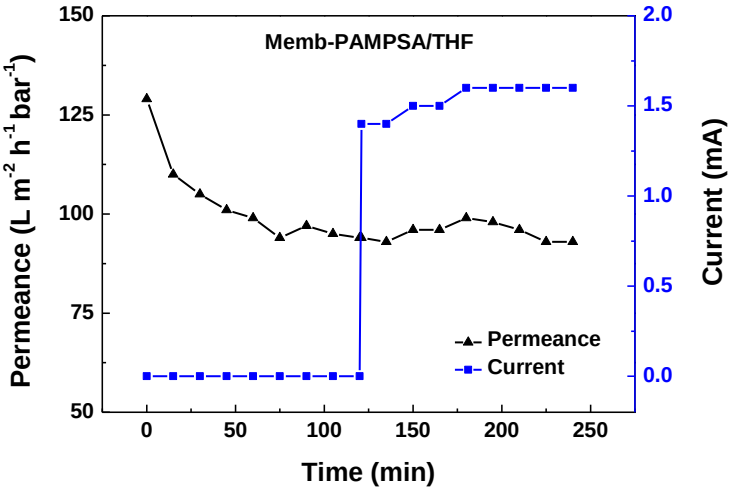

Fig. 9-8 Water permeance and current of Memb-PAMPSA/THF under applied potential with and without potential (30 V).

These results show that a denser membrane top layer is not sufficient to improve the MWCO, conductivity and electrical tuneability of the selectivity and permeance of these Memb-PAMPSA/THF. Combined with the inability of EG incorporation with and without secondary doping with DBSA to produce high conductivity membranes with MWCO in the NF/low UF range, it is clear that

another approach is needed in future work to achieve the membranes required. This may include the following:

- Incorporation of a smaller polymer dopant, which could be a smaller MW PAMPSA or another polymer dopant altogether.
- Incorporation of smaller conductive particles into the PANI membrane that do not in themselves introduce macro porosity like the EG does. This may include small particles of graphene, carbon nanotubes and/or metal and/or semiconductor/conductive micro and nanoparticles.
- The use of another volatile co-solvent other than THF which does not decrease the conductivity of the resulting PANI membrane. This could be dioxane – a common solvent used as a volatility enhancer in membranes cast with DMF as a solvent.

9.9 Conclusions

Highly volatile solvents, THF and acetone, were selected as co-solvents in an attempt to tighten the MWCO of Memb-PAMPSA into the range of small acid doped membranes. The results in this chapter showed that:

- THF as a co-solvent produced a more viscous solution while acetone as a co-solvent led to gelation of casting solution which could not be casted into membranes. Membranes prepared by THF as a co-solvent with a longer evaporation time exhibited a thicker skin layer, followed by a distinguishable transition region with a porous structure, compared to a shorter evaporation time.
- Memb-PAMPSA/THF (mainly the membrane prepared at an evaporation time of 60 s) showed a slight enhancement in the mechanical strength compared to Memb-PAMPSA. This can be explained by the formation of denser skin layer by utilising THF as a co-solvent.
- Compared to Memb-PAMPSA, the water permeance of Memb-PAMPSA/THF decreased by 59.6% and the rejection of PEG 1000-6000 improved to 30%-40% from 10%-30% of Memb-PAMPSA.
- However, the membranes cannot be tightened into the MWCO range of small acid doped membranes, indicating the increased porosity in Memb-PAMPSA was mainly due to the incorporation of large MW of acid dopants. Furthermore,

the membrane displayed decreased electrical conductivity which probably caused the loss of electrical tuneability under applied potential.

10 Stimuli-Responsive Composite PANI Membranes to Solve Fouling

10.1 Introduction

Fouling is one of the main challenges in pressure-driven membrane processes, hampering practical implementations [60]. Generally, fouling is induced by the accumulation of colloids, particles, salts and bacteria on the membrane surface or within the pores [49]. Fouling reduces membrane flux and degrades the quality of the permeate produced. Fouling propensity is closely related to the physical or chemical interaction between foulants and membrane surface. Previous studies have focussed on pre-treatment of the feed, modification of the membrane surface, physical or chemical cleaning to control or reduce fouling to some extent [49, 323]. Among these techniques, pre-treatment generally comes at a great cost with limited effect [47]. Chemical cleaning removes fouling to a degree at the expense of interrupting the filtration process [48]. Surface modification has a significant effect on the initial stage of filtration. However, it cannot play a long-lasting role in fouling suppression once the surface is covered by deposited foulants [49]. Regardless of all the mentioned approaches, the membrane would eventually be contaminated during filtration. In this regard, it is of great interest to develop tuneable membranes with switchable separation properties which allow the cleaning of fouled membranes in-situ upon external stimuli [51].

At present, the fabrication of electrically conductive membranes with tuneable transport properties under applied potential has attracted considerable attention [60]. Many studies have focused on the anti-fouling behaviour of such membranes using external electrical potential on the membrane surface [61-63]. Polyaniline is a conjugated polymer which has the ability to reversibly switch between doping and undoping states, providing a convenient way to modify the separation properties [148]. In the previous chapters, it has been demonstrated that the transport properties (e.g. permeance and selectivity) of electrically conductive PANI membranes can be tuned in-situ by applying an electrical potential. The applied potential can cause the rearrangement of polymer structures, changes the charge and electric field in and on the membrane, changes the membrane chemical properties and brings about changes on the membrane free volume and the interaction between the solutes and solvents and the membranes. This gives a promising solution to in-situ membrane

fouling removal by tuning the membrane separation performance using external stimuli.

The overall aim of this research is to develop unique conducting PANI membranes that can be electrically tuneable to different fluxes and selectivity. The target application is in a membrane reactor, where the primary aim of the new generated tuneable membrane is to allow the fouling layer to be pushed off/through membrane by external potential. Based on this, the fabricated four kinds of conductive PANI membranes from the three previous chapters were applied, including small acid doped PANI membrane (Memb-HCl), PAMPSA doped PANI membrane (Memb-PAMPSA), Memb-PAMPSA incorporated with EG (Memb-PAMPSA-EG) and Memb-PAMPSA-EG secondary doped by DBSA (Memb-PAMPSA-EG/DBSA).

BSA is one of the most commonly used foulants for fouling studies of membranes and membrane reactors [61, 324]. It was chosen as a model foulant in this chapter to determine the fouling removal ability of the aforementioned membranes under applied potential. The concentration of BSA in the wash solution was measured using UV-Vis. Dead-end filtration was conducted to determine the membrane permeance recovery corresponding to the applied electrical potential. All the membranes (virgin, BSA fouled, cleaned) were characterised by FTIR, SEM and CSLM to further evaluate the performance of in-situ fouling removal under applied potential.

10.2 Possible Mechanisms of Fouling Reduction

Previous studies pointed out that an externally electrical potential triggered in-situ fouling removal on the electrically conductive membranes and there were two major mechanisms contributed to the electricity driven fouling reduction [60, 309, 325].

(1) The electrically conductive membrane serves as working electrodes by the application of electrical potential. The water can be electrolysed into hydrogen and oxygen molecules upon electrical potential. The generated gas bubbles at the interface of foulants and membranes can force the deposited BSA to detach from the solid-liquid interface, and attach to the liquid-vapour interface. In this way, the protein at the liquid-vapour interface can be washed away while the protein at the solid-liquid interface stays on the membrane surface [325, 326].

(2) The applied current across the conductive membrane provides a large number of free electrons, causing direct or indirect oxidation of foulants (e.g. BSA) on the membrane surface [327]. The electrolytic oxidation can lead to the degradation or dehydration of foulants like protein, resulting in the release of deposited contaminants from membranes.

However, since these membranes are electrically tuneable (as discussed in previous chapters), three additional mechanisms may also help remove the foulants. An electrically conductive PANI membrane could possibly be dynamically responsive by applying an external electrical potential across the membrane, thus inducing several changes in membrane properties that could produce more general membrane tuneability beyond the ion separations that PANI membranes have in the main been applied to thus far. These electrically induced changes include: changing surface charge controlling Donnan exclusion, change in pore size/free volume (via incorporation or expulsion of ions from the acid dopant site) controlling pore flow transport, and chemical property changes controlling solution diffusion and volume swelling. Combined, these make polyaniline an excellent candidate for a more universally electrically tuneable membrane investigation.

These all indicated that acid doped PANI membranes are very promising candidates for in-situ removal of fouling.

10.3 Electrical Conductivity of Membranes

In terms of the four kinds of membranes used for the fouling removal detection, Fig. 10-1 presents the electrical conductivities of these membranes. Memb-HCl possessed the highest electrical conductivity while Memb-PAMPSA exhibited the lowest conductivity. The electrical conductivity of Memb-PAMPSA was improved by two orders of magnitude with the addition of EG, and could be further enhanced by twenty times using a long chain acid DBSA as a secondary dopant. As discussed in previous chapters, the membrane tuneable separation properties (permeance and selectivity) were closely related to the electrical conductivity. A higher electrical conductivity resulted in a more significant change in membrane permeance and rejection under applied potential. In terms of in-situ defouling by the application of electrical stimulus, it is assumed that the different electrical conductivities can result in different membrane defouling ability.

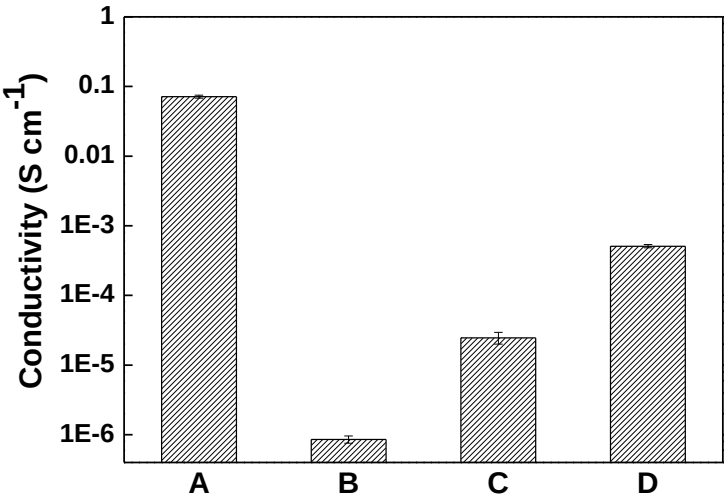

Fig. 10-1 Electrical conductivity of the four different kinds of PANI membranes compared. (A=Memb-HCl; B=Memb-PAMPSA; C=Memb-PAMPSA-EG; D= Memb-PAMPSA-EG/DBSA)

10.4 Memb-HCl Fouling Removal

Memb-HCl exhibited a reduced permeance and MWCO in the presence of applied potential in the electrically connected cross-flow filtrations in Chapter 5. It was proposed that electrical stimulus could trigger the movement of acid dopants, changing the dopants attachment or steric position in the polymer structure that would slightly swell the polymer chains. This behaviour would reduce the pore size of Memb-HCl and result in a tighter structure. Taking this initial tuneability proof into account, an applied potential was utilised to further investigate its influence on fouling removal of Memb-HCl.

10.4.1 BSA Concentration in the Wash Solution

Measuring BSA concentration in the wash solution is a direct way to evaluate the foulants washed away from the membrane. As shown in Fig. 10-2, Memb-HCl showed fast fouling removal response in the first 30 min under applied voltage, and the removal efficiency decreased with time. The rapid defouling response was likely to be induced by the high electrical conductivity of Memb-HCl. As observed in Chapter 5, the small acid leached out from the membrane during a long-term operation. It was deduced that the decreased fouling reduction efficiency was due to the dopant loss, resulting in less significantly tuneable properties with time.

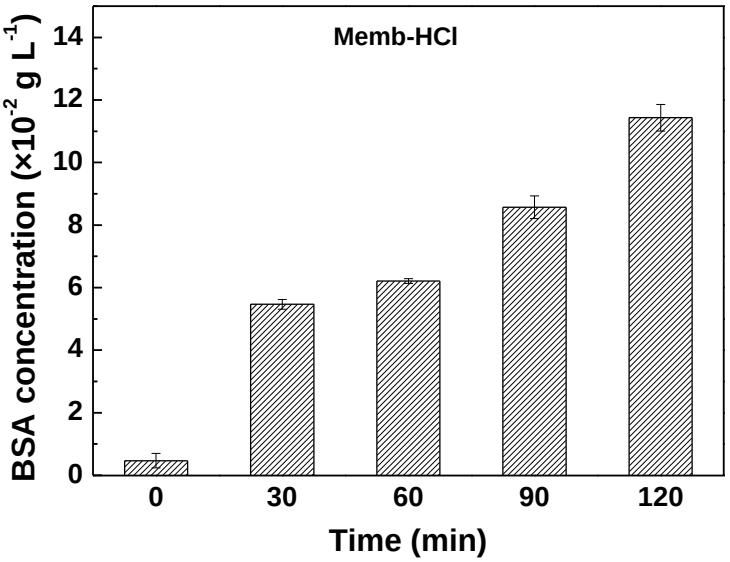

Fig. 10-2 BSA concentration in the wash solution of Memb-HCl with time.

For the mechanism of fouling removal on Memb-HCl, it was observed that some bubbles were produced around the membranes (Fig. D1, Appendix D) and the colour of BSA in the wash solution slightly altered to light yellow (Fig. D2, Appendix D). It should be noted that these phenomena occurred in all the four kinds of membranes. Therefore, it was hypothesised that the bubble generation and BSA oxidation were two main reasons for the membrane defouling behavior. In the case of Memb-HCl, the membrane structure was found to get tightened in the presence of applied voltage as mentioned in Chapter 5. Consequently, it was less likely for the foulants trapped inside the pores to be washed out when voltage was applied.

In addition, two control experiments were run on BSA fouled Memb-HCl in the absence of applied potential and BSA fouled Memb-EB in the presence of applied potential, and BSA was not found in the wash solution of both cases. This confirms that the fouling removal only occurred on the conductive membrane under applied potential (Fig. D3, Appendix D).

10.4.2 Permeance Recovery in Dead-end Filtration

To better understand the defouling action upon electrical potential, dead-end filtration was used to assess the permeance recovery of Memb-HCl. Fig. 10-3 shows that the membrane permeance reduced after BSA fouling as expected, from 3.7±0.1 to 1.9±0.3 $L \cdot m^{-2} \cdot h^{-1} \cdot bar^{-1}$. Although it was found that the some BSA had been removed using the applied electrical potential in Fig. 10-2, there was no

significant permeance recovery after the cleaning process. The membrane fouling was induced by the deposited BSA on the membrane surface as well as the particles trapped within the pores. It was deduced that the cake layer formed on the membrane surface became detached under applied potential and could be removed with time. On the other hand, it was difficult for the foulants within the pores to be washed out and these foulants could cause more serious pore clogging due to the tightened membrane structure by the application of electrical potential. This can be considered as irreversible fouling, which affected the permeate recovery.

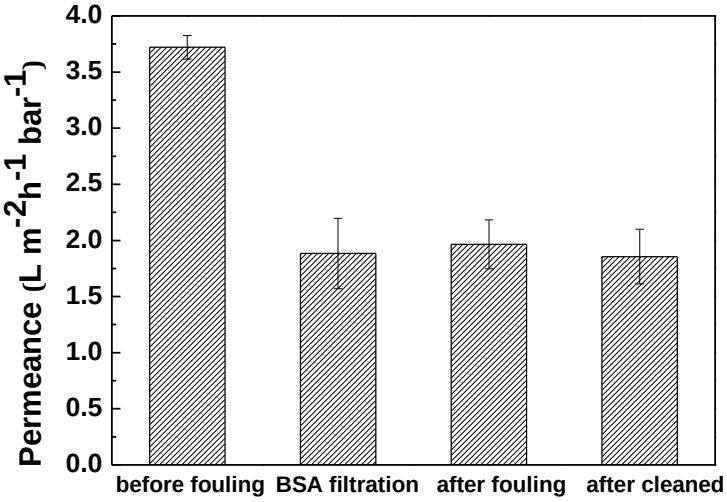

Fig. 10-3 Permeance of Memb-HCl (virgin, BSA fouled, after fouled and cleaned).

10.4.3 FTIR and Colour of Memb-HCl (virgin, fouled and cleaned)

Fig. 10-4 (a) shows the FTIR spectra of BSA. There are two regions in the BSA spectra, namely 1700-1600 cm^{-1} and 1550-1500 cm^{-1}, unique to the protein secondary structure amide I and amine II, respectively. The amine I region is typically used for BSA structure analysis due to signal intensity [328]. Therefore, this region would be used for fouling study in this research. It can be observed from Fig. 10-4 (b) that there was no obvious variation in the spectra between virgin Memb-HCl and control test of 30 V without fouling. This showed that the applied voltage of 30 V did not deteriorate Memb-HCl. The presence of a peak at 1700-1600 cm^{-1} in fouled Memb-HCl shows that BSA fouling formed on the membrane surface. After cleaning by the application of electrical stimulus, the peak intensity at 1700-1600 cm^{-1} became weak, implying that BSA fouling on the membrane surface was reduced. Moreover, the quinoid ring shifted from 1567 to 1597 cm^{-1} after BSA fouling, indicating that acid leaching occurred during filtration. Colour

analysis in Fig. 10-4 (c) presents that the membrane colour cannot be recovered to that of the virgin one by defouling using applied potential. Scanned membrane photos can be seen in Fig. D4, Appendix D. One probable explanation was that the acid leached out of the membrane and changed the membrane colour from dark green to purple bronze. Another possible factor was that the fouling on the membrane surface could not be completely removed.

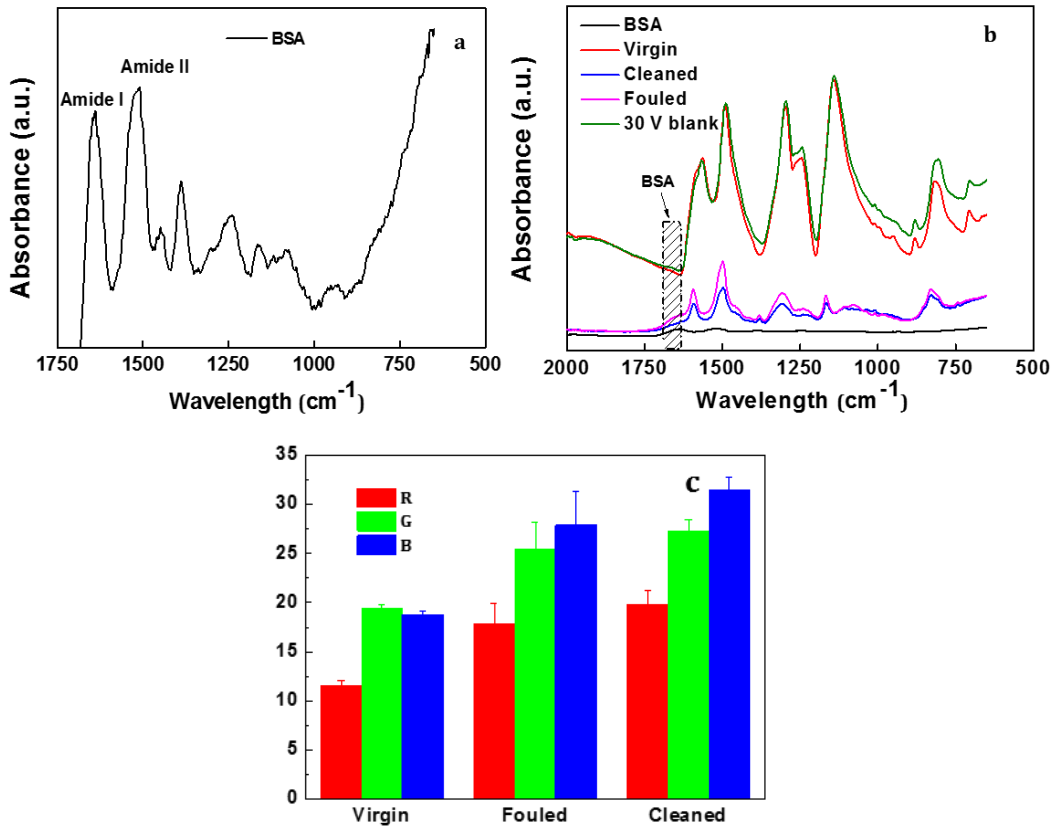

Fig. 10-4 FTIR of (a) BSA and (b) membranes and (c) colour change of Memb-HCl (virgin, BSA fouled and cleaned).

10.4.4 SEM of Memb-HCl (virgin, fouled and cleaned)

Fig. 10-5 presents the surface morphologies of virgin, BSA fouled and cleaned Memb-HCl. It can be observed that the fouled membrane surface was partially covered by the protein cluster. Generally, a membrane with a smaller pore size or a tighter structure exhibits the tendency of accumulating contaminants on the membrane surface [304]. Memb-HCl possessed the tightest structure among the four kinds of membranes. Therefore, it was surmised that BSA contaminants were prone to stay on the surface of Memb-HCl. The hydraulic pressure during filtration forced BSA to deposit onto the membrane surface or into the pores, promoting the

interactions between protein molecules and membrane materials. High acidity of HCl in the membrane structure could result in the aggregation and denaturation of BSA. When an external electrical potential was applied, the protein cluster might get further denatured and become mobile as a result of bubble generation. This could explain the looser and more scattered fouling pattern observed on the membrane surface after applying the electrical potential.

It was also noticed that the Memb-HCl surface exhibited less fouling in comparison to the other three kinds of membranes. Membrane fouling typically depends on the roughness of the membrane surface and membranes with more rough surfaces tend to trap foulants within valleys and get fouled more easily than smoother surfaces [304, 329]. Memb-HCl displayed the smoothest surface, which made the fouling most difficult to deposit on the surface. It was also reported that the antifouling performance of membranes could be improved under acidic conditions due to the strong electrostatic repulsion [98]. Based on this, HCl leaching could increase the ionic strength of the feed and effectively reduce the extent of protein adsorption [330]. Furthermore, HCl with higher acidity has a stronger electrostatic repulsion with BSA than PAMPSA, which could also reduce the deposition of BSA on the membrane surface.

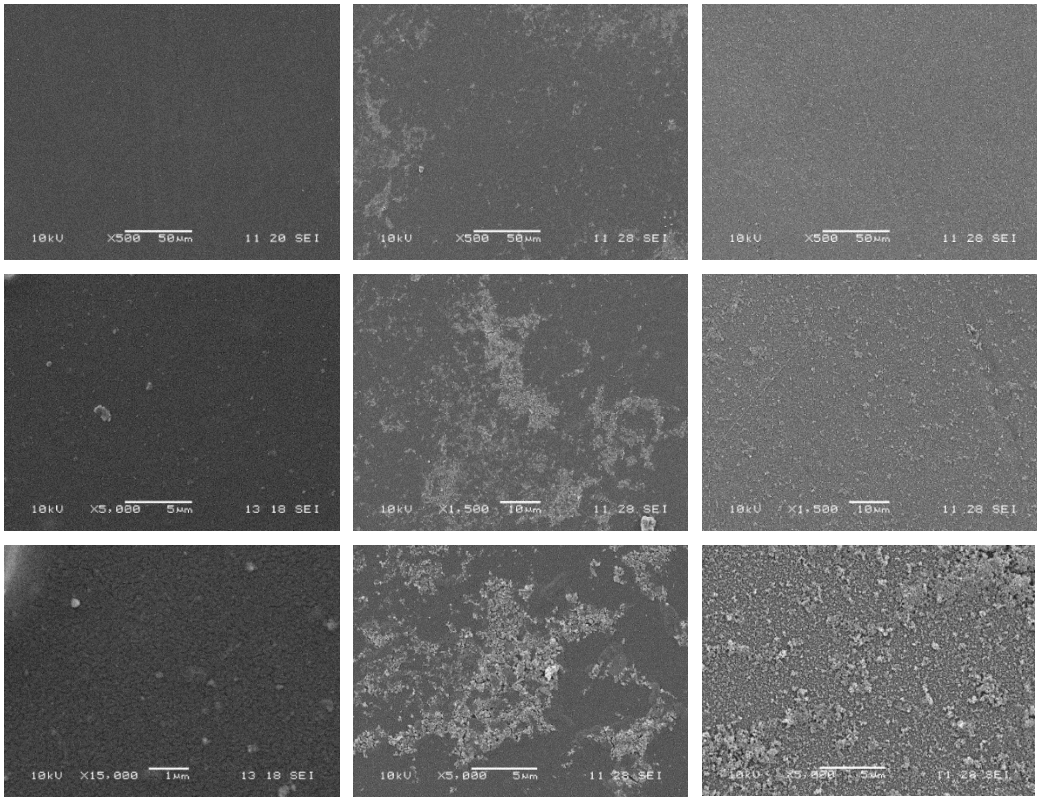

Memb-HCl Virgin Memb-HCl Fouled Memb-HCl Cleaned

Fig. 10-5 SEM images of virgin, BSA fouled and cleaned (left to right) Memb-HCl with scale bar of 50, 10, 5 µm (top to bottom), respectively.

10.4.5 CLSM of Memb-HCl (virgin, fouled and cleaned)

To obtain an independent verification of the SEM results using a technique that does not require putting a sample in a vacuum, CSLM was employed to visualise the BSA-fluorescein on the membrane surface and distinguish the membrane defouling action upon electrical stimulus [331]. The observed green colour of virgin Memb-HCl in Fig. 10-6 shows the presence of fluorescein on the membrane. After filtration with BSA, it can be observed that the membrane surface was partially fouled by contaminants, consistent with SEM images in Fig. 10-5. After cleaning process with an applied potential, the membrane turned lighter in colour. In terms of defouling action observed in Fig. 10-5, it is postulated that the colour change was caused by more scattered and looser BSA fouling on the membrane surface upon applied potential. Alternately, it could be ascribed to the leaching of HCl which resulted in different interactions between Memb-HCl and fluorescein, altering the distribution of fluorescein on the membrane surface.

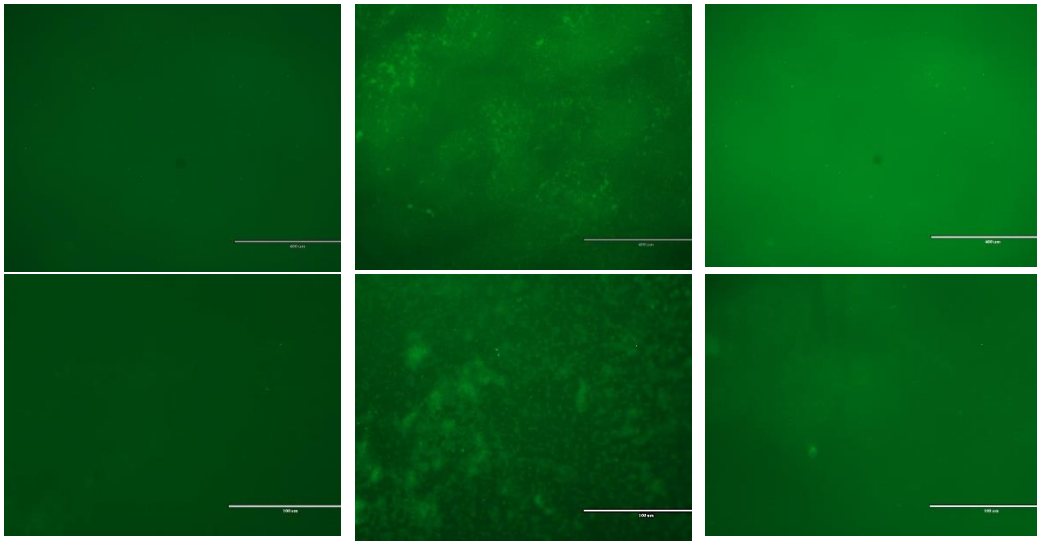

Memb-HCl-Virgin Memb-HCl-Fouled Memb-HCl-Washed

Fig. 10-6 Microscopy of virgin, BSA fouled and cleaned (left to right) Memb-HCl with scale bar of 400, 100 μm (top to bottom), respectively.

10.5 Memb-PAMPSA Fouling Removal

In Chapter 7, it was found that the electrical potential caused an enhanced permeance and decreased PEG rejection of Memb-PAMPSA. As stated in Chapter 7, an applied potential can bring about several changes that could produce a more general membrane tuneability beyond ion separations. These include: changing surface charge controlling Donnan exclusion, change in pore size/free volume (via incorporation or expulsion of ions from the acid dopant site) controlling pore flow transport, and chemical property changes controlling solution diffusion. Applying an electrical potential to the membrane resulted in a large void formation associated with great free volume in the membrane when PAMPSA arranged its structure under electrical potential. This could provide free space for larger solutes to pass through the membranes. In terms of the initial tuneability of Memb-PAMPSA, the fouling removal ability by the application of an electrical potential was examined.

10.5.1 BSA Concentration in the Wash Solution

BSA concentration in the Memb-PAMPSA wash solution as a function of time is illustrated in Fig. 10-7. Compared to Memb-HCl, Memb-PAMPSA performed reduced fouling removal efficiency but more stable fouling removal with time. The final BSA concentration in the wash solution was $(5.4\pm0.3) \times10^{-2}$ g L^{-1} for Memb-PAMPSA compared to $(11.4\pm0.4) \times10^{-2}$ g L^{-1} for Memb-HCl.

As mentioned previously, bubble production and BSA oxidation by the application of an electrical potential facilitated the fouling removal. In the case of Memb-PAMPSA, the looser membrane structure due to the external electrical potential could be another contributing factor to the fouling reduction. It is postulated that some foulants inside the pores could be denatured by the applied voltage and move out during the washing process. In comparison with Memb-HCl, the decreased BSA concentration of Memb-PAMPSA in the wash solution could be explained by the low electrical conductivity, which limited the bubble generation, foulants oxidation and free volume formation. On the other hand, BSA concentration of Memb-PAMPSA in the wash solution smoothly increased with time. The more stable defouling behaviour under applied potential was due to the "double-stranded" structure between PAMPSA and PANI chains (as discussed in Section 7.3.6).

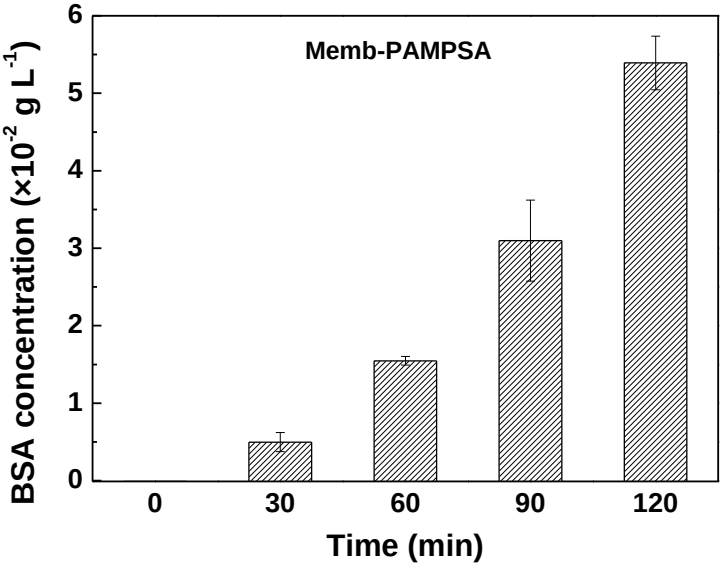

Fig. 10-7 BSA concentration in the wash solution of Memb-PAMPSA with time.

10.5.2 Permeance Recovery in Dead-end Filtration

Fig. 10-8 displays the permeance recovery behaviour of Memb-PAMPSA. As expected, the permeance loss happened due to BSA fouling, from 193±5 to 25±10 $L \cdot m^{-2} \cdot h^{-1} \cdot bar^{-1}$. After cleaning, the water permeance improved up to 46.6% of the initial flux. In combination with the ascending BSA concentration in the wash solution (Fig. 10-7), it can be concluded that the presence of applied potential promoted the removal of BSA fouling.

In contrast to Memb-HCl, it was observed that the permeance drop of Mem-PAMPSA due to BSA fouling was more significant. As mentioned in Section

10.4.4, Memb-PAMPSA with a rougher surface and lower acidity possessed a weaker repulsion to BSA, therefore it was relatively easier for BSA to deposit on the membrane surface. Furthermore, the incorporation of PAMPSA into the PANI polymer chain triggered a porous and loose microstructure (as outlined in Chapter 7). This type of structure accelerated the deposition of BSA into the pores and caused pore plugging, thereby hampering the membrane filtration performance. It is clear that the applied potential only removes BSA on the membrane surface and not inside the pores.

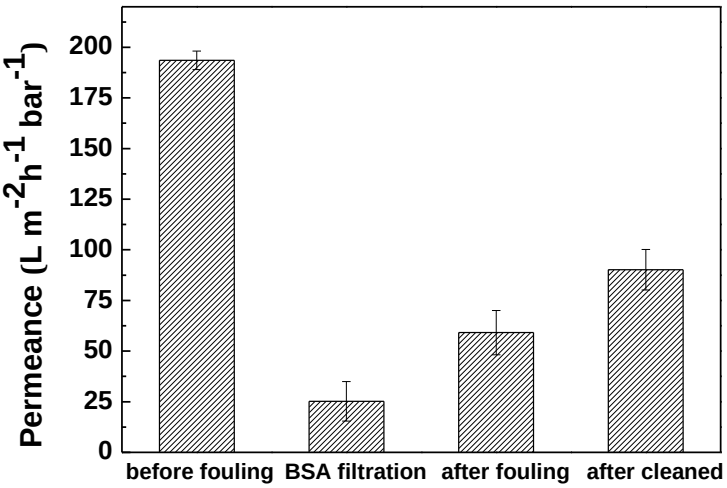

Fig. 10-8 Permeance of Memb-PAMPSA (virgin, BSA fouled, after fouled and cleaned).

10.5.3 FTIR and Colour of Memb-PAMPSA (virgin, fouled and cleaned)

Fig. 10-9 (a) presents the FTIR spectra of virgin, fouled and cleaned Memb-PAMPSA. Similarly, no obvious variation was seen in the spectra between virgin Memb-PAMPSA and control test of 30 V without fouling, indicating that the applied voltage was unable to degrade the membrane. Imine I peak was observed at 1700-1600 cm^{-1} in the fouled membrane, showing that BSA fouling formed on the membrane surface. After cleaning, imine I peak fouling can still be detected on the membrane surface. This implies that the applied voltage could only partially remove the BSA fouling. Colour characterisation in Fig. 10-9 (b) shows that the membrane colour was partially recovered after in-situ self-cleaning applying electrical potential. These results agree well with the permeance recovery data, suggesting that applied potential facilitated the in-situ defouling behaviour of Memb-PAMPSA.

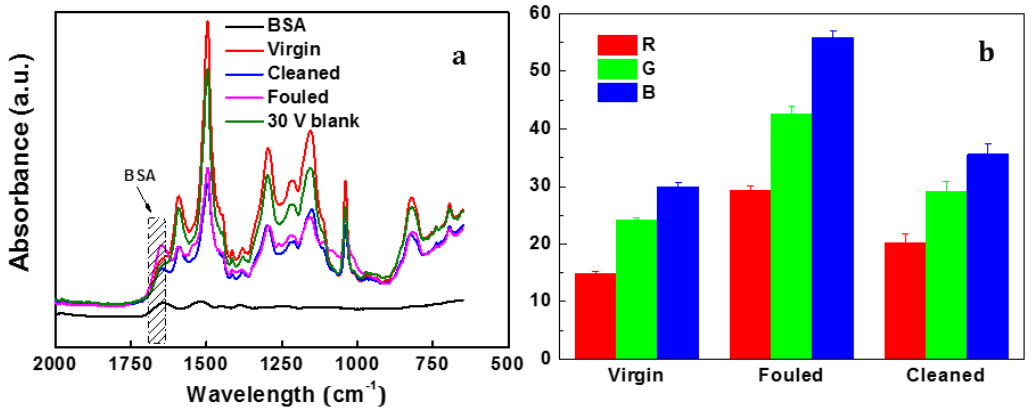

Fig. 10-9 (a) FTIR and (b) colour change of Memb-PAMPSA (virgin, BSA fouled and cleaned).

10.5.4 SEM of Memb-PAMPSA (virgin, fouled and cleaned)

SEM images in Fig. 10-10 illustrate the surface difference between virgin, fouled and cleaned Memb-PAMPSA. The membrane surface showed an evenly distributed fouling layer after being contaminated by BSA. In combination with permeance results, it confirms that the surface of Memb-PAMPSA was more heavily fouled than that of Memb-HCl. This could also explain the more considerable permeance drop of Memb-PAMPSA compared to Memb-HCl. After cleaning, it was evident that some contaminants had been washed away from membrane surface. This is in good agreement with the previous results, indicating that the presence of applied potential was able to remove membrane fouling.

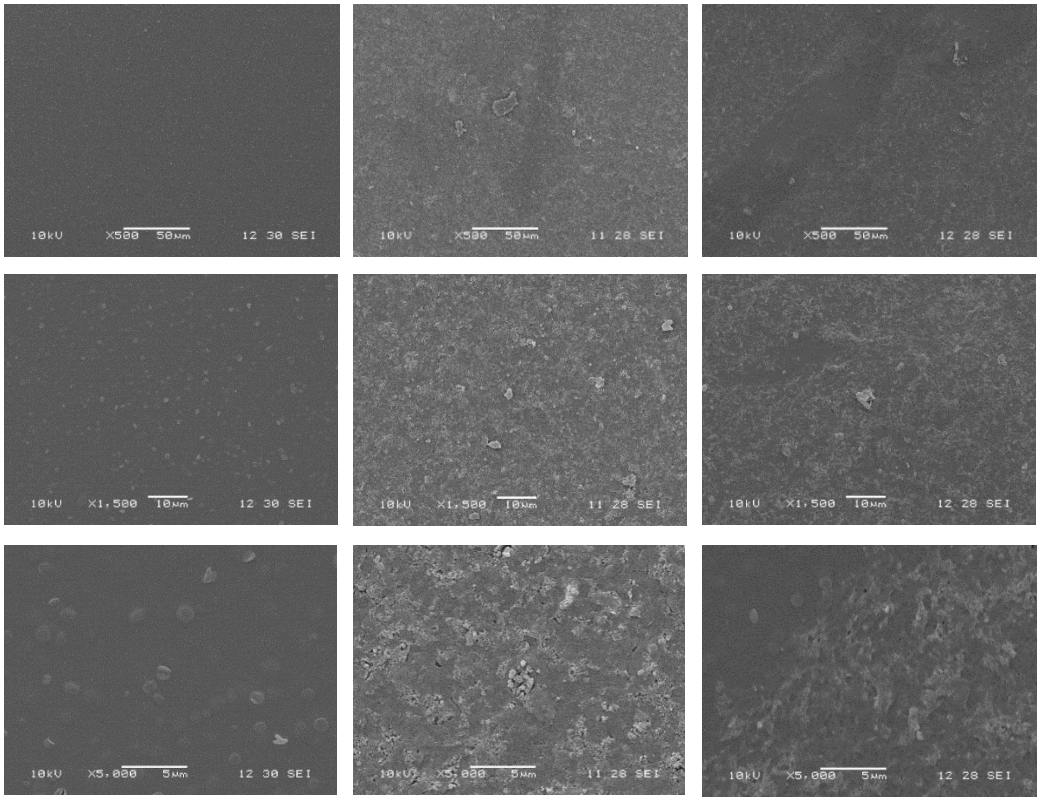

Memb-PAMPSA Virgin Memb-PAMPSA Fouled Memb-PAMPSA Washed

Fig. 10-10 SEM images of virgin, BSA fouled and cleaned (left to right) Memb-PAMPSA with scale bar of 50, 10, 5 µm (top to bottom), respectively.

10.5.5 CSLM of Memb-PAMPSA (virgin, fouled and cleaned)

CSLM in Fig. 10-11 provides visualised images for the defouling action of Memb-PAMPSA. The virgin Memb-PAMPSA displayed green colour by introduction of fluorescein into the membrane. The fouled membrane surface altered to a uniformly brighter colour, suggesting that the surface was completely covered by BSA foulants. After cleaning by the application of electrical potential, some parts of the membrane surface exhibited a black colour, illustrating that the fouling had been washed out from the membrane. The microscopy images are related very well with the SEM images in Fig. 10-10. These all indicate that the presence of applied voltage could dislodge deposited foulants and reduce membrane fouling.

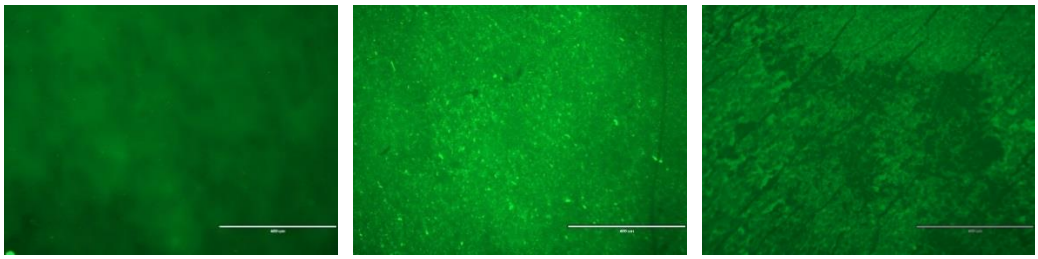

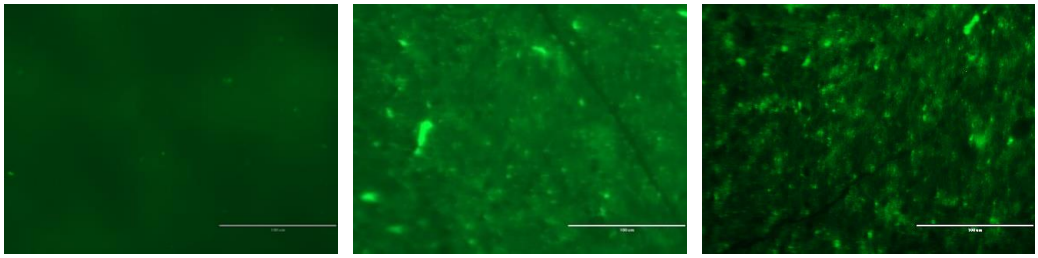

Memb-PAMPSA-Virgin Memb-PAMPSA-Fouled Memb-PAMPSA-Washed

Fig. 10-11 Microscopy of virgin, BSA fouled and cleaned (left to right) Memb-PAMPSA with scale bar of 400, 100 μm (top to bottom), respectively.

10.6 Memb-PAMPSA-EG Fouling Removal

It was found in Chapter 8 that Memb-PAMPSA-EG exhibited a much higher conductivity than Memb-PAMPSA and the membrane showed an increase in the permeance but no noticeable change in PEG rejection under applied potential. The incorporation of EG resulted in more cavities in the microstructure, leading to more porous membranes. The rejection variation with and without electrical potential was surmised to be not detectable by the NF/low UF PEG MWCO method used and so the tuneability of the membranes could not be determined. However, the membranes should be tight enough to retain and be fouled by BSA. Based on this, attempts were made to further examine the defouling ability of Memb-PAMPSA-EG upon applied potential.

10.6.1 BSA Concentration in the Wash Solution

Fig. 10-12 shows the BSA concentration of Memb-PAMPSA-EG in the wash solution. The BSA concentration gradually increased with time and the final BSA solution in the wash solution was (12.1±0.7) $\times 10^{-2}$ g L^{-1}, in contrast to (5.4±0.3) $\times 10^{-2}$ g L^{-1} for Memb-PAMPSA and (11.4±0.4) $\times 10^{-2}$ g L^{-1} for Memb-HCl. Memb-PAMPSA-EG displayed enhanced efficiency on the fouling removal compared to Memb-PAMPSA and more stable fouling removal ability than Memb-HCl.

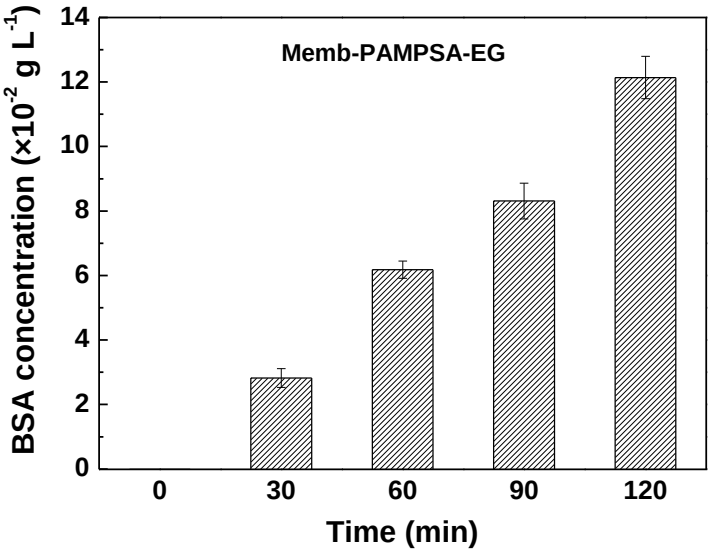

Fig. 10-12 BSA concentration in the wash solution of Memb-PAMPSA-EG with time.

The electrical conductivity of Memb-PAMPSA-EG was known to be two orders of magnitude higher than Memb-PAMPSA. The incorporation of EG facilitated faster charge transport and allowed more electrons movement under applied potential. This in turn accelerated bubbles generation and foulant (BSA) oxidation, consequently contributed to the foulant reduction [60]. In addition, applied potential can bring about several changes that could produce a more general membrane tuneability beyond ion separations, which was outlined in Section 10.2. EG possesses highly mobile electrons and more polarons are expected to form in the polymer backbone upon applying voltage, thereby causing more significant tuneability, potentially allowing the fouling move out from the membrane.

10.6.2 Permeance Recovery in Dead-end Filtration

The filtration behaviour of virgin, fouled and cleaned Memb-PAMPSA-EG is depicted in Fig. 10-13. Permeance decline occurred because of the protein fouling, from 399±19 to 27±12 $L \cdot m^{-2} \cdot h^{-1} \cdot bar^{-1}$. The water permeance of the cleaned membrane was almost twice of the fouled membrane, implying that the application of electrical stimulus reduced the fouling and improved the membrane filtration performance. As explained before, the generated bubble at the interface of liquid and solid as well as BSA denaturation facilitated the fouling reduction. Furthermore, the membrane free volume change caused by chain movement and surface charge change under applied potential could also promote the in-situ cleaning of Memb-PAMPSA-EG.

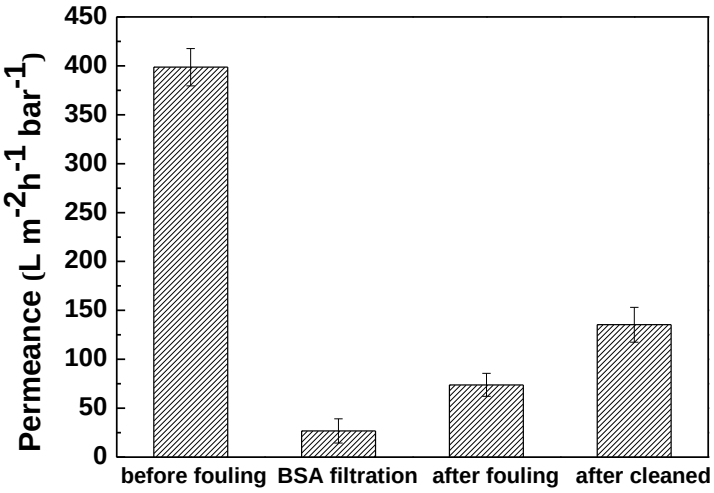

Fig. 10-13 Permeance of Memb-PAMPSA-EG (virgin, BSA fouled, after fouled and cleaned).

10.6.3 FTIR and Colour of Memb-PAMPSA-EG (virgin, fouled and cleaned)

FTIR spectra in Fig. 10-14 (a) illustrates the membrane fouling removal behaviour. The rather similar spectra between virgin Memb-PAMPSA-EG and control test of 30 V indicated that the membrane and polymer did not break down at the applied voltage. The functional group of BSA appears in the FTIR spectra of the membrane surface after BSA filtration, confirming that the membrane was fouled by protein. After cleaning using applied voltage, imine I peak could still be detected, again like the other membranes implying that the fouling could not be completely removed. The colour variation in Fig. 10-14 (b) suggests that the cleaned Memb-PMAPSA-EG tended to recover its colour to that of the virgin one. These all show that the stimuli-responsive Memb-PAMPSA-EG could in-situ self-clean itself with applied potential.

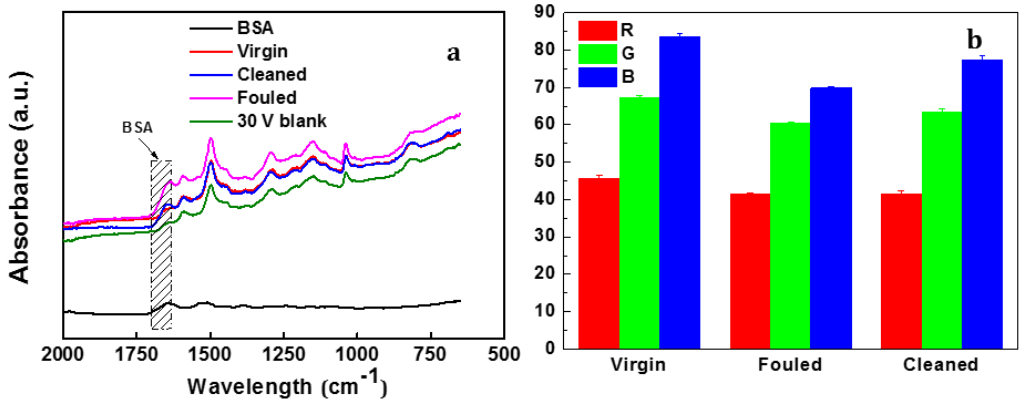

Fig. 10-14 (a) FTIR and (b) colour change of Memb-PAMPSA-EG (virgin, BSA fouled and cleaned).

10.6.4 SEM of Memb-PAMPSA-EG (virgin, fouled and cleaned)

SEM images in Fig. 10-15 show the surface morphology of virgin, fouled and cleaned Memb-PAMPSA-EG. It can be observed that the fouled membrane surface was fully covered by contaminants, rather similar to Memb-PAMPSA. However, the fouling layer seemed to become thinner and some clean parts of the membrane surface could be observed after applying electrical potential. Compared with Memb-HCl, the fouling was found to be more severe in Memb-PAMPSA-EG. As discussed before, the rougher membrane surface and lower acidity of doped acids led to weaker repulsion to the contaminants and thus Memb-PAMPSA-EG suffered from greater foulant deposition. In contrast to Memb-PAMPSA, the incorporation of EG formed a looser structure with a rougher surface, which enabled greater foulant accumulation, resulting in more significant permeance drop to the initial flux.

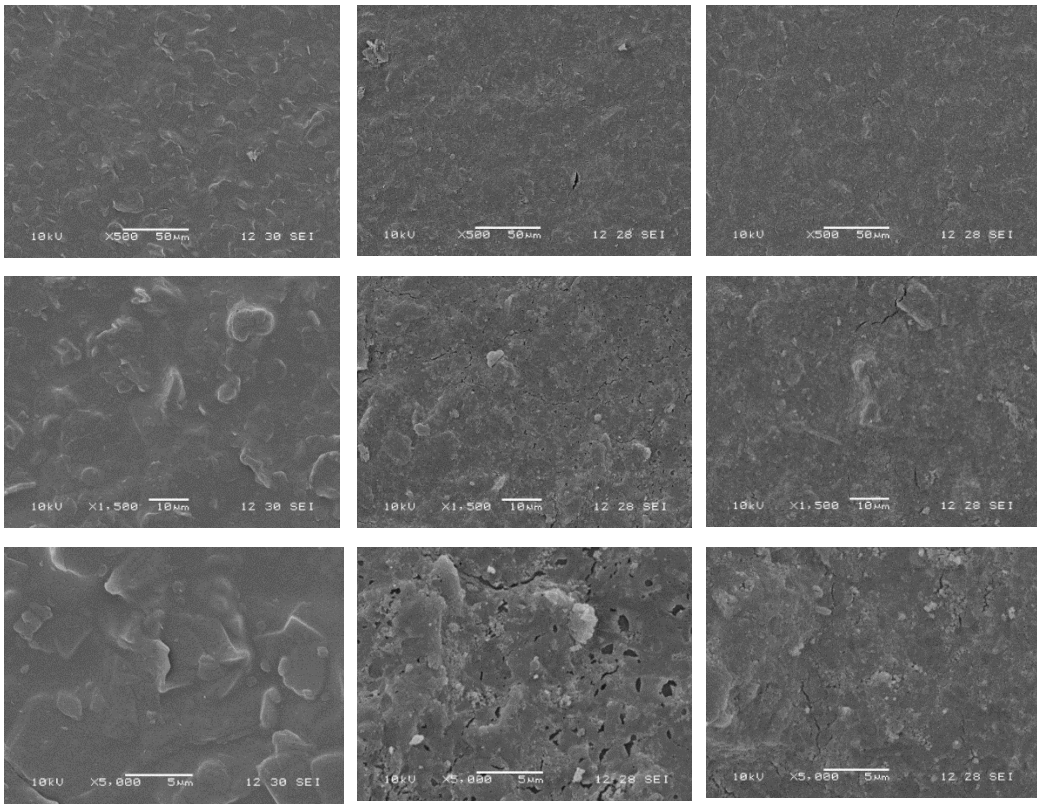

Memb-PAMPSA-EG Virgin Memb-PAMPSA-EG Fouled Memb-PAMPSA-EG Washed

Fig. 10-15 SEM images of virgin, BSA fouled and cleaned (left to right) Memb-PAMPSA-EG with scale bar of 50, 10, 5 μm (top to bottom), respectively.

10.6.5 CLSM of Memb-PAMPSA-EG (virgin, fouled and cleaned)

BSA fouling on the surface of Memb-PAMPSA-EG was further characterised by CLSM in Fig. 10-16. The virgin membrane showed green colour due to the addition of fluorescein. The fouled membrane became brighter in colour as a result of protein deposition. The colour became weaker after applying voltage on the Memb-PAMPSA-EG, illustrating that BSA deposition on the membrane surface was reduced by the application of electrical potential. This is in good accordance with SEM images in Fig. 10-15, confirming the defouling behaviour of Memb-PAMPSA-EG upon applied potential.

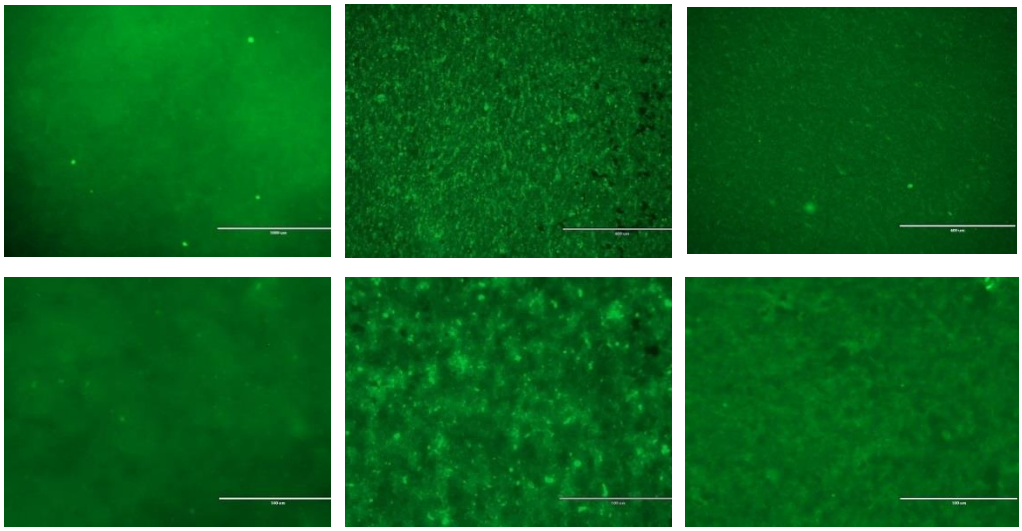

Memb-PAMPSA-EG Virgin Memb-PAMPSA-EG Fouled Memb-PAMPSA-EG Washed

Fig. 10-16 Microscopy of virgin, BSA fouled and cleaned (left to right) Memb-PAMPSA-EG with scale bar of 400, 100 μm (top to bottom), respectively.

10.7 Memb-PAMPSA-EG/DBSA fouling removal

DBSA was utilised as a secondary dopant of Memb-PAMPSA-EG membranes to further increase electrical conductivity. An increased permeance and decreased rejection were observed in Memb-PAMPSA-EG/DBSA by the application of applied potential in Chapter 8. In terms of the initial tuneability, further investigation was carried out on the fouling reduction behaviour of Memb-PAMPSA-EG/DBSA under an applied potential of 30 V.

10.7.1 BSA Concentration in the Wash Solution

BSA concentration of Memb-PAMPSA-EG/DBSA in the wash solution with time is illustrated in Fig. 10-17. The BSA concentration steadily improved with time in the first 90 min and then no significant increase was observed from 90 to 120 min.

The final BSA concentration in the wash solution was (13.7±0.5) $\times 10^{-2}$ g L^{-1}, compared with (11.4±0.4) $\times 10^{-2}$ g L^{-1} for Memb-HCl, (5.4±0.3) $\times 10^{-2}$ g L^{-1} for Memb-PAMPSA and (12.1±0.7) $\times 10^{-2}$ g L^{-1} for Memb-PAMPSA-EG. Memb-PAMPSA-EG/DBSA was found to possess the highest BSA concentration in the wash solution among the four kinds of membranes. This is likely to be because Memb-PAMPSA-EG/DBSA exhibited a relatively high electrical conductivity - two orders of magnitude higher than Memb-PAMPSA and more than twenty times higher than Memb-PAMPSA-EG. Although Memb-HCl possessed a higher initial conductivity than Memb-PAMPSA-EG/DBSA, the serious acid leaching caused decreased electrical conductivity and reduced the fouling removal efficiency.

It can be concluded that there is a close relationship between the defouling ability and electrical conductivity of these PANI membranes. An increase in electrical conductivity was associated with an enhancement in membrane fouling removal. The membranes with higher conductivities provided more electrons and accelerated the charge delocalisation, allowing more significant and efficient bubble production, protein oxidation, surface charge change and polymer chain movement. This promoted the fouling removal from the membranes as discussed in Section 10.2. In addition, it was noticed that the defouling of Memb-PAMPSA-EG/DBSA was effective in the first 90 min. Fouling reduction became less after 90 min, however this is most probably because most of the fouling had been removed in the first 90 min.

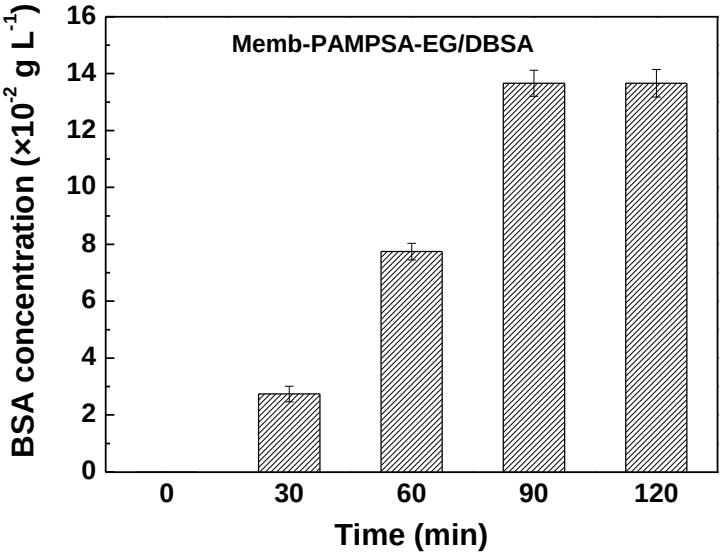

Fig. 10-17 BSA concentration in the wash solution of Memb-PAMPSA-EG/DBSA with time.

10.7.2 Permeance Recovery in Dead-end Filtration

The permeance of virgin, fouled and cleaned Memb-PAMPSA-EG/DBSA is shown in Fig. 10-18. There was a significant permeance reduction after BSA fouling – from 357±24 to 32±10 $L \cdot m^{-2} \cdot h^{-1} \cdot bar^{-1}$. It can be seen that the fouled Memb-PAMPSA, Memb-PAMPSA-EG and Memb-PAMPSA-EG/DBSA exhibited a very similar permeance. Observations of membranes after fouling showed a gel-like BSA fouling on the surface of the membranes, which was therefore the major reason for the permeance reduction and what was wanted for these experiments. As measured in Chapter 8, the above mentioned three kinds of membranes exhibited above 90% rejection of BSA, indicating similar contents of BSA deposited on the membrane surface and/or within the pores. This consequently induced rather similar resistance to the solute while filtrating, thereby producing the similar permeance.

After cleaning under applied potential, the permeance increased to approximately three times of the fouled Memb-PAMPSA-EG/DBSA and the membrane permeance recovery arrived at 46.2% of the virgin membranes. Again, it is thought that the two mentioned factors (namely gas generation and protein oxidation directly or indirectly) were the major causes of the fouling removal. Additionally, the applied potential could trigger the surface charge change and induce the reorganization of the polymer chains, permitting a more opened membrane structure. This could also facilitate the fouling reduction in terms of pore plugging in Memb-PAMPSA-EG/DBSA. Memb-PAMPSA-EG/DBSA gave the best fouling removal compared to Memb-PAMPSA and Memb-PAMPSA-EG; this is consistent with the findings in Section 10.7.1, which can be attributed to the high electrical conductivity of Memb-PAMPSA-EG/DBSA.

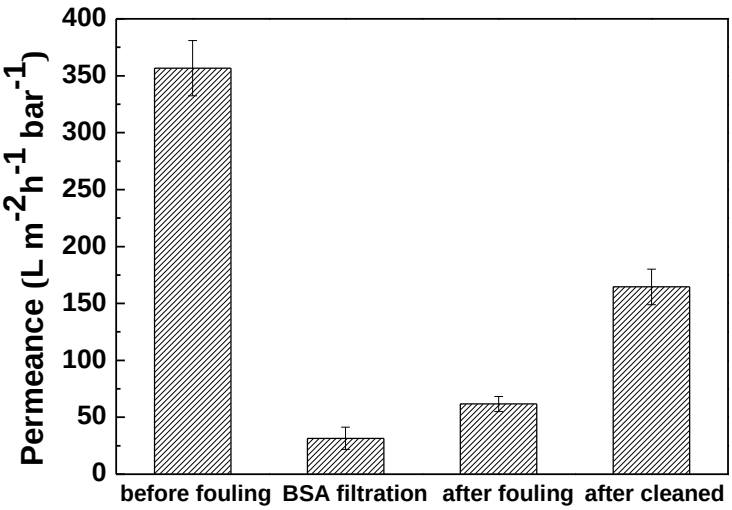

Fig. 10-18 Permeance of Memb-PAMPSA-EG/DBSA (virgin, BSA fouled, after fouled and cleaned).

10.7.3 FTIR and Colour of Memb-PAMPSA-EG/DBSA (virgin, fouled and cleaned)

Fig. 10-19 (a) presents the FTIR spectra of virgin, fouled and cleaned Memb-PAMPSA-EG/DBSA. Virgin Memb-PAMPSA and a control test of 30 V without fouling displayed a similar spectrum, indicating that the membrane and polymer does not break down at the applied voltage of 30 V. The Imine I functional group of BSA was observed in the fouled Memb-PAMPSA-EG/DBSA, again confirming that fouling was successful. After applying the external voltage, the imine I peak still appeared in the cleaned Memb-PAMPSA-EG/DBSA. It can be concluded that the electrical potential application still does not remove all the BSA foulant, even if Memb-PAMPSA-EG/DBSA exhibited the best defouling performance.

Fig. 10-19 (b) shows that the colour of fouled Memb-PAMPSA-EG/DBSA almost recovered to the virgin state, indicating most of the contaminants had been washed out from the membrane surface. Therefore, there is further room for improvement for these experiments and membranes. This should include the production of less rough membrane surfaces and the testing of the defouling of these membranes in a cross-flow rig to examine the combined (and hopefully synergetic) effect of cross-flow velocity, in pore flow through the membrane and applied potential on fouling reduction from the membrane surface and within the pores.

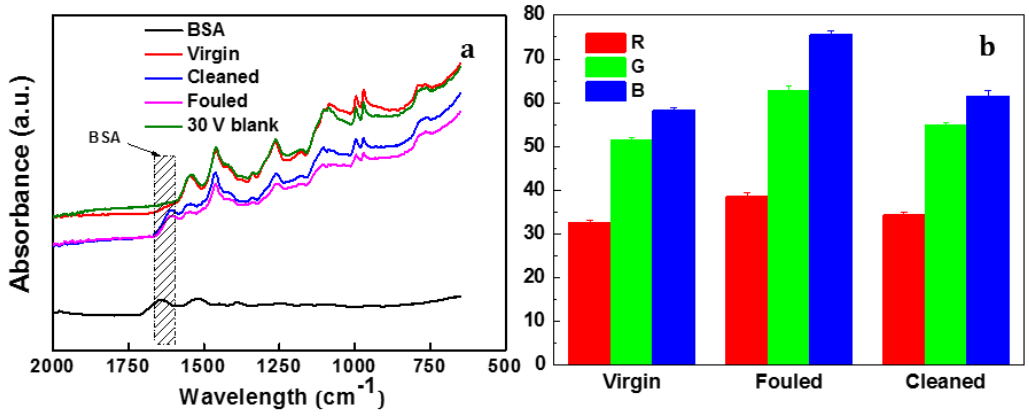

Fig. 10-19 (a) FTIR and (b) colour change of Memb-PAMPSA-EG/DBSA (virgin, BSA fouled and cleaned).

10.7.4 SEM of Memb-PAMPSA-EG/DBSA (virgin, fouled and cleaned)

Fig. 10-20 presents the surface morphology of virgin, fouled and cleaned Memb-PAMPSA-EG/DBSA. As can be seen, the membrane was fully covered by foulant after BSA filtration. A similar cake layer formation was also observed in Memb-PAMPSA and Memb-PAMPSA-EG, which could account for the similar membrane permeance during BSA filtration as discussed in Section 10.7.2. The application of an electrical potential removed most of the contaminants on the membrane surface, again confirming that membranes with a higher electrical conductivity possessed better defouling ability. It was reported by other researchers that a long treatment time could release EG from membranes, forming aggregation with BSA into clusters [325]. This behaviour was not observed in the current work as EG was still in a good interfacial contact with the membrane surface after use.

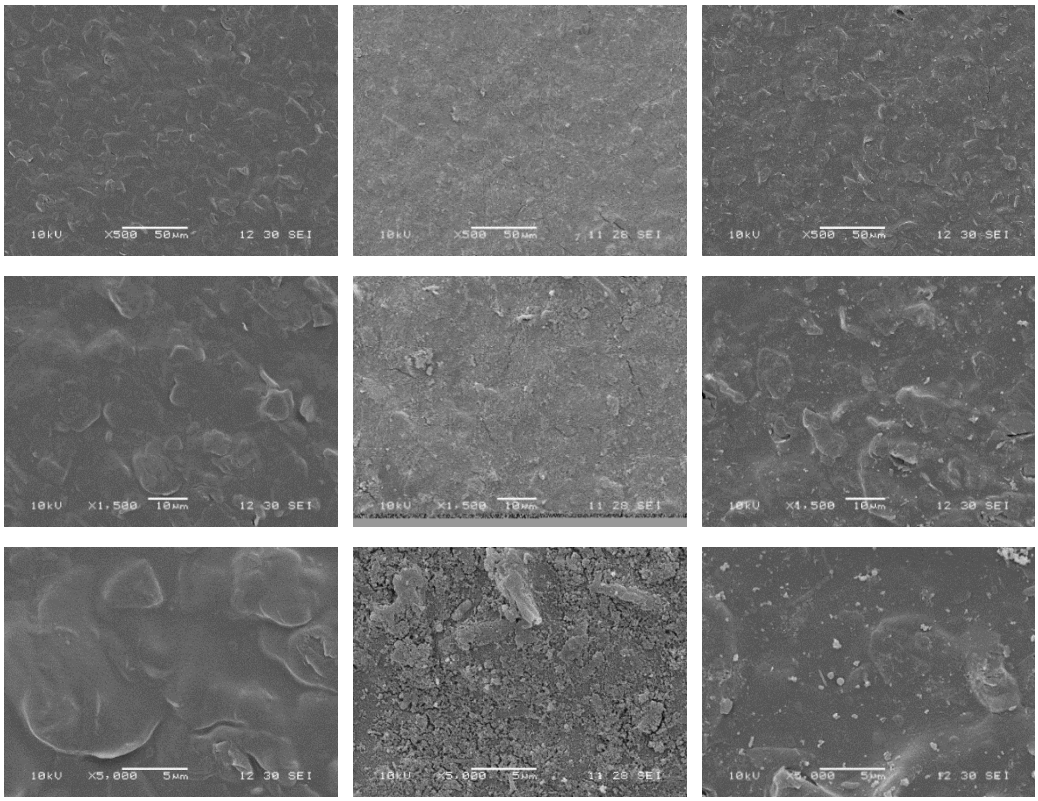

Memb-PAMPSA-EG/DBSA Virgin | Memb-PAMPSA-EG/DBSA Fouled | Memb-PAMPSA-EG/DBSA Washed

Fig. 10-20 SEM images of virgin, BSA fouled and cleaned (left to right) Memb-PAMPSA-EG/DBSA membranes with scale bar of 50, 10, 5 μm (top to bottom), respectively.

Although the membranes demonstrated the feasibility of defouling upon applied potential, it is worth noting that the electric field cannot completely remove the fouling within the treatment time.

10.7.5 CLSM of Memb-PAMPSA-EG/DBSA (virgin, fouled and cleaned)

Fig. 10-21 shows CLSM images of virgin, fouled and cleaned Memb-PAMPSA-EG/DBSA. The membrane exhibited a dark green colour from the incorporation of fluorescein. The presence of BSA foulants on the membrane surface changed the colour into much greener one. After applying potential, most of the membrane surface changed back to dark green colour, suggesting that only few foulants were left on the membrane surface. The obtained microscopy images agree well with SEM images in Fig. 10-20. It can be concluded that that most of the surface foulants on the Memb-PAMPSA-EG/DBSA had been removed by the application of electrical potential. This indicates that in pore (irreversible fouling) is the main fouling zone not removed by the applied potential treatment and should be the focus of future work.

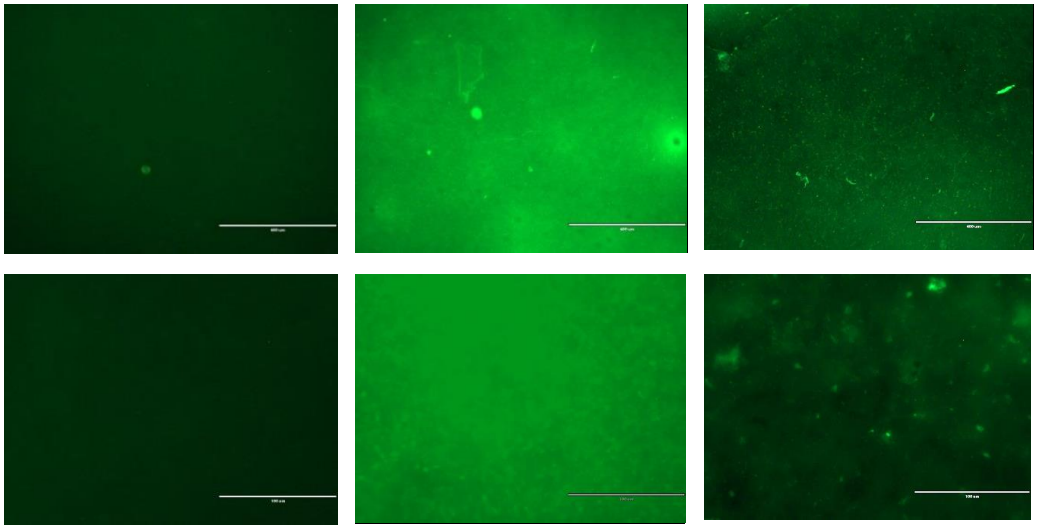

Memb-PAMPSA-EG/DBSA Virgin | Memb-PAMPSA-EG/DBSA Fouled | Memb-PAMPSA-EG/DBSA Washed

Fig. 10-21 Microscopy of virgin, BSA fouled and cleaned (left to right) Memb-PAMPSA-EG/DBSA with scale bar of 400, 100 μm (top to bottom), respectively.

10.8 Conclusions

This chapter provided evidence for fouling removal from the surface of electrically conductive PANI membranes by applying an electrical potential. Four kinds of conductive PANI membranes, including Memb-HCl, Memb-PAMPSA, Memb-PAMPSA-EG and Memb-PAMPSA-EG/DBSA, were applied to determine the membrane in-situ fouling removal under applied voltage. The results show that:

- Small acid doped membranes showed faster fouling removal response in the first 30 min under applied voltage, but the removal efficiency decreased with the leaching of small acids.
- Compared to Memb-HCl, Memb-PAMPSA displayed reduced fouling removal efficiency but more stable fouling removal behaviour with time.
- Memb-PAMPSA-EG exhibited enhanced fouling removal efficiency compared to Memb-PAMPSA, and the membrane fouling removal efficiency could be further improved by secondary doping with a long chain acid DBSA. The membrane permeance recovery of Memb-PAMPSA-EG/DBSA arrived at 46.2% of the virgin membranes.
- The membranes (virgin, fouled, cleaned) characterised by FTIR, colour, SEM and CSLM demonstrated their potential for in-situ fouling removal and the defouling ability was closely related to the stability and conductivity of the

membranes. Membranes with higher conductivity and better stability displayed more efficient in-situ fouling removal under applied potential.

In summary, the stimulating responsive PANI membrane can be considered as a promising solution to remove the membrane fouling in-situ by the application of external electrical potential.

11 Conclusions and Recommendations for Future Work

11.1 Conclusions

11.1.1 Influence of T_{poly} on Electrical Tuneability of Flux and MWCO of Memb-HCl

This work demonstrates that T_{poly} has a significant effect on the properties of the PANI powder, and then further influences the morphology, transport performance and electrical tuneability of the membranes. A lower T_{poly} was related to a membrane with relatively lower electrical conductivity and higher mechanical strength with fewer macrovoids. The conductive Memb-HCl showed a decreased permeance and MWCO under the applied potential in the PEG cross-flow filtrations. The greater tuneability was found to be related to the membranes with relatively higher electrical conductivity. The optimal T_{poly} was found to be 15°C, with higher membrane mechanical strength than higher T_{poly} and improved electrical conductivity than lower T_{poly}. The membrane (T_{poly} = 15°C) exhibited the greatest MWCO reduction (down to 2800 g mol^{-1}) at 30 V.

It is also noticed that a range of parameters like synthesis, doping and external stimuli affect the tuneable separation performance of HCl doped membranes. Understanding the detailed mechanism of membrane transport properties under applied potential is desirable to produce the most versatile electrically tuned separation. Future work can be done to optimise the parameters to control the in-situ tuneable separations of these membranes – detailed in Section 11.2.

11.1.2 One-filtration MWCO Method for Aqueous based NF and UF Membranes using PEGs

A reliable, cost effective, high resolution, single filtration MWCO evaluation method for aqueous based NF and UF membranes has been developed using a wide range of PEG oligomers as MWCO probes. This method was enabled by a new, high resolution oligomer separation and detection using HPLC coupled with an ELSD. The refined method can determine the MWCO of membranes over a MW range from 678 to 4594 g mol^{-1} with a molecular weight difference of just 44 g mol^{-1} and a bonus further one point extension to 6000 g mol^{-1} – covering a wider MW range than any other MWCO method for aqueous based NF and low MWCO UF membranes. MWCO determination of five commercial membranes from GE

Osmonics™ and Millipore showed good agreement with manufacturer and literature values, confirming the accuracy of the method. As this new method has significant advantages over all other existing aqueous MWCO determinations (i.e. single filtration, higher resolution over a wider MW range, low cost MWCO molecular probes), it is suggested that it be adopted as the new standard for determining aqueous MWCO over a MW range from 678 to 6000 g mol^{-1}.

11.1.3 Fabrication and Characterisation of Stimulating Responsive PAs Doped PANI Membranes

Four kinds of PAs, including PAMPSA, PSSA, PAAc and PMVEA, have been used as dopants to overcome the two challenges (namely acid leaching and membrane brittleness) of Memb-HCl. Based on this, a new membrane preparation method is proposed to prepare PAs doped membranes. In this new method, PAs were incorporated into PANI during the chemical oxidation of aniline, and the produced PANI-PA complexes were directly used as the membrane materials to prepare PAs doped PANI membrane. Among the four kinds of PANI-PA complexes produced (PANI-PAMPSA, PANI-PSSA, PANI-PMVEA, PANI-PAAc), PANI-PAMPSA was found to produce the best practical membrane films under the casting conditions and solvents considered.

Memb-PAMPSA exhibited improved mechanical strength, with the Young's modulus and tensile strength twice higher than Memb-HCl (24 h doping time). The stable permeate pHs in the dead-end filtration implied the reduced acid leaching during filtration. However, Memb-PAMPSA exhibited a decreased electrical conductivity, with $(8.56\pm1.01) \times10^{-7}$ and $(8.68\pm0.89) \times10^{-4}$ S cm^{-1} measured in a dry and wet state, respectively, which were not conductive enough to produce a significant tuneability in terms of the permeance and selectivity change under applied potential. The incorporation of large acids facilitated the formation of a PANI membrane with a loose microstructure, with MWCO in the loose UF range (much higher than 6, 000 g mol^{-1} but lower than 60, 000 g mol^{-1}). These results combined suggest that the Memb-PAMPSA was not tight enough as desired NF range and further work is needed to tighten the membrane MWCO and improve the electrical conductivity.

11.1.4 Enhancing Memb-PAMPSA as a Stimulating-responsive Membrane by EG Incorporation and DBSA Treatment

Considering the low conductivity of Memb-PAMPSA, EG and a secondary dopant DBSA were incorporated into these membranes. It was also found that the membrane conductivity could be improved by two orders of magnitude by the incorporation of EG using a solution mixing method, and further enhanced by twenty times using a long chain acid DBSA as a secondary dopant. The membranes displayed more significant dynamic contact angle change because of the enhanced electrical conductivity, which gives a further quantitative indication of the electrical tuneability of these membranes. Memb-PAMPSA-EG/DBSA with DBSA as a secondary dopant was more stable in filtration compared with small acid doped PANI membranes.

On the other hand, the addition of EG has made the membrane surface more hydrophilic with the contact angle changing from 54 ± 2^{o} to 62 ± 2^{o} and the permeance of Memb-PAMPSA-EG was twice higher than Memb-PAMPSA. However, the addition of EG further decreased the membrane rejection and the membranes were too porous to exhibit a discernible permeance or selectivity change under applied potential. Therefore, further work needs to be done to find a solution to tighten the MWCO of these membranes.

11.1.5 Effect of Co-solvent and Evaporation Time on the Performance of Memb-PAMPSA

Therefore, tightening of PAMPSA doped PANI membranes was addressed. Attempts were made by adding highly volatile co-solvents (THF and acetone) into the polymer solution. The addition of acetone as a co-solvent into the casting solution led to gel formation, while THF as a co-solvent produced a viscous solution. Membranes prepared by THF as a co-solvent with a longer evaporation time (namely 45, 60 and 120 s) exhibited a thicker skin layer, followed by a distinguishable transition region with a porous structure, compared to a shorter evaporation time. The water permeance of Memb-PAMPSA/THF (mainly the membrane prepared at an evaporation time of 60 s) decreased by 59.6% compared to Memb-PAMPSA and the rejection of PEG 1000-6000 improved to 30%-40% from 10%-30% of Memb-PAMPSA. The membrane also showed an enhancement

in the mechanical strength compared to Memb-PAMPSA, which can be explained by the formation of denser skin layer.

However, the MWCO range was similar to that of Memb-PAMPSA produced without THF, indicating the increased porosity in Memb-PAMPSA was mainly due to the incorporation of large acid dopants and so could not be modified out using a more volatile solvent to produce a denser skin/active layer. Furthermore, the membrane displayed decreased electrical conductivity which most likely caused a loss of electrical tuneability under applied potential. The current membranes however possess sufficiently low MWCO to be used for large molecule filtrations – such as model foulant BSA – which can be used to determine the anti-fouling behaviour of membranes.

11.1.6 Stimuli-responsive Composite Polymer Membranes to Solve Fouling

The overall aim of this research is to develop unique conducting PANI membranes that can be electrically tuneable to different fluxes and selectivity. The target application is in a membrane reactor, where the primary aim of the new generated tuneable membrane is to allow the fouling layer to be pushed off/through membrane by external potential. Based on this, four of the different variants of fabricated conductive PANI membranes from Chapter 5, 7 and 8 were applied (the membranes from Chapter 9 were not included due to the lower conductivity determined). All the membranes demonstrated their potential for in-situ fouling removal under applied potential and the defouling ability was closely related to the electrical conductivity and the acid stability. Higher conductivity and better acid stability are desirable for the membrane defouling efficiency by the application of electrical potential.

Memb-HCl showed faster fouling removal response, but the removal efficiency decreased with the leaching of small acids. Memb-PAMPSA displayed reduced fouling removal efficiency but stable stimuli response. Memb-PAMPSA-EG exhibited enhanced fouling removal efficiency compared to Memb-PAMPSA, and the membrane fouling removal efficiency could be further improved by secondary doping with DBSA. Memb-PAMPSA-EG/DBSA gave the best fouling removal among the four kinds of membranes, and the permeance of cleaned membrane increased to approximately three times of the fouled membrane and the permeance

recovery arrived at 46.2% of the virgin membrane. In summary, the electrically tuneable PANI membranes can be considered as a promising solution to remove membrane fouling in-situ by the application of external electrical potential.

11.2 Recommendations for Future Work

This work has established a number of novel new PANI-PA polymers that have been used in membranes and have shown the potential of these membranes to be used in changing membrane transport properties when in use and for the in-situ removal of a model foulant. In doing so several new questions and work streams have been opened which can be addressed in future work.

In terms of low conductivity of polymer acid doped membrane, exploring new potential acid dopants that have lower pKa and smaller MWs is a potential way. This could minimise dopants wash out during filtration and lead to better tuneable transportation under applied potential. Additionally, blending PAs with other smaller MW acids could be a promising solution to improve the membrane conductivity.

Considering the loose membrane structure caused by the incorporation of PAs and EG, two approaches could be used to tighten the membrane structure. One way is to incorporate smaller conductive particles into the membrane that do not in themselves introduce macro porosity like the EG does. This may include small particles of graphene, CNTs and/or metal and/or semiconductor/conductive micro and nanoparticles. The other way is to select another volatile co-solvent other than THF which does not decrease the conductivity of the resulting PANI membrane. This could be 4-dioxane – a common solvent used as a volatility enhancer in membranes cast with DMF as a solvent.

The detailed fouling removal mechanism under applied potential is insufficiently understood. Cyclic voltammetry is a useful characterisation technique to evaluate the membrane electrochemical properties. Some preliminary measurements have been done (Fig. E1, Appendix E) and more work is underway. Electrical impedance spectroscopy is also an advantageous tool which enables the early detection of membrane fouling as well as the in-situ investigation of membrane self-cleaning under external stimuli. Understanding the detailed mechanism of

membrane defouling can assist the timely cleaning of the membrane, and improve the membrane long-term performance.

The selection of polymer/solvent/non-solvent systems in NIPS method is crucial to form membranes with the desired performance. PANI-PAMPSA partially lost its conductivity after being cast from NMP solvent, indicating that NMP was not a “good” membrane film making solvent for the PANI-PAMPSA. Finding a “good” solvent is favourable to better dissolve the PANI-PAMPSA complexes and change the molecular conformation of doped PANI from “compact coil” structures to more expanded structures, which are desirable for the high conductivity.

In this study, 30 V of applied potential was provided on the membranes. In terms of energy consumption by applying an electrical potential, improving the design of the setup is a promising way to decrease the electrical potential used and reduce the energy consumption.

In terms of membrane defouling behaviour, only one kind of model foulants (BSA) was used to investigate the membrane defouling ability. More foulants, such as humid acid, sodium alginate and silicon dioxide particles, can be tried to further determine the effect of electrical potential on the fouling removal caused by different model foulants.

References

[1] F. Meng, S.-R. Chae, A. Drews, M. Kraume, H.-S. Shin, F. Yang, Recent advances in membrane bioreactors (MBRs): membrane fouling and membrane material, Water research, 43 (2009) 1489-1512.

[2] A. Drews, Membrane fouling in membrane bioreactors—characterisation, contradictions, cause and cures, Journal of membrane science, 363 (2010) 1-28.

[3] R.B. Kaner, Gas, liquid and enantiomeric separations using polyaniline, Synthetic metals, 125 (2001) 65-71.

[4] M. Sairam, S.K. Nataraj, T.M. Aminabhavi, S. Roy, C.D. Madhusoodana, Polyaniline Membranes for Separation and Purification of Gases, Liquids, and Electrolyte Solutions, Separation & Purification Reviews, 35 (2006) 249-283.

[5] J. Pellegrino, The Use of Conducting Polymers in Membrane-Based Separations, Annals of the New York Academy of Sciences, 984 (2003) 289-305.

[6] R. Rohani, Linking the Microstructural and Separation Properties of Electrically Tuneable Polyaniline Pressure Filtration Membranes, in, University of Auckland, 2013.

[7] M. Sairam, X.X. Loh, K. Li, A. Bismarck, J.H.G. Steinke, A.G. Livingston, Nanoporous asymmetric polyaniline films for filtration of organic solvents, Journal of Membrane Science, 330 (2009) 166-174.

[8] H. Hu, J.L. Cadenas, J.M. Saniger, P. Nair, Electrically conducting polyaniline–poly (acrylic acid) blends, Polymer International, 45 (1998) 262-270.

[9] B.D. Malhotra, S. Ghosh, R. Chandra, Polyaniline/Polymeric acid composite, a novel conducting rubber, Journal of Applied Polymer Science, 40 (1990) 1049-1052.

[10] L. Zhang, H. Peng, J. Sui, P.A. Kilmartin, J. Travas-Sejdic, Polyaniline nanotubes doped with polymeric acids, Current Applied Physics, 8 (2008) 312-315.

[11] J. Tarver, J.E. Yoo, T.J. Dennes, J. Schwartz, Y.-L. Loo, Polymer acid doped polyaniline is electrochemically stable beyond pH 9, Chemistry of Materials, 21 (2008) 280-286.

[12] L. Hechavarría, H. Hu, M.E. Rincón, Polyaniline–poly (2-acrylamido-2-methyl-1-propanosulfonic acid) composite thin films: structure and properties, Thin Solid Films, 441 (2003) 56-62.

[13] H. Hu, J.M. Saniger, J.G. Bañuelos, Thin films of polyaniline–polyacrylic acid composite by chemical bath deposition, Thin Solid Films, 347 (1999) 241-247.

[14] L. Sun, H. Liu, R. Clark, S.C. Yang, Double-strand polyaniline, Synthetic metals, 84 (1997) 67-68.

[15] T.M. Su, I.J. Ball, J.A. Conklin, S.-C. Huang, R.K. Larson, S.L. Nguyen, B.M. Lew, R.B. Kaner, Polyaniline/polyimide blends for pervaporation and gas separation studies, Synthetic metals, 84 (1997) 801-802.

[16] Y. Kang, M.-H. Lee, S.B. Rhee, Electrochemical properties of polyaniline doped with poly (styrenesulfonic acid), Synthetic metals, 52 (1992) 319-328.

[17] S. Judd, B. Jefferson, Membranes for industrial wastewater recovery and re-use, Elsevier, 2003.

[18] DARRELL ALEC PATTERSON, CHRISTOPHER JOHN DAVEY, R. ROHANI, Membrane separations: From purifications, minimisation, reuse and recycling to process intensification, Chemical Processes for a Sustainable Future, (2014) 467.

[19] B. Van der Bruggen, C. Vandecasteele, T. Van Gestel, W. Doyen, R. Leysen, A review of pressure-driven membrane processes in wastewater treatment and drinking water production, Environmental progress, 22 (2003) 46-56.

[20] M. Mulder, Basic Principles of Membrane Technology Second Edition, Kluwer Academic Pub, 1996.

[21] R. Baker, Membrane technology and applications, John Wiley & Sons, 2012.

[22] N. Hilal, H. Al-Zoubi, N. Darwish, A. Mohamma, M. Abu Arabi, A comprehensive review of nanofiltration membranes: Treatment, pretreatment, modelling, and atomic force microscopy, Desalination, 170 (2004) 281-308.

[23] L.F. Greenlee, D.F. Lawler, B.D. Freeman, B. Marrot, P. Moulin, Reverse osmosis desalination: water sources, technology, and today's challenges, Water research, 43 (2009) 2317-2348.

[24] C. Fritzmann, J. Löwenberg, T. Wintgens, T. Melin, State-of-the-art of reverse osmosis desalination, Desalination, 216 (2007) 1-76.

[25] F. Carstensen, A. Apel, M. Wessling, < i> In situ</i> product recovery: Submerged membranes< i> vs.</i> external loop membranes, Journal of Membrane Science, 394 (2012) 1-36.

[26] M. Mota, J.A. Teixeira, A. Yelshin, Influence of cell-shape on the cake resistance in dead-end and cross-flow filtrations, Separation and purification technology, 27 (2002) 137-144.

[27] J. Wijmans, The role of permeant molar volume in the solution-diffusion model transport equations, Journal of membrane science, 237 (2004) 39-50.

[28] J. Wijmans, R. Baker, The solution-diffusion model: a review, Journal of membrane science, 107 (1995) 1-21.

[29] H. Strathmann, L. Giorno, E. Drioli, Introduction to membrane science and technology, Wiley-VCH Verlag & Company, 2011.

[30] H.K. Lonsdale, W. Pusch, A. Walch, Donnan-membrane effects in hyperfiltration of ternary systems, Journal of the Chemical Society, Faraday Transactions 1: Physical Chemistry in Condensed Phases, 71 (1975) 501-514.

[31] Y.S. Toh, X. Loh, K. Li, A. Bismarck, A. Livingston, In search of a standard method for the characterisation of organic solvent nanofiltration membranes, Journal of membrane science, 291 (2007) 120-125.

[32] L. Giorno, E. Drioli, Biocatalytic membrane reactors: applications and perspectives, Trends in biotechnology, 18 (2000) 339-349.

[33] I. Pinnau, B. Freeman, Formation and modification of polymeric membranes: overview, in: ACS Symposium series, ACS Publications, 2000, pp. 1-22.

[34] H. Strathmann, Membrane separation processes: current relevance and future opportunities, AIChE Journal, 47 (2001) 1077-1087.

[35] I. Pinnau, W.J. Koros, Relationship between substructure resistance and gas separation properties of defect-free integrally skinned asymmetric membranes, Industrial & engineering chemistry research, 30 (1991) 1837-1840.

[36] P. Pandey, R. Chauhan, Membranes for gas separation, Progress in Polymer Science, 26 (2001) 853-893.

[37] M. Ulbricht, Advanced functional polymer membranes, Polymer, 47 (2006) 2217-2262.

[38] W. Pusch, A. Walch, Synthetic membranes—preparation, structure, and application, Angewandte Chemie International Edition in English, 21 (1982) 660-685.

[39] G. Lu, J. Diniz da Costa, M. Duke, S. Giessler, R. Socolow, R. Williams, T. Kreutz, Inorganic membranes for hydrogen production and purification: a critical review and perspective, Journal of colloid and interface science, 314 (2007) 589-603.

[40] D. Shekhawat, D.R. Luebke, H.W. Pennline, A review of carbon dioxide selective membranes, US Department of Energy, (2003).

[41] R.D. Noble, D.L. Gin, Perspective on ionic liquids and ionic liquid membranes, Journal of Membrane Science, 369 (2011) 1-4.

[42] C.J. Davey, D. Leak, D.A. Patterson, Hybrid and Mixed Matrix Membranes for Separations from Fermentations, Membranes, 6 (2016) 17.

[43] M. Goosen, S. Sablani, H. Al-Hinai, S. Al-Obeidani, R. Al-Belushi, D. Jackson, Fouling of reverse osmosis and ultrafiltration membranes: a critical review, Separation Science and Technology, 39 (2005) 2261-2297.

[44] J.C. Chen, Q. Li, M. Elimelech, In situ monitoring techniques for concentration polarization and fouling phenomena in membrane filtration, Advances in Colloid and Interface Science, 107 (2004) 83-108.

[45] N. D'SOUZA, A. Mawson, Membrane cleaning in the dairy industry: a review, Critical reviews in food science and nutrition, 45 (2005) 125-134.

[46] D. Potts, R. Ahlert, S. Wang, A critical review of fouling of reverse osmosis membranes, Desalination, 36 (1981) 235-264.

[47] H. Huang, K. Schwab, J.G. Jacangelo, Pretreatment for low pressure membranes in water treatment: a review, Environmental science & technology, 43 (2009) 3011-3019.

[48] G.S. Ajmani, D. Goodwin, K. Marsh, D.H. Fairbrother, K.J. Schwab, J.G. Jacangelo, H. Huang, Modification of low pressure membranes with carbon nanotube layers for fouling control, water research, 46 (2012) 5645-5654.

[49] D. Rana, T. Matsuura, Surface modifications for antifouling membranes, Chemical reviews, 110 (2010) 2448-2471.

[50] H. Hasbullah, S. Kumbharkar, A. Ismail, K. Li, Preparation of polyaniline asymmetric hollow fiber membranes and investigation towards gas separation performance, Journal of Membrane Science, 366 (2011) 116-124.

[51] Y. Liao, X.-G. Li, E.M. Hoek, R.B. Kaner, Carbon nanotube/polyaniline nanofiber ultrafiltration membranes, Journal of Materials Chemistry A, 1 (2013) 15390-15396.

[52] D. Wandera, S.R. Wickramasinghe, S.M. Husson, Stimuli-responsive membranes, Journal of Membrane Science, 357 (2010) 6-35.

[53] D. Roy, J.N. Cambre, B.S. Sumerlin, Future perspectives and recent advances in stimuli-responsive materials, Progress in Polymer Science, 35 (2010) 278-301.

[54] C. Liangyin, X. Rui, J. Xiaojie, Stimuli-responsive membranes: smart tools for controllable mass-transfer and separation processes, Chinese Journal of Chemical Engineering, 19 (2011) 891-903.

[55] M.A.C. Stuart, W.T. Huck, J. Genzer, M. Müller, C. Ober, M. Stamm, G.B. Sukhorukov, I. Szleifer, V.V. Tsukruk, M. Urban, Emerging applications of stimuli-responsive polymer materials, Nature materials, 9 (2010) 101-113.

[56] D.L. Pile, A.C. Hillier, Electrochemically modulated transport through a conducting polymer membrane, Journal of membrane science, 208 (2002) 119-131.

[57] C. Weidlich, K.-M. Mangold, Electrochemically switchable polypyrrole coated membranes, Electrochimica Acta, 56 (2011) 3481-3484.

[58] Q. Yang, S. Wickramasinghe, Responsive Membranes for Water Treatment, Responsive Membranes and Materials, (2012) 143-162.

[59] H.H. Himstedt, K.M. Marshall, S.R. Wickramasinghe, pH-responsive nanofiltration membranes by surface modification, Journal of membrane science, 366 (2011) 373-381.

[60] F. Ahmed, B.S. Lalia, V. Kochkodan, N. Hilal, R. Hashaikeh, Electrically conductive polymeric membranes for fouling prevention and detection: A review, Desalination, 391 (2016) 1-15.

[61] J. Huang, Z. Wang, J. Zhang, X. Zhang, J. Ma, Z. Wu, A novel composite conductive microfiltration membrane and its anti-fouling performance with an external electric field in membrane bioreactors, Scientific reports, 5 (2015).

[62] A.V. Dudchenko, J. Rolf, K. Russell, W. Duan, D. Jassby, Organic fouling inhibition on electrically conducting carbon nanotube–polyvinyl alcohol composite ultrafiltration membranes, Journal of Membrane Science, 468 (2014) 1-10.

[63] Q. Zhang, C.D. Vecitis, Conductive CNT-PVDF membrane for capacitive organic fouling reduction, Journal of Membrane Science, 459 (2014) 143-156.

[64] G. Schaule, A. Rumpf, C. Weidlich, K.-M. Mangold, H.-C. Flemming, Effects of electric polarization of indium tin oxide (ITO) and polypyrrole on biofilm formation, Water Science & Technology, 58 (2008).

[65] A.D. Enevoldsen, E.B. Hansen, G. Jonsson, Electro-ultrafiltration of industrial enzyme solutions, Journal of Membrane science, 299 (2007) 28-37.

[66] S. Bhadra, D. Khastgir, N.K. Singha, J.H. Lee, Progress in preparation, processing and applications of polyaniline, Progress in Polymer Science, 34 (2009) 783-810.

[67] A. Malinauskas, Self-doped polyanilines, Journal of power sources, 126 (2004) 214-220.

[68] Y. Nicolau, D. Djurado, Novel crystalline structures of polyaniline, Synthetic metals, 55 (1993) 394-401.

[69] E. Genies, A. Boyle, M. Lapkowski, C. Tsintavis, Polyaniline: a historical survey, Synthetic Metals, 36 (1990) 139-182.

[70] Z. Wei, C.F.J. Faul, Aniline Oligomers – Architecture, Function and New Opportunities for Nanostructured Materials, Macromolecular Rapid Communications, 29 (2008) 280-292.

[71] G.G. Wallace, P.R. Teasdale, G.M. Spinks, L.A. Kane-Maguire, Conductive electroactive polymers: intelligent polymer systems, CRC press, 2008.

[72] J.Y. Shimano, A.G. MacDiarmid, Polyaniline, a dynamic block copolymer: key to attaining its intrinsic conductivity?, Synthetic Metals, 123 (2001) 251-262.

[73] Y. Cao, A. Andreatta, A.J. Heeger, P. Smith, Influence of chemical polymerization conditions on the properties of polyaniline, Polymer, 30 (1989) 2305-2311.

[74] I. Sapurina, J. Stejskal, The mechanism of the oxidative polymerization of aniline and the formation of supramolecular polyaniline structures, Polymer International, 57 (2008) 1295-1325.

[75] J. Jang, Conducting polymer nanomaterials and their applications, in: Emissive Materials Nanomaterials, Springer, 2006, pp. 189-260.

[76] A. Pron, F. Genoud, C. Menardo, M. Nechtschein, The effect of the oxidation conditions on the chemical polymerization of polyaniline, Synthetic metals, 24 (1988) 193-201.

[77] P. Adams, P. Laughlin, A. Monkman, A. Kenwright, Low temperature synthesis of high molecular weight polyaniline, Polymer, 37 (1996) 3411-3417.

[78] M. Bláha, M. Varga, J. Prokeš, A. Zhigunov, J. Vohlídal, Effects of the polymerization temperature on the structure, morphology and conductivity of polyaniline prepared with ammonium peroxodisulfate, European Polymer Journal, 49 (2013) 3904-3911.

[79] J. Stejskal, A. Riede, D. Hlavatá, J. Prokeš, M. Helmstedt, P. Holler, The effect of polymerization temperature on molecular weight, crystallinity, and electrical conductivity of polyaniline, Synthetic Metals, 96 (1998) 55-61.

[80] M. Abe, A. Ohtani, Y. Umemoto, S. Akizuki, M. Ezoe, H. Higuchi, K. Nakamoto, A. Okuno, Y. Noda, Soluble and high molecular weight polyaniline, Journal of the Chemical Society, Chemical Communications, (1989) 1736-1738.

[81] P. Chapman, X.X. Loh, A.G. Livingston, K. Li, T.A.C. Oliveira, Polyaniline membranes for the dehydration of tetrahydrofuran by pervaporation, Journal of Membrane Science, 309 (2008) 102-111.

[82] S. Yang, J. Chen, The effect of synthesis conditions on the properties of polyaniline film, Synthetic Metals, 69 (1995) 153-154.

[83] A.G. Macdiarmid, A.J. Epstein, Polyaniline: interrelationships between molecular weight, morphology, Donnan potential and conductivity, in: MRS Proceedings, Cambridge Univ Press, 1992, pp. 565.

[84] G. Boara, M. Sparpaglione, Synthesis of polyanilines with high electrical conductivity, Synthetic Metals, 72 (1995) 135-140.

[85] A. Ohtani, M. Abe, M. Ezoe, T. Doi, T. Miyata, A. Miyake, Synthesis and properties of high-molecular-weight soluble polyaniline and its application to the 4MB-capacity barium ferrite floppy disk's antistatic coating, Synthetic Metals, 57 (1993) 3696-3701.

[86] J. Lee, M. Cho, H. Choi, M. Jhon, Effect of polymerization temperature on polyaniline based electrorheological suspensions, Colloid and Polymer Science, 277 (1999) 73-76.

[87] P. Adams, P. Laughlin, A. Monkman, Synthesis of high molecular weight polyaniline at low temperatures, Synthetic Metals, 76 (1996) 157-160.

[88] Y. Moo Lee, S. Yong Nam, S. Yong Ha, Pervaporation of water/isopropanol mixtures through polyaniline membranes doped with poly (acrylic acid), Journal of membrane science, 159 (1999) 41-46.

[89] Z. Sun, Y. Geng, J. Li, X. Wang, X. Jing, F. Wang, Catalytic oxidization polymerization of aniline in an H2O2 Fe2+ system, Journal of applied polymer science, 72 (1999) 1077-1084.

[90] G. Illing, K. Hellgardt, R. Wakeman, A. Jungbauer, Preparation and characterisation of polyaniline based membranes for gas separation, Journal of Membrane Science, 184 (2001) 69-78.

[91] M. Sairam, X.X. Loh, K. Li, A. Bismarck, J.H.G. Steinke, A.G. Livingston, Nanoporous asymmetric polyaniline films for filtration of organic solvents, Journal of Membrane Science, 330 (2009) 166-174.

[92] X.X. Loh, M. Sairam, J.H. Steinke, A.G. Livingston, A. Bismarck, K. Li, Polyaniline hollow fibres for organic solvent nanofiltration, Chemical communications, (2008) 6324-6326.

[93] X. Loh, M. Sairam, A. Bismarck, J. Steinke, A. Livingston, K. Li, Crosslinked integrally skinned asymmetric polyaniline membranes for use in organic solvents, Journal of Membrane Science, 326 (2009) 635-642.

[94] M. Sairam, X. Loh, Y. Bhole, I. Sereewatthanawut, K. Li, A. Bismarck, J. Steinke, A. Livingston, Spiral-wound polyaniline membrane modules for organic solvent nanofiltration (OSN), Journal of Membrane Science, 349 (2010) 123-129.

[95] P. Wang, K.L. Tan, E.T. Kang, K.G. Neoh, Preparation and characterization of semi-conductive poly(vinylidene fluoride)/polyaniline blends and membranes, Applied Surface Science, 193 (2002) 36-45.

[96] S. Zhao, Z. Wang, J.X. Wang, S.B. Yang, S.C. Wang, PSf/PANI nanocomposite membrane prepared by in situ blending of PSf and PANI/NMP, Journal of Membrane Science, 376 (2011) 83-95.

[97] S. Tan, J.H. Tieu, D. Bélanger, Chemical polymerization of aniline on a poly (styrene sulfonic acid) membrane: controlling the polymerization site using different oxidants, The Journal of Physical Chemistry B, 109 (2005) 14085-14092.

[98] Z. Fan, Z. Wang, M. Duan, J. Wang, S. Wang, Preparation and characterization of polyaniline/polysulfone nanocomposite ultrafiltration membrane, Journal of Membrane Science, 310 (2008) 402-408.

[99] G. Tishchenko, J. Dybal, J. Stejskal, V. Kůdela, M. Bleha, E.Y. Rosova, G. Elyashevich, Electrical resistance and diffusion permeability of microporous polyethylene membranes modified with polypyrrole and polyaniline in solutions of electrolytes, Journal of membrane science, 196 (2002) 279-287.

[100] J.-Y. Kim, J.-H. Lee, S.-J. Kwon, The manufacture and properties of polyaniline nano-films prepared through vapor-phase polymerization, Synthetic metals, 157 (2007) 336-342.

[101] G. Illing, K. Hellgardt, M. Schonert, R.J. Wakeman, A. Jungbauer, Towards ultrathin polyaniline films for gas separation, Journal of Membrane Science, 253 (2005) 199-208.

[102] M. Delvaux, J. Duchet, P.-Y. Stavaux, R. Legras, S. Demoustier-Champagne, Chemical and electrochemical synthesis of polyaniline micro-and nano-tubules, Synthetic Metals, 113 (2000) 275-280.

[103] W. Yang, B. Rånby, Radical living graft polymerization on the surface of polymeric materials, Macromolecules, 29 (1996) 3308-3310.

[104] A.I. Schäfer, A.G. Fane, T.D. Waite, Nanofiltration: principles and applications, Access Online via Elsevier, 2005.

[105] G.R. Guillen, Y. Pan, M. Li, E.M. Hoek, Preparation and characterization of membranes formed by nonsolvent induced phase separation: a review, Industrial & Engineering Chemistry Research, 50 (2011) 3798-3817.

[106] I.D. Norris, A.G. Fadeev, J. Pellegrino, B.R. Mattes, Development of Integrally Skinned Asymmetric Polyaniline Hollow Fibers for Membrane Applications, Synthetic Metals, 153 (2005) 57-60.

[107] H. Deligöz, Preparation of self-standing polyaniline-based membranes: Doping effect on the selective ion separation and reverse osmosis properties, Journal of Applied Polymer Science, 105 (2007) 2640-2645.

[108] I.J. Ball, S.-C. Huang, R.A. Wolf, J.Y. Shimano, R.B. Kaner, Pervaporation studies with polyaniline membranes and blends, Journal of Membrane Science, 174 (2000) 161-176.

[109] P. Gajendran, R. Saraswathi, Polyaniline-carbon nanotube composites, Pure and Applied Chemistry, 80 (2008) 2377-2395.

[110] J. Li, L. Zhu, Y. Wu, Y. Harima, A. Zhang, H. Tang, Hybrid composites of conductive polyaniline and nanocrystalline titanium oxide prepared via self-assembling and graft polymerization, Polymer, 47 (2006) 7361-7367.

[111] S. Stankovich, D.A. Dikin, G.H. Dommett, K.M. Kohlhaas, E.J. Zimney, E.A. Stach, R.D. Piner, S.T. Nguyen, R.S. Ruoff, Graphene-based composite materials, Nature, 442 (2006) 282-286.

[112] A.K. Geim, Graphene: status and prospects, Science, 324 (2009) 1530-1534.

[113] P. Vandezande, X. Li, L.E. Gevers, I.F. Vankelecom, High throughput study of phase inversion parameters for polyimide-based SRNF membranes, Journal of Membrane Science, 330 (2009) 307-318.

[114] Y.H. See-Toh, M. Silva, A. Livingston, Controlling molecular weight cut-off curves for highly solvent stable organic solvent nanofiltration (OSN) membranes, Journal of Membrane Science, 324 (2008) 220-232.

[115] C. Kong, M. Kanezashi, T. Yamomoto, T. Shintani, T. Tsuru, Controlled synthesis of high performance polyamide membrane with thin dense layer for water desalination, Journal of Membrane Science, 362 (2010) 76-80.

[116] Y.H. See-Toh, F.C. Ferreira, A.G. Livingston, The influence of membrane formation parameters on the functional performance of organic solvent nanofiltration membranes, Journal of Membrane Science, 299 (2007) 236-250.

[117] I. Soroko, M. Makowski, F. Spill, A. Livingston, The effect of membrane formation parameters on performance of polyimide membranes for organic solvent nanofiltration (OSN). Part B: Analysis of evaporation step and the role of a co-solvent, Journal of Membrane Science, 381 (2011) 163-171.

[118] A.F. Ismail, P.Y. Lai, Effects of phase inversion and rheological factors on formation of defect-free and ultrathin-skinned asymmetric polysulfone membranes for gas separation, Separation and Purification Technology, 33 (2003) 127-143.

[119] O. Breuer, U. Sundararaj, Big returns from small fibers: a review of polymer/carbon nanotube composites, Polymer composites, 25 (2004) 630-645.

[120] G. Ćirić-Marjanović, Recent advances in polyaniline composites with metals, metalloids and nonmetals, Synthetic Metals, 170 (2013) 31-56.

[121] M. Baibarac, I. Baltog, S. Lefrant, J. Mevellec, O. Chauvet, Polyaniline and carbon nanotubes based composites containing whole units and fragments of nanotubes, Chemistry of Materials, 15 (2003) 4149-4156.

[122] X.-h. Li, B. Wu, J.-e. Huang, J. Zhang, Z.-f. Liu, H.-l. Li, Fabrication and characterization of well-dispersed single-walled carbon nanotube/polyaniline composites, Carbon, 41 (2003) 1670-1673.

[123] H. Zengin, G. Kalaycı, Synthesis and characterization of polyaniline/activated carbon composites and preparation of conductive films, Materials Chemistry and Physics, 120 (2010) 46-53.

[124] K.R. Reddy, B.C. Sin, K.S. Ryu, J. Noh, Y. Lee, < i> In situ</i> self-organization of carbon black–polyaniline composites from nanospheres to nanorods: Synthesis, morphology, structure and electrical conductivity, Synthetic Metals, 159 (2009) 1934-1939.

[125] M.R. Karim, C.J. Lee, M.S. Lee, Synthesis and characterization of conducting polyaniline-activated carbon nanocomposites, Journal of applied polymer science, 103 (2007) 1973-1977.

[126] S. Bourdo, Z. Li, A.S. Biris, F. Watanabe, T. Viswanathan, I. Pavel, Structural, Electrical, and Thermal Behavior of Graphite-Polyaniline Composites with Increased Crystallinity, Advanced Functional Materials, 18 (2008) 432-440.

[127] C. Xiang, L. Li, S. Jin, B. Zhang, H. Qian, G. Tong, Expanded graphite/polyaniline electrical conducting composites: Synthesis, conductive and dielectric properties, Materials Letters, 64 (2010) 1313-1315.

[128] L. Nikzad, S. Alibeigi, M.R. Vaezi, B. Yazdani, M.R. Rahimipour, Synthesis of a Graphite-Polyaniline Nanocomposite and Evaluation of Its Electrochemical Properties, Chemical engineering & technology, 32 (2009) 861-866.

[129] S.E. Bourdo, B.A. Warford, T. Viswanathan, Electrical and thermal properties of graphite/polyaniline composites, Journal of Solid State Chemistry, 196 (2012) 309-313.

[130] X. Du, M. Xiao, Y. Meng, Synthesis and characterization of polyaniline/graphite conducting nanocomposites, Journal of Polymer Science Part B: Polymer Physics, 42 (2004) 1972-1978.

[131] R. Saito, G. Dresselhaus, M.S. Dresselhaus, Physical properties of carbon nanotubes, World Scientific, 1998.

[132] H. Zengin, W. Zhou, J. Jin, R. Czerw, D.W. Smith, L. Echegoyen, D.L. Carroll, S.H. Foulger, J. Ballato, Carbon nanotube doped polyaniline, Advanced materials, 14 (2002) 1480-1483.

[133] M.S. Shaffer, X. Fan, A. Windle, Dispersion and packing of carbon nanotubes, Carbon, 36 (1998) 1603-1612.

[134] Y.-k. Zhou, B.-l. He, W.-j. Zhou, J. Huang, X.-h. Li, B. Wu, H.-l. Li, Electrochemical capacitance of well-coated single-walled carbon nanotube with polyaniline composites, Electrochimica Acta, 49 (2004) 257-262.

[135] K. Zhang, L.L. Zhang, X. Zhao, J. Wu, Graphene/polyaniline nanofiber composites as supercapacitor electrodes, Chemistry of Materials, 22 (2010) 1392-1401.

[136] Q. Wu, Y. Xu, Z. Yao, A. Liu, G. Shi, Supercapacitors based on flexible graphene/polyaniline nanofiber composite films, Acs Nano, 4 (2010) 1963-1970.

[137] C. Yan, Y.W. Kanaththage, R. Short, C.T. Gibson, L. Zou, Graphene/Polyaniline nanocomposite as electrode material for membrane capacitive deionization, Desalination, 344 (2014) 274-279.

[138] H. Wang, Q. Hao, X. Yang, L. Lu, X. Wang, A nanostructured graphene/polyaniline hybrid material for supercapacitors, Nanoscale, 2 (2010) 2164-2170.

[139] D.-W. Wang, F. Li, J. Zhao, W. Ren, Z.-G. Chen, J. Tan, Z.-S. Wu, I. Gentle, G.Q. Lu, H.-M. Cheng, Fabrication of graphene/polyaniline composite paper via in situ anodic electropolymerization for high-performance flexible electrode, Acs Nano, 3 (2009) 1745-1752.

[140] C. Yan, L. Zou, R. Short, Polyaniline-modified activated carbon electrodes for capacitive deionisation, Desalination, 333 (2014) 101-106.

[141] O. Misoon, K. Seok, Effect of dodecyl benzene sulfonic acid on the preparation of polyaniline/activated carbon composites by in situ emulsion polymerization, Electrochimica Acta, 59 (2012) 196-201.

[142] X. Du, M. Xiao, Y. Meng, Facile synthesis of highly conductive polyaniline/graphite nanocomposites, European Polymer Journal, 40 (2004) 1489-1493.

[143] S. Bourdo, T. Viswanathan, Graphite/Polyaniline (GP) composites: Synthesis and characterization, Carbon, 43 (2005) 2983-2988.

[144] M. Cochet, W.K. Maser, A.M. Benito, M.A. Callejas, M.T. Martínez, J.-M. Benoit, J. Schreiber, O. Chauvet, Synthesis of a new polyaniline/nanotube composite:“in-situ” polymerisation and charge transfer through site-selective interaction, Chemical communications, (2001) 1450-1451.

[145] Y. Qiao, C.M. Li, S.-J. Bao, Q.-L. Bao, Carbon nanotube/polyaniline composite as anode material for microbial fuel cells, Journal of Power Sources, 170 (2007) 79-84.

[146] C. Yan, L. Zou, R. Short, Single-walled carbon nanotubes and polyaniline composites for capacitive deionization, Desalination, 290 (2012) 125-129.

[147] H. Bai, Y. Xu, L. Zhao, C. Li, G. Shi, Non-covalent functionalization of graphene sheets by sulfonated polyaniline, Chem. Commun., (2009) 1667-1669.

[148] M.R. Anderson, B.R. Mattes, H. Reiss, R.B. Kaner, Conjugated polymer films for gas separations, Science, 252 (1991) 1412-1415.

[149] M. Anderson, B. Mattes, H. Reiss, R. Kaner, Gas separation membranes: A novel application for conducting polymers, Synthetic Metals, 41 (1991) 1151-1154.

[150] S.-A. Chen, H.-T. Lee, Structure and properties of poly (acrylic acid)-doped polyaniline, Macromolecules, 28 (1995) 2858-2866.

[151] J. Hwang, S. Yang, Morphological modification of polyaniline using polyelectrolyte template molecules, Synthetic Metals, 29 (1989) 271-276.

[152] A.A. Nekrasov, O.L. Gribkova, V.F. Ivanov, A.V. Vannikov, Electroactive films of interpolymer complexes of polyaniline with polyamidosulfonic acids: advantageous features in some possible applications, Journal of Solid State Electrochemistry, 14 (2010) 1975-1984.

[153] J.E. Yoo, J.L. Cross, T.L. Bucholz, K.S. Lee, M.P. Espe, Y.-L. Loo, Improving the electrical conductivity of polymer acid-doped polyaniline by controlling the template molecular weight, Journal of Materials Chemistry, 17 (2007) 1268-1275.

[154] M. Angelopoulos, N. Patel, R. Saraf, Amic acid doping of polyaniline: characterization and resulting blends, Synthetic metals, 55 (1993) 1552-1557.

[155] B. Mattes, M. Anderson, J. Conklin, H. Reiss, R. Kaner, Morphological modification of polyaniline films for the separation of gases, Synthetic metals, 57 (1993) 3655-3660.

[156] R. Nagarajan, S. Tripathy, J. Kumar, F.F. Bruno, L. Samuelson, An enzymatically synthesized conducting molecular complex of polyaniline and poly (vinylphosphonic acid), Macromolecules, 33 (2000) 9542-9547.

[157] G.E. Asturias, G.W. Jang, A.G. Macdiarmid, K. Doblhofer, C. Zhong, Membrane-Properties of Polymer Films: The Acid-Doping Reaction of Polyaniline, Berichte der Bunsengesellschaft für physikalische Chemie, 95 (1991) 1381-1384.

[158] A. Nekrasov, O. Gribkova, T. Eremina, A. Isakova, V. Ivanov, V. Tverskoj, A. Vannikov, Electrochemical synthesis of polyaniline in the presence of poly (amidosulfonic acid) s with different rigidity of polymer backbone and characterization of the films obtained, Electrochimica Acta, 53 (2008) 3789-3797.

[159] C.A. Amarnath, J. Kim, K. Kim, J. Choi, D. Sohn, Nanoflakes to nanorods and nanospheres transition of selenious acid doped polyaniline, Polymer, 49 (2008) 432-437.

[160] Y. Xia, J.M. Wiesinger, A.G. MacDiarmid, A.J. Epstein, Camphorsulfonic acid fully doped polyaniline emeraldine salt: conformations in different solvents studied by an ultraviolet/visible/near-infrared spectroscopic method, Chemistry of Materials, 7 (1995) 443-445.

[161] Y. Cao, P. Smith, A.J. Heeger, Counter-ion induced processibility of conducting polyaniline and of conducting polyblends of polyaniline in bulk polymers, Synthetic metals, 48 (1992) 91-97.

[162] M. Jayakannan, P. Anilkumar, A. Sanju, Synthesis and characterization of new azobenzenesulfonic acids doped conducting polyaniline, European polymer journal, 42 (2006) 2623-2631.

[163] P. Anilkumar, M. Jayakannan, Single-molecular-system-based selective micellar templates for polyaniline nanomaterials: control of shape, size, solid state ordering, and expanded chain to coillike conformation, Macromolecules, 40 (2007) 7311-7319.

[164] G. Lu, C. Li, G. Shi, Polypyrrole micro-and nanowires synthesized by electrochemical polymerization of pyrrole in the aqueous solutions of pyrenesulfonic acid, Polymer, 47 (2006) 1778-1784.

[165] I. Kulszewicz-Bajer, M. Zagorska, J. Nizioł, A. Proń, W. Łużny, Esters of 5-sulfo-i-phthalic acid as new dopants improving the solution processibility of polyaniline: spectroscopic, structural and transport properties of the doped polymer, Synthetic metals, 114 (2000) 125-131.

[166] R.K. Paul, C.K.S. Pillai, Thermal properties of processable polyaniline with novel sulfonic acid dopants, Polymer international, 50 (2001) 381-386.

[167] C. Ong, S. Goh, H. Chan, Conductive polyaniline/poly (vinylphosphonic acid) blends, Polymer bulletin, 39 (1997) 627-632.

[168] I. Kulszewicz-Bajer, J. Pretula, A. Proń, Poly (alkylene phosphates) as new dopants of polyaniline, J. Chem. Soc., Chem. Commun., (1994) 641-642.

[169] I. Kulszewicz-Bajer, J. Sobczak, M. Hasik, J. Pretula, Spectroscopic studies of polyaniline protonation with poly (alkylene phosphates), Polymer, 37 (1996) 25-30.

[170] L. Zhang, H. Peng, C.F. Hsu, P.A. Kilmartin, J. Travas-Sejdic, Self-assembled polyaniline nanotubes grown from a polymeric acid solution, Nanotechnology, 18 (2007) 115607.

[171] L. Xiao, H. Zhang, E. Scanlon, L. Ramanathan, E.-W. Choe, D. Rogers, T. Apple, B.C. Benicewicz, High-temperature polybenzimidazole fuel cell membranes via a sol-gel process, Chemistry of Materials, 17 (2005) 5328-5333.

[172] H.-K. Song, B. Toste, K. Ahmann, D. Hoffman-Kim, G. Palmore, Micropatterns of positive guidance cues anchored to polypyrrole doped with polyglutamic acid: a new platform for characterizing neurite extension in complex environments, Biomaterials, 27 (2006) 473-484.

[173] S.-A. Chen, M.-Y. Hua, Compatibilities and electrostatic interactions in the blends of self-acid-doped conjugated conducting polymer, poly [2-(3'-thienyl) ethanesulfonic acid], and its sodium salt with poly (vinyl alcohol), Macromolecules, 29 (1996) 4919-4925.

[174] N.V. Blinova, J. Stejskal, M. Trchová, G. Ciric-Marjanovic, I. Sapurina, Polymerization of aniline on polyaniline membranes, The Journal of Physical Chemistry B, 111 (2007) 2440-2448.

[175] A.A. Qaiser, M.M. Hyland, D.A. Patterson, Polyaniline deposition site control on microporous mixed cellulose ester membranes: Surface and in-pore polymerization, in: IOP Conference Series: Materials Science and Engineering, IOP Publishing, 2009, pp. 012009.

[176] S. Jeong Kim, N. Rae Lee, B.J. Yi, S.I. Kim, Synthesis and characterization of polymeric acid-doped polyaniline interpenetrating polymer networks, Journal of Macromolecular Science Part A: Pure and Applied Chemistry, 43 (2006) 497-505.

[177] S. Kuwabata, C.R. Martin, Investigation of the gas-transport properties of polyaniline, Journal of membrane science, 91 (1994) 1-12.

[178] S.-C. Huang, I.J. Ball, R.B. Kaner, Polyaniline membranes for pervaporation of carboxylic acids and water, Macromolecules, 31 (1998) 5456-5464.

[179] B. Vijaya Kumar Naidu, M. Sairam, K. Raju, T.M. Aminabhavi, Pervaporation separation of water+ isopropanol mixtures using novel nanocomposite membranes of poly (vinyl alcohol) and polyaniline, Journal of membrane science, 260 (2005) 142-155.

[180] F.D.R. Amado, E. Gondran, J.Z. Ferreira, M.A.S. Rodrigues, C.A. Ferreira, Synthesis and characterisation of high impact polystyrene/polyaniline composite membranes for electrodialysis, Journal of Membrane Science, 234 (2004) 139-145.

[181] S. Tan, A. Laforgue, D. Bélanger, Characterization of a cation-exchange/polyaniline composite membrane, Langmuir, 19 (2003) 744-751.

[182] A. MacDiarmid, J. Chiang, A. Richter, A. Epstein, Polyaniline: a new concept in conducting polymers, Synthetic Metals, 18 (1987) 285-290.

[183] C. Dhand, M. Das, M. Datta, B. Malhotra, Recent advances in polyaniline based biosensors, Biosensors and Bioelectronics, 26 (2011) 2811-2821.

[184] S. Bhadra, S. Chattopadhyay, N.K. Singha, D. Khastgir, Improvement of conductivity of electrochemically synthesized polyaniline, Journal of Applied Polymer Science, 108 (2008) 57-64.

[185] A.A. Syed, M.K. Dinesan, Polyaniline: Reaction stoichiometry and use as an ion-exchange polymer and acid/base indicator, Synthetic metals, 36 (1990) 209-215.

[186] W. Richard Bowen, T.A. Doneva, Atomic force microscopy characterization of ultrafiltration membranes: correspondence between surface pore dimensions and molecular weight cut-off, Surface and Interface Analysis, 29 (2000) 544-547.

[187] Sterlitech, GE Osmonics Flat Sheet Membrane, GE, Composite PA, UF, 47 mm, 5/Pk, in, 2016.

[188] F. Ellouze, N.B. Amar, A. Deratani, Étude comparative de deux méthodes de caractérisation de membranes d'ultrafiltration et de nanofiltration : la porométrie bi-liquide et le transport de solutés neutres, Comptes Rendus Chimie, 18 (2015) 482-491.

[189] J. Vanneste, A. Sotto, C.M. Courtin, V. Van Craeyveld, K. Bernaerts, J. Van Impe, J. Vandeur, S. Taes, B. Van der Bruggen, Application of tailor-made membranes in a multi-stage process for the purification of sweeteners from Stevia rebaudiana, Journal of Food Engineering, 103 (2011) 285-293.

[190] Sterlitech, GE Osmonics Flat Sheet Membrane, GH, TFC, UF, 47 mm, 5/Pk, in, 2016.

[191] Sterlitech, GE Osmonics Flat Sheet Membrane, GK, TFC, UF, 47 mm, 5/Pk, in, 2016.

[192] Sterlitech, TriSep Flat Sheet Membrane, UA60, PPA, UF, 47 mm, 5/Pk, in, 2016.

[193] Sigma-Aldrich, Ultrafiltration disk membranes, Millipore® PLAC cellulosic (regenerated cellulose) disks, MWCO 1,000 Da, diam. 44.5 mm in, 2016.

[194] Sigma-Aldrich, Ultrafiltration disk membranes, Millipore® MWCO 3,000 Da, PLBC cellulosic (regenerated cellulose) disks, diam. 44.5 mm in, 2016.

[195] F. Vargas-Romero, N. Guitierrez-Najera, G. Mendoza-Hernández, D. Ortega-Bernal, R. Hernández-Pando, M. Castañón-Arreola, Secretome profile analysis of hypervirulent Mycobacterium tuberculosis CPT31 reveals increased production of EsxB and proteins involved in adaptation to intracellular lifestyle, Pathogens and Disease, 74 (2016).

[196] M. Liu, K. Tzou, R. Gregory, Influence of the doping conditions on the surface energies of conducting polymers, Synthetic metals, 63 (1994) 67-71.

[197] S.M. Long, K.R. Brenneman, A. Saprigin, R.S. Kohlman, A.J. Epstein, M. Angelopoulos, S.L. Buchwalter, A. Rossi, W. Zheng, A.G. MacDiarmid, Aggregation and interchain “self” doping in emeraldine base, Synthetic Metals, 84 (1997) 809-810.

[198] D. Yang, A.G. Fadeev, P.N. Adams, B.R. Mattes, GPC characterization of emeraldine base in NMP containing ionic liquids, Synthetic Metals, 157 (2007) 988-996.

[199] D. Yang, B.R. Mattes, Polyaniline emeraldine base in N-methyl-2-pyrrolidinone containing secondary amine additives: B. Characterization of solutions and thin films, Synthetic Metals, 129 (2002) 249-260.

[200] D. Yang, G. Zuccarello, B.R. Mattes, Physical stabilization or chemical degradation of concentrated solutions of polyaniline emeraldine base containing secondary amine additives, Macromolecules, 35 (2002) 5304-5313.

[201] X. Li, F. Monsuur, B. Denoulet, A. Dobrak, P. Vandezande, I.F. Vankelecom, Evaporative light scattering detector: toward a general molecular weight cutoff characterization of nanofiltration membranes, Analytical chemistry, 81 (2009) 1801-1809.

[202] R. Rohani, M. Hyland, D. Patterson, A refined one-filtration method for aqueous based nanofiltration and ultrafiltration membrane molecular weight cut-off determination using polyethylene glycols, Journal of Membrane Science, 382 (2011) 278-290.

[203] C. Causserand, S. Rouaix, A. Akbari, P. Aimar, Improvement of a method for the characterization of ultrafiltration membranes by measurements of tracers retention, Journal of Membrane Science, 238 (2004) 177-190.

[204] N.C. Megoulas, M.A. Koupparis, Twenty years of evaporative light scattering detection, Critical reviews in analytical chemistry, 35 (2005) 301-316.

[205] J. Davey, S. Ralph, C. Too, G. Wallace, Synthesis, characterisation and ion transport studies on polypyrrole/polyvinylphosphate conducting polymer materials, Synthetic metals, 99 (1999) 191-199.

[206] M.J. Ariza, T.F. Otero, Ionic diffusion across oxidized polypyrrole membranes and during oxidation of the free-standing film, Colloids and Surfaces A: Physicochemical and Engineering Aspects, 270 (2005) 226-231.

[207] D.L. Feldheim, C.M. Elliott, Switchable gate membranes. Conducting polymer films for the selective transport of neutral solution species, Journal of membrane science, 70 (1992) 9-15.

[208] H. Lomax, Towards greener membrane processes: stimuli responsive membranes for fouling reduction, Centre for Sustainable Chemical Technologies CDT MRes project 2 thesis, University of Bath, (2012).

[209] P.P. Sengupta, B. Adhikari, Influence of polymerization condition on the electrical conductivity and gas sensing properties of polyaniline, Materials Science and Engineering: A, 459 (2007) 278-285.

[210] M. Cortés, E. Sierra, Effect of synthesis parameters in polyaniline: influence on yield and thermal behavior, Polymer Bulletin, 56 (2006) 37-45.

[211] W.-S. Huang, B.D. Humphrey, A.G. MacDiarmid, Polyaniline, a novel conducting polymer. Morphology and chemistry of its oxidation and reduction in aqueous electrolytes, Journal of the Chemical Society, Faraday Transactions 1: Physical Chemistry in Condensed Phases, 82 (1986) 2385-2400.

[212] Y. Geng, J. Li, Z. Sun, X. Jing, F. Wang, Polymerization of aniline in an aqueous system containing organic solvents, Synthetic metals, 96 (1998) 1-6.

[213] A. Malinauskas, R. Holze, Cyclic UV-Vis spectrovoltammetry of polyaniline, Synthetic metals, 97 (1998) 31-36.

[214] S. Pruneanu, E. Veress, I. Marian, L. Oniciu, Characterization of polyaniline by cyclic voltammetry and UV-Vis absorption spectroscopy, Journal of materials science, 34 (1999) 2733-2739.

[215] J. Albuquerque, L.C. Mattoso, D. Balogh, R. Faria, J. Masters, A. MacDiarmid, A simple method to estimate the oxidation state of polyanilines, Synthetic Metals, 113 (2000) 19-22.

[216] J.E. de Albuquerque, L.H.C. Mattoso, R.M. Faria, J.G. Masters, A.G. MacDiarmid, Study of the interconversion of polyaniline oxidation states by optical absorption spectroscopy, Synthetic Metals, 146 (2004) 1-10.

[217] D. Yang, W. Lu, R. Goering, B.R. Mattes, Investigation of polyaniline processibility using GPC/UV–vis analysis, Synthetic Metals, 159 (2009) 666-674.

[218] T. Zhou, S. Xing, C. Zhang, Y. Wu, C. Zhao, Influence of external voltage on the reprotonated polyaniline films by Fourier Transform Infrared spectroscopy, Spectrochimica acta. Part A, Molecular and biomolecular spectroscopy, 73 (2009) 84-88.

[219] J. Huang, J.A. Moore, J.H. Acquaye, R.B. Kaner, Mechanochemical route to the conducting polymer polyaniline, Macromolecules, 38 (2005) 317-321.

[220] M. Bláha, M. Riesová, J. Zedník, A. Anžlovar, M. Žigon, J. Vohlídal, Polyaniline synthesis with iron(III) chloride–hydrogen peroxide catalyst system: Reaction course and polymer structure study, Synthetic Metals, 161 (2011) 1217-1225.

[221] D.A. Patterson, A. Havill, S. Costello, Y.H. See-Toh, A.G. Livingston, A. Turner, Membrane characterisation by SEM, TEM and ESEM: The implications of dry and wetted microstructure on mass transfer through integrally skinned polyimide nanofiltration membranes, Separation and Purification Technology, 66 (2009) 90-97.

[222] A.K. Hołda, B. Aernouts, W. Saeys, I.F. Vankelecom, Study of polymer concentration and evaporation time as phase inversion parameters for polysulfone-based SRNF membranes, Journal of membrane science, 442 (2013) 196-205.

[223] A.K. Hołda, I.F. Vankelecom, Understanding and guiding the phase inversion process for synthesis of solvent resistant nanofiltration membranes, Journal of Applied Polymer Science, 132 (2015).

[224] E. Ruckenstein, W. Yin, Polyaniline co-doped with camphor sulfonic and hydrochloric acids by chemical oxidation in aqueous solution, Journal of applied polymer science, 79 (2001) 80-85.

[225] J. Yang, S.M. Burkinshaw, J. Zhou, A.P. Monkman, P.J. Brown, Fabrication and Characteristics of 2-Acrylamido-2-methyl-1-propanesulfonic Acid-Doped Polyaniline Hollow Fibers, Advanced materials, 15 (2003) 1081-1084.

[226] Y. Geng, J. Li, X. Jing, F. Wang, Interaction of N-methylpyrrolidone with doped polyaniline, (1997).

[227] S.A. Chen, H.T. Lee, Polyaniline plasticized with 1-methyl-2-pyrrolidone: structure and doping behavior, Macromolecules, 26 (1993) 3254-3261.

[228] J. Libert, J. Cornil, D. Dos Santos, J. Brédas, From neutral oligoanilines to polyanilines: a theoretical investigation of the chain-length dependence of the electronic and optical properties, Physical Review B, 56 (1997) 8638.

[229] A.G. MacDiarmid, A.J. Epstein, Secondary doping in polyaniline, Synthetic Metals, 69 (1995) 85-92.

[230] I.C. Kim, H.G. Yoon, K.H. Lee, Formation of integrally skinned asymmetric polyetherimide nanofiltration membranes by phase inversion process, Journal of applied polymer science, 84 (2002) 1300-1307.

[231] J. Qin, T.-S. Chung, Effect of dope flow rate on the morphology, separation performance, thermal and mechanical properties of ultrafiltration hollow fibre membranes, Journal of membrane science, 157 (1999) 35-51.

[232] L. Xu, W. Chen, A. Mulchandani, Y. Yan, Reversible conversion of conducting polymer films from superhydrophobic to superhydrophilic, Angewandte Chemie International Edition, 44 (2005) 6009-6012.

[233] M. Schneemilch, W.J. Welters, R.A. Hayes, J. Ralston, Electrically induced changes in dynamic wettability, Langmuir, 16 (2000) 2924-2927.

[234] V. Lifton, J. Taylor, B. Vyas, P. Kolodner, R. Cirelli, N. Basavanhally, A. Papazian, R. Frahm, S. Simon, T. Krupenkin, Superhydrophobic membranes with electrically controllable permeability and their application to “smart” microbatteries, Applied Physics Letters, 93 (2008) 043112.

[235] E.M. Andrade, F.V. Molina, M.I. Florit, D. Posadas, Volume Changes of Poly (2-methylaniline) upon Redox Switching Anion and Relaxation Effects, Electrochemical and Solid-State Letters, 3 (2000) 504-507.

[236] L. Lizarraga, E.M.a. Andrade, F.V. Molina, Swelling and volume changes of polyaniline upon redox switching, Journal of Electroanalytical Chemistry, 561 (2004) 127-135.

[237] E. Smela, N. Gadegaard, Volume change in polypyrrole studied by atomic force microscopy, The Journal of Physical Chemistry B, 105 (2001) 9395-9405.

[238] M. Wan, J. Yang, Mechanism of proton doping in polyaniline, Journal of applied polymer science, 55 (1995) 399-405.

[239] T. Zhou, S. Xing, C. Zhang, Y. Wu, C. Zhao, Influence of external voltage on the reprotonated polyaniline films by Fourier Transform Infrared spectroscopy, Spectrochimica Acta Part A: Molecular and Biomolecular Spectroscopy, 73 (2009) 84-88.

[240] C.M. Tam, A.Y. Tremblay, Membrane pore characterization—comparison between single and multicomponent solute probe techniques, Journal of Membrane Science, 57 (1991) 271-287.

[241] J. Ren, Z. Li, F.-S. Wong, A new method for the prediction of pore size distribution and MWCO of ultrafiltration membranes, Journal of membrane science, 279 (2006) 558-569.

[242] A. Morão, M.T. Pessoa de Amorim, A. Lopes, I. Escobar, J.A. Queiroz, Characterisation of ultrafiltration and nanofiltration membranes from rejections of neutral reference solutes using a model of asymmetric pores, Journal of Membrane Science, 319 (2008) 64-75.

[243] N. Hilal, M. Al-Abri, H. Al-Hinai, M. Abu-Arabi, Characterization and retention of NF membranes using PEG, HS and polyelectrolytes, Desalination, 221 (2008) 284-293.

[244] J. Kwiatkowski, M. Cheryan, Performance of nanofiltration membranes in ethanol, Separation science and technology, 40 (2005) 2651-2662.

[245] P. Mulherkar, R. van Reis, Flex test: a fluorescent dextran test for UF membrane characterization, Journal of Membrane Science, 236 (2004) 171-182.

[246] G. Schock, A. Miquel, R. Birkenberger, Characterization of ultrafiltration membranes: cut-off determination by gel permeation chromatography, Journal of Membrane Science, 41 (1989) 55-67.

[247] G. Tkacik, S. Michaels, A rejection profile test for ultrafiltration membranes & devices, Nature Biotechnology, 9 (1991) 941-946.

[248] P. Aimar, M. Meireles, V. Sanchez, A contribution to the translation of retention curves into pore size distributions for sieving membranes, Journal of membrane science, 54 (1990) 321-338.

[249] C. Causserand, P. Aimar, C. Vilani, T. Zambelli, Study of the effects of defects in ultrafiltration membranes on the water flux and the molecular weight cut-off, Desalination, 149 (2002) 485-491.

[250] R. Nobrega, H. De Balmann, P. Aimar, V. Sanchez, Transfer of dextran through ultrafiltration membranes: a study of rejection data analysed by gel permeation chromatography, Journal of membrane science, 45 (1989) 17-36.

[251] Y.H. See-Toh, F.C. Ferreira, A.G. Livingston, The influence of membrane formation on functional performance of organic solvent nanofiltration membranes, Desalination, 199 (2006) 242-244.

[252] L.S. White, Transport properties of a polyimide solvent resistant nanofiltration membrane, Journal of Membrane Science, 205 (2002) 191-202.

[253] K. Yoon, B.S. Hsiao, B. Chu, High flux nanofiltration membranes based on interfacially polymerized polyamide barrier layer on polyacrylonitrile nanofibrous scaffolds, Journal of Membrane Science, 326 (2009) 484-492.

[254] T. Tsuru, S.-i. Wada, S. Izumi, M. Asaeda, Silica–zirconia membranes for nanofiltration, Journal of Membrane Science, 149 (1998) 127-135.

[255] X. Yang, A. Livingston, L.F. Dos Santos, Experimental observations of nanofiltration with organic solvents, Journal of Membrane Science, 190 (2001) 45-55.

[256] C. Li, Y. Ma, H. Li, G. Peng, A convenient method for the determination of molecular weight cut-off of ultrafiltration membranes, Chinese Journal of Chemical Engineering.

[257] S.-S. Chen, J.S. Taylor, L.A. Mulford, C.D. Norris, Influences of molecular weight, molecular size, flux, and recovery for aromatic pesticide removal by nanofiltration membranes, Desalination, 160 (2004) 103-111.

[258] Y. Kiso, T. Kon, T. Kitao, K. Nishimura, Rejection properties of alkyl phthalates with nanofiltration membranes, Journal of Membrane Science, 182 (2001) 205-214.

[259] B. Van der Bruggen, J. Schaep, D. Wilms, C. Vandecasteele, Influence of molecular size, polarity and charge on the retention of organic molecules by nanofiltration, Journal of Membrane Science, 156 (1999) 29-41.

[260] K. Boussu, B. Van der Bruggen, A. Volodin, C. Van Haesendonck, J. Delcour, P. Van Der Meeren, C. Vandecasteele, Characterization of commercial nanofiltration membranes and comparison with self-made polyethersulfone membranes, Desalination, 191 (2006) 245-253.

[261] M. Dalwani, N.E. Benes, G. Bargeman, D. Stamatialis, M. Wessling, A method for characterizing membranes during nanofiltration at extreme pH, Journal of Membrane Science, 363 (2010) 188-194.

[262] M.V. Tres, H.C. Ferraz, R.M. Dallago, M. Di Luccio, J.V. Oliveira, Characterization of polymeric membranes used in vegetable oil/organic solvents separation, Journal of Membrane Science, 362 (2010) 495-500.

[263] M. Urgun-Demirtas, P.L. Benda, P.S. Gillenwater, M.C. Negri, H. Xiong, S.W. Snyder, Achieving very low mercury levels in refinery wastewater by membrane filtration, Journal of Hazardous Materials, 215–216 (2012) 98-107.

[264] Y. Zhang, C. Causserand, P. Aimar, J.P. Cravedi, Removal of bisphenol A by a nanofiltration membrane in view of drinking water production, Water Research, 40 (2006) 3793-3799.

[265] M. Bulut, L.E. Gevers, J.S. Paul, I.F. Vankelecom, P.A. Jacobs, Directed development of high-performance membranes via high-throughput and combinatorial strategies, Journal of combinatorial chemistry, 8 (2006) 168-173.

[266] M.F. Rubner, S.K. Tripathy, J. Georger Jr, P. Cholewa, Structure-property relationships of polyacetylene/polybutadiene blends, Macromolecules, 16 (1983) 870-875.

[267] L. Li, L. Ferng, Y. Wei, C. Yang, H.-F. Ji, Effects of acidity on the size of polyaniline-poly (sodium 4-styrenesulfonate) composite particles and the stability of corresponding colloids in water, Journal of colloid and interface science, 381 (2012) 11-16.

[268] J.-M. Liu, S.C. Yang, Novel colloidal polyaniline fibrils made by template guided chemical polymerization, Journal of the Chemical Society, Chemical Communications, (1991) 1529-1531.

[269] X.M. Feng, R.M. Li, Y.W. Ma, R.F. Chen, N.E. Shi, Q.L. Fan, W. Huang, One-Step Electrochemical Synthesis of Graphene/Polyaniline Composite Film and Its Applications, Advanced Functional Materials, 21 (2011) 2989-2996.

[270] J. Jang, J. Ha, J. Cho, Fabrication of Water-Dispersible Polyaniline-Poly (4-styrenesulfonate) Nanoparticles For Inkjet-Printed Chemical-Sensor Applications, Advanced materials, 19 (2007) 1772-1775.

[271] J.-W. Jeon, J. O'Neal, L. Shao, J.L. Lutkenhaus, Charge storage in polymer acid-doped polyaniline-based layer-by-layer electrodes, ACS applied materials & interfaces, 5 (2013) 10127-10136.

[272] N.V. Blinova, J. Stejskal, M. Trchová, J. Prokeš, Control of polyaniline conductivity and contact angles by partial protonation, Polymer International, 57 (2008) 66-69.

[273] L. Tarachiwin, P. Kiattibutr, L. Ruangchuay, A. Sirivat, J. Schwank, Electrical conductivity response of polyaniline films to ethanol–water mixtures, Synthetic Metals, 129 (2002) 303-308.

[274] M. Angelopoulos, N. Patel, J.M. Shaw, N.C. Labianca, S.A. Rishton, Water soluble conducting polyanilines: applications in lithography, Journal of Vacuum Science & Technology B, 11 (1993) 2794-2797.

[275] J. Yue, Z.H. Wang, K.R. Cromack, A.J. Epstein, A.G. MacDiarmid, Effect of sulfonic acid group on polyaniline backbone, Journal of the American Chemical Society, 113 (1991) 2665-2671.

[276] M. Aroon, A. Ismail, M. Montazer-Rahmati, T. Matsuura, Morphology and permeation properties of polysulfone membranes for gas separation: effects of non-solvent additives and co-solvent, Separation and Purification Technology, 72 (2010) 194-202.

[277] S. Bhadra, N.K. Singha, D. Khastgir, Effect of aromatic substitution in aniline on the properties of polyaniline, European Polymer Journal, 44 (2008) 1763-1770.

[278] W. Li, M. Wan, Porous polyaniline films with high conductivity, Synthetic metals, 92 (1998) 121-126.

[279] A. Mukherjee, R. Menon, The role of molecular recognition in charge transport properties of doped polyaniline, Applied biochemistry and biotechnology, 96 (2001) 145-153.

[280] G.R. Guillen, G.Z. Ramon, H. PirouzKavehpour, R.B. Kaner, E. Hoek, Direct microscopic observation of membrane formation by nonsolvent induced phase separation, Journal of Membrane Science, (2013).

[281] P. Sukitpaneenit, T.-S. Chung, Molecular elucidation of morphology and mechanical properties of PVDF hollow fiber membranes from aspects of phase inversion, crystallization and rheology, Journal of Membrane Science, 340 (2009) 192-205.

[282] D. Wang, K. Li, W.K. Teo, Porous PVDF asymmetric hollow fiber membranes prepared with the use of small molecular additives, Journal of Membrane Science, 178 (2000) 13-23.

[283] J.E. Yoo, T.L. Bucholz, S. Jung, Y.-L. Loo, Narrowing the size distribution of the polymer acid improves PANI conductivity, Journal of Materials Chemistry, 18 (2008) 3129-3135.

[284] J.E. Yoo, Understanding the Processing-Structure-Property Relationships of Water-Dispersible, Conductive Polyaniline, The University of Texas at Austin, (2009).

[285] S.C. George, S. Thomas, Transport phenomena through polymeric systems, Progress in Polymer Science, 26 (2001) 985-1017.

[286] T. Okada, M. Yoshikawa, T. Matsuura, A study on the pervaporation of ethanol/water mixtures on the basis of pore flow model, Journal of membrane science, 59 (1991) 151-168.

[287] L. Al-Mashat, K. Shin, K. Kalantar-Zadeh, J.D. Plessis, S.H. Han, R.W. Kojima, R.B. Kaner, D. Li, X. Gou, S.J. Ippolito, Graphene/polyaniline nanocomposite for hydrogen sensing, The Journal of Physical Chemistry C, 114 (2010) 16168-16173.

[288] K. Ghanbari, M.F. Mousavi, M. Shamsipur, H. Karami, Synthesis of polyaniline/graphite composite as a cathode of Zn-polyaniline rechargeable battery, Journal of Power Sources, 170 (2007) 513-519.

[289] Y. Ma, W. Cheung, D. Wei, A. Bogozi, P.L. Chiu, L. Wang, F. Pontoriero, R. Mendelsohn, H. He, Improved conductivity of carbon nanotube networks by in situ polymerization of a thin skin of conducting polymer, Acs Nano, 2 (2008) 1197-1204.

[290] K.S. Lee, Water-dispersible, conductive polyaniline for organic thin-film electronics, ProQuest, 2007.

[291] K.-S. Ho, Effect of phenolic based polymeric secondary dopants on polyaniline, Synthetic metals, 126 (2002) 151-158.

[292] R. Dweiri, J. Sahari, Electrical properties of carbon-based polypropylene composites for bipolar plates in polymer electrolyte membrane fuel cell (PEMFC), Journal of Power Sources, 171 (2007) 424-432.

[293] Z. Mo, H. Shi, H. Chen, G. Niu, Z. Zhao, Y. Wu, Synthesis of graphite nanosheets/polyaniline nanorods composites with ultrasonic and conductivity, Journal of applied polymer science, 112 (2009) 573-578.

[294] A. Celzard, J.F. Marêché, F. Payot, G. Furdin, Electrical conductivity of carbonaceous powders, Carbon, 40 (2002) 2801-2815.

[295] S. Heo, J. Yun, K. Oh, K. Han, Influence of particle size and shape on electrical and mechanical properties of graphite reinforced conductive polymer composites for the bipolar plate of PEM fuel cells, Advanced Composite Materials, 15 (2006) 115-126.

[296] K. Kalaitzidou, H. Fukushima, L.T. Drzal, A new compounding method for exfoliated graphite–polypropylene nanocomposites with enhanced flexural properties and lower percolation threshold, Composites Science and Technology, 67 (2007) 2045-2051.

[297] H.-C. Kuan, C.-C.M. Ma, K.H. Chen, S.-M. Chen, Preparation, electrical, mechanical and thermal properties of composite bipolar plate for a fuel cell, Journal of Power Sources, 134 (2004) 7-17.

[298] B. Debelak, K. Lafdi, Use of exfoliated graphite filler to enhance polymer physical properties, Carbon, 45 (2007) 1727-1734.

[299] I. Zaman, H.C. Kuan, Q. Meng, A. Michelmore, N. Kawashima, T. Pitt, L. Zhang, S. Gouda, L. Luong, J. Ma, A facile approach to chemically modified graphene and its polymer nanocomposites, Advanced Functional Materials, 22 (2012) 2735-2743.

[300] S. Araby, Q. Meng, L. Zhang, H. Kang, P. Majewski, Y. Tang, J. Ma, Electrically and thermally conductive elastomer/graphene nanocomposites by solution mixing, Polymer, 55 (2014) 201-210.

[301] Y. Hernandez, V. Nicolosi, M. Lotya, F.M. Blighe, Z. Sun, S. De, I. McGovern, B. Holland, M. Byrne, Y.K. Gun'Ko, High-yield production of graphene by liquid-phase exfoliation of graphite, Nature nanotechnology, 3 (2008) 563-568.

[302] S. Giordani, S.D. Bergin, V. Nicolosi, S. Lebedkin, M.M. Kappes, W.J. Blau, J.N. Coleman, Debundling of single-walled nanotubes by dilution: observation of large populations of individual nanotubes in amide solvent dispersions, The journal of physical chemistry B, 110 (2006) 15708-15718.

[303] S. Majeed, D. Fierro, K. Buhr, J. Wind, B. Du, A. Boschetti-de-Fierro, V. Abetz, Multi-walled carbon nanotubes (MWCNTs) mixed polyacrylonitrile (PAN) ultrafiltration membranes, Journal of Membrane Science, 403–404 (2012) 101-109.

[304] J.-H. Choi, J. Jegal, W.-N. Kim, Fabrication and characterization of multi-walled carbon nanotubes/polymer blend membranes, Journal of Membrane Science, 284 (2006) 406-415.

[305] G.H. Chen, D.J. Wu, W.G. Weng, W.L. Yan, Preparation of polymer/graphite conducting nanocomposite by intercalation polymerization, Journal of Applied Polymer Science, 82 (2001) 2506-2513.

[306] L. Lu, H. Sun, F. Peng, Z. Jiang, Novel graphite-filled PVA/CS hybrid membrane for pervaporation of benzene/cyclohexane mixtures, Journal of membrane science, 281 (2006) 245-252.

[307] W. Li, C.L. Johnson, H.-L. Wang, Preparation and characterization of monolithic polyaniline–graphite composite actuators, Polymer, 45 (2004) 4769-4775.

[308] Y.J. Ren, C.L. Zeng, Effect of conducting composite polypyrrole/polyaniline coatings on the corrosion resistance of type 304 stainless steel for bipolar plates of proton-exchange membrane fuel cells, Journal of Power Sources, 182 (2008) 524-530.

[309] H. Saveyn, P. Van der Meeren, R. Hofmann, W. Stahl, Modelling two-sided electrofiltration of quartz suspensions: importance of electrochemical reactions, Chemical engineering science, 60 (2005) 6768-6779.

[310] S. Bhadra, N.K. Singha, S. Chattopadhyay, D. Khastgir, Effect of different reaction parameters on the conductivity and dielectric properties of polyaniline synthesized electrochemically and modeling of conductivity against reaction parameters through regression analysis, Journal of Polymer Science Part B: Polymer Physics, 45 (2007) 2046-2059.

[311] J. Janata, M. Josowicz, Conducting polymers in electronic chemical sensors, Nature materials, 2 (2003) 19-24.

[312] J.E. Yoo, W.P. Krekelberg, Y. Sun, J.D. Tarver, T.M. Truskett, Y.-L. Loo, Polymer conductivity through particle connectivity, Chemistry of Materials, 21 (2009) 1948-1954.

[313] A. Pron, P. Rannou, Processible conjugated polymers: from organic semiconductors to organic metals and superconductors, Progress in polymer science, 27 (2002) 135-190.

[314] X. Liu, K.J. Gilmore, S.E. Moulton, G.G. Wallace, Electrical stimulation promotes nerve cell differentiation on polypyrrole/poly (2-methoxy-5 aniline sulfonic acid) composites, Journal of neural engineering, 6 (2009) 065002.

[315] M.A. Aroon, A.F. Ismail, M.M. Montazer-Rahmati, T. Matsuura, Morphology and permeation properties of polysulfone membranes for gas separation: Effects of non-solvent additives and co-solvent, Separation and Purification Technology, 72 (2010) 194-202.

[316] P. Vandezande, L.E. Gevers, I.F. Vankelecom, Solvent resistant nanofiltration: separating on a molecular level, Chemical Society Reviews, 37 (2008) 365-405.

[317] I. Soroko, Y. Bhole, A.G. Livingston, Environmentally friendly route for the preparation of solvent resistant polyimide nanofiltration membranes, Green Chemistry, 13 (2011) 162-168.

[318] F.G. Paulsen, S.S. Shojaie, W.B. Krantz, Effect of evaporation step on macrovoid formation in wet-cast polymeric membranes, Journal of Membrane Science, 91 (1994) 265-282.

[319] H.L. Wang, R.J. Romero, B.R. Mattes, Y. Zhu, M.J. Winokur, Effect of processing conditions on the properties of high molecular weight conductive polyaniline fiber, Journal of Polymer Science Part B: Polymer Physics, 38 (2000) 194-204.

[320] D. Yang, B. Mattes, Polyaniline emeraldine base in N-methyl-2-pyrrolidinone containing secondary amine additives: A rheological investigation of solutions, Journal of Polymer Science Part B: Polymer Physics, 40 (2002) 2702-2713.

[321] D. Wang, K. Li, W. Teo, Polyethersulfone hollow fiber gas separation membranes prepared from NMP/alcohol solvent systems, Journal of Membrane Science, 115 (1996) 85-108.

[322] J.E. Yoo, K.S. Lee, A. Garcia, J. Tarver, E.D. Gomez, K. Baldwin, Y. Sun, H. Meng, T.-Q. Nguyen, Y.-L. Loo, Directly patternable, highly conducting polymers for broad applications in organic electronics, Proceedings of the National Academy of Sciences, 107 (2010) 5712-5717.

[323] K. Kimura, Y. Hane, Y. Watanabe, G. Amy, N. Ohkuma, Irreversible membrane fouling during ultrafiltration of surface water, Water Research, 38 (2004) 3431-3441.

[324] H. Susanto, H. Arafat, E.M. Janssen, M. Ulbricht, Ultrafiltration of polysaccharide–protein mixtures: elucidation of fouling mechanisms and fouling control by membrane surface modification, Separation and Purification Technology, 63 (2008) 558-565.

[325] Z. Wu, H. Chen, Y. Dong, H. Mao, J. Sun, S. Chen, V.S.J. Craig, J. Hu, Cleaning using nanobubbles: Defouling by electrochemical generation of bubbles, Journal of Colloid and Interface Science, 328 (2008) 10-14.

[326] A. Agarwal, W.J. Ng, Y. Liu, Principle and applications of microbubble and nanobubble technology for water treatment, Chemosphere, 84 (2011) 1175-1180.

[327] C.D. Vecitis, M.H. Schnoor, M.S. Rahaman, J.D. Schiffman, M. Elimelech, Electrochemical multiwalled carbon nanotube filter for viral and bacterial removal and inactivation, Environmental science & technology, 45 (2011) 3672-3679.

[328] T. Maruyama, S. Katoh, M. Nakajima, H. Nabetani, T.P. Abbott, A. Shono, K. Satoh, FT-IR analysis of BSA fouled on ultrafiltration and microfiltration membranes, Journal of Membrane Science, 192 (2001) 201-207.

[329] B.T. McVerry, J.A. Temple, X. Huang, K.L. Marsh, E.M. Hoek, R.B. Kaner, Fabrication of low-fouling ultrafiltration membranes using a hydrophilic, self-doping polyaniline additive, Chemistry of Materials, 25 (2013) 3597-3602.

[330] S. Salgın, S. Takaç, T.H. Özdamar, Adsorption of bovine serum albumin on polyether sulfone ultrafiltration membranes: Determination of interfacial interaction energy and effective diffusion coefficient, Journal of Membrane Science, 278 (2006) 251-260.

[331] M. Ferrando, A. Rŏžek, M. Zator, F. Lopez, C. Güell, An approach to membrane fouling characterization by confocal scanning laser microscopy, Journal of Membrane Science, 250 (2005) 283-293.

Appendix A- Electrically Tuneable Polyaniline Membranes

A.1 Increasing the Mechanical Robustness of PANI Membranes: Effect of Doping Time

Table A1 Effect of doping time on the mechanical properties of the Memb-ES-15.

Doping time/h	Tensile strength/MPa	Young modulus/GPa	Elongation at break/%
2	10.1±0.19	1.23±0.031	0.028±0.002
6	8.29±0.27	1.07±0.062	0.026±0.001
24	8.31±0.1	0.89±0.045	0.019±0.001

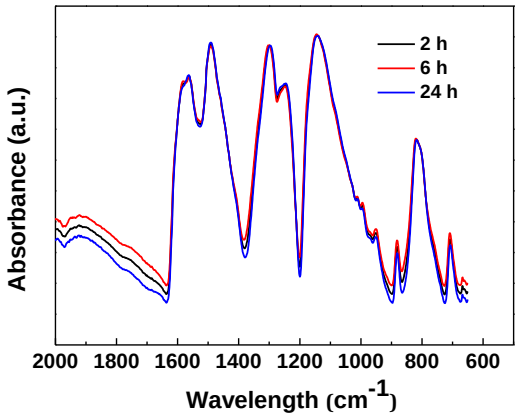

Fig A1. FTIR of PANI Memb-ES-15 at different doping times (2, 6 and 24 h).

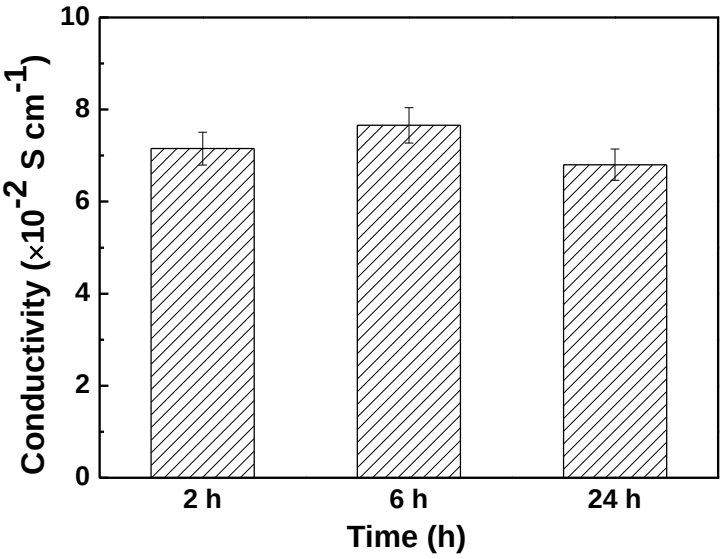

Fig A2. The conductivity of Memb-ES-15 at different doping times

A.2 Small acid leaching during filtration

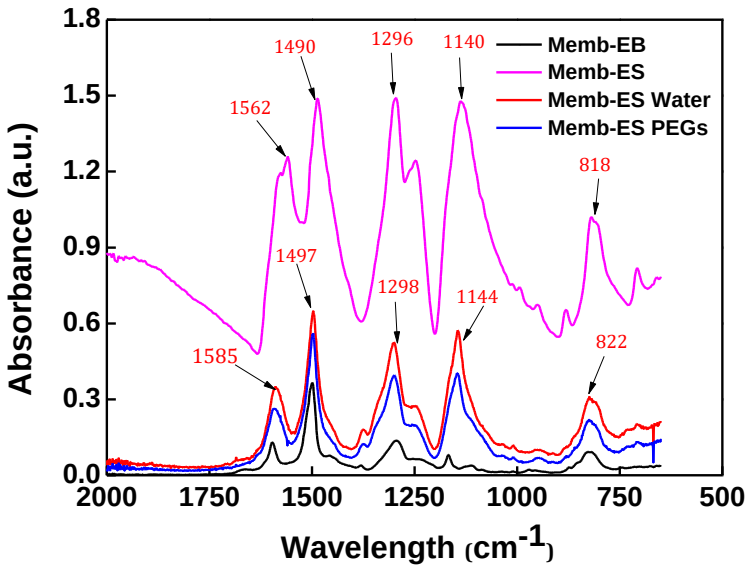

Fig A3. FTIR spectra of membranes before and after cross flow filtration.

Table A2 Colour characterisation of membranes before and after cross flow filtration.

Membrane	Red	Green	Blue
Memb-EB	12.6	18.8	18.4
Memb-ES	11.3	19.8	20.6
Memb-ES (Water)	12.0	19.9	20.5
Memb-ES (PEG UF)	12.0	20.1	20.9

A.3 Membrane permeance in cross flow filtration

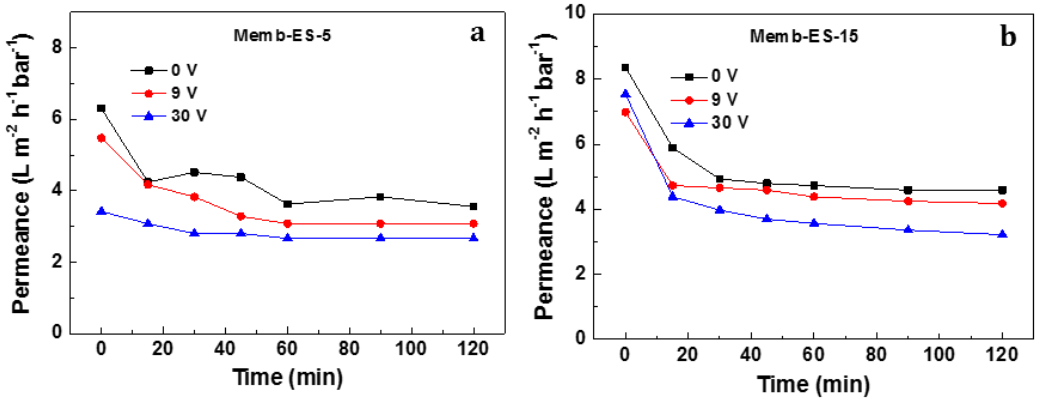

Fig A4. Variation of PEG permeance of (a) Memb-ES-5 and (b) Memb-ES-15 under applied voltage from 0 V to 30 V (20 bar, 25℃, PEG).

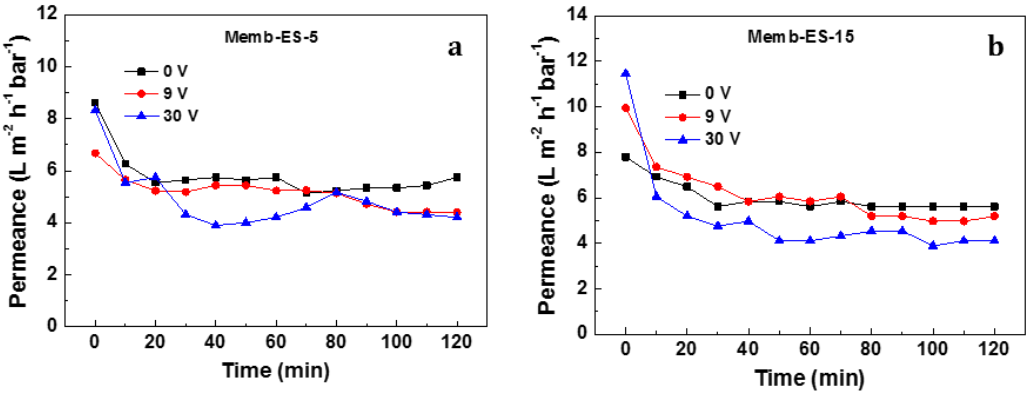

Fig A5. Variation of water permeance of (a) Memb-ES-5 and (b) Memb-ES-15 under applied voltage from 0 V to 30 V (20 bar, 25℃, DI water).

A.4 Membrane permeance and MWCO in dead end filtration

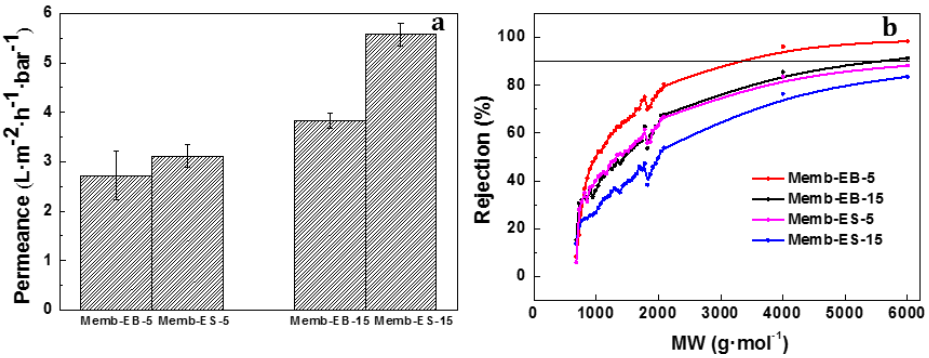

Fig A6. (a) Water permeance and (b) MWCO of Memb-EB and Memb-ES by the dead-end filtration.

A.4 Membrane thickness

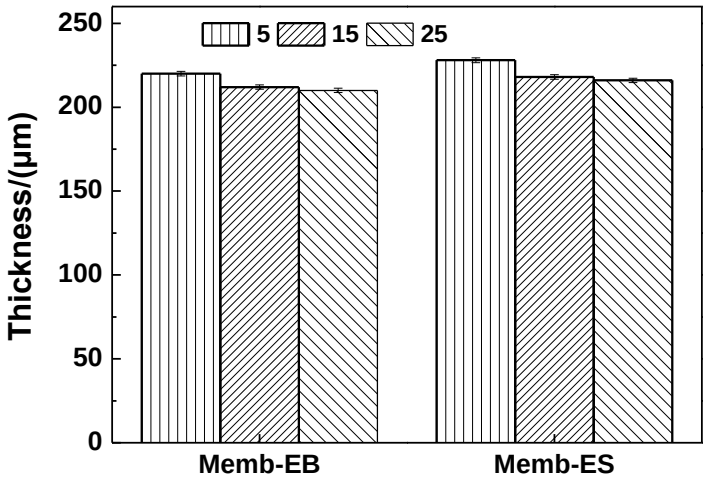

Fig A7**.** The thickness of Memb-EB and Memb-ES from different polymerisation temperatures.

Appendix B- MWCO Method for Aqueous Based NF and UF Membranes Using PEGs

B.1 Identification of individual PEG oligomers

Table B1 show the oligomer peak MW attribution in the purer PEG 1000 standard and commercial PEG mixtures. The peak time and area are matched to the MW of each oligomer.

Table B1 The oligomer peak MW attribution in Purer PEG 1000

MW/g·mol^{-1}	Time/min	Area
678	4.49	10.73
722	4.72	27.86
766	4.92	66.96
810	5.11	138.49
854	5.31	216.99
898	5.51	290.82
942	5.73	350.21
986	5.98	371.21
1030	6.25	356.94
1074	6.57	306.45
1118	6.92	242.96
1162	7.31	167.73
1206	7.76	112.57
1250	8.26	66.06
1294	8.83	37.78
1338	9.48	8.51
1382	9.51	7.36

Table B2 The oligomer peak MW attribution in the PEG mixtures

MW/g·mol^{-1}	Time/min	MW/g·mol^{-1}	Time/min
678	4.49	2746	44.23
722	4.71	2790	44.73
766	4.91	2834	45.22
810	5.10	2878	45.67
854	5.29	2922	46.14
898	5.49	2966	46.59
942	5.71	3010	47.04
986	5.96	3054	47.46
1030	6.23	3098	47.89
1074	6.53	3142	48.30
1118	6.88	3186	48.73
1162	7.26	3230	49.15
1206	7.68	3274	49.56
1250	8.16	3318	49.97
1294	8.68	3362	50.37
1338	9.28	3406	50.76
1382	9.95	3450	51.14
1426	10.72	3494	51.50
1470	11.61	3538	51.87
1514	12.61	3582	52.23
1558	13.79	3626	52.60
1602	15.10	3670	52.94
1646	16.66	3714	53.28
1690	18.42	3758	53.61
1734	20.52	3802	53.93

1778	22.88	3846	54.26
1822	25.25	3890	54.58
1866	27.11	3934	54.90
1910	28.69	3978	55.21
1954	30.10	4022	55.51
1998	31.36	4066	55.80
2042	32.50	4110	56.13
2086	33.56	4154	56.43
2130	34.55	4198	56.72
2174	35.47	4242	57.03
2218	36.34	4286	57.33
2262	37.15	4330	57.62
2306	37.95	4374	57.89
2350	38.69	4418	58.19
2394	39.42	4462	58.50
2438	40.12	4506	58.77
2482	40.78	4550	59.05
2526	41.41	4594	59.33
2570	42.02	4638	59.59
2614	42.62	4682	59.86
2658	43.18	4726	60.11
2702	43.71	6000	65.85

B.2 Obtaining calibration curves

Different concentrations of the commercial PEG mixtures were run and external calibration curves were established for each MW of PEG oligomer. In this work, there were "combined" peaks in the chromatogram, thereby peak areas were attributed to a combination of the concentration of this MW in both commercial PEGs. As suggested in the literature [202], the concentration of each peak can be calculated using Equation B1 and B2:

$$C_i = \frac{A_i}{[\sum_{i=1}^{n} A_i]_{PEG\ mix}} [C_{total}]_{PEG\ mix} \quad (1)$$

$$= \frac{\sum_{x=1}^{z} m_x}{V_{total}} = \frac{m_{PEG1000} + m_{PEG1500} + m_{PEG2000} + m_{PEG3000} + m_{PEG4000}}{V_{total}} \quad (2)$$

Where:

$[C_{total}]_{PEG\ mix}$ is the total concentration of all PEG oligomers in the total mixture; C_i and A_i are the concentration and area of each oligomer corresponding to peak i, respectively;

$[\sum_{i=1}^{n} A_i]_{PEG\ mix}$ is the total area of all peaks in the commercial grade PEG mix, where n is the number of PEG oligomer peaks, m_x is the mass of commercial grade PEG_x, V_{total} is the total volume, and z is the total number of commercial grade PEGs used in the mixture (which is 5 in this work).

Fig. B1 shows the resulting calibration curves of all of the different PEG oligomers correlating peak areas to oligomer concentration for PEG oligomers with MWs from 678 g mol^{-1} to 4594 g mol^{-1} with a MW difference of 44 g mol^{-1} and followed by one composite peak attributed to a PEG MW of 6000 g mol^{-1}.

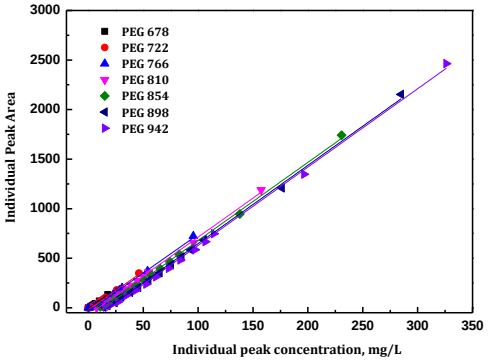
PEG 678
PEG 722
PEG 766
PEG 810
PEG 854
PEG 898
PEG 942
Individual Peak Area
Individual peak concentration, mg/L

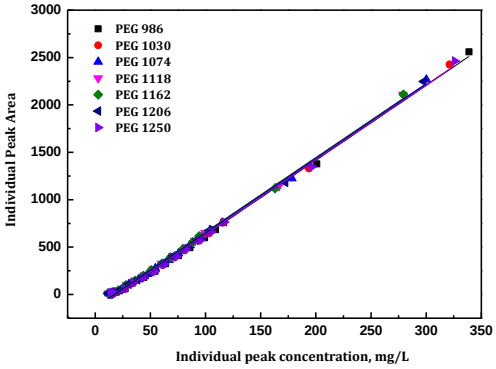
PEG 986
PEG 1030
PEG 1074
PEG 1118
PEG 1162
PEG 1206
PEG 1250
Individual Peak Area
Individual peak concentration, mg/L

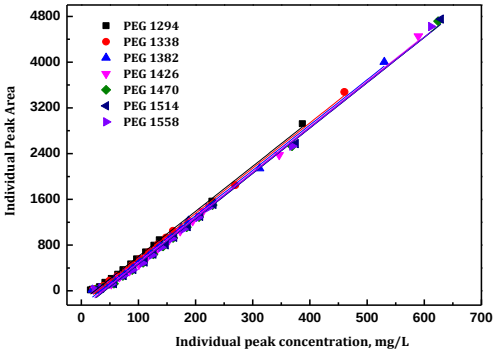
PEG 1294
PEG 1338
PEG 1382
PEG 1426
PEG 1470
PEG 1514
PEG 1558
Individual Peak Area
Individual peak concentration, mg/L

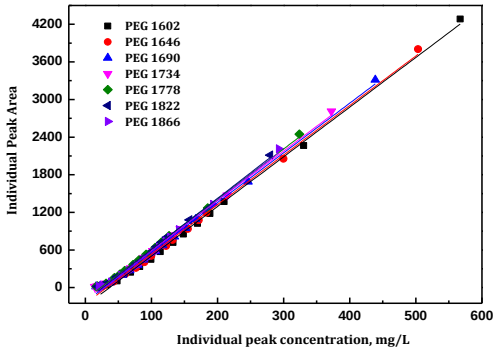
PEG 1602
PEG 1646
PEG 1690
PEG 1734
PEG 1778
PEG 1822
PEG 1866
Individual Peak Area
Individual peak concentration, mg/L

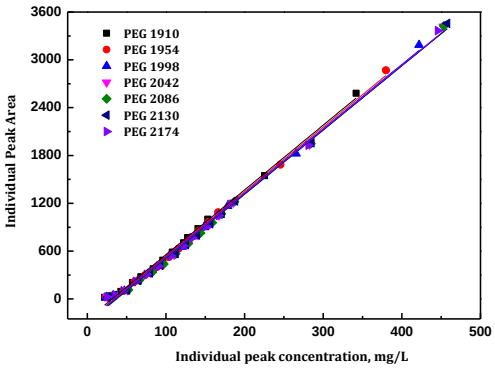
PEG 1910
PEG 1954
PEG 1998
PEG 2042
PEG 2086
PEG 2130
PEG 2174
Individual Peak Area
Individual peak concentration, mg/L

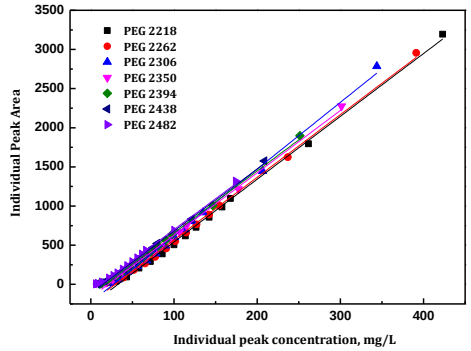
PEG 2218
PEG 2262
PEG 2306
PEG 2350
PEG 2394
PEG 2438
PEG 2482
Individual Peak Area
Individual peak concentration, mg/L

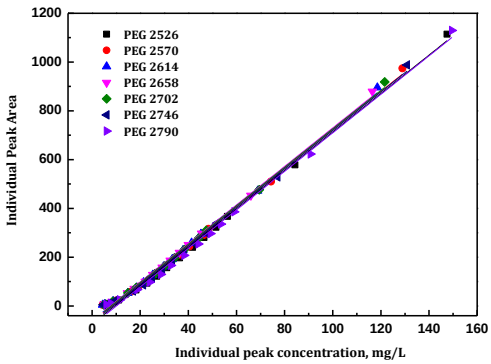
PEG 2526
PEG 2570
PEG 2614
PEG 2658
PEG 2702
PEG 2746
PEG 2790
Individual Peak Area
Individual peak concentration, mg/L

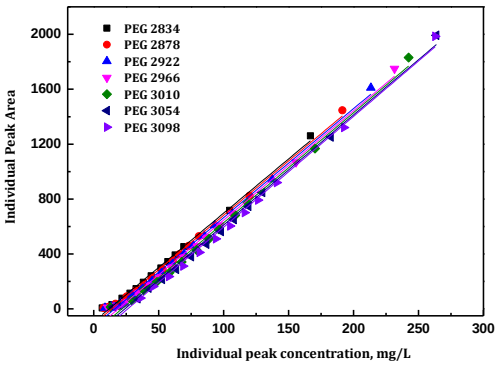
PEG 2834
PEG 2878
PEG 2922
PEG 2966
PEG 3010
PEG 3054
PEG 3098
Individual Peak Area
Individual peak concentration, mg/L

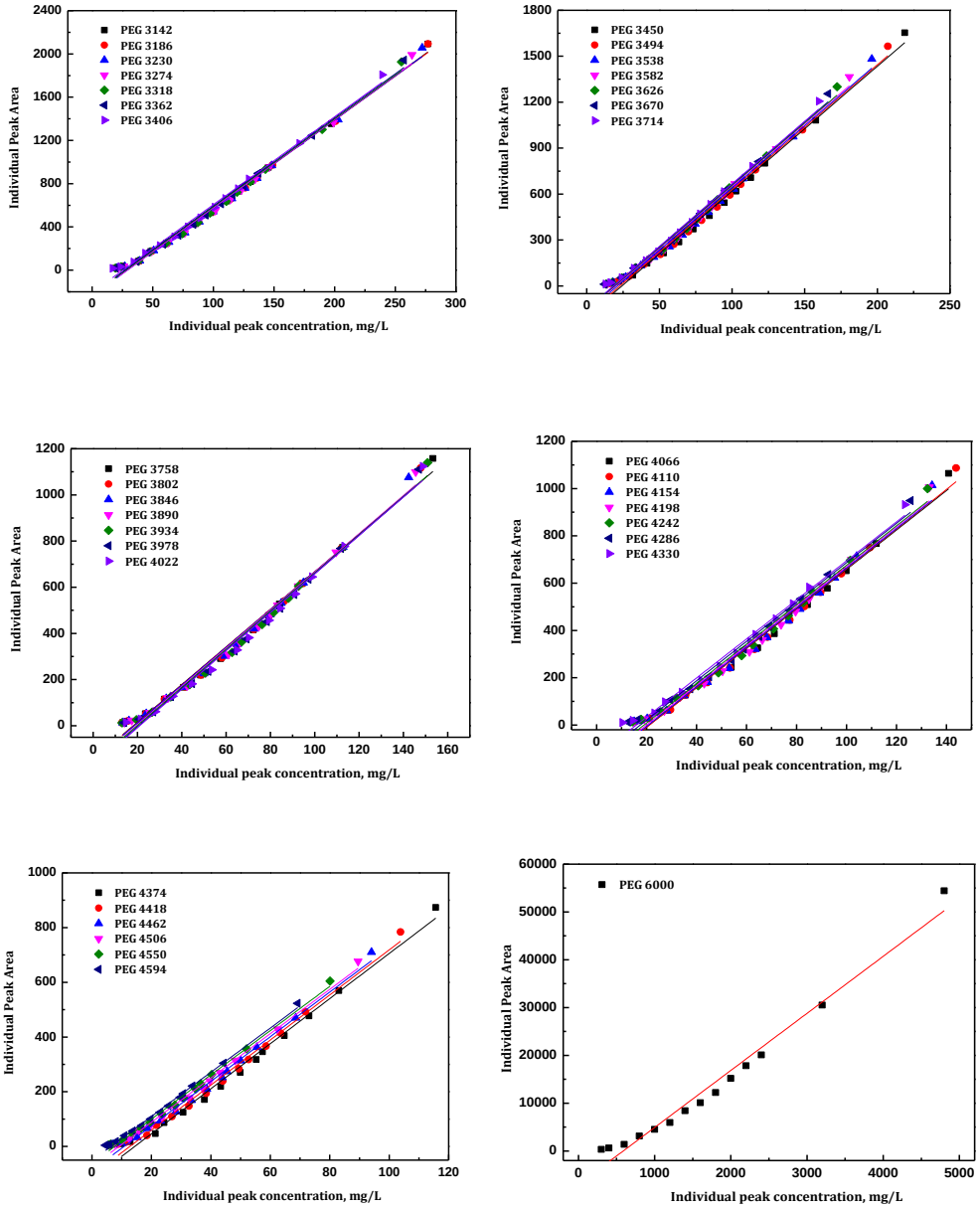

Fig. B1 Calibration curves of for all of the PEG oligomers identified.

B.3 Resulting HPLC chromatograms obtained from commercial membranes

Fig. B2-B6 present the HPLC chromatograms of feed, retentate and permeate from filtering PEG mixtures through the six commercial membranes chosen. The permeates all gave HPLC chromatograms with higher MW PEG oligomers with lower ELSD responses than the feed, indicating that these higher MW oligomers were rejected by the membranes.

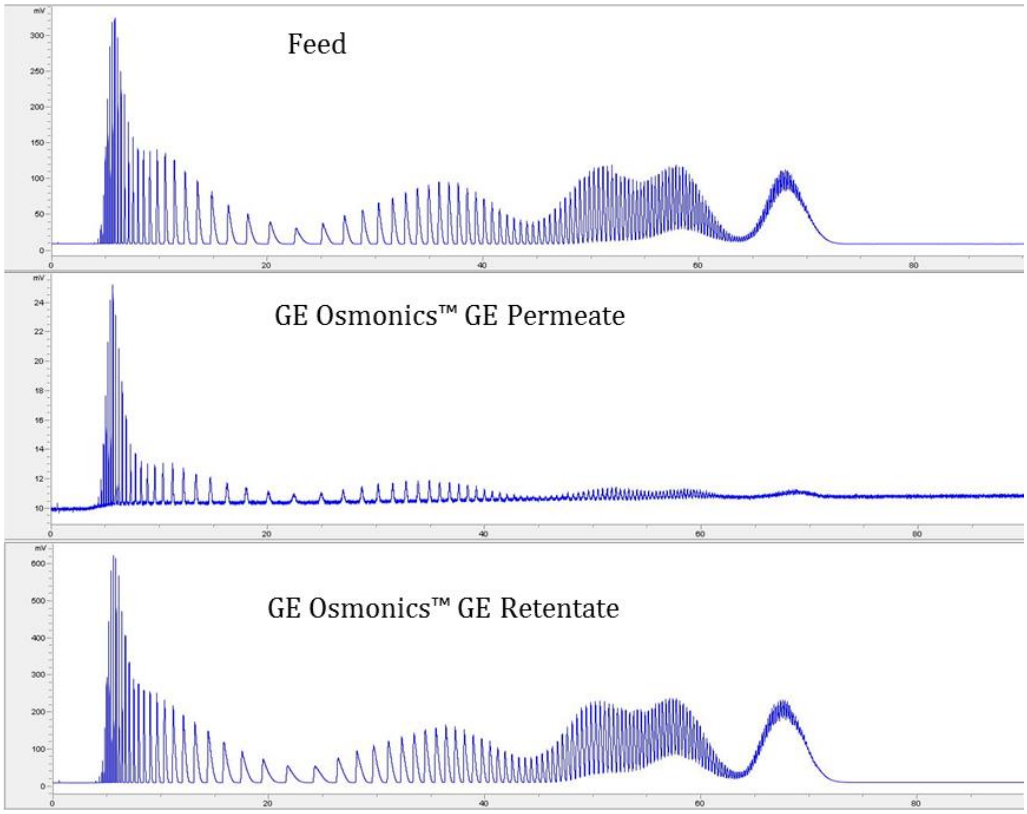

Fig. B2 HPLC chromatograms of the feed, permeate and retentate from GE Osmonics™ GE.

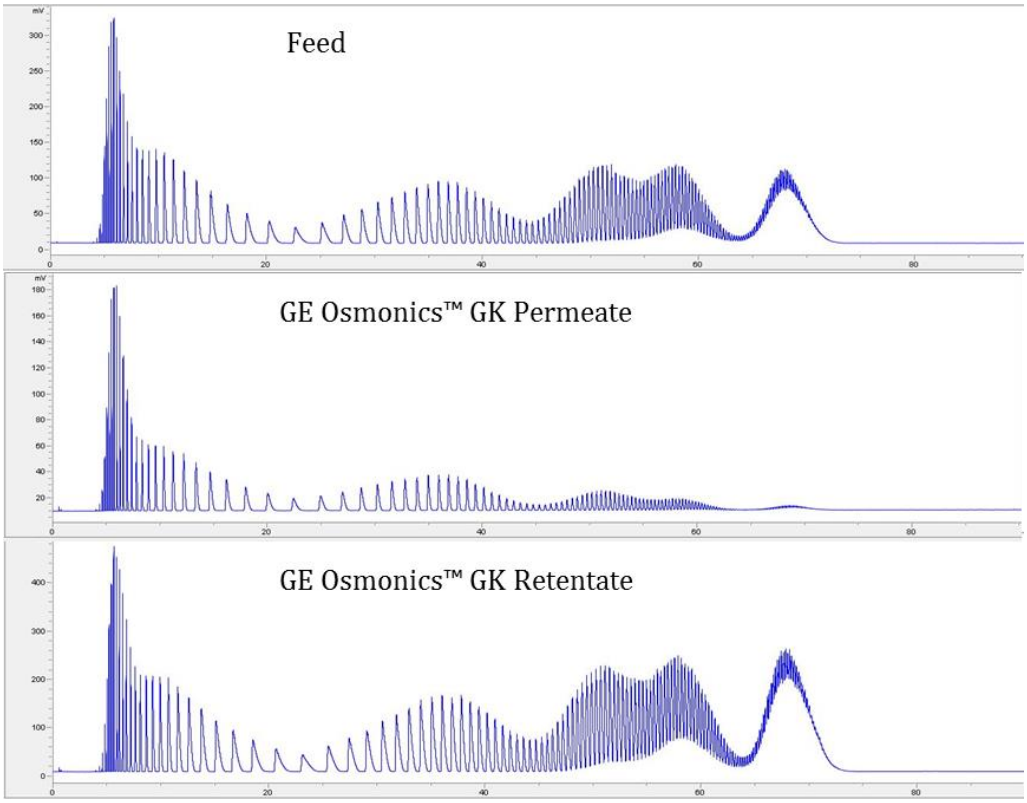

Fig. B3 HPLC chromatograms of the feed, permeate and retentate from GE Osmonics™ GK.

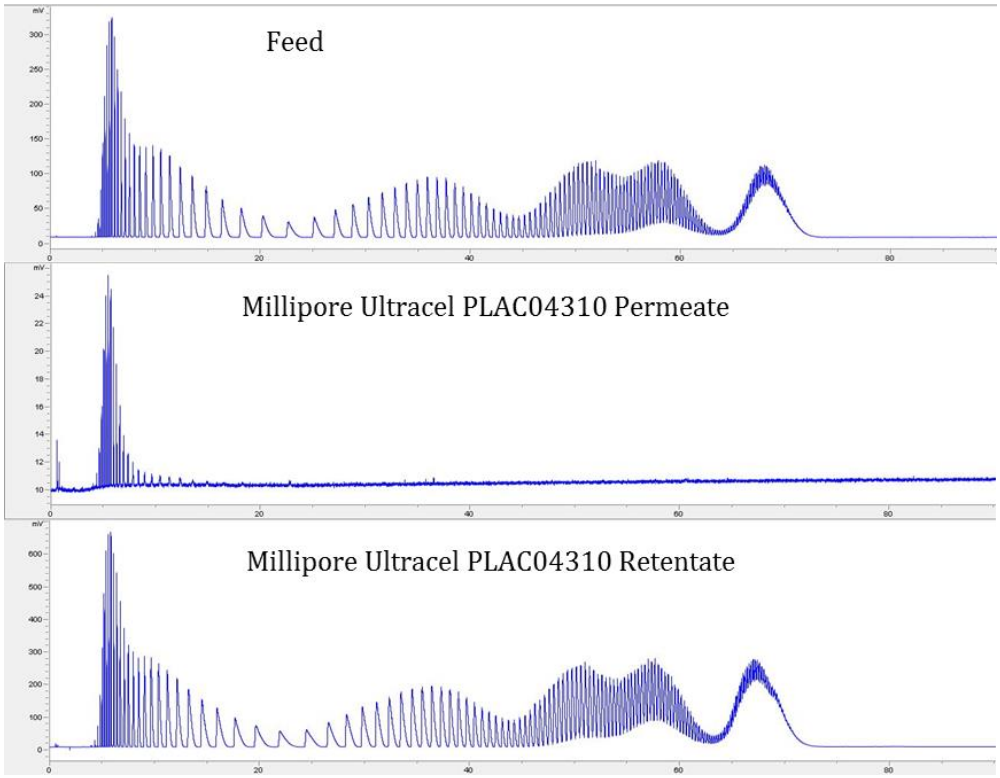

Fig. B4 HPLC chromatograms of the feed, permeate and retentate from Millipore Ultracel PLAC04310.

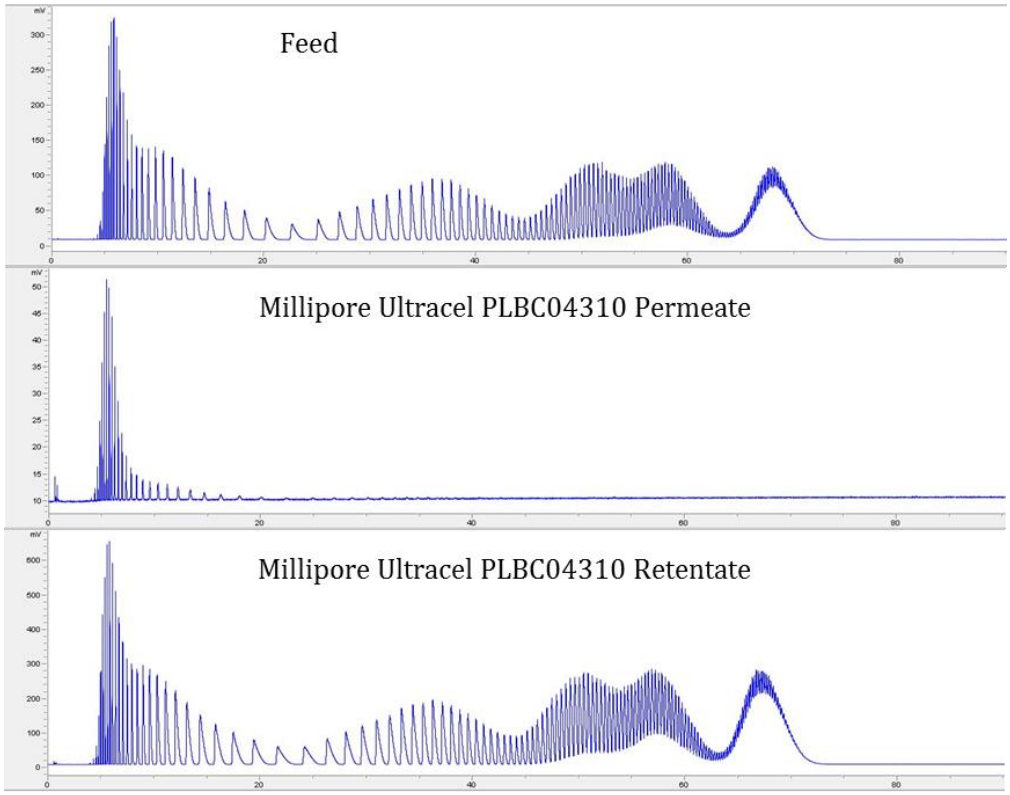

Fig. B5 HPLC chromatograms of the feed, permeate and retentate from Millipore Ultracel PLBC04310.

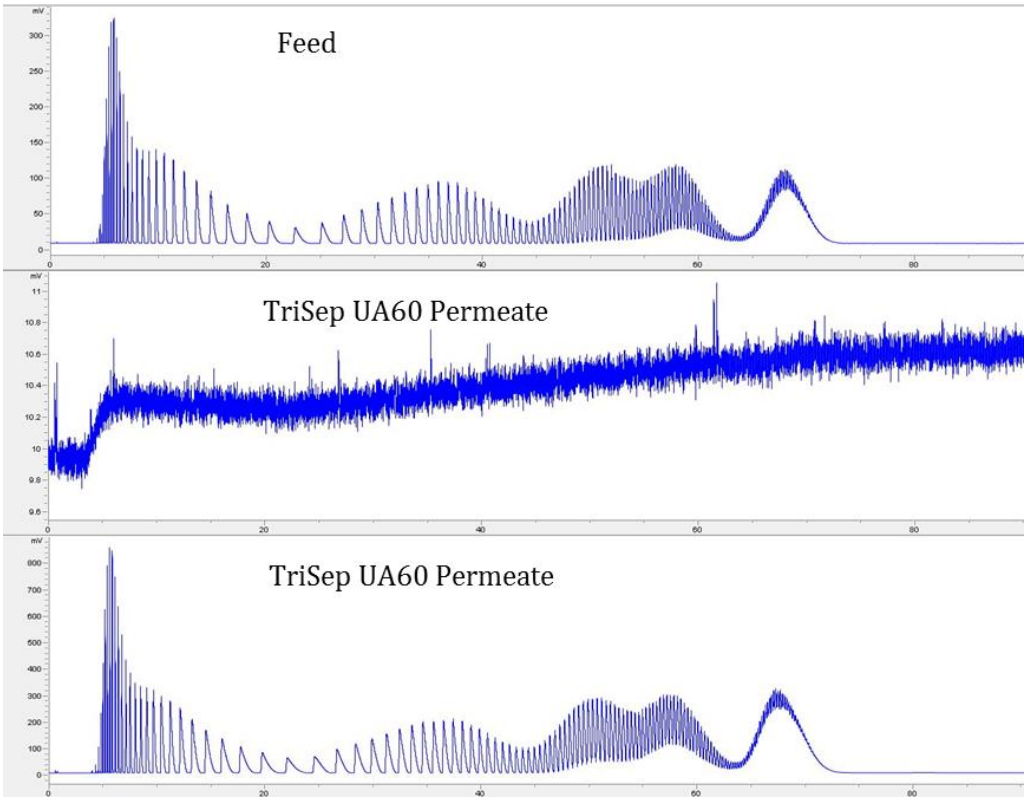

Fig. B6 HPLC chromatograms of the feed, permeate and retentate from TriSep UA60.

Fig. B7 shows the UV-Vis spectra of Rose Bengal from the permeate, retentate and feed of TriSep UV60. The permeate did not show any absorbance, indicating the rose Bengal was totally rejected by the membrane and the MWCO of TriSep UA60 used in the study was below 974 g mol^{-1} by using this method.

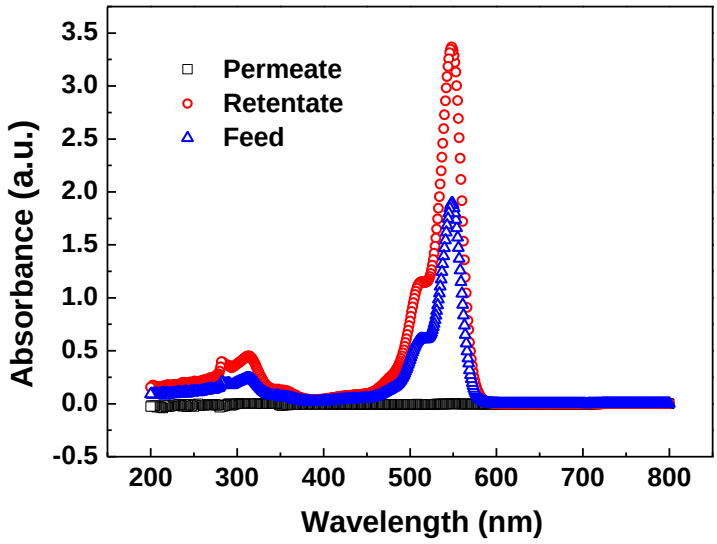

Fig. B7 UV-Vis spectra of Rose Bengal from the permeate, retentate and feed of TriSep UV60.

Appendix C- Enhancing Memb-PAMPSA as a Stimulating-responsive Membrane by EG Incorporation and DBSA Treatment

C.1 Electrically Connected Cross-flow Filtration of Membranes

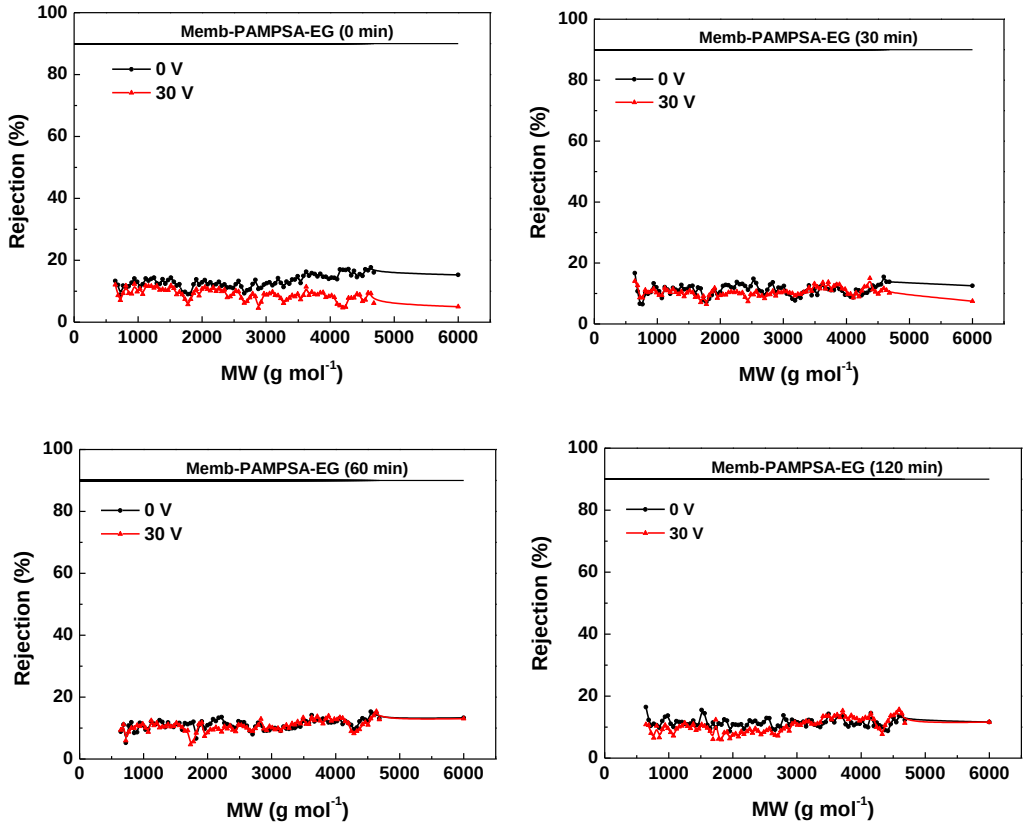

Fig. C1 The rejection of Memb-PAMPSA-EG at different filtration times (0, 30, 60 and 120 min) under applied potential of 0 and 30 V (2 bar, 25℃, PEG mixtures).

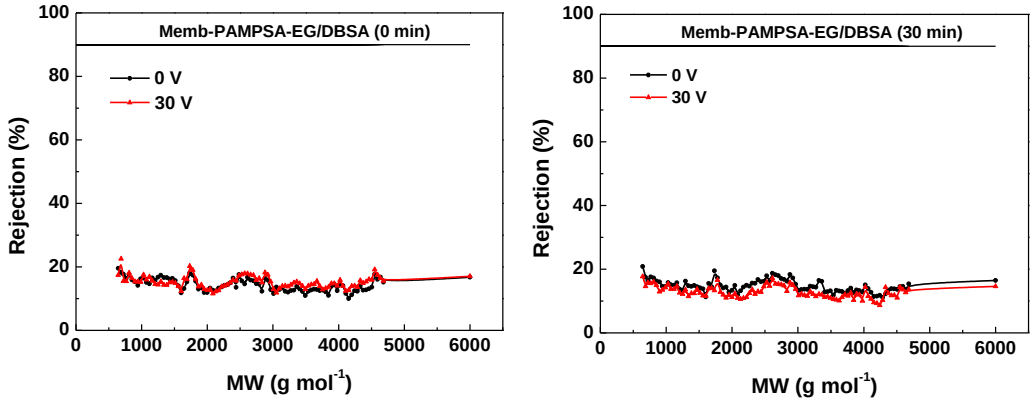

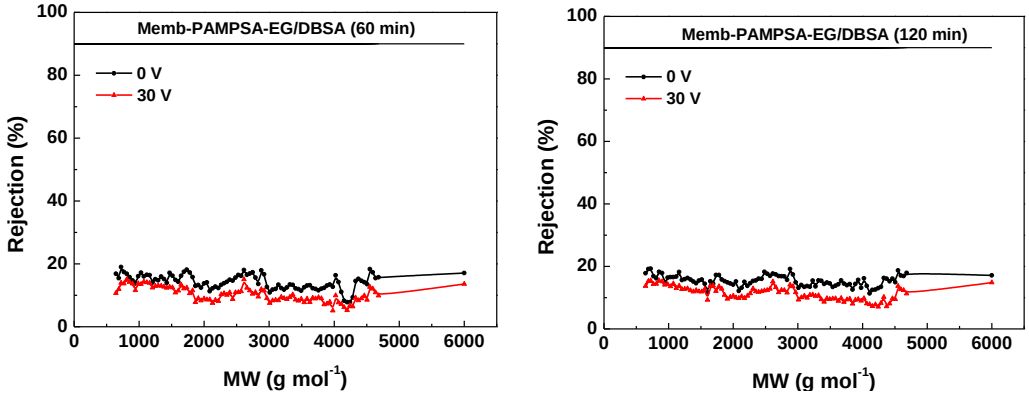

Fig. C2 The rejection of Memb-PAMPSA-EG/DBSA at different filtration times (0, 30, 60 and 120 min) under applied potential of 0 and 30 V (2 bar, 25℃, PEG mixtures).

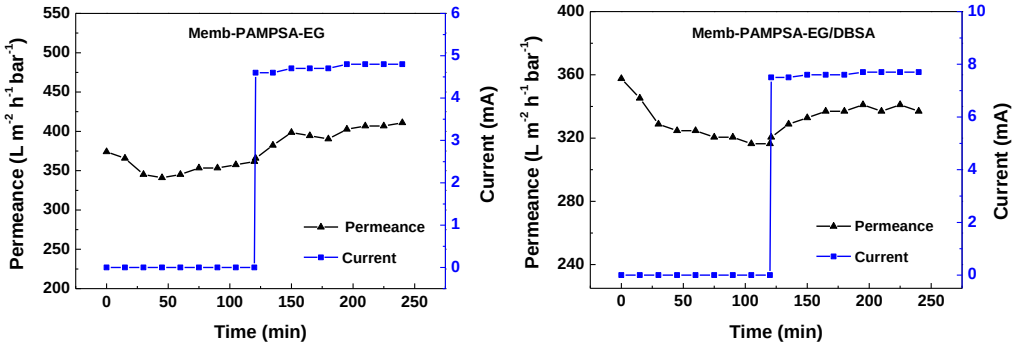

Fig. C3 Permeance and current of Memb-PAMSA-EG and Memb-PAMSA-EG DBSA under applied potential of 0 and 30 V (2 bar, 25℃, PEG mixtures).

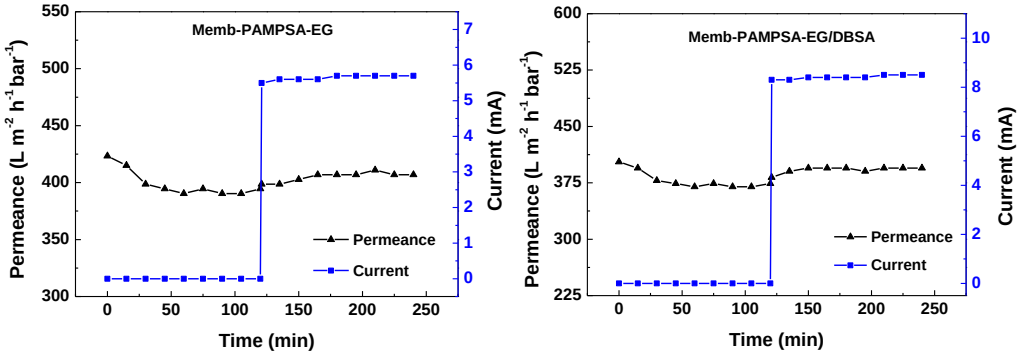

Fig. C4 Water permeance and current of Memb-PAMSA-EG and Memb-PAMSA-EG DBSA under applied potential of 0 and 30 V (2 bar, 25℃, DI Water).

Appendix D- Stimuli-Responsive Composite PANI Membranes to Solve Fouling

D.1 Fouling removal under applied potential

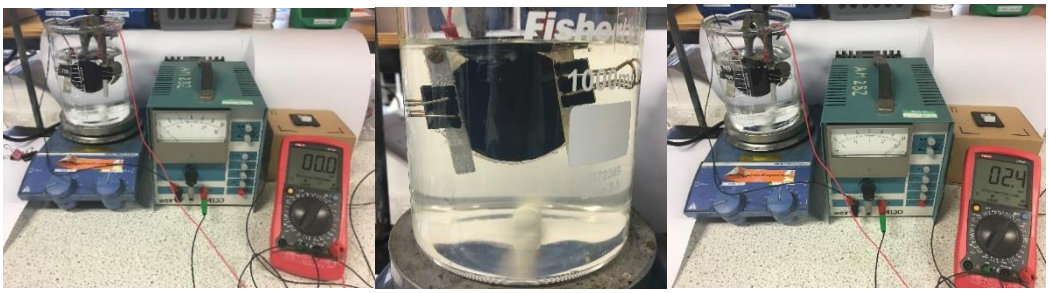

Fig. D1 Photos of membrane fouling removal under applied potential

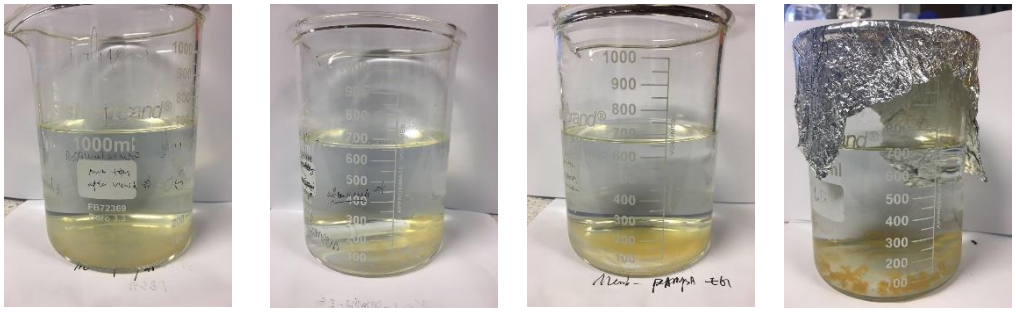

Memb-HCl | Memb-PAMPSA | Memb-PAMPSA-EG | Memb-PAMPSA-EG (DBSA)

Fig. D2 Photos of membrane wash solution after applied potential

D.2 Blank experiment

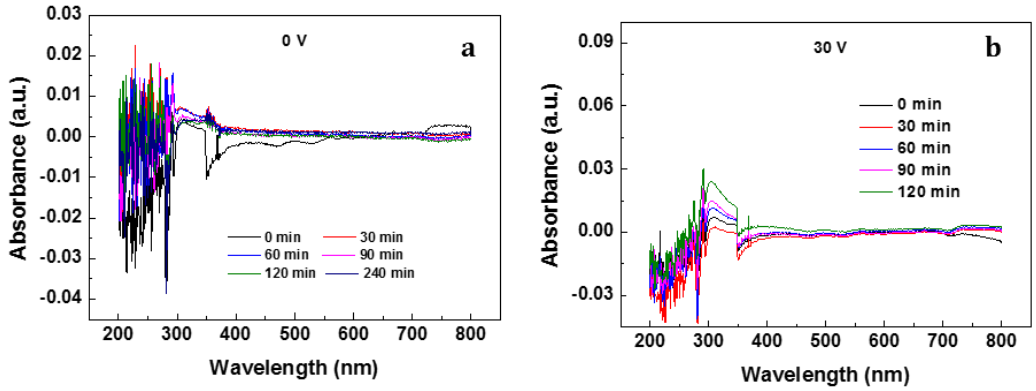

Fig. D3 UV-Vis spectra (a) wash solution of fouled membrane in the absence of applied potential (b) wash solution of virgin membrane in the presence of applied potential (30 V).

D.3 Colour change

Fig. D4 Scanned photos of Memb-HCl, Memb-PAMPSA, Memb-PAMPSA-EG and Memb-PAMPSA-EG/DBSA.

Appendix E-Electrochemical Properties of Membranes

E.1 Cyclic voltammetry (helped by Professor Frank Marken)

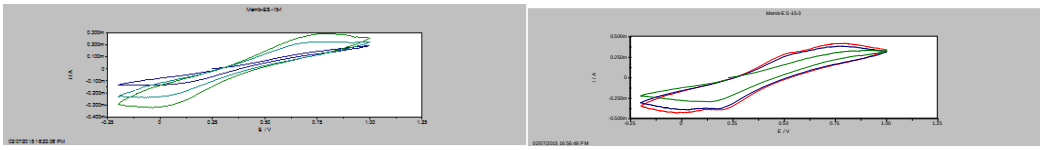

Memb-HCl

Memb-PAMPSA

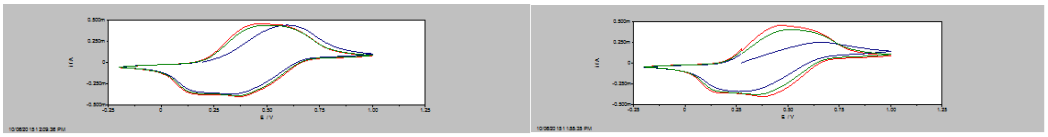

Memb-PAMPSA-EG Memb-PAMPSA-EG DBSA

Fig. E1 Cyclic voltammetry of Memb-HCl, Memb-PAMPSA, Memb-PAMPSA-EG and Memb-PAMPSA-EG/DBSA.